EXH. JPH-16
DOCKETS UE-240004/UG-240005
2024 PSE GENERAL RATE CASE
WITNESS: JAMES P. HOGAN

BEFORE THE
WASHINGTON UTILITIES AND TRANSPORTATION COMMISSION

WASHINGTON UTILITIES AND TRANSPORTATION COMMISSION, Complainant, v. PUGET SOUND ENERGY, Respondent.	Docket UE-240004 Docket UG-240005

FIFTEENTH EXHIBIT (NONCONFIDENTIAL) TO THE PREFILED DIRECT TESTIMONY OF

JAMES P. HOGAN

ON BEHALF OF PUGET SOUND ENERGY

FEBRUARY 15, 2024

SUBMITTED TO:
Puget Sound Energy
1600 Park Lane
Burlington, WA 98233

BY:
Shannon & Wilson
400 N. 34th Street, Suite 100
Seattle, WA 98103

(206) 632-8020
www.shannonwilson.com

GEOTECHNICAL REPORT
FOUNDATION FAILURE MODES REPORT

Upper Baker Dam

CONCRETE, WASHINGTON

SHANNON & WILSON

December 22, 2022

Shannon & Wilson No: 105102-033

Submitted To: Puget Sound Energy
1600 Park Lane
Burlington, WA 98233
Attn: Mr. John Bickford

Subject: GEOTECHNICAL REPORT
FOUNDATION FAILURE MODES REPORT, UPPER BAKER DAM, CONCRETE, WASHINGTON

Shannon & Wilson, Inc. (Shannon & Wilson) prepared this report and participated in this project as a consultant to Puget Sound Energy (PSE). Our original scope of services was specified in Agreement Number 4600014598 with PSE dated May 21, 2020. On December 17, 2020, a revised Statement of Work (SOW) No. CW2230087 was executed under a new Master Services Agreement (No. CW2229967, dated December 4, 2020). In partial completion of the SOW deliverables, a Foundation Failure Modes Assessment Geotechnical Report (original) was delivered to PSE on April 6, 2021.

Shannon & Wilson and PSE executed Change Order No. 1 on October 12, 2021, to evaluate the subsurface conditions in the Upper Baker Dam spillway slope. The Foundation Failure Modes Assessment Geotechnical Report presented herein is an updated version of the original report. This report includes the new information and revised analyses resulting from the Change Order No. 1 explorations and was prepared under the direction of the undersigned.

We appreciate the opportunity to be of service to you on this project. If you have questions concerning this report, or we may be of further service, please contact us.

Sincerely,

SHANNON & WILSON, INC.

REX WHISTLER
STATE OF WASHINGTON
22021356
REGISTERED PROFESSIONAL ENGINEER
Expires: 11/22/2023

Rex Whistler, PE
Senior Geological Engineer

Samantha Kleich
Geological Engineer

SJK:RAW/mds:mmb

EXECUTIVE SUMMARY

Upper Baker Dam is part of Puget Sound Energy's (PSE's) Upper Baker Development for the Baker River Hydroelectric Project, FERC Number 2150. The Baker River Hydroelectric Project includes the Lower Baker Development and Upper Baker Development. In addition to Upper Baker Dam, the Upper Baker Development includes West Pass Dike, Auxiliary Dike, Depression Lake Dike, and other associated facilities. In 2019, HDR, Inc. (HDR) in conjunction with the Eleventh Independent Consultant's Safety Inspection, performed a Potential Failure Mode Analysis (PFMA) for the Baker River Hydroelectric Project (HDR, 2019). This report presents the geologic conditions and an assessment of selected potential failure modes (PFMs) related to the stability of Upper Baker Dam, particularly related to movement within the dam foundation, stability of the spillway slope, and erosion and stability of the slope downstream of the spillway. The following PFMs are introduced or addressed in this report:

- PFMs N-UB-2A, F-UB-2A, and S-UB-2A, which pertain to shear displacement along a foliation surface within the rock mass below Monoliths 18/19;
- PFMs N-UB-2B, F-UB-2B, and S-UB-2B, which pertain to shear displacement along a discontinuity within the rock mass below Monoliths 9/10;
- PFMs N-UB-2C, F-UB-2C, and S-UB-2C, which pertain to sliding along an adversely oriented discontinuity (or discontinuities) in the foundation below Monoliths 4/5;
- PFMs S-UB-3, F-UB-3B, and F-UB-3A, which pertain to stability of the spillway slope downstream of Monoliths 16/17 with the potential to undermine and lead to damage or loss of the spillway and undermining of Monoliths 16/17;
- PFMs N-UB-8 and F-UB-8, and S-UB-6, which pertain to sliding along a shallow foliation surface within the rock mass, a short distance below and parallel to the concrete-to-rock interface at Monoliths 18/19; and
- PFM F-UB-3C, which pertains to stability of the slope downstream of the spillway with the potential to undermine and lead to damage or loss of the spillway and undermining of Monoliths 16/17.

To assess the foundation geologic conditions at Upper Baker Dam, Shannon & Wilson, Inc. (Shannon & Wilson) completed a field investigation program between 2014 and 2017 that consisted of geologic mapping, photogrammetry survey, and rock core drilling. The geologic mapping of rock exposures in the left and right abutments was completed by Shannon & Wilson on June 19, 2014. In 2016 and 2017, eleven (11) borings from within the dam gallery and three (3) borings on the exterior of the dam were completed using a combination of HQ3 rock coring methods and rotosonic drilling methods. Laboratory testing was performed on representative rock cores, including uniaxial compressive strength tests, direct shear tests, and petrographic analysis. Select borings were surveyed using televiewer imagery, packer tested, and instrumented with joint meters, flow monitors, vibrating wire piezometers, multiple-point borehole extensometers, and/or inclinometer casing. Then, in March 2020, the structural geologic mapping effort was augmented with an unmanned aerial vehicle photogrammetry survey performed by Terrane Geosciences. To assess the spillway slope geologic conditions, four (4) borings were completed in 2021 using HQ3 rock coring methods. Laboratory testing was performed on representative rock cores, including uniaxial compressive strength tests, and direct shear tests. The borings were surveyed using televiewer imagery and instrumented with three (3) vibrating wire piezometers per boring.

Analyses of kinematically admissible blocks for Upper Baker Dam were divided into groups of concrete monoliths (described in previous reports as concrete 'blocks'; therefore, because a 'Monolith' was previously described as a 'Block', this terminology is still depicted in some of our previous analyses). Five (5) areas beneath the dam foundation were identified as having kinematically admissible failure modes and were investigated further, including the foundations under concrete Monoliths 1, 2, and 3; Monoliths 4 and 5; Monoliths 6 through 10; Monoliths 17, 18, and 19; and Monoliths 20 and 21. Additionally, the spillway slope was identified as having kinematically admissible failure modes and was investigated further. The major structures identified beneath Monoliths 1, 2, and 3; beneath Monoliths 4 and 5; and beneath Monoliths 6, 7, 8, 9, and 10 do not form kinematically admissible wedges that would daylight downstream of the dam. A potential kinematically admissible rock wedge was identified beneath Monoliths 17, 18, and 19, but the Hatch three-dimensional numerical model determined that Monolith 18 is locked up against Monolith 19, and the sliding surface will not daylight in the slope in proximity to the dam. Additionally, offsets observed in the vicinity of Monoliths 20 and 21 are interpreted to be related to the historic movement of Monoliths 18 and 19. In summary, the major structures identified in the foundation rock mass do not pose a stability issue for the Upper Baker Dam given the present geologic interpretation.

To address the identified kinematically admissible failure modes in the spillway slope, two-dimensional limit equilibrium stability analyses were performed. In addition to evaluating the existing slope, two alternative spillway stabilization designs were developed: a rock anchor support pattern and a grouted rock buttress. Both the rock anchor support pattern and grouted rock buttress were designed to meet the design criteria established in Geotechnical Design Memorandum 1. The grouted rock buttress alternative is the preferred option.

CONTENTS

CONTENTS

CONTENTS

CONTENTS

CONTENTS

CONTENTS

Exhibits

CONTENTS

CONTENTS

CONTENTS

CONTENTS

Tables

CONTENTS

Figures

The figures appended to this report are larger-scale versions of the in-text exhibits.

Plates

Appendices

ACRONYMS

2D	two-dimensional
3D	three-dimensional
AVD	acceleration, velocity, displacement
BOC	Board of Consultants
CDMG	California Division of Mines and Geology
FERC	Federal Energy Regulatory Commission
FS	factor of safety
GD	Geotechnical Design Memorandum
GLE/Morgenstern	generalized limit equilibrium/Morgenstern-Price
GPS	global positioning system
GSI	Geological Strength Index
i	joint roughness angle
I.D.	inside diameter
Ja	Joint alteration number
$JCond_{(89)}$	Joint condition
JCS	Joint Compressive Strength
Jn	Number of discontinuity sets
Jr	Joint roughness number
JRC	Joint Roughness Coefficient
Jw	Joint water reduction
ksi	kips per square inch
LA	left abutment road cut
LA_SW	spillway rock slope
LE	limit equilibrium
lidar	light detection and ranging
LSA	lower south abutment
MCE	maximum credible earthquake
mi	material constant
mm	millimeters
MPBX	multiple-point borehole extensometers
NAVD88	North American Vertical Datum of 1988
NGVD29	National Geodetic Vertical Datum of 1929
O.D.	outside diameter
pcf	pounds per cubic foot
PFM	potential failure mode
PFMA	Potential Failure Mode Analysis
PGA	peak ground acceleration
PMF	probable maximum flood

ACRONYMS

PSE	Puget Sound Energy
psf	pounds per square foot
psi	pounds per square inch
Q-system	Tunneling Quality Index
RA	right abutment and adjacent to the dam
RA_DS	downstream canyon wall
RMR_{89}	Rock Mass Rating
RQD	Rock Quality Designation
SOW	Statement of Work
STID	strike in the downstream direction
UAV	Unmanned Aerial Vehicle
UCS	uniaxial compressive strength
UNA	upper north abutment
USA	upper south abutment
USGS	U.S. Geological Survey
VWP	vibrating wire piezometer

1 INTRODUCTION

This document presents the geologic conditions and an assessment of selected potential failure modes (PFMs) related to Upper Baker Dam. Upper Baker Dam is part of Puget Sound Energy's (PSE's) Upper Baker Development for the Baker River Hydroelectric Project, Federal Energy Regulatory Commission (FERC) Number 2150. The Baker River Hydroelectric Project includes the Lower Baker Development and Upper Baker Development. In addition to Upper Baker Dam, the Upper Baker Development includes West Pass Dike, Auxiliary Dike, Depression Lake Dike, and other associated facilities.

The purpose of this study is to address selected stability PFMs identified in the Potential Failure Mode Analysis (PFMA) for the Baker River Hydroelectric Project by HDR, Inc. (HDR) in conjunction with the Eleventh Independent Consultant's Safety Inspection (HDR, 2019). The PFMs identified by HDR for Upper Baker Dam that are addressed in this study generally include movement within the dam foundation, stability of the spillway slope, and erosion and stability of the slope downstream of the spillway. Specific failure modes addressed by this study are described in Section 1.4.

1.1 Scope of Work

Our original scope of services was specified in Change Order No. 5 to PSE Outline Agreement No. 4600007357, Task 5.3 (Review and update August 28, 2012, Letter Report), Task 5.4 (Preliminary Design for Spillway Support), Task 5.5 (Preliminary Design Slope Protection Downstream of Spillway), and PSE Outline Agreement No. 400014598, dated May 21, 2020. On December 17, 2020, a revised Statement of Work (SOW) No. CW2230087 was executed under a new Master Services Agreement (No. CW2229967, dated December 4, 2020). The scope of engineering services for these contracts included delivery of the following work elements:

- Updated the geologic model,
- Updated rock mass characterization,
- Revised evaluation of PFMs with regard to stability of selected blocks,
- Analyzed the stability of the existing spillway and designed support to increase the stability of the spillway and underlying rock slope,
- Performed slope stability analyses and designed slope protection for area downstream of spillway, and

- Prepared a Foundation Failure Modes Assessment Geotechnical Report (Original), delivered to PSE on April 6, 2021.

In response to the Baker River Project FERC Project 2150 Board of Consultants (BOC) Report for Meeting No. 10 in April 2021, PSE contracted Shannon & Wilson to perform additional geotechnical explorations in the spillway slope and revise spillway slope analyses under Change Order No. 1, dated October 12, 2021. The scope of engineering services for Change Order No. 1 includes the following work elements:

- Updating spillway slope rock mass characterization,
- Updating spillway slope groundwater conditions characterization,
- Updating stability analyses of the existing spillway slope and support designs, and
- Preparing this revised Foundation Failure Modes Assessment Geotechnical Report.

1.2 Previous Studies

Several previous studies have been performed to characterize Upper Baker Dam. These primary sources of data are described below and include:

- Historical photographs circa 1960 (PSE, 1960). These photographs provided a basis for estimation of joint location, persistence, orientation and spacing, and comparison to field observation.
- Geology of Dam Site (Stone & Webster Engineering Corporation, 1960b). This report details information observed and recorded during the construction of the site, including geology, foundation preparation, grout curtain construction, and subsurface drainage. The cross-section and profile along the axis of the dam note several mud seams, indicating the location, orientation, and extent of through-going discontinuities. This report is included as Appendix I.
- Report on Additional Drainage – Monoliths 5 through 10 (Stone & Webster, 1963). This report provides information on the occurrence of increased uplift pressures in Monolith 8 and vicinity in 1963, including the additional drainage boring logs, contraction joint measurements, geologic conditions in the foundation of the dam, recording uplift pressures, and emplacement of a cinder blanket on the upstream face of the dam. The addition of 16 drains and cinder blanket was effective in reducing the uplift pressures.
- Report on Analysis of Movements (Stone & Webster, 1972). This report details an analysis of the extensometer, micrometer, and taut wire measurement systems. Stone & Webster found that based on micrometer data, there was "virtually no net motion between Monoliths 6 and 7, Monoliths 9 and 10, Monoliths 17 and 18, and Monoliths 19 and 20." Furthermore, the data indicate the extensometers are stable, indicating that Monolith 18 is stable relative to the surface (depths 5 to 10 feet) of the foundation rock and that Monolith 19 is stable relative to depths of 80 to 90 feet.

- Periodic Safety Inspection Report No. 3 (Stone & Webster, 1978). This report provides a summary of a FERC letter describing the movement of Monolith 18 as the result of a rotation with a center deep in the rock mass.
- Seismic Analyses of the Baker River Dams, Volume Three and Appendices (Stone & Webster, 1984 [revised 1987]). This report includes seismic and static stability analyses. Stone & Webster evaluated the potential for foundation instabilities created by a rock wedge formed by the intersection of two (2) planes of weakness underneath the dam, sliding either on the line of intersection of the planes or along one planar surface. Stone & Webster's results relied on limited field mapping of the dam abutments and two (2) rock and concrete borings. Because no discontinuity was identified along which sliding would likely occur below the dam and the bedding plane orientation identified in the left and right abutments was thought to be acceptably stable, Stone & Webster concluded that no large-scale instabilities existed. They reported that the stability of the dam was adequate for normal static loading conditions and that the dam's response to a hypothetical earthquake would be acceptable.
- Upper Baker Dam Drainage System Study (Stone & Webster, 1988b). This study reviews previous reports, camera borehole logs, and drain hole pressure readings. The review summarizes hydrogeologic conditions under the right abutment and provides an interpretation of geologic structure contributing to the increased uplift pressures.
- Concrete Rock Interface (Shannon & Wilson, 2008). This report details the creation of a digital surface for the elevation of the rock existing underneath the dam. The topographic contours from this report formed part of the base map used in this study.
- Foundation Drain Inspection (Shannon & Wilson, 2009). This report provides details of the drains within the gallery noting depth, orientation, water levels, flows, and a visual record of the drains. Notes from this study are presented in Drawing C-01.
- History of Monolith 18/19 Relative Movements (PSE, 2009). This report details the construction history, observed offsets, and monitoring of movements of Monoliths 18 and 19.
- Stress and stability analysis, final report, Rev. 2 (Hatch, 2009). This report details a three-dimensional (3D) non-linear stability analysis using 3DEC to evaluate sliding along the dam foundation interface.
- Rock Abutment Stability Assessment Rev. 2 (Shannon & Wilson, 2010). This report investigates possible modes of failure for concrete gravity dams, characterizes the rock mass of the abutments, and summarizes available information on site geology, engineering observations, and past geotechnical reports.
- Camera Inspection of Drains (Shannon & Wilson, 2013). This report provides details of the drains within the gallery noting depth, orientation, water levels, flows, and a visual record of the drains. The report also reviewed available documentation on piezometers, long-term monitoring results, and flow volumes.

- Dam Safety Instrumentation Upgrades (Shannon & Wilson, 2018). This report provides details of geotechnical explorations and geotechnical instrumentation upgrades, including flowmeters, joint meters at contraction joints, installation of vibrating wire piezometers (VWPs), multiple-point borehole extensometers (MPBXs), and borehole inclinometers.
- Camera Inspection of Drains (Shannon & Wilson, 2020a). This report provides details of the drains within the gallery noting depth, flows, and a visual record of the drains.
- Geotechnical Report, Earthquake Time History Development for Baker Project (Shannon & Wilson, 2020b). This report presents the earthquake time histories developed for the Baker River Hydroelectric Project that are used in engineering analyses of the spillway slope.
- Geotechnical Design Memorandum GD-1, Rev. 1, (Shannon & Wilson, 2022), Upper Baker Dam, Concrete, Washington Spillway Support Analyses Criteria. Presented as Appendix M.

Other reports and documentation reviewed for this study include:

- Dam Safety Inspection Report (FERC, 2008)
- Upper Baker Development FERC Part 12 Safety Inspection Report (MWH Americas, Inc., 2004)
- Evaluation of Sliding Stability (MWH Americas, 2009)
- Revised Downstream Contours (Pacific Geomatic Services, 2014)
- History of Monolith 18/19 Movement (PSE, 2009)
- Upper Baker Dam Instrumentation (PSE, 2013)
- Rock Abutment Stability (Shannon & Wilson, 2012)
- Foundation Drainage Investigation Upper Baker River Dam, Volumes 1 and 2 (Stone & Webster, 1990)
- Periodic Safety Inspection Report No. 4 (Stone & Webster, 1983)
- Periodic Safety Inspection Report No. 5 (Stone & Webster, 1988a)
- Seismic Analyses of the Baker River Dams, Volume Three and Appendices (Stone & Webster, 1984 [revised 1987])
- Files on CD presented to Shannon & Wilson by PSE, BOC Meeting October 28 – November 1, 2013, Baker River Hydro Project, Upper Baker Dam
- Upper Baker Spillway Estimate of Stream Power (Falvey & Associates, 2016), provided in Appendix G

- Pressures on Invert of Upper Baker Dam Spillway (Falvey & Associates, 2019), provided in Appendix G
- Upper Baker Dam Instrumentation Data Set, Appendix C of the 2021 Dam Safety Surveillance and Monitoring Report provided to Shannon & Wilson by PSE, provided in Appendix K

1.3 Potential Failure Modes (PFMs)

HDR completed a PFMA for the Baker River Hydroelectric Project in conjunction with the Eleventh Independent Consultant's Safety Inspection (HDR, 2019). PFMs evaluated concern movement within the dam foundation, stability of the spillway slope, and erosion and stability of the slope downstream of the spillway. PFMs related to sliding along or in proximity to the concrete-to-rock interface, gate malfunction, or other PFMs not related to the foundation are not considered in this report. Each failure mode was assigned to one of the following categories, as follows:

- Category I – Highlighted (significant concerns): 3
- Category II – Considered but not Highlighted (credible but of lesser significance): 5
- Category III – More Information Needed to Classify: 4
- Category IV – Ruled Out (remote probability of occurrence, very low consequences, or not physically possible): 4
- Ruled Out Without Development: 0

Additionally, the PFMs were categorized based on loading conditions with the following breakdown:

- Normal (pool elevation): 4
- Flood (pool elevation): 7
- Seismic: 5
- Volcanic: 0
- Other: 0

All PFMs that are addressed by this study are included in the following sections and summarized in Exhibit 1-1 by category and loading condition.

Exhibit 1-1: Identified PFMs for Upper Baker Dam Addressed by this Study

	Loading Condition					
Category	Normal	Flood	Volcanic	Seismic	Other	Total
Category I	1	1	0	1	0	3
Category II	1	2	0	2	0	5
Category III	1	2	0	1	0	4
Category IV	1	2	0	1	0	4
Ruled Out Without Development	0	0	0	0	0	0
Total	4	7	0	5	0	16

1.4 Potential Failure Modes (PFMs) Addressed by this Study

This section discusses Category I, Category II, Category III, and Category IV PFMs and how this study addresses those PFMs.

1.4.1 PFMs N-UB-2A, F-UB-2A, and S-UB-2A

N-UB-2A, F-UB-2A, and S-UB-2A are Category I PFMs. The description for these three failure modes is similar and pertains to sliding within the foundation below Monoliths 18 and 19, with only the loading condition differing among them.

- N-UB-2A: "Under normal pool conditions, shear displacement along a foliation surface within the rock mass below Monoliths 18/19 reduces the shear strength along the surface. The displacement continues gradually and without detection until a shallow foliation surface that daylights downstream of the dam is no longer capable of resisting the sliding forces imposed by the reservoir. Monoliths 18/19 slide suddenly, resulting in a breach of the dam, uncontrolled release of the reservoir to the foundation level at the location of the breach, and downstream flooding."
- F-UB-2A: "As the result of a flood, the reservoir elevation rises above the historic high level. The reservoir rise produces an increase in the hydrostatic load on the dam and higher uplift pressure within the dam foundation. Under the influence of the higher loads, the concrete dam slides along one or more foliation surfaces within the foundation beneath Monoliths 18/19. The displacement continues until a shallow foliation surface that daylights downstream of the dam is no longer capable of resisting the sliding forces imposed by the reservoir. Monoliths 18/19 slide suddenly, resulting in a breach of the dam, uncontrolled release of the reservoir to the foundation level at the location of the breach, and downstream flooding."
- S-UB-2A: "Cyclic movement caused by an earthquake reduces the shear strength along a foliation surface within the rock mass below Monoliths 18/19. The strength reduction is sufficient to allow the monoliths to slide under the static loads that remain following the

earthquake. The displacement continues gradually and without detection until a shallow foliation surface that daylights downstream of the dam is no longer capable of resisting the sliding forces imposed by the reservoir. Monoliths 18/19 slide suddenly, resulting in a breach of the dam, uncontrolled release of the reservoir to the foundation level at the location of the breach, and downstream flooding."

The PFMs described above all relate to sliding along foliation or along the line of intersection of the foliation surface and Joint Set 4 in the foundation below Monoliths 18/19. The potential for sliding to occur along the foliation surface or along the foliation surface and Joint Set 4 is related to the depth, orientation, shear strength properties, groundwater uplift pressures along the sliding surface, and other external loading conditions. The potential that the sliding plane, either along foliation or along the trend and plunge of the intersection of foliation and Joint Set 4, does not daylight downstream of the dam also impacts this PFM.

In this study, the geometry of the sliding was based on locations of observed movement in the foundation, the range of orientation of foliation and Joint Set 4 obtained from field mapping and downhole televiewer surveys, and downstream topography. Shear strength properties along foliation and Joint Set 4 were based on direct shear laboratory testing. Groundwater conditions were based on VWPs installed in selected borings.

1.4.2 PFMs N-UB-2B, F-UB-2B, and S-UB-2B

N-UB-2B, F-UB-2B, and S-UB-2B are Category II PFMs. The description for these three failure modes is similar and pertains to sliding in the foundations below Monoliths 9 and 10, with only the loading condition differing among them.

- N-UB-2B: "Under normal pool conditions, shear displacement occurs along a discontinuity within the rock mass below Monoliths 9/10. The shear strength along the discontinuity decreases as displacement increases. Movement continues gradually and without detection until a shallow discontinuity that daylights downstream of the dam is no longer capable of resisting the sliding forces imposed by the reservoir. Monoliths 9/10 slide suddenly, resulting in a breach of the dam, uncontrolled release of the reservoir to the foundation level at the location of the breach, and downstream flooding."
- F-UB-2B: "As the result of a flood, the reservoir elevation rises above the historic high level. The reservoir rise produces an increase in the hydrostatic load on the dam and higher uplift pressure within the dam foundation. Under the influence of the higher loads, shear displacement occurs along a discontinuity within the rock mass below Monoliths 9/10. Movement continues gradually and without detection until a shallow discontinuity that daylights downstream of the dam is no longer capable of resisting the sliding forces imposed by the reservoir. Monoliths 9/10 slide suddenly, resulting in a

breach of the dam, uncontrolled release of the reservoir to the foundation level at the location of the breach, and downstream flooding."

- S-UB-2B: "Cyclic movement caused by an earthquake reduces the shear strength along a foliation surface within the rock mass beneath Monoliths 9 and 10. The strength reduction is sufficient to allow the monoliths to slide under the static loads that remain following the earthquake. The displacement continues gradually and without detection until a shallow foliation surface that daylights downstream of the dam is no longer capable of resisting the sliding forces imposed by the reservoir. Monoliths 9 and 10 slide suddenly, resulting in a breach of the dam, uncontrolled release of the reservoir to the foundation level at the location of the breach, and downstream flooding."

The PFMs described above all relate to sliding along an adversely oriented discontinuity in the foundation below Monoliths 6 through 10 (previously restricted to Monoliths 9 and 10). The potential for sliding to occur along this geologic structure is related to the depth, orientation, shear strength properties, groundwater uplift pressures along the sliding surface, and other external loading conditions related to offsets observed in existing drain holes. The interpretation that the sliding plane does not daylight downstream of the dam also impacts the classification of this PFM.

In this study, the geometry of the sliding plane was based on locations of observed historic movement in the foundation. The orientation of the sliding plane is based on the orientation of natural fractures observed in geotechnical borings in Monoliths 9 and 10 at depths that can be correlated to the observed offsets in adjacent drain holes. Groundwater conditions were based on VWPs installed in selected borings and measurements in existing drain holes.

1.4.3 PFMs N-UB-2C, F-UB-2C, and S-UB-2C

N-UB-2C, F-UB-2C, and S-UB-2C are Category IV PFMs. The description for these three failure modes is similar and pertains to sliding in the foundations below Monoliths 4 and 5, with only the loading condition differing among them.

- N-UB-2C: "Under normal pool conditions, shear displacement occurs along a discontinuity within the rock mass below Monoliths 4/5. The shear strength along the discontinuity decreases as displacement increases. Movement continues gradually and without detection until a shallow discontinuity that daylights downstream of the dam is no longer capable of resisting the sliding forces imposed by the reservoir. Monoliths 4/5 slide suddenly, resulting in a breach of the dam, uncontrolled release of the reservoir to the foundation level at the location of the breach, and downstream flooding."
- F-UB-2C: "As the result of a flood, the reservoir elevation rises above the historic high level. The reservoir rise produces an increase in the hydrostatic load on the dam and higher uplift pressure within the dam foundation. Under the influence of the higher

loads, the concrete dam slides along one or more foliation surfaces within the foundation beneath Monoliths 4/5. The amount of movement is sufficient to open a gap in the dam. Reservoir water flowing through the gap causes additional erosion and monolith movement that quickly develops into a dam breach and results in a rapid and uncontrollable release of the reservoir and downstream flooding."

- S-UB-2C: "Inertial forces produced by an earthquake cause sliding along foliation surfaces within the dam foundation beneath Monoliths 4/5. The sliding removes many of the asperities on the foliation surfaces and reduces the shear strength of the surfaces. With the shear strengths reduced, Monoliths 4/5 are no longer able to withstand the hydrostatic load imposed by the reservoir. Monoliths 4/5 slide, opening a gap in the left side of the dam. Reservoir water flowing through gap causes additional erosion and monolith movement that quickly develops into a dam breach and results in a rapid and uncontrollable release of the reservoir and downstream flooding."

The PFMs described above all relate to sliding along an adversely oriented discontinuity (or discontinuities) in the foundation below Monoliths 4 and 5. The potential for sliding is related to the depth, orientation, shear strength properties, groundwater uplift pressures along the sliding surface(s), and other external loading conditions. The interpretation that a kinematically admissible wedge does not exist under Monoliths 4 and 5 also impacts the classification of this PFM.

In this study, the geometry of the sliding surface(s) was based on the orientation of major and minor structures obtained from field mapping and downhole televiewer surveys.

1.4.4 PFMs S-UB-3, F-UB-3A, and F-UB-3B

S-UB-3 and F-UB-3A are Category II PFMs. F-UB-3B is a Category III PFM. All three failure modes pertain to stability of the spillway slope downstream of Monoliths 16 and 17 with the potential to undermine and lead to damage or loss of the spillway and undermining of Monoliths 16 and 17.

- S-UB-3: "Inertial forces produced by an earthquake cause sliding of the rock wedge supporting the spillway. A flood event occurs before repairs can be made, and the spillway is operated for an extended period of time. The exposed rock erodes, and the erosion progresses upstream, eventually undermining the spillway and one or more monoliths fail, resulting in downstream flooding."
- F-UB-3A: "During a large flood, the spillway is operated for an extended period of time. The dynamic forces on the spillway chute overstress the chute and it fails. Continued spillway discharge erodes the rock foundation below the chute, the erosion progresses upstream, eventually undermining the spillway monoliths and one or more monoliths fail, resulting in downstream flooding."

- F-UB-3B: "During a large flood, the spillway is operated for an extended period of time. The water pressure in the rock foundation beneath the spillway chute increases, resulting in a sliding failure of the rock wedge supporting the chute. Continued spillway discharge erodes the rock foundation below the chute, the erosion progresses upstream, eventually undermining the spillway monoliths and one or more monoliths fail, resulting in downstream flooding."

PFMs S-UB-3 and F-UB-3B relate to loss or damage to the spillway as a result of plane shear sliding along foliation in the spillway slope. The potential for sliding to occur along the foliation surface is related to the inclination of the foliation, persistence of the foliation surfaces, shear strength properties of the foliation surface and general rock mass, groundwater uplift pressures along the sliding surface, and other external loading conditions.

In this study, the geometry of the sliding plane was based on the range of orientation of foliation obtained via downhole televiewer surveys from geotechnical borings drilled in the spillway slope. Shear strength properties along the sliding surfaces were based on direct shear laboratory testing of spillway slope rock core samples. Groundwater conditions are based on the piezometric data collected from the spillway borings.

PFM F-UB-3A relates to failure of the spillway chute and resulting loss of material downslope of the spillway as a result of extended spillway flows. The erosion progresses upstream, eventually undermining the spillway monoliths. This report does not address the structural integrity of the spillway structure; however, options to improve the stability of the slope using either post-tensioned rock anchors or a grouted rock buttress will preclude foundation failure as a contributing factor to this PFM.

1.4.5 PFMs N-UB-8, F-UB-8, and S-UB-6

N-UB-8, F-UB-8, and S-UB-6 are Category III PFMs. All three failure modes pertain to sliding along a shallow foliation surface within the rock mass, a short distance below and parallel to the concrete-to-rock interface at Monoliths 18 and 19, with only the loading condition differing among them. These PFMs are not addressed in this report and were not addressed by Hatch. Hatch completed a stress and stability analysis evaluating sliding along the concrete-to-rock interface (Hatch, 2009) and sliding along a foliation surface within the rock mass beneath Monoliths 18/19 (Hatch, 2015). They are described below as information only.

- N-UB-8: "Under normal pool conditions, shear displacement in the downstream direction along a shallow foliation surface within the rock mass, a short distance below and parallel to the concrete/rock interface at Monoliths 18/19, reduces the shear strength along the surface. The displacement continues gradually and without detection until a shallow foliation surface that daylights downstream of the dam is no longer capable of resisting the sliding forces imposed by the reservoir. Monoliths 18/19 slide suddenly, resulting in a breach of the dam, uncontrolled release of the reservoir to the foundation level at the location of the breach, and downstream flooding. Based on construction photographs, Monoliths 18 and 19 appear to be founded on foliation planes in the phyllite, which have a dip of 40 degrees and strike in the downstream direction (STID). The foliation planes associated with this PFM are parallel to and slightly below the concrete/rock interface."

- F-UB-8: "Under flood conditions, shear displacement in the downstream direction along a shallow foliation surface within the rock mass, a short distance below and parallel to the concrete/rock interface at Monoliths 18/19 reduces the shear strength along the surface. The displacement continues gradually and without detection until a shallow foliation surface that daylights downstream of the dam is no longer capable of resisting the sliding forces imposed by the reservoir. Monoliths 18/19 slide suddenly, resulting in a breach of the dam, uncontrolled release of the reservoir to the foundation level at the location of the breach, and downstream flooding. Based on construction photographs, Monoliths 18 and 19 appear to be founded on foliation planes in the phyllite, which have a dip of 40 degrees and STID. The foliation planes associated with this PFM are parallel to and slightly below the concrete/rock interface."
- S-UB-6: "Under normal pool conditions, shear displacement in the downstream direction along a shallow foliation surface within the rock mass, a short distance below and parallel to the concrete/rock interface at Monoliths 18/19 reduces the shear strength along the surface. An earthquake occurs, applying additional seismic load. The additional load results in a shallow foliation surface developing that daylights downstream of the dam. The dam is no longer capable of resisting the sliding forces imposed by the reservoir along the degraded foundation. Monoliths 18/19 slide suddenly, resulting in a breach of the dam, uncontrolled release of the reservoir to the foundation level at the location of the breach, and downstream flooding. Based on construction photographs, Monoliths 18 and 19 appear to be founded on foliation planes in the phyllite, which have a dip of 40 degrees and STID. The foliation planes associated with this PFM are parallel to and slightly below the concrete/rock interface."

1.4.6 PFM F-UB-3C

F-UB-3C is a Category IV PFM. This failure mode pertains to stability of the slope downstream of the spillway with the potential to undermine and lead to damage or loss of the spillway and undermining of Monoliths 16 and 17.

- F-UB-3C: "During a large flood, the spillway is operated for an extended period of time. Erosion of the rock downstream of the spillway occurs as a result of tailwater scour. The erosion progresses upstream, undermining the spillway chute, and causing a failure of

> the spillway chute. Rock erosion continues to progress upstream, eventually undermining the spillway monoliths and one or more monoliths slide, opening a gap in the dam. Reservoir water flowing through the gap causes additional erosion and monolith movement that quickly develops into a breach and results in a rapid and uncontrollable release of the reservoir and downstream flooding."

PFM F-UB-3C relates to loss of material downslope of the spillway as a result of extended spillway flows. The erosion progresses upstream, eventually undermining the spillway monoliths. The potential for downslope erosion to occur is related to the inclination of the foliation, persistence of the foliation surfaces, shear strength properties of the foliation surface, erodibility of the rock mass, and stream power of spillway flows.

In this study, the geometry of the sliding was based on the range of orientation of foliation obtained from field mapping, downhole televiewer surveys, and downstream topography. Shear strength properties along foliation were based on direct shear laboratory testing. Rock mass properties are based on surface mapping and geotechnical borings completed in Monoliths 17, 18, and 19.

2 SITE DESCRIPTION

Upper Baker Dam is part of the Upper Baker Development, Baker River Hydroelectric Project, located upstream of Concrete, Washington, as shown in Exhibit 2-1. The Upper Baker Dam is a 312-foot-high, 1,200-foot-long concrete gravity dam that impounds Baker Lake.

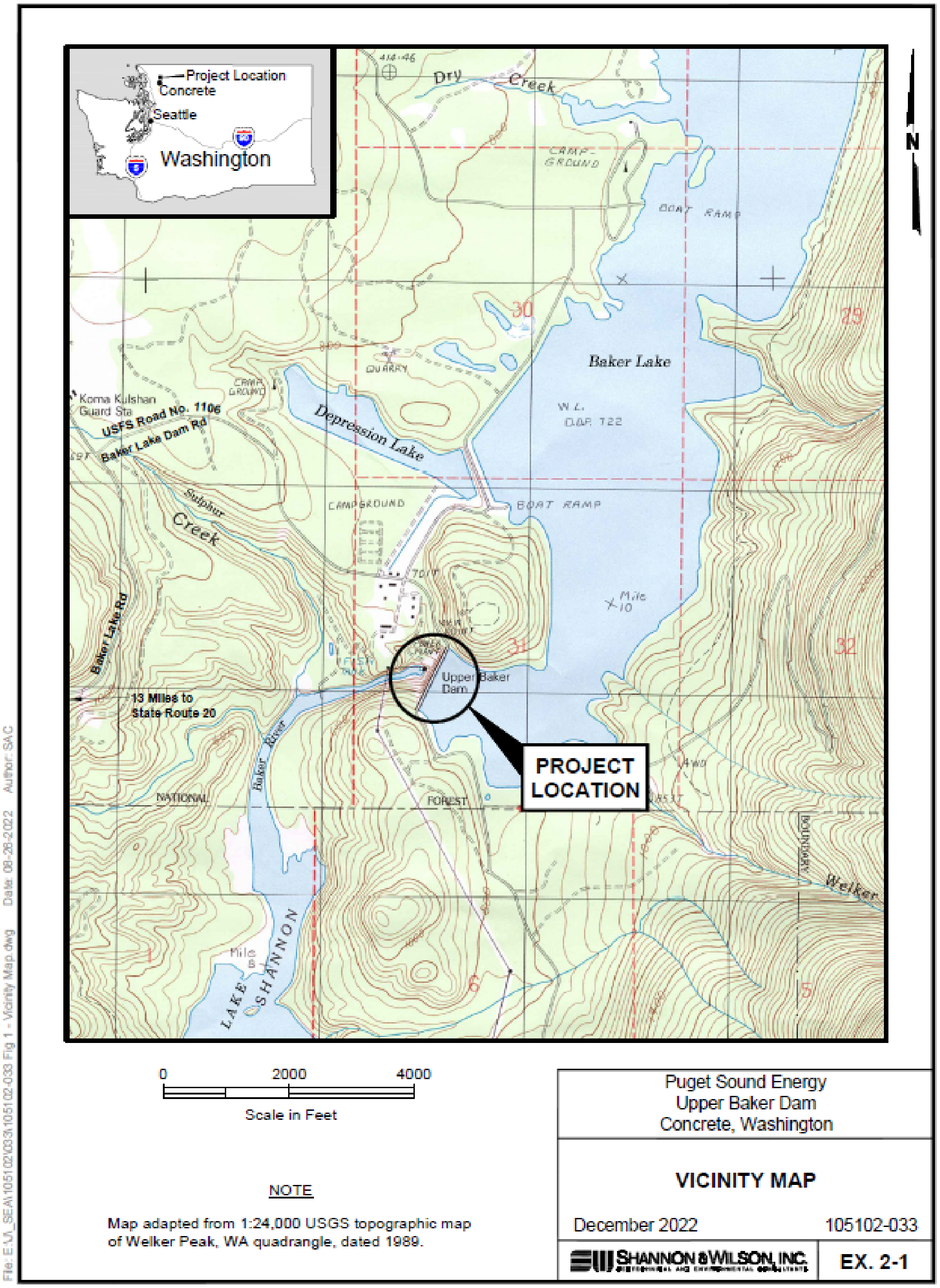

Exhibit 2-1: Upper Baker Dam Vicinity Map

The dam is constructed of 25 monoliths, each approximately 50 feet wide, with no structural connection except for vertical keyways cast near the upstream face of the dam. At the time of construction, elevations were reported using the National Geodetic Vertical Datum of 1929 (NGVD29) (1947 adjustment). In 2004, in order to standardize elevations in documents, drawings, and maps related to the Baker River Hydroelectric Project, PSE decided to consistently use the North American Vertical Datum of 1988 (NAVD88). To convert from NGVD29 (1947 adjustment) to NAVD88, 3.77 feet is added. All elevations in this report are NAVD88 unless otherwise stated.

The primary benchmark for the Upper Baker development is a concrete monument at the top of the dam; the elevation of this monument is 735.77 feet NAVD88 (Leonard and others, 2008). According to Leonard, Boudinot, and Skodje (2008), the documented Upper Baker and Lower Baker benchmark elevations are on the same datum and are 0.15 foot lower than a U.S. Geological Survey (USGS) benchmark (B61-1934) located at the old railroad depot in Concrete, Washington. Due to the large number of existing drawings that date back to 1925, PSE decided to disregard the 0.15-foot elevation difference and use the existing NAVD88 elevations. Future elevation readings taken at the Baker River Hydroelectric Project using a global positioning system (GPS) will need to have 0.15 foot subtracted to check against documented project elevations.

3 SITE HISTORY

Construction of Upper Baker Dam began in June 1956, and the concrete monoliths were completed by July 1959. The reservoir was filled to an elevation of 708 feet (NGVD29), and 711.77 feet (NAVD88), for the first time in September 1959. By 1963, uplift pressures "exceeding design limits" had developed and cracks and/or displacements could be observed in several monoliths of the dam (Stone & Webster, 1963). Investigations, mitigation measures, and monitoring programs have been performed as a response to these conditions (PSE, 2009).

3.1 Grouting Program

A foundation drilling program for grouting and drainage began on May 21, 1957 and was completed on October 30, 1958. Grouting started on June 18, 1957 and was completed June 11, 1958. This program was completed during construction to "…make impervious any faults of shear planes that may be present and to consolidate the rock into essentially a monolithic mass" (Stone & Webster, 1960b). During this program, 211 holes were drilled and filled with approximately 5,200 sacks of cement. A Type II cement was used ranging in water/cement ratio from 4:1 to 0.5:1. "Since most the rock was generally tight, most of the grouting was done with the 4:1 water/cement ratio" (Stone & Webster, 1960b). The majority of holes were drilled along a single line approximately three (3) feet downstream of the dam axis. The foundation grouting program in the left abutment was abandoned in Monoliths 16, 20, and 21 because it was "practically impossible" to prevent the grout from filling the drains (MWH Americas, 2004; Stone & Webster, 1960b, 1963, and 1990). Furthermore, 123 drain holes were drilled across the gallery and downstream of the dam (Stone & Webster, 1960b).

3.2 Historical Monolith Movements

During an inspection of the dam in 1963, Stone & Webster noted displacements at each contraction joint across the dam at the upstream curb with the exception of Monolith 12/13 (Stone & Webster, 1963). Additional measurements of contraction joint movements, where observed, were taken in the drainage gallery and at the downstream curb. These displacements were measured in three (3) axes: dilation of the contraction joint, translation of one monolith downstream relative to another, and a drop in elevation of one monolith relative to another. Displacements for contraction joint dilation, translation, and drop ranged from 0.00 to 0.25 inch, 0.00 to 0.25 inch, and 0.00 to 0.35 inch, respectively (Stone & Webster, 1963). Stone & Webster (1963) recorded the following notable monolith displacements:

- Monolith 10 had moved down relative to Monolith 9 by approximately 0.3 inch, and Monolith 9 had moved downstream relative to Monolith 8 by approximately 0.2 inch;
- Monolith 18 had translated downstream relative to Monolith 19 by 0.25 inch, dropped 0.06 inch, and the contraction joint between Monoliths 18 and 19 dilated 0.14 inch;
- A 4-foot-long crack, approximately 1/16 inch in aperture, was observed in Monolith 18 approximately 2 feet from the upstream curb, and in Monolith 19, an approximately 20-foot-long crack was observed running from the downstream curb to the contraction joint with Monolith 18;
- Similar in magnitude to Monoliths 18/19, Monoliths 2/3 dilated 0.25 inch, Monolith 3 translated downstream 0.25 inch, and Monolith 2 dropped 0.19 inch;
- The Monolith 20/21 contraction joint dilated 0.30 inch, and Monolith 20 translated downstream and dropped in elevation 0.25 and 0.06 inch, respectively, similar in magnitude to Monoliths 18/19.

Displacements on the order of 0.1 inches were recorded for the majority of the monoliths. Stone & Webster recorded a "maximum deflection in the tallest monoliths of approximately 2¼ inch, which is in close agreement with a computed deflection of 2⅜ inch from elastic deformation and plastic flow of the concrete" (Stone & Webster, 1963).

During a full inspection of the dam in 1968, a second crack, measuring about two (2) feet long, had developed in Monolith 18 approximately 24 inches from the upstream curb (excerpt from "Periodic Safety Report No. 1, 1968" as shown in PSE, 2009). In accordance with a recommendation by the BOC, additional instrumentation and measurements were performed to better evaluate the mode of failure causing the cracks (Stone & Webster, 1972). Three (3) types of measurement systems were utilized: extensometers in Monoliths 18/19 installed in 1969; aluminum angles and plates (crackmeters) measured with a micrometer across contraction joints 6/7, 9/10, 17/18, 18/19, and 19/20 installed in 1965; and a taut wire system that extended from Monolith 16 to Monolith 20. Of these, the taut wire system was discontinued in 1999 after being deemed unreliable (PSE, 2009). Four (4) extensometers were installed into Monoliths 18 and 19. The extensometers in Monoliths 18, 18A, and 18B are embedded approximately five (5) and 10 feet into bedrock, respectively, whereas the rods in Monoliths 19, 19A, and 19B are embedded approximately 70 and 80 feet, respectively (Stone & Webster, 1972). Two (2) rods were installed in each monolith: one vertical and the other angled 30 degrees from vertical in a downstream direction and perpendicular to the axis of the dam. The crackmeters measure relative movement between monoliths across the contraction joint in three (3) axes (Stone & Webster, 1972). Extensometers in Monoliths 18 and 19 are used to measure the deformation magnitude of the concrete monoliths relative to the fixed anchor depth. These were used in combination with the manually read joint meters in Monoliths 18 and 19 to calculate the absolute movement of Monolith 18 in a coordinate system relative to the dam. Monitoring of manually read crackmeters installed in 1965 and manually read extensometers installed in 1969 has been discontinued.

A review of the micrometer data from 1965 to 1972 indicates that there has been no net relative movement between Monoliths 2/3, 3/4, 6/7, 9/10, 16/17, 17/18, 19/20, and 20/21. The relative horizontal movement over this time span between Monoliths 18/19 averages 0.015 inch a year (Stone & Webster, 1972). A review of the extensometer data shows a cyclic movement of Monoliths 18 and 19 in response to reservoir elevation and temperature fluctuations. The conclusion is therefore drawn that, "…Monolith 19 is not moving relative to the foundation rock at depth and that Monolith 18 is not moving relative to the surface of the foundation rock" (Stone & Webster, 1972).

In 2009, PSE completed a comprehensive summary of previous studies and reports regarding relative movements between monoliths in the dam, with emphasis on Monoliths 18/19. Excerpts from the 1978 Periodic Safety Inspection No. 3, the 1983 Fourth Periodic Safety Inspection Report, the 1988 Fifth Periodic Safety Inspection Report, and the 1999 Periodic Safety Inspection No. 7 all state that a review of the measurements to date shows no or little displacement of the concrete monoliths, and the conclusion of the BOC is that

"Monoliths 18 and 19 are in a condition of equilibrium" (PSE, 2009, excerpt from Fifth Periodic Safety Inspection Report, 1988). However, as part of the summary in PSE's 2009 report, it was concluded that "Monolith 18 appears to be moving horizontally and vertically at a consistent rate of 0.0015 inch per year relative to rock at an 80-foot depth."

Contraction joint micrometer measurements have been recorded for joints 2/3, 3/4, 6/7, 9/10, 16/17, 17/18, 18/19, 19/20, and 20/21 since the mid-1960s. The joint measurement system is set up to measure relative movements between monoliths in three (3) dimensions: horizontal, vertical, and axial. Review of this data provided by PSE from 1992 through 2013 does not indicate ongoing relative movements of the monoliths. Movements are interpreted to be elastic deformation related to several factors including, but not limited to, lake elevation, sensor temperature, and operator torque/error, all of which can affect the precision and accuracy of the measurements (PSE, 2014). This joint meter system is now inactive and was replaced by vibrating wire displacement transducers (joint meters) installed in 2015.

3.3 Uplift Pressures

In 1963, water was observed discharging from the top of a drain in Monolith 8. Stone & Webster (1963) performed an investigation and determined that uplift pressures in Monoliths 7 through 10 exceeded design criteria. Mitigation measures included the installation of 12 additional drains in Monoliths 7 through 10 and 4 additional drains in Monoliths, 5, 6, and 7. A cinder blanket was also placed on the upstream portion of the dam where water infiltration was suspected (Stone & Webster, 1963). The additional drains are B5-D3, SD6-1, SD6-2, SD7-1, SD7-2, SD7-3, SD8-1, SD8-2, SD8-3, B8-G12, SD9-1, SD9-2, SD9-3, SD9-4, SD10-1, and SD10-2 and are shown in Drawings C-01 and Drawing C-02.

Piezometer B9-P1 was drilled in Monolith 9 to assess the effectiveness of the additional drains. The cinder blanket extended from approximately the middle of Monolith 8 to the middle of Monolith 10, to a distance of approximately 35 feet upstream of the upstream face of the dam and ranged in thickness from two (2) to three (3) feet (Stone & Webster, 1963). This program was successful in reducing uplift pressures until the spring of 1985 when increased pressures were once again recorded in Monoliths 8 and 9. It is presumed that the cinder blanket was scoured away during this period. However, uplift pressures decreased by the summer of 1985 and no actions were taken. Pressure increased again in the spring of 1986, and PSE flushed the drain system, which resulted in a decrease in uplift pressures. Uplift pressures increased again in the spring of 1987, and mitigation measures were taken that included the installation of 12 foundation drains and 11 piezometers. These actions were successful in decreasing the uplift pressures (MWH Americas, 2004).

Currently, 38 piezometers are used to monitor and calculate drain efficiencies and uplift pressures. These are B7-P1, B9-P2, B10-P1 Upper, B11-P1 Upper, B12-P1, B13-P1, B16-P1 Upper, B17-P1, B19-P1, and 29 VWPs installed in Borings IN-0500 (four (4) VWPs), -0900 (five (5) VWPs), -1000 (four (4) VWPs), -1700 (four (4) VWPs), -1802 (four (4) VWPs), -1801 (four (4) VWPs), and -1900 (four (4) VWPs). The nine (9) VWPs installed in Borings BH-401 (four (4) VWPs), BH-402 (four (4) VWPs), and BH-403 (three (3) VWPs) are not used to evaluate uplift pressures because all three (3) borings are located downstream of Monoliths 3 and 4. Monitoring of piezometer levels since 1987 indicates that the mitigation measures are still functioning at maintaining allowable uplift pressures (PSE, 2013).

4 FIELD EXPLORATION PROGRAM

To assess the foundation geologic conditions at Upper Baker Dam, Shannon & Wilson completed a field investigation program between 2014 and 2017 that consisted of geologic mapping, photogrammetry survey, and rock core drilling. The geologic mapping of rock exposures in the left and right abutments was completed by Shannon & Wilson on June 19, 2014. Then, in March 2020, the geologic mapping effort was augmented with an unmanned aerial vehicle (UAV) photogrammetry survey performed by Terrane Geosciences. In 2016 and 2017, 11 borings from within the dam gallery and three (3) borings on the exterior of the dam were completed using a combination of HQ3 rock coring methods and rotosonic drilling methods. Laboratory testing was performed on representative rock cores, including uniaxial compressive strength tests, direct shear tests, and petrographic analysis. Select borings were surveyed using televiewer imagery, packer tested, and instrumented with joint meters, flow monitors, VWPs, MPBXs, and/or inclinometer casing. The results of these were incorporated in Leapfrog Geo™ software to develop a 3D geologic model.

To assess the spillway slope geologic conditions, four (4) borings were completed in 2021 using HQ3 rock coring methods. Laboratory testing was performed on representative rock cores, including uniaxial compressive strength tests, and direct shear tests. The borings were surveyed using televiewer imagery and instrumented with three (3) VWPs per boring.

4.1 Geologic Mapping

4.1.1 Outcrop Mapping

Geologic mapping was performed in 2014 to identify and characterize lithologic units, lithologic boundaries, and lithologic structure, including major geologic structure and minor geologic structure. Information on the properties of rock discontinuities was collected from surface observations. These properties include orientation, persistence, spacing, and surface characteristics of discontinuities. Orientations of discontinuities were measured in surface outcrop by Brunton compass. The data collected by Shannon & Wilson showing rock discontinuity orientations and rock mass properties observed in rock exposures are presented in Table 1. Locations of the 2014 mapping locations are shown in yellow in Exhibit 4-1.

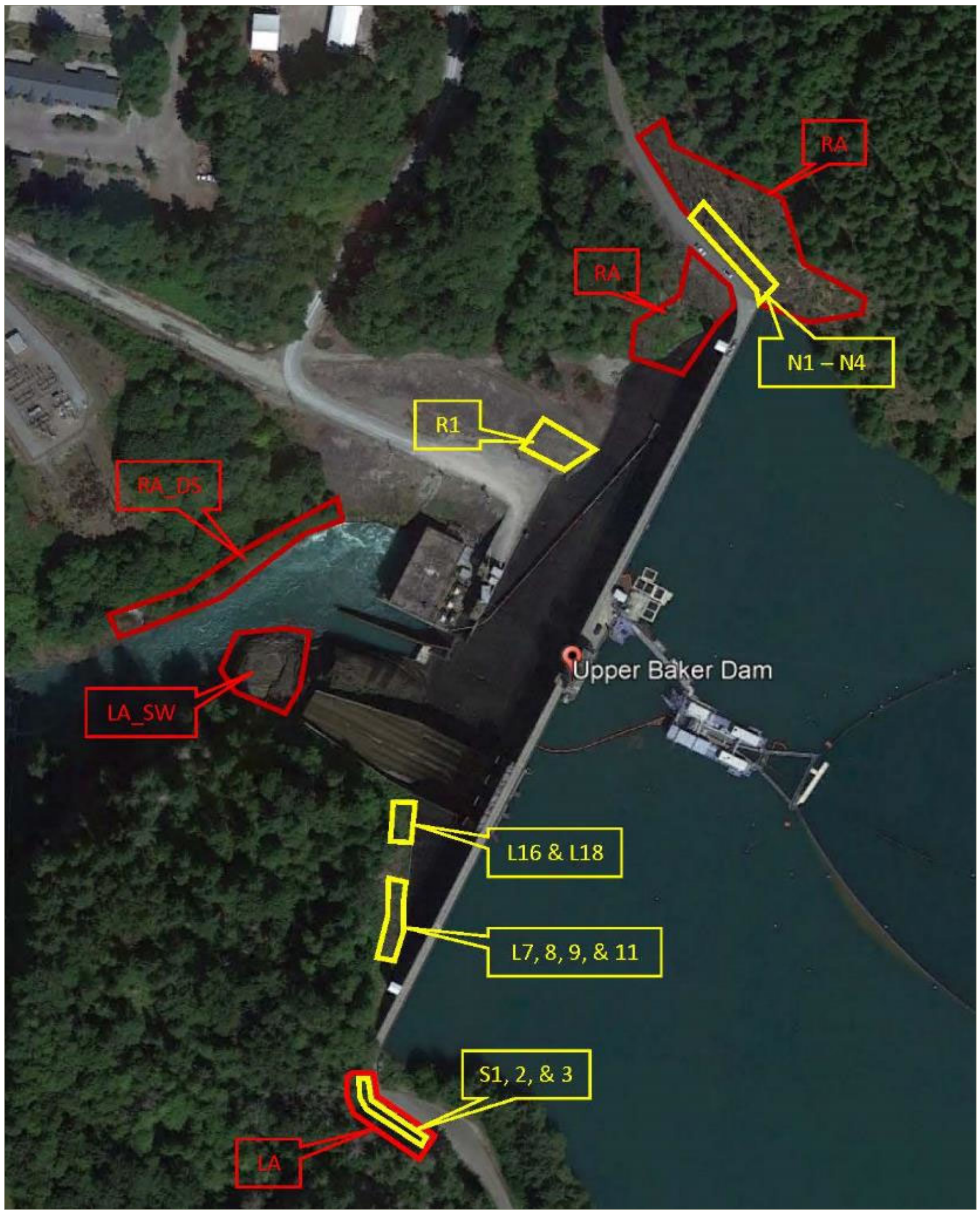

Exhibit 4-1: Mapping Locations Shown in Yellow from 2014 and Red from 2020

4.1.2 Unmanned Aerial Vehicle (UAV) Photogrammetry Survey

The 2020 UAV survey by Terrane Geosciences included the right abutment above and adjacent to the dam (RA), downstream canyon wall (RA_DS), spillway rock slope (LA_SW), and the left abutment road cut (LA). The locations of the 2020 UAV survey are shown in red in Exhibit 4-1. The survey was completed using a multirotor UAV and a high-resolution camera for aerial photography and digital elevation modeling. Surveys were flown at an altitude of 50 and 150 feet above ground level, yielding a ground resolution of one (1) to three (3) inches (3.0 to 7.0 centimeters). This resolution and vertical accuracy decrease significantly in vegetated areas.

Data from the four (4) survey areas were georeferenced and checked for accuracy before final processing in Agisoft™, a 3D photogrammetry software. Georeferencing was accomplished using a combination of the UAV's internal GPS and ground control points distributed throughout the project area. A bare-earth point cloud was generated from the verified data set and used to produce a textured 3D mesh model (digital elevation model with orthophoto draped over) suitable for import into a 3D modeling platform.

Digital structural geology mapping was carried out on the textured 3D meshes to identify the location and orientation of major and minor discontinuities in the rock mass. This analysis was done using Leapfrog Geo™ software and merged with the existing 3D geological model for the dam and surrounding abutments. The location and orientation of major and minor discontinuities in the rock mass identified during digital structural geology mapping in Leapfrog Geo™ were provided to Shannon & Wilson for quality assurance/quality control and data verification in the field.

A total of 1,125 measurements were recorded by visually aligning a "structural disc" parallel to each planar discontinuity identified on the mesh. Each disc provides an x, y, and z location coordinate and true dip direction of the measured plane. The rock discontinuity orientations collected via UAV survey are presented with the entire discontinuity data set in Appendix C, Table C-2.

4.2 Geotechnical Drilling

The purpose of the core drilling program was to obtain data and information to better understand and address PFMs (specifically related to potential sliding monoliths in proximity to Monoliths 4 and 5, 9 and 10, and 17, 18, and 19) and to implement appropriate instrumentation systems to monitor identified failure modes such as deformations in the dam foundations, uplift pressures, flow through the drainage systems, and stability of the spillway slope.

The drilling exploration program included vertical borings from within the dam gallery, both vertical and inclined borings near the downstream toe of Monoliths 3 and 4, and vertical borings adjacent to the spillway. Soil samples and rock cores were recovered using rotosonic drilling and HQ3 rock coring, respectively. These methods are described in the following paragraphs. Boring locations, depths, and other details are summarized in Table 2 with location and depth shown on Drawing C-01 through Drawing C-03.

Rotosonic drilling was performed in accordance with ASTM International D6914, Standard Practice for Sonic Drilling for Site Characterization and the Installation of Subsurface Monitoring Devices (ASTM, 2010a). The sonic core drilling method uses high-frequency vibratory motion applied to the top of the drill column, along with down-pressure and rotation, to obtain nearly continuous core samples in soil. Soil samples are obtained using a 5-inch outside diameter (O.D.) core barrel. As the drill column is advanced into the ground, a core of soil slides up and enters the core barrel (3.75-inch inside diameter [I.D.]). After advancing the core barrel a specific distance (termed a core "run"), the drill column and core barrel are then removed from the borehole and the soil core is extracted from the core barrel, collected into flexible plastic bags, organized in core boxes, and logged by a Shannon & Wilson geologist. After retrieval of the soil core for a specific interval, a temporary casing is vibrated to the bottom of the sampled interval. The casing is then cleared of slough, and the next core sample is collected starting at the bottom of the temporary casing.

Rock coring was performed in accordance with ASTM D2113, Standard Practice for Rock Core Drilling and Sampling of Rock for Site Exploration (ASTM, 2014a). The HQ3 rock coring method uses an HQ (about 3.8 inches O.D. and 2.5 inches I.D.) triple-tube core barrel. The triple-tube core barrel consists of inner and outer barrels and a split inner core tube, often referred to as splits. The outer barrel rotates while the inner barrel and inner split tube remain stationary. As the core barrel is advanced, rock core enters the split tube. This system protects the core from the drilling fluid (water for this application) and reduces the torsional forces transmitted to the core. After each core run, a wireline is used to retrieve the inner core barrel and splits. The splits are then pushed from the inner core barrel and opened to allow a detailed visual analysis of the relatively undisturbed core. During drilling, the borehole is cleared of cuttings by circulating water through the drill casing. A second split tube is placed inside the inner core barrel and lowered back into the outer barrel before advancing the next core run.

A Shannon & Wilson geologist was on-site for the duration of the drilling to log the recovered core in the field, photograph the core, place the core into wooden core boxes, and coordinate the geophysics and instrumentation installation. In each core box, core was arranged in descending sequence beginning at the upper left end of the core box partition and continuing in the other partitions from left to right. Each core run was separated from the preceding run by blocks labeled with the run number, depth, run length, and core recovery. Zones of core loss were indicated with blocks labeled with the depth interval where the loss occurred. If the zone of core loss was uncertain, the core loss was assigned to the bottom of the run. After completion of the drilling operations, the core boxes were reopened, and the core was photographed dry and wet. Boring logs for the 18 boreholes drilled are included in Appendix A. Core photographs are presented in Appendix B.

4.2.1 Foundation Borings

Nicholson Construction Company performed the drilling and installations within the gallery of the dam. Holt Services and Crux Subsurface performed the explorations at the downstream toe of Monoliths 3 and 4. Eleven borings were drilled within the gallery and three (3) borings were drilled on the exterior of the dam adjacent to Monoliths 3 and 4. Borings drilled in the gallery were advanced through the floor of the gallery, through the concrete base of the dam, and into bedrock using HQ3 rock coring methods. Rotosonic drilling was performed in Borings BH-401 and BH-402 drilled at the base of Monoliths 3 and 4 to advance through overburden soil and rock debris. HQ3 rock coring methods were then used to advance the boring through bedrock to the final depth. Core runs using HQ3 rock coring are generally one (1) to two (2) feet in the gallery borings and five (5) feet in length in borings downstream of Monoliths 3 and 4, although core runs may have been shortened in certain zones to improve recovery in highly fractured or poor rock quality rock.

4.2.2 Spillway Borings

Crux Subsurface performed the drilling adjacent to the spillway. Four (4) borings were drilled adjacent to the spillway downstream of Monoliths 16 and 17: BH-16-1, BH-16-2, BH-17-1, and BH-17-2. Borings drilled adjacent to the spillway were advanced with HQ3 rock coring methods.

4.3 Instrumentation

The foundation and spillway boreholes were instrumented after the completion of geotechnical explorations. The instrumentation systems installed in the foundation were designed to monitor identified failure modes such as deformations in the dam foundations, uplift pressures, and flow through the drainage systems. The instrumentation systems installed in the spillway borings were designed to better characterize the groundwater conditions of the spillway rock mass.

4.3.1 Foundation Instrumentation

The foundation instrumentation program included the installation of an array of sensors and equipment, including 3D joint meters, flow monitors, VWPs, MPBXs, and inclinometer casing. Details on the process of installation and locations of the foundation instruments are presented in two Shannon & Wilson reports:

- Phase 2 Instrumentation Design Report, Dam Safety Instrumentation Upgrades, 100 Percent – Issued for Construction, Puget Sound Energy, Upper Baker Dam, Concrete, Washington, September 8, 2016, submitted to Mr. Nabil Dbaibo, and
- Dam Safety Instrumentation Upgrades, Puget Sound Energy, Upper Baker Dam, Concrete, Washington, October 31, 2018, submitted to Mr. Tom Danielson.

This geotechnical report relies on the data from seven (7) inclinometers and four (4) MPBXs that were installed within the gallery to assess deformation of the rock foundation: IN-0500, EX-0900, IN-0900, IN-1000, EX-1000, IN-1700, IN-1802, EX-1800, IN-1801, IN-1900, and EX-1900. This report also relies on the nine (9) previously installed inclinometers and observed movements. Discussions of the data are presented in Section 10.2.1, Monoliths 1, 2, and 3; Section 10.2.2, Monoliths 4 and 5; Section 10.2.3, Monoliths 6 through 10; Section 10.2.4, Monoliths 17, 18, 19; and Section 10.2.5, Monoliths 20 and 21.

4.3.2 Spillway Instrumentation

The spillway instrumentation program included the installation of three (3) VWPs (VWP1, VWP2, and VWP3) in each of the four (4) spillway slope borings. This geotechnical report relies on the piezometric head measured in the spillway slope VWPs. Discussions of the piezometric data and the engineering implications for the spillway design are presented in Section 10.3.

4.4 Borehole Televiewer

Acoustic and optical survey methods provide a "virtual" oriented core that can be analyzed to determine the orientation, spacing, and physical characteristics of discontinuities intersected by the borehole. The optical televiewer survey provides the natural color of the rock, indicating zones of more intense weathering and the types of infilling of discontinuities, whereas the acoustic televiewer survey can more easily detect tight aperture joints in the rock mass. The acoustic method requires fluid, such as water, to be present within the borehole. Acoustic televiewing may also determine discontinuity orientations when the rock mass is dark in color or when fluid is opaque, as opposed to the optical survey which cannot get a clear image in these conditions.

4.4.1 Foundation Televiewer Surveys

Televiewer surveys were performed by Global Geophysics and Crux Subsurface for the 11 borings drilled in the gallery and the three (3) borings drilled downstream of Monoliths 3 and 4. Televiewer surveys were used in combination with observations of the core and engineering tests performed on selected specimens to further our understanding of the rock mass of the dam foundation as related to PFMs of sliding in the dam foundation. Borehole televiewer data is included in Appendix F.

4.4.2 Spillway Televiewer Surveys

Televiewer surveys were performed by Crux Subsurface for the four (4) borings drilled adjacent to the spillway slope. Televiewer surveys were used in combination with observations of the core and engineering tests performed on selected specimens to further our understanding of the rock mass of the spillway slope as related to PFMs of spillway slope stability. Borehole televiewer data is included in Appendix F.

4.5 Packer Pressure Testing

In situ water pressure (packer) tests were performed within the bedrock portion of the borings drilled in the gallery and downstream of Monoliths 3 and 4, except BH-403. It was determined by Shannon & Wilson and PSE that pressure testing in BH-403 would not provide test results different from boreholes BH-401 and BH-402 based on its proximity to them. The tests were performed in 10-foot intervals in ascending stages using a double-packer system to isolate and evaluate the permeability of specific zones within the rock. A single-packer system was used in the lowest test section of the borehole. In general, the test duration was at least 10 minutes at each increment, and the applied pressure was 5 to 10 pounds per square inch (psi) above the natural hydrostatic pressure. The test procedures are described in the design report (Shannon & Wilson, 2016), and the test results are presented in the instrumentation report (Shannon & Wilson, 2018).

5 LABORATORY TESTING

Laboratory testing conducted on representative rock cores consisted of unit weight, uniaxial compressive strength tests, direct shear tests, and petrographic analysis. Laboratory result reports are presented in Appendix D.

5.1 Uniaxial Compressive Strength (UCS) and Unit Weight

The uniaxial compressive strength (UCS) provides an indication of the strength of the intact rock material, which is the strength of the rock not considering joints and other planes of weakness. In the UCS test, a cylindrical sample (often in the form of a rock core) is compressed parallel to its longitudinal axis. The presented tests were performed under subcontract to Shannon & Wilson in general accordance with ASTM International D7012, Standard Test Method for Compressive Strength and Elastic Moduli of Intact Rock Core Specimens under Varying States of Stress and Temperatures (ASTM, 2014b). As a part of the UCS testing, unit weight determinations were performed in general accordance with ASTM D2216, Unit Weight of Rock (ASTM, 2010b).

5.1.1 Foundation UCS Testing

A total of 18 uniaxial compressive tests were performed on rock core samples collected from foundation borings. The borings include three from previous studies—lower south abutment (LSA), upper north abutment (UNA), and upper south abutment (USA)—and six (6) borings from the 2016 to 2017 drill exploration program: BH-401, BH-402, EX-1000, IN-0500, IN-1802, and BH-403. The boring locations are shown on Drawing C-01. The tests were performed by three companies: Vector Engineering, Inc. of Grass Valley, California; Geo-Logic Associates of Grass Valley, California; and GeoTesting Express of Acton, Massachusetts. Samples were selected from lengths of core where planes of weakness were not visible, and an attempt was made in the field to select samples that were representative of the rock mass. Testing included a determination of UCS, Young's Modulus, Poisson's Ratio, and unit weight for those samples tested by Vector Engineering. Testing by Geo-Logic Associates and GeoTesting Express included determination of UCS and unit weight.

The results of the uniaxial compressive tests are presented in Table 3. The test results indicate that the UCS for phyllite range from approximately 4.5 to 14.5 kips per square inch (ksi) with a mean UCS of 8.4 ksi. The UCS for the mylonitic phyllite ranges from approximately 1.5 to 6.7 ksi with a mean UCS of 4.1 ksi. The UCS for the metagraywacke ranges from approximately 16.4 to 29.6 ksi with a mean UCS of 22.9 ksi.

5.1.2 Spillway UCS Testing

A total of 11 uniaxial compressive tests were performed on rock core samples collected from spillway borings. The borings include four (4) borings from the spillway drilling exploration program: BH-16-1, BH-16-2, BH-17-1, and BH-17-2. The boring locations are shown on Drawing C-01. The tests were performed by GeoTesting Express.

The results of the uniaxial compressive tests are presented in Table 3. The test results indicate that the UCS for all samples from spillway borings range from approximately 1.3 to 24.4 ksi with a mean UCS of 5.5 ksi and median of 3.2 ksi. Nine (9) of the 11 tests failed through a combination of intact rock and along a discontinuity (Failure Type C), and two (2) tests failed only along a discontinuity. For the purposes of our engineering analyses, we employed the laboratory testing statistics of the Failure Type C samples, with a median UCS of 3.2 ksi.

5.2 Direct Shear

The shear strength along discontinuities was evaluated through direct shear tests of saw-cut surfaces. In a direct shear test, normal load is applied perpendicular to a sample of rock, and the sample is displaced parallel to the saw-cut surface. The shear load is measured as the force required to displace the sample of rock. Procedures for this test are provided in ASTM D5607, Laboratory Direct Shear Strength Test of Rock Specimens Under Constant Normal Force (ASTM, 2008). The normal stress on the discontinuity or saw-cut surface and the shear strength of the discontinuity is obtained by dividing the applied normal load and applied maximum shear load by the area of the surface, respectively. Tests performed on saw-cut surfaces result in base friction angles. Discontinuity shear strength is further discussed in Section 8.2.2.

5.2.1 Foundation Direct Shear Testing

For this report, eight (8) direct shear (saw-cut) tests were performed on rock core samples from foundation borings BH-401, BH-402, IN-1000, and IN-1802, and six (6) direct shear (saw-cut) tests were reviewed from previous studies and included rock core samples from borings UNA and USA. Tests were performed by Vector Engineering and by Geo-Logic Associates under subcontract to Shannon & Wilson. Each sample was sheared at three different normal stresses, ranging from 50 to 300 psi, and is in the range of anticipated overburden stress in the dam foundation.

The results of the direct shear tests are presented in Table 4. The table summarizes the normal stress, maximum shear stress, and the calculated base friction angle for each load increment. The friction angle is calculated as the arctangent of the ratio of the maximum shear stress to the applied normal stress and represents the frictional resistance of the rock discontinuity if it is assumed that the rock discontinuity has no cohesion. The base friction angle for phyllite on sawed surfaces ranges from 25 to 35 degrees, with a mean friction angle of 29 degrees (for phyllite samples tested on the left abutment). The base friction angle for mylonitic phyllite on sawed surfaces ranges from 15 to 25 degrees, with a mean friction angle of 18 degrees. The base friction angle for metagraywacke on sawed surfaces ranges from 24 to 34 degrees, with a mean friction angle of 29 degrees. The mylonitic phyllite and metagraywacke were only observed in the right abutment.

5.2.2 Spillway Direct Shear Testing

Eight (8) direct shear (saw-cut) tests were performed on rock core samples from spillway borings BH-16-1, BH-16-2, BH-17-1, and BH-17-2. Tests were performed by GeoTesting Express under subcontract to Shannon & Wilson. The normal stresses for testing were adjusted from the previous foundation direct shear tests to reflect the normal stresses underneath the spillway. Each sample was sheared at the following normal stresses: 25 psi, 50 psi, and 100 psi.

The results of the direct shear tests are presented in Table 4. The table summarizes the normal stress, maximum shear stress, and the calculated base friction angle for each load increment. The friction angle is calculated as the arctangent of the ratio of the maximum shear stress to the applied normal stress and represents the frictional resistance of the rock discontinuity if it is assumed that the rock discontinuity has no cohesion. The peak shear strength base friction angle for phyllite on saw-cut surfaces ranges from 38 to 74 degrees, with a mean friction angle of 51 degrees and a median friction angle of 44 degrees. The post-peak shear strength base friction angles ranged from 33 to 74 degrees, with a mean and median of 48 and 41 degrees, respectively. All direct shear (saw-cut) tests were performed on phyllite samples taken from the spillway borings.

5.3 Petrographic Analyses

Petrographic analyses were performed on thin sections prepared from foundation rock core samples to provide a deeper understanding of the geologic framework at Upper Baker Dam and to resolve inconsistencies with the lithologic identification of the rock masses in the foundation of Upper Baker Dam. Previous reports have called the rock mass under and in the vicinity of Monoliths 1 to 13 dolomitic hornfels to impure dolomitic marble (Stone & Webster, 1984 [revised 1987]). In addition to evaluating thin section samples with a polarizing microscope, several samples were subject to thin section X-ray scans. X-ray scans of thin sections can provide important data to distinguish between minerals that may not be readily apparent from thin section petrography.

For this report, thin section samples include BH-402, from 101-101.2 feet; BH-403, from 0-1 feet, 38.6-38.7 feet, 117.6-117.8 feet, and 144.1-144.4 feet; IN-1900 from 23.5-23.9 feet; RA-1 surface sample; and UNA-2A. Petrographic analyses were performed by Willamette Geological Service of Philomath, Oregon, under subcontract to Shannon & Wilson. The results of the analysis indicate that the lithologic types in the foundation of Upper Baker

Dam vary from metagraywacke, phyllite, and mylonitic phyllite under Monoliths 1 through 5 to phyllite under Monoliths 5 through 25. The full report provided by Willamette Geological Service is provided as Appendix E.

6 GEOLOGIC CONDITIONS AND MAJOR STRUCTURE

6.1 Regional Geology

6.1.1 Introduction

The Upper Baker Dam is situated within a deep canyon of the Baker River basin. The Baker River basin is located along the western flank of the North Cascades physiographic province that includes the Baker River Valley and the peaks of Mt. Baker (10,775 feet), Mt. Shuksan (9,127 feet), and the Pickett Range, among others. Valley bottoms and low-lying areas are covered by a Pacific Temperate Rainforest, whereas alpine glacial and perennial snowfields occur above an elevation of approximately 6,000 feet. The Baker River has been affected by various episodes of glaciation as well as volcanic events that have altered its course. The modern Baker River at the location of Upper Baker Dam was incised into bedrock during the late Pleistocene (MWH Americas, 2004; Stone & Webster, 1960b).

6.1.2 Regional Geology

The Baker River basin is located on the western flank of the North Cascades physiographic province in Western Washington. The North Cascades province is a region of extremely rugged mountains that average between 6,000 and 8,000 feet in elevation and is bounded on the east by the Okanogan Highlands and the Columbia Plateau and on the west by the Puget Sound Lowland. The Baker River basin includes the deeply glaciated Baker River Valley and the peaks of Mt. Baker (10,775 feet), Mt. Shuksan (9,127 feet), the Pickett Range, and many lesser peaks. Alpine glaciers occupy the higher peaks, and perennial snowfields are common above an elevation of 6,000 feet.

The bedrock underlying the Baker River basin, as portrayed in Exhibit 6-1 and Exhibit 6-2, consists predominantly of Mesozoic and Paleozoic volcanic and sedimentary strata that have been metamorphosed, deformed, and juxtaposed along major tectonic boundaries. The western two-thirds of the basin are underlain primarily by the Paleozoic-age Chilliwack Group, which includes partly metamorphosed volcanic flows and pyroclastic rocks, sandstone, siltstone, shale, limestone, and chert. Locally, the Chilliwack Group rocks are in fault contact with much older ultramafic and metamorphic rocks. The eastern third of the basin is underlain primarily by mid-Cretaceous bedrock of the Shuksan Metamorphic Suite, which consists of greenschists, blueschists, and phyllites that were emplaced along the major north-trending Excelsior Ridge thrust fault. In the late Mesozoic and Tertiary times, the bedrock units were further metamorphosed and deformed by faulting, intrusion, and uplift. The Chilliwack Batholith, which consists of quartz diorite and granodiorite, was intruded in Tertiary time along what is now the eastern part of the Baker River basin.

Overlying the Mesozoic and Paleozoic bedrock in the western part of the basin are basaltic and andesitic lava flows and breccias that were extruded in Quaternary time from Mt. Baker and older associated volcanic vents. In the Baker River Valley, these volcanic deposits are interstratified with and overlain by sediments derived from multiple advances and retreats of continental and alpine glaciers. The youngest strata in the basin are the alluvial sediments that have been deposited by the Baker River drainage system since the end of the most recent glaciations.

The basin's present-day landforms have been sculpted by repeated glaciations and stream erosion during Quaternary time. Alpine glaciation produced sharp peaks and ridges and eroded the deep valleys. Continental glaciation rounded the landforms at lower elevations and scoured-out pre-existing drainages. The continental glaciers also created ice dams behind which large glacial lakes were formed and into which sediment-laden streams deposited thick accumulations of alluvium.

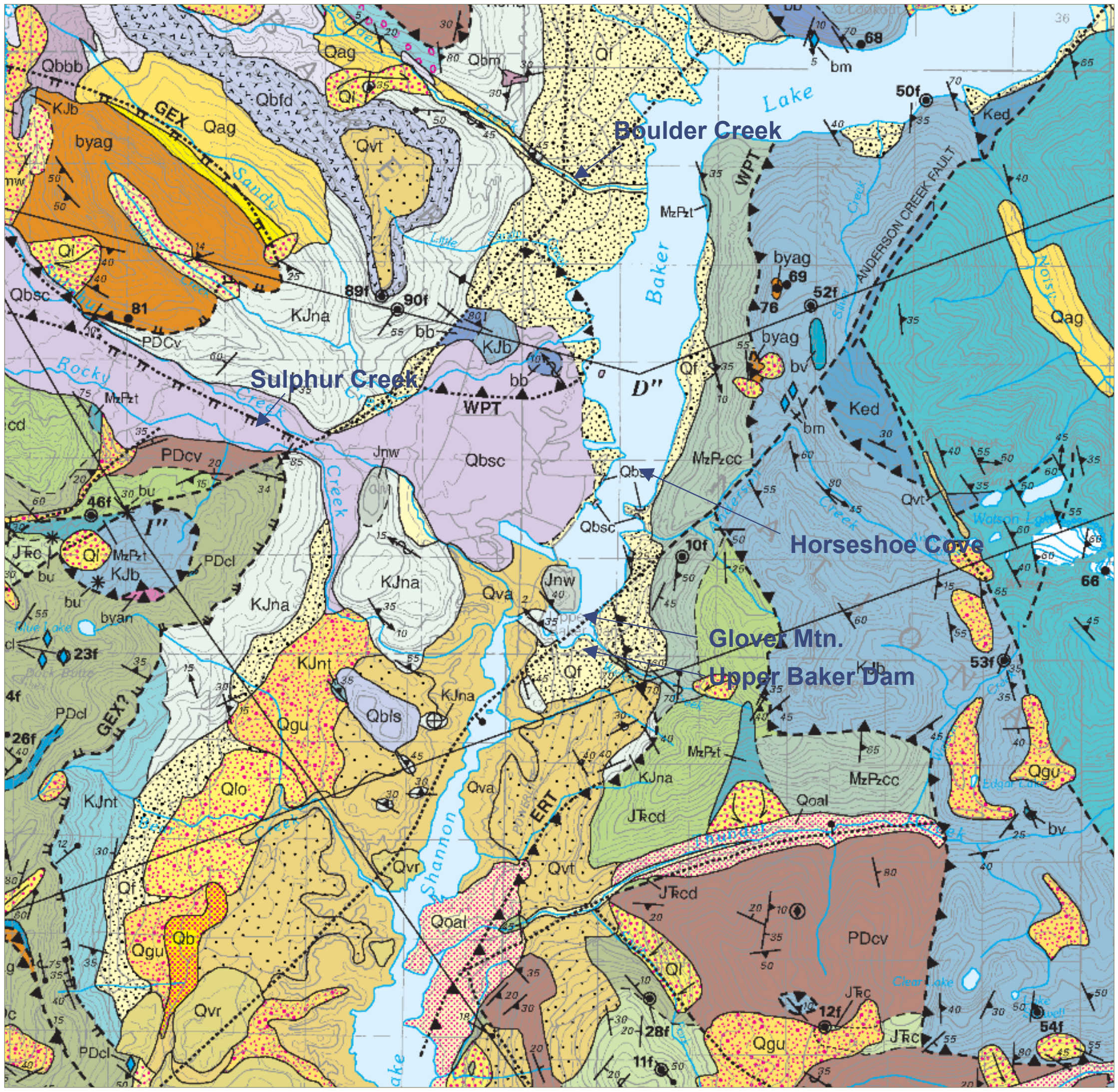

Exhibit 6-1: Baker River Project Geologic Map after Tabor and Others, 2003

Exhibit 6-2: Baker River Project Geologic Map after Tabor and Others, 2003, Continued

The relatively recent geologic history of the Baker River basin is characterized by both volcanic and glacial activity. Beginning in Pleistocene time, the ancestral Baker River Valley, which had been carved in bedrock, was modified by alpine glaciers that filled much of the valley with till. This glacial till was subsequently buried by thick glacial lake sediments, and outwash sand and gravel deposits that accumulated in the ancestral Baker Lake. This lake occupied the basin in the Late Pleistocene time when the continental ice sheet in the Puget Lowland monolithed the Skagit River Valley. The ancestral Baker Lake was one finger of an enormous glacially impounded lake that occupied the upper Skagit River Valley and its tributaries.

After retreat of the ice sheet about 13,000 years ago, the Baker River re-established its grade by incising its channel into the lake deposits and into bedrock (near its confluence with the Skagit River). Since then, the geologic history of the upper Baker River Valley has been dominated by a series of volcanic events along the flanks of Mt. Baker that sent mudflows, pyroclastic flows, and lava flows down tributary valleys into the Baker River Valley. Between approximately 7,000 and 10,000 years ago, one or more lava flows originating from a vent at Schreiber's Meadow flowed about 8 miles down the Sulphur Creek Valley, burying the Baker River channel under several hundred feet of lava. The lava forced the Baker River against the eastern side of its valley, temporarily impounding it until the water was high enough to overtop its embankments and erode a new channel. As a result, when the Baker River channel re-established itself, it abandoned its ancestral channel about 2 miles to the west of Glover Mountain and incised a new channel in the bedrock to the east of Glover Mountain where Upper Baker Dam is now located.

Lava that erupted from the vent at Schreiber's Meadow filled the Sulphur Creek valley to a depth of over 300 feet. As the lava entered the Baker River Valley, it spread out upriver and pushed Sandy Creek to the northern side of its valley. Mudflows, alluvium, and colluvium have subsequently filled in pre-existing drainages to considerable depths. The largest mudflow appears to have been associated with a massive avalanche of hydrothermally altered rock from near Sherman Peak about 6,000 years ago. This mudflow extended 19 miles down the Middle Fork Nooksack River valley to the west of Sherman Peak and seven (7) to eight (8) miles down the Sulphur Creek valley.

The Sulphur Creek lava flows are typically fractured and permeable. As a result, these flows readily transmit groundwater that originates as precipitation at higher elevations and discharges that groundwater as springs in the Baker River Valley. The largest spring issues from these lavas along lower Sulphur Creek and at Horse Bridge Springs near Horseshoe Cove. The springs at Horseshoe Cove were inundated by the filling of Baker Lake in 1959, and the flow from the springs is believed to have been reversed, at least in part, augmenting the discharge of the springs along Sulphur Creek.

6.1.3 Site Geology and Foundation Conditions

Upper Baker Dam is founded entirely on bedrock of the Chilliwack Group. Locally, the rock mass consists of fine- and medium-grained strata that dips moderately to the northeast. The broad general picture of the bedrock beneath the dam is that of a homocline, dipping on average 31 degrees at an azimuth of 39 degrees. The fabric is locally convoluted and undulating, showing variability by as much as 20 degrees or more over a few tens of feet (Stone & Webster, 1960b).

The rocks appear to become coarser up the stratigraphic sequence as shale and phyllite in the south give way to interbedded shale, graywacke, and sandstone in the north, as is typical of a turbidite sequence. The bedrock below the dam extending from Monolith 25 to approximately Monolith 5 consists of a medium-strong to strong, fresh to slightly weathered, thin to medium foliated, close to medium jointed, dark gray to black phyllite — former claystones and siltstones that have been metamorphosed slightly beyond slate. This rock exhibits highly persistent bedding, which is roughly equivalent to foliation because of the low-grade metamorphism of the rock.

The rock mass occupying the right abutment (north of Monolith 5) is primarily medium-strong to very strong, fresh, medium to very widely jointed, dark gray phyllite and gray coarse-grained metagraywacke—former shale, claystones, siltstones, and sandstones that have been slightly metamorphosed—grading to the north to un-metamorphosed shale. Unlike the phyllite at the south abutment, the foliation in this rock is not well expressed and has low persistence. Where exposed at the base of the dam (below Monolith 7) at the north end of the parking lot, the rock mass is low to moderate strength, fresh to slightly weathered phyllite, with tightly deformed foliation containing discontinuous quartz lenses up to about ¼-inch thick. The phyllite at this outcrop is thinly foliated and widely jointed.

Additional subsurface exploration at the base of Monolith 4 intersected a previously unknown major structure. This structure was referred to as a mylonite zone, which has rock mass characteristics similar to those of other soft seams and is probably geologically related to Soft Seam C. The mylonite zone does not form a kinematically admissible wedge with Soft Seam C or other major structures.

A potential rock wedge exists under Monoliths 6 through 10. The wedge boundaries are interpreted to be formed by a master joint and the Monolith 10 deformation zone and Soft Seam D major structures. The rock wedge is based on the discrete offsets and fracture zones within the drain holes that were constructed at the same time as the dam and on the results of the 2016-2017 subsurface exploration program.

The modeled rock wedge under Monoliths 18 and 19 is based on the interpretation of the historical measurements of deformation between Monoliths 18 and 19, discrete offsets and fracture zones within drains of Monolith 18, and the results of the 2016-2017 subsurface exploration program. The rock wedge is formed by foliation (as the slide plane), Joint Set 1 or 3 (as the upstream release plane), and Joint 4 or one side of a wedge with foliation (a side-release plane). This rock wedge possibly compresses a series of vertical open joints from Joint Set 1 or 3, or the U2 Fault downstream of Monolith 18. The foliation plane under Monolith 18 does not daylight downstream.

6.1.4 Deformation History

The geology of the western section of the Baker River basin is structurally complex, consisting of the regional-scale fault nappes comprised of recumbent folds, shear zones, and imbricate stacks, all of which have been offset by later cross-cutting extensional faulting. The rocks have undergone at least three major tectonic events resulting from continental-scale processes. These deformation events ("D") include:

a. Pre-mid-Cretaceous assembly of terranes (volcanic island arcs, oceanic arcs, etc.) onto the western margin of the North American craton (D1);
b. Mid- to late-Cretaceous crustal thickening through thrusting, pluton emplacement, and volcanism (D2); and
c. Eocene extensional tectonics, including faulting and plutonism (D3) (Tabor and others, 2003).

These major orogenic events were followed by continued continental magmatic arc development (i.e., volcanic activity) in the Oligocene through Holocene and eventually by several periods of glaciation throughout the recent Quaternary period.

Near Upper Baker Dam, mid-Cretaceous compression (D2) resulted in the Chilliwack strata being tilted approximately 50 to 75 degrees to the northeast, or at low angles to the southwest. The rock has also undergone localized low-grade metamorphism to greenschist facies, resulting in a foliation generally sub-parallel to bedding (Brown and others, 1987). Later extensional brittle faulting (D3) crosscuts the dominant northeast fabric.

6.2 Structural Geology

A total of 11 significant geologic structures previously identified as soft seams, mylonite zones, or lineaments visible in regional lidar (light detection and ranging) have been identified as occurring in the bedrock foundation of the dam. These features are summarized in Exhibit 6-3. Ten of these features, identified as major mappable structures, are presented in Exhibit 6-4. A more detailed analysis of each major structure is presented in the fault atlas (Appendix H). For consistency, the same terminology used in the historical reports is used herein to describe the geological features identified. Specifically, the term "soft seam" was first used in the Stone & Webster (1960b) report to describe a zone where the rock was disintegrated or decomposed to the consistency of soil/mud. It is assumed that soft seams represent altered or weathered rock along a pre-existing geologic structure such as a fault, shear, or persistent joint. In some cases, these soft seams can be traced for considerable distance and are considered major mappable structures. In addition, several highly persistent joints intersected in recent borings (2016-2018) are referred to herein as "master joints" since they do not exhibit the characteristics of fault zones but are linked across multiple borings and display evidence of minor offsets and or inflow in the historic drain holes.

Exhibit 6-3: Summary of Major Geologic Structure in Dam Foundation

Feature	Location	Type	Dip[1]	Dip/Dir[1]	Comments
Fault A	Monolith 1	Fault	73	016	Limited extent
Soft Seam B	Monoliths 1-3	Soft Seam	65	215	Limited extent
Mylonite Zone	Monolith 4	Shear Zone	59	028	Regional structure, sub-parallel to foliation
Soft Seam C	Monolith 5	Soft Seam	83	054	Sub-parallel to foliation. Possible splay
Soft Seam D	Monoliths 7-9	Soft Seam	83	162	Limited data
Block 6-10_Discontinuity	Monoliths 8-10	Master Joint	36	270	Persistent joint with minor offset
Block 10_Deformation Zone	Monolith 10	Fault	53	047	Regional structure, sub-parallel to foliation
U1	Monolith 12	Fault	38	044	Sub-parallel to foliation
U2	Monoliths 14-16	Fault	64	349	Limited data
Foliation	Monoliths 1-25	Master Joint	43	033	Ranges in dip from 15-70 degrees and dip/dir from 0-70 degrees
Block 18 Discontinuity	Monoliths 17-19	Master Joint	47	027	Parallel to foliation

NOTE:

1 Dip and Dip Direction (Dip/Dir) are in degrees and have been corrected for magnetic declination.

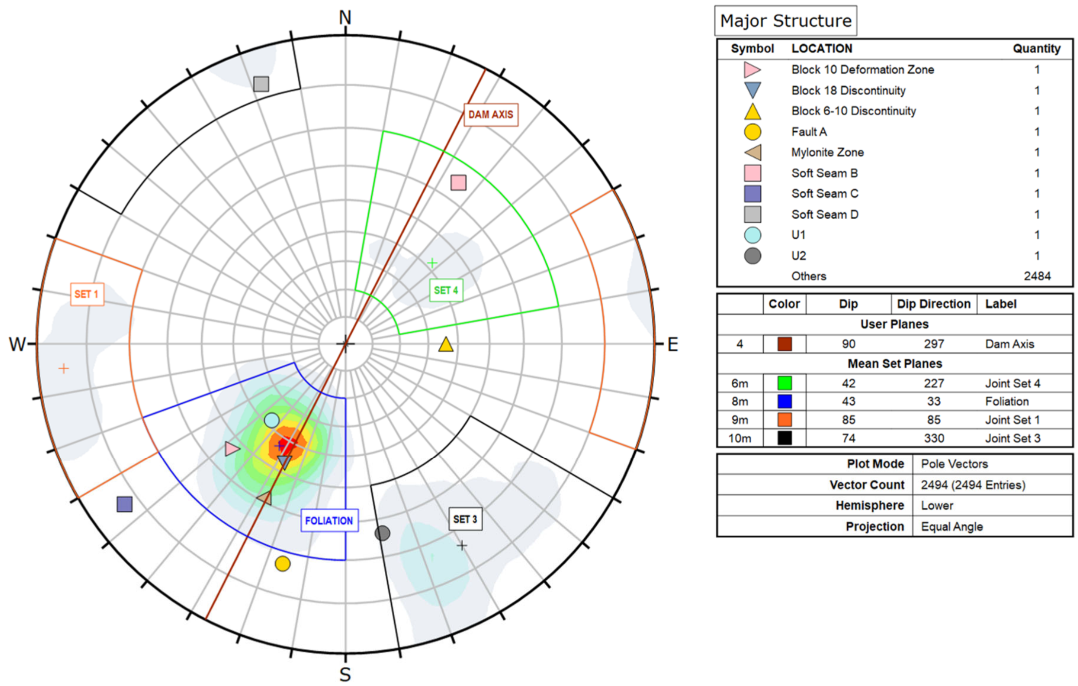

Exhibit 6-4: Lower Hemisphere Stereonet Showing Poles to the Plane of Major Mappable Structure

All major mappable structures were modeled in 3D using Leapfrog Geo™ to better understand their geometry and potential interaction with each other as well as dam infrastructure. This information was then used to perform kinematic analyses, and in some instances limit equilibrium analyses, which will be detailed in later sections. A summary of the 3D modeling results and cross-section is shown in Exhibit 6-5 and Exhibit 6-6, respectively.

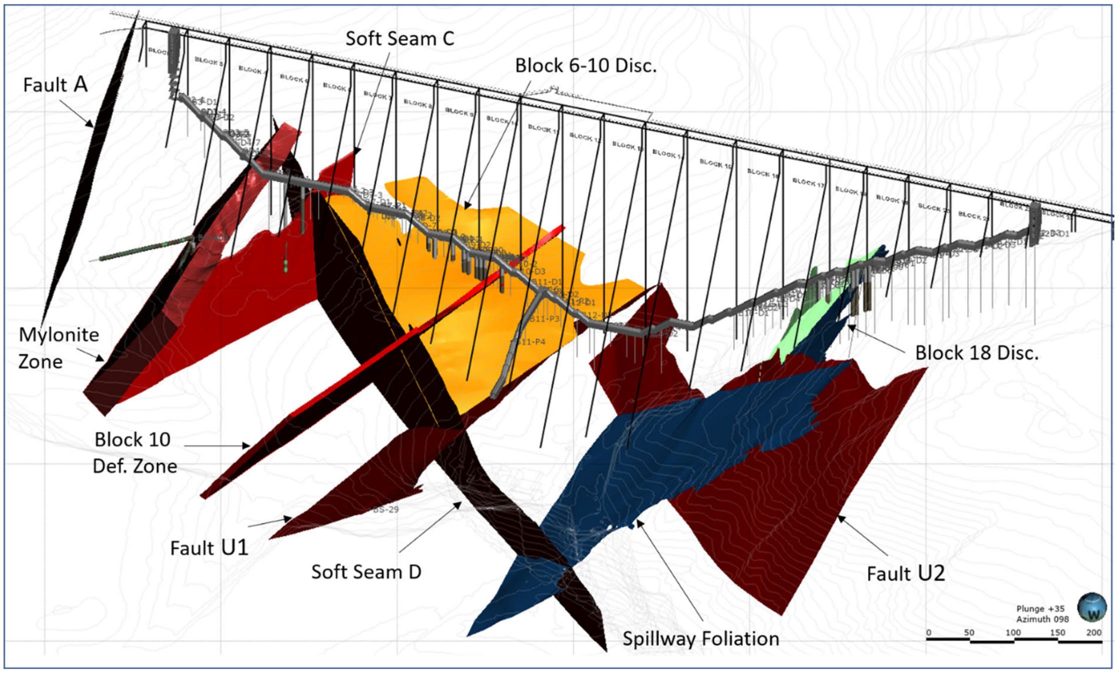

Exhibit 6-5: Three-Dimensional Representation of Modeled Major Structure

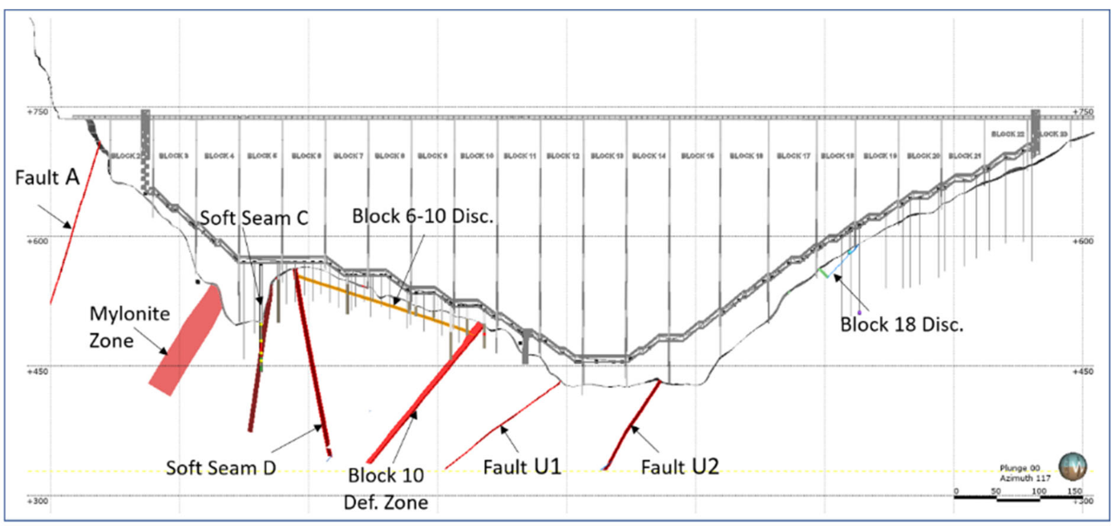

Exhibit 6-6: Cross Section Parallel to Axis of the Dam Showing Modeled Major Structure

6.3 Major Structure

6.3.1 Faulting

Geological investigations have been conducted to identify the major fault zones closest to the dam and to determine whether any of these faults show signs of renewed activity. The Straight Creek Fault, the Shuksan Thrust, and a series of linear topographic scarps suggestive of young faulting about 20 miles east of Upper Baker Dam at the southern edge of the Chilliwack Batholith were investigated for signs of recent movement. Tephrochronology—using ash deposits from known volcanic eruptions to date stratigraphic layers—confirmed that neither the scarps nor the southern edge of the batholith had experienced movement over the last 6,600 years (Forest Service, 2002). There is no evidence, even prior to the last 6,600 years, that either the Shuksan Thrust or the Straight Creek Fault has experienced movement.

6.3.2 Mylonite Zone

Of the geologic features identified beneath the dam, at least two can be attributed to regional-scale faulting processes. A mylonite shear zone forms a prominent regional lineament evident in the lidar, extending approximately one (1) mile to the northwest of the dam and two (2) miles to the southeast (Exhibit 6-7). A portion of this lineament along Sulphur Creek has been mapped as an extensional fault zone by the USGS in 1994 and 2003 (Tabor and others, 2003). The location at which the lineament bisects the axis of the dam corresponds to the location of a "deep trench" and soft seam under Monoliths 4 and 5 that was identified during dam construction and grout curtain installation (Stone & Webster, 1960b). The presence of the lineament was also confirmed in borings BH-401 and BH-402, where mylonite and intensely sheared phyllite intersected (Shannon & Wilson, 2022). The survey of the excavated bedrock surface also shows that at least 55 feet of material was excavated from this trench prior to dam construction. Slickensides—polished joint surfaces—are present throughout the variable jointing, foliation, and bedding in the mylonitic phyllite. The modeled orientation of this feature at the dam is 59/028 (Dip/Dip Direction) degrees, with an estimated true thickness of 25 to 30 feet.

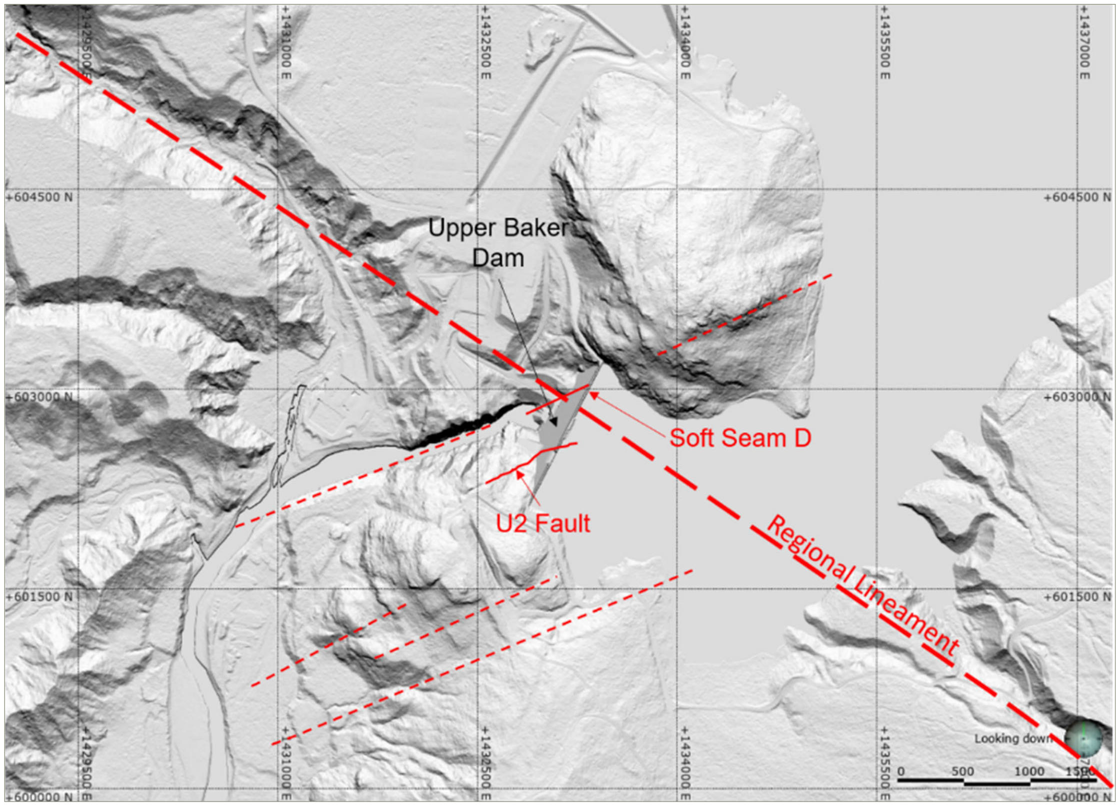

Exhibit 6-7: Regional Plan View Showing Surface Trace of the U2 Fault, Soft Seam D, and Parallel Lineaments to the North and South

6.3.3 Soft Seam D

USGS mapping also identified a northeast-trending high-angle fault—the Anderson Creek Fault—that they inferred to pass within about 0.3 miles south of Upper Baker Dam (Exhibit 6-1). An alternate interpretation of the Anderson Creek Fault alignment is that it corresponds to Soft Seam D, which crosses Monolith 6 through Monolith 9 before leaving the dam foundation area on the downstream side and extending along the tailrace channel (Exhibit 6-7 and Exhibit 6-8). Soft Seam D was first identified during construction (Stone & Webster, 1960b), where they located Soft Seam D in the foundation below Monolith 7 rather than Monolith 6. The soft seam has an estimated orientation of 83/162 degrees. The parallel trend to the Anderson Creek Fault is an indication that the bedrock under the dam is likely influenced by the southwest extension of this fault system. The U2 Fault also has a similar trend, but dips in the opposite direction to the northeast; its relationship to the Anderson Creek Fault is unclear at this time.

Although the USGS did not indicate the age of the Anderson Creek Fault, crosscutting relationships suggest that the Anderson Creek Fault pre-dates the intrusion of the Tertiary Chilliwack Batholith and post-dates the Mesozoic Shuksan Thrust. It is also overlain by undisturbed Quaternary deposits along much of its 22-mile mapped length. Thus, the fault appears to have last moved in Mesozoic or early Tertiary time, with no evidence of Quaternary displacement observed.

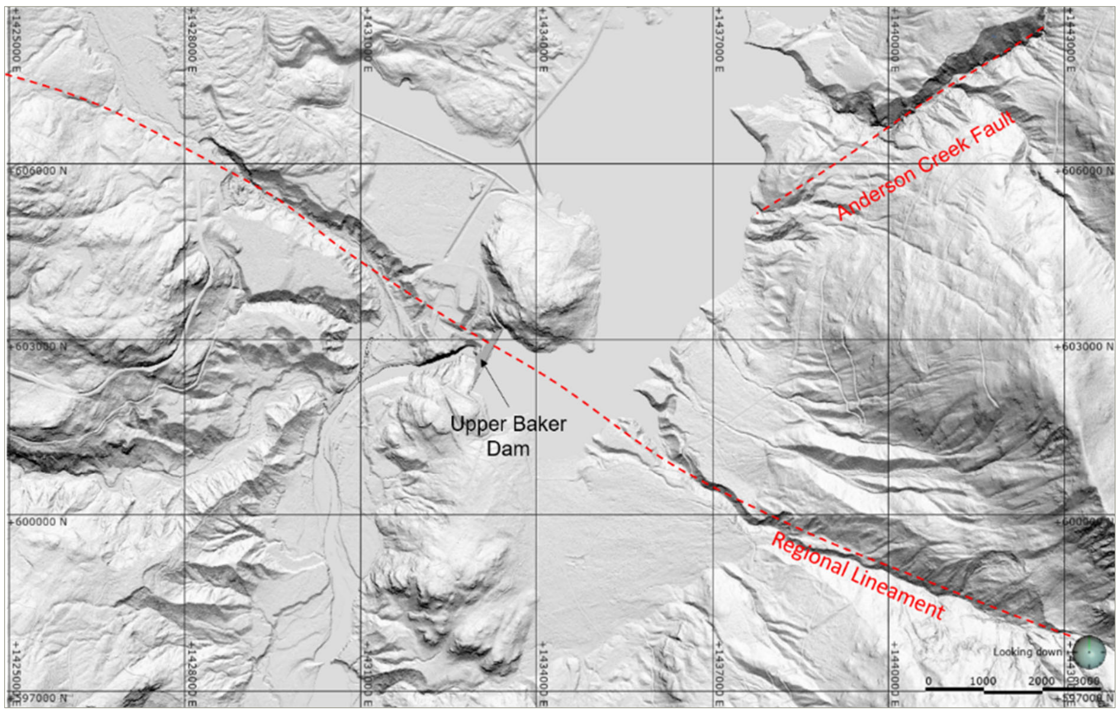

Exhibit 6-8: Regional Structure Identified in Lidar Traversing Beneath the Dam in the Location of Known Structure

6.3.4 Fault U2

Fault U2 extends from the upstream side of Monolith 14, crosses Monoliths 15 and 16, and continues through Monolith 17 before leaving the dam foundation area on the downstream side (Exhibit 6-5, Exhibit 6-6, Drawings C-01 and C-02). The fault was first identified during construction (Stone & Webster, 1960a). Stone & Webster (1960a) refer to this feature as a clay seam in their report and as a fault on the foundation drainage plate, Drawing Number 9548-FH-7D.

Fault U2 is oriented 64/349 degrees, making it parallel to the canyon downstream of the dam and coincident with a series of parallel lineaments in the area (Exhibit 6-7 and Drawing C-01). From a regional perspective, the lineaments occur along trend of the Anderson Creek

Fault to the northeast, indicating that the U2 Fault likely forms part of the southwest extension of this fault system. Regardless of its provenance, the coincident sub-parallel lineaments are indicative that the U2 Fault is one in a series of faults or associated splays of a similar orientation that are responsible for the linear trend of the canyon downstream of the dam.

6.3.5 Fault A

Fault A is located in the right abutment and extends underneath Monolith 1 at an approximate orientation of 73/016 degrees. This fault was identified by Stone & Webster and is shown in Drawing C-01 and Drawing C-02 (Stone & Webster, 1960b). The fault is readily visible as a continuous structure in outcrop and in the lidar data but has not been intersected in any of the exploration borings.

6.3.6 Block 10 Deformation Zone

A fault-bounded deformation zone consisting of complexly folded and deformed phyllite was encountered in the 2017 borings under Monolith 10 (Exhibit 6-5 and Exhibit 6-6). In contrast to the surrounding country rock, the interval contains between 20 and 30% calcite veining that has undergone multiple episodes of folding and offsets. The calcite is indicative that the zone was once a brecciated zone that acted as a pathway for hydrothermal fluids. The deformed zone is oriented at 53/047 degrees and has a true thickness of about seven (7) feet. It may correspond to the fault noted by Stone & Webster (1960b) as dipping 42 degrees toward the right abutment.

6.3.7 Soft Seam B

Soft Seam B was not exposed in the foundation during construction and has not been observed in the geotechnical borings; thus, its extent and orientation are poorly constrained. Stone & Webster (1960b) did not provide sufficient detail to evaluate the orientation of Soft Seam B. It was located in numerous grout holes during construction and estimated to have an apparent dip approximately parallel to the right abutment slope, extending from Monolith 1 to midway through Monolith 3; estimated orientation is 65/215 degrees. As Soft Seam B was not intercepted or observed in the geotechnical borings, it is likely the structure does not persist into Monolith 4.

6.3.8 Soft Seam C

Soft Seam C is a deformation zone approximately 5-feet thick comprised of very weak to strong, slightly weathered to completely weathered, close to moderately jointed, dark-gray mylonitic phyllite. It occurs adjacent and slightly oblique to the Mylonite Zone discussed above, indicating it is most likely a splay off the main shear zone. Soft Seam C was encountered in borings BH-401 and BH-402. The foliation and bedding are highly variable and offset, with brecciated and mylonitic zones containing quartz and calcite replacement. Slickensides are present throughout the variable jointing, foliation, and bedding in the mylonitic phyllite rock. Soft Seam C extends under Monolith 3, Monolith 4, and Monolith 5, having an approximate orientation of 83/054 (Exhibit 6-5 and Exhibit 6-6).

6.3.9 Fault U1

Fault U1 was also identified during construction (Stone & Webster, 1960b). It extends beneath Monolith 12 near the base of the canyon and has an orientation of 38/044 degrees, making it parallel to the dominant foliation trend that has an average dip and dip direction of 43/033 (Exhibit 6-5 and Exhibit 6-6). It is postulated that Fault U1 is the result of significant displacement from slippage that has occurred along the pre-existing zone of weakness.

7 DISCONTINUITY CHARACTERISTICS

7.1 Minor Structure

The orientations of features characterized as minor structures were obtained from geologic field reconnaissance, downhole televiewer surveys of the 2016-2017 borings, a 2020 photogrammetry survey, and the 2021 spillway borings. A total of 2,494 orientations were imported into Dips v. 8.021 (Rocscience, 2022) to generate stereonet plots. The orientations of these discontinuities are represented as poles to planes plotted on a lower hemisphere, equal-angle, polar projection. Minor structure orientations are presented in Exhibit 7-1.

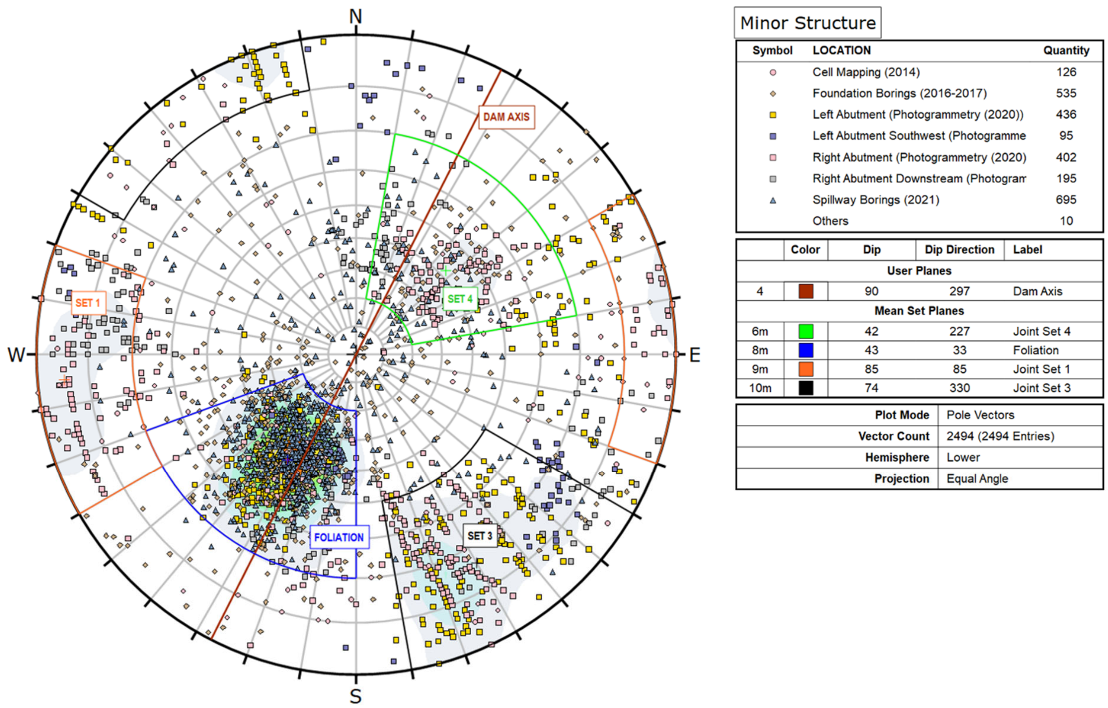

Exhibit 7-1: Lower Hemisphere Showing Poles to the Plane of Minor Structure

The discontinuity data was divided into four clusters or sets:

- Foliation: Foliation forms the cluster with the greatest number of observations. The average orientation is 43/033 degrees, with individual discontinuities ranging in dip from 15 to 60 degrees direction from approximately zero (0) to 80 degrees. Previous studies mention the foliation as smooth, planar, having apertures less than an inch, and free of infilling (Stone & Webster, 1984 [revised 1987]). Field observations support this description and indicate persistence is upward of 150 feet. A previously identified, Joint Set 2 had an orientation of 74/011 but is now included with foliation and not identified separately.
- Joint Set 1: Joint Set 1 is near vertical and strikes approximately parallel to the axis of the dam with an average dip/dip direction of 85/085 degrees. Joint Set 1 has fewer observations in the televiewer data due to the vertical direction of the majority of the borings and the steep inclination of the joint set. However, this joint set is also visible in the photogrammetry data, historic photographs, and in outcrop. Individual orientations generally range in dip from 60 to 90 degrees, and dip direction from 60 to 120 degrees and 240 to 300 degrees.
- Joint Set 3: Joint Set 3 is steeply inclined and has an average dip/dip direction of 74/330 degrees, and thus, is nearly orthogonal to Joint Set 1. Individual orientations generally range in dip from 55 to 90 degrees, and dip direction from zero (0) to 300 degrees, typically around 175 degrees. Joint Set 3 also has fewer observations in the televiewer

data due to borehole direction bias. Stone & Webster (1960b) identified several discontinuities in Joint Sets 1 and 3 that contained soft, clay-like material and had an open aperture. Joint persistence is often greater than 100 feet as seen in construction-era photographs (Exhibit 7-2).

- Joint Set 4: Joint Set 4 has an average dip/dip direction of 42/227 degrees. This set is generally smooth, planar, tight, and free of infilling with a measured persistence upward of 50 feet.

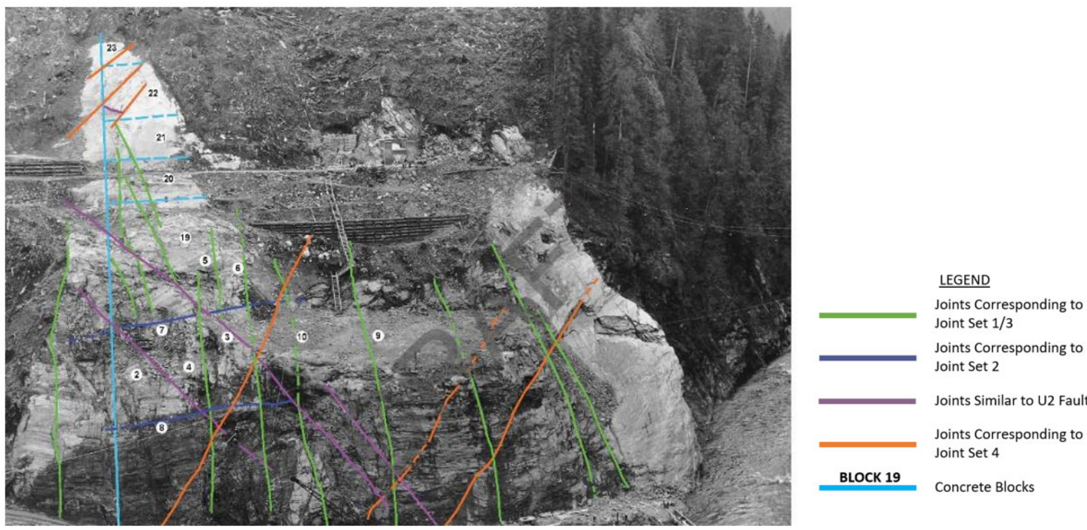

Exhibit 7-2: Photograph of the Left Abutment during Construction Showing Selected Joint Sets

Characteristics of the minor structure discontinuities include orientation, persistence, spacing, infilling material(s), aperture and surface profile, and roughness. These characteristics were compiled from the exploration and surface mapping programs and incorporated into our analyses. Minor structure includes joints, shears, and bedding planes; collectively described as discontinuities.

7.1.1 Orientation

The orientation of the discontinuity is expressed as (a) dip and (b) dip direction (i.e., Dip/Dip Direction). The dip is the angle that the discontinuity is inclined from horizontal and the dip direction is the angle in degrees from true north measured in the maximum down-dip direction. In outcrops, discontinuity orientation was measured using a Brunton compass. In geotechnical holes, orientations were calculated from the optical or acoustic televiewer methods. For the photogrammetry survey, discontinuity orientations were obtained using Leapfrog Geo™. Mean orientation for each joint set are presented in Exhibit 7-3.

Exhibit 7-3: Joint Set Orientation Summary

Type	Dip[1] (degrees)	Dip Direction[1] (degrees)
Joint Set 1	85	085
Joint Set 2 (included with Foliation)	--	--
Joint Set 3	74	330
Joint Set 4	42	227
Foliation	43	033

NOTE:
1 Dip and Dip Direction are in degrees and have been corrected for magnetic declination.

7.1.2 Persistence

Persistence is the distance that a discontinuity extends through the rock mass. For this project, persistence was measured along outcrops or estimated from historical photographs and ranges from very low (less than 3 feet) to very high (greater than 60 feet). During mapping, we also recorded whether one end, two ends, or neither end of a discontinuity could be observed in outcrop. One end was observed in about 35% of discontinuities, two ends were observed in about 10% of discontinuities, and neither end was observed in about 50% of discontinuities. About 5% of discontinuities did not have documentation on whether one end, two ends, or neither end was observed during mapping.

7.1.3 Spacing

The true distance between individual discontinuities of the same joint set was measured from surface discontinuity surveys and ranges from very close spacing (1 to 2.5 inches) to very wide spacing (6 to 20 feet), with values ranging from one (1) inch to about 12 feet. The average observed spacing from surface discontinuity surveys is approximately 29 inches (2.4 feet).

The apparent distance between individual discontinuities and structures of all joint sets was measured from observations of all boring logs to date. These distances range from extremely close spacing (less than 1 inch) to very wide spacing (6 to 20 feet), with values ranging from about 0.10 inches to about seven (7) feet. The average observed spacing from borehole discontinuities is approximately 0.5 inches.

7.1.4 Infilling

The type of material occurring within joints was observed in discontinuities exposed at the surface and in core specimens collected from the Shannon & Wilson geotechnical boring exploration program. Summation of infilling types may total over 100% due to multiple types of material occurring within joints (i.e., having a joint with infilling of both clay and calcite).

From surface mapping, we observed that joints were mostly clean with little having infill of quartz as shown by the following approximate distribution of infilling types:

- Clean, 65%;
- Quartz, about 18%; and
- Unspecified, about 17%.

From observation of discontinuities exposed in core specimens collected from the Shannon & Wilson geotechnical exploration program, we observed the following approximate distribution of infilling types for minor structure:

- Clean (no filling), 64%;
- Clay, 17%;
- Rock fragments, 10%;
- Iron oxide, 5%;
- Calcite, less than 5%;
- Unidentified mineral, less than 5%; and
- Quartz, less than 5%.

7.1.5 Aperture

The width of discontinuity openings observed during mapping ranges from tight (less than 1/16 inch) to very wide (1 inch) but were typically observed as tight.

The width of discontinuity openings observed within core specimens collected from the Shannon & Wilson geotechnical exploration program ranges from tight (less than 1/16 inch) to an estimated six (6) inches. This is likely an overestimate due to core dilation during the coring process.

7.1.6 Surface Profile and Roughness

The profile of joints observed during mapping are typically smooth to very rough. The joint roughness coefficient ranges from 3 (smooth) to 20 (very rough). About 70% of joint profiles are smooth, about 25% of joint profiles are rough, and about 5% of joint profiles are very rough.

The profile of joints observed are typically slickensided, smooth, slightly rough, rough, or very rough. The joint roughness coefficient (JRC) ranges from 0 to 2 (slickensided) to 18 to 20 (very rough), with an average JRC of approximately 6 for all borings and 7 for the spillway borings. Slickensided surfaces were observed on less than 10% of the discontinuities.

8 ENGINEERING PROPERTIES

The analysis included an evaluation of the rock mass. A rock mass includes both intact rock and discontinuities. The strength of the intact rock, the strength of the discontinuities, and the spacing and orientation of the discontinuities collectively affect the overall strength and engineering performance of the rock mass. The engineering properties of the rock mass were primarily determined from observation of rock core collected during the subsurface exploration program and laboratory testing, supplemented by information gathered from mapping as well as acoustic and optical televiewer data.

Rock mass design parameters were estimated based on our evaluation of engineering properties and were used to develop shear strength values for our design analyses. For the purpose of this report, the geologic rock masses observed in the foundation of Upper Baker Dam have been combined into three engineering lithologies based on laboratory testing and engineering characteristics: phyllite, mylonitic phyllite, and metagraywacke. The engineering and geologic characteristics that separate these lithologies include the UCS, shear strength, Geological Strength Index (GSI), and lithographic composition.

The shear strength values are based on Hoek-Brown failure criterion, which considers equivalent rock continuum properties accounting for strength contributions from both intact rock and discontinuities throughout the rock mass, and characterization of the discontinuities, which considers direct shear laboratory testing and roughness of the discontinuities to evaluate the frictional shear strength. From the Hoek-Brown criterion, Mohr-Coulomb criteria, which considers the strength of discontinuities and rock bridges, were approximated based on anticipated confining stresses (Hoek and others, 1995).

8.1 Intact Rock Design Parameters

The UCS for the three engineering lithologies are presented in Exhibit 8-1 and the UCS for two failure types are presented in Exhibit 8-2 (ASTM D7012). A total of 18 uniaxial compressive tests were performed on rock core samples collected from foundation borings and a total of 11 uniaxial compressive tests were performed on rock core samples collected from spillway borings, as discussed in Section 5.1 and presented in Appendix D. Design parameters for UCS used in our analyses are based on the median Failure Type C (combination of through intact rock and along a discontinuity) UCS value from laboratory testing of spillway borings: 3.2 ksi.

Exhibit 8-1: Summary of Uniaxial Compressive Strength of Engineering Lithologies from UCS Tests Conducted on Rock Core Samples Collected from Foundation Borings

	Uniaxial Compressive Strength (ksi)			
Engineering Lithologies	Minimum	Maximum	Mean	Number of Samples
Mylonitic Phyllite	1.5	6.7	4.1	5
Phyllite	4.5	14.5	8.4	6
Metagraywacke	16.4	29.6	22.9	7

Exhibit 8-2: Summary of Uniaxial Compressive Strength from Tests Conducted on Rock Core Samples Collected from Spillway Borings

	Uniaxial Compressive Strength (ksi)			
Failure Type	Minimum	Maximum	Median	Number of Samples
Failure Type A[1]	1.3	1.4	1.3	2
Failure Type C[2]	1.4	24.4	3.2	9

NOTE:
1 Failure Type A is a failure that occurs along a discontinuity.
2 Failure Type C is a combination failure in which the failure occurs both through the intact rock and along a discontinuity.

8.2 Equivalent Rock Mass Design Parameters

8.2.1 Rock Mass Rating (RMR_{89}) and Geological Strength Index (GSI)

Equivalent rock mass properties were evaluated using the Rock Mass Rating (RMR_{89}) system developed by Bieniawski (1989); the Tunneling Quality Index (Q-system) (Barton et al., 1974); and the GSI as described by Hoek and Brown (1997) and equations for GSI by Hoek, Carter, and Diederichs (2013). These rating systems consider the combined contributions of discontinuities and intact rock within a rock mass. The RMR_{89} and Q-system were used to evaluate GSI, which was used to calculate the Hoek-Brown failure criterion for the rock mass.

RMR_{89} system ratings range from zero (0) to 100, with a rating of zero (0) corresponding to "Very Poor Rock" and a rating of 100 corresponding to "Very Good Rock." RMR_{89} is determined based on the intact rock UCS, the Rock Quality Designation (RQD), the typical discontinuity spacing, the typical condition of the discontinuities, typical groundwater conditions, and discontinuity orientation relative to the slope considered. RQD is measured as a percentage of drill core that has lengths greater than 4 inches (Deere and Miller, 1966); it was calculated for each core run. RMR_{89} for all borings ranged from 33 to 82, with an average RMR_{89} of 58. RMR_{89} for spillway borings ranged from 42 to 68, with a weighted average of 60.

The Q-system is an empirically based rock mass rating system that was developed specifically for the design of tunnel support systems but has since been expanded, like the $RMR_{(89)}$ system, for other rock engineering applications. Under the Q-system, rock mass quality is divided into nine classes ranging from "exceptionally poor" (Q of 0.001 to 0.01) to "exceptionally good" (Q of 400 to 1,000). The Q-system considers six parameters:

- RQD;
- Number of discontinuity sets (Jn);
- Joint roughness number (Jr), based on the most unfavorable discontinuity;
- Joint alteration number (Ja), dependent on the degree of alteration or filling along the weakest discontinuity;
- Joint water reduction (Jw), dependent on the worst-case water inflow conditions; and
- Stress Reduction Factor, dependent on estimates of the state of stress in the slope or surrounding the tunnel perimeter.

GSI ranges from zero (0) to 100, with a lower rating corresponding to a lower-quality rock mass and a higher rating corresponding to a higher-quality rock mass. The RMR_{89} and Q-system were used to evaluate GSI, which was further used to calculate the Hoek-Brown failure criterion for the rock mass. GSI is based on "surface condition" closely resembling the joint condition rating criteria in RMR_{89} and rock mass structure, corresponding to the interlocking characteristics of the rock mass (analogous to the degree of natural fracturing of the rock mass relative to the scale of the engineering problem). According to Hoek and Brown (1997), GSI can be calculated as RMR_{89} less five (5). GSI calculated from RMR_{89} according to Hoek, Carter, and Diederichs (2013) is dependent upon the joint condition ($JCond_{(89)}$) and RQD. GSI calculated from the Q-system is dependent upon joint roughness (Jr), joint alternation (Ja), and RQD (Hoek and others, 2013).

GSI was calculated for each core run as the average of two of the three methods described above: (1) GSI calculated from RMR_{89} dependent upon $JCond_{(89)}$ and RQD, and (2) GSI calculated from the Q-system dependent upon Jr, Ja, and RQD. GSI calculations are presented in Appendix C. For the purposes of the limit equilibrium engineering analyses, the GSI was evaluated for both the foundation and spillway borings: IN-0500, BH-401, BH-402, BH-403, EX-0900, EX-1000, IN-0900, IN-1000, EX-1800, EX-1900, IN-1700, IN-1801, IN-1802, IN-1900, BH-16-1, BH-16-2, BH-17-1, and BH-17-2. The GSI of the rock mass for all borings ranged from nine (9) to 94, with an average GSI of 54. The GSI of the rock mass for the spillway borings ranged from 23 to 77, with an approximate weighted average of 60 (Table C-1).

8.2.2 Discontinuity Strength

The shear strength along discontinuities was evaluated through direct shear tests along discontinuities and saw-cut surfaces and is presented in Table 4 (ASTM D5607). A total of 14 direct shear tests from foundation borings and eight (8) direct shear tests from spillway borings were performed on saw-cut surfaces of rock core samples, as discussed in Section 5.2 and presented in Appendix D. Higher normal stresses were used in previous laboratory testing to reflect the stresses of potential slip surfaces under the foundation of the dam. The normal stresses used in direct shear testing on samples collected from the spillway borings was changed to reflect the range of normal stresses acting along the potential slip surfaces in the spillway slope.

The base friction angle for the rock mass on sawed surfaces for all tested lithologies within foundation borings ranges from 15 to 35, with a mean base friction angle of 26 degrees.

Exhibit 8-3 summarizes the minimum, maximum, and mean base friction angle of the engineering lithologies resulting from shear strength laboratory testing.

The peak shear strength friction angle for the rock mass on sawed surfaces from rock core samples within spillway borings ranges from 38 to 74 degrees, with a median of 44 degrees and a mean of 51 degrees. The post-peak shear strength friction angle for the rock mass on sawed surfaces from rock core samples within spillway borings ranges from 33 to 74, with a median of 41 degrees and a mean of 48 degrees. Exhibit 8-4 summarizes the minimum, maximum, median, and mean friction angles for peak and post-peak shear strength of each spillway boring resulting from laboratory testing. For purposes of the spillway stability limit equilibrium analyses, we used the minimum saw-cut peak shear strength friction angle of 38 degrees plus 10 degrees accounting for joint roughness angle to obtain a total joint frictional component of 48 degrees (Wyllie and Mah, 2004). A joint roughness angle of 10 degrees was used as it is the minimum joint roughness calculated using Equation 3.9 from Wyllie and Mah (2004). The joint roughness added to the base friction is based on the joint roughness coefficient observed during core logging and not the larger and longer amplitude waviness or roughness of the foliation surfaces observed at the outcrop scale. An average and median JRC of 7 and 5 was observed from the spillway borings, respectively. We selected the median JRC of 5 for use in Equation 3.9 from Wyllie and Mah (2004). We also used a saw-cut post-peak shear strength friction angle of 41 degrees for the post-earthquake condition, which represents the median post-peak shear strength values of 41 degrees.

Exhibit 8-3: Summary of Discontinuity Shear Strength of Engineering Lithologies from Direct Shear Tests Conducted on Rock Core Samples Collected from Foundation Borings

Engineering Lithologies	Friction Angle (degrees) Minimum	Maximum	Mean	Number of Samples
Mylonitic Phyllite	15	25	18	4
Phyllite	25	35	29	7
Metagraywacke	24	34	29	3

Exhibit 8-4: Summary of Discontinuity Shear Strength from Direct Shear Tests Conducted on Rock Core Samples Collected from Spillway Borings

	Friction Angle (degrees)								
	Peak Shear Strength				Post-Peak Shear Strength				
Boring No.	Min	Max	Median	Mean	Min	Max	Median	Mean	Number of Samples
BH-16-1	41	44	42	42	37	40	39	39	2
BH-16-2	38	42	40	40	33	39	36	36	2
BH-17-1	61	74	68	68	60	74	67	67	2
BH-17-2	45	61	53	53	42	58	50	50	2
Total	**38**	**74**	**44**	**51**	**33**	**74**	**41**	**48**	**8**

9 POTENTIAL FAILURE MODES (PFMS)

9.1 Typical Failure Modes for Concrete Gravity Dams

For this study, the identification of PFMs in the foundation of Upper Baker Dam is based on geologic data collected through field observations and borehole logging as well as geologic data collected in previous studies. For a rock mass to have a kinematically admissible wedge there must be discontinuities for sliding to occur on, release joints to free the wedge from the surrounding rock mass, and an open space for the mass to move into. Fell and others (2005) illustrate typical modes of foundation instability for concrete gravity dams displayed in Exhibit 9-1 and described below:

- Mode 1 consists of shear along the interface between the concrete and rock, at or near the base of the dam.
- Mode 2 consists of development of a non-compression zone along the upstream portion of the rock/concrete contact, combined with shear along the downstream portion of the rock/concrete contact at the base of the dam.

- Modes 3 and 4 consist of shear along either single or multiple planar discontinuities in the rock formation. For these failure modes, the discontinuities should both be approximately parallel to the base of the dam and daylight downstream of the dam.
- Mode 5 consists of the failure through highly jointed or weak rock mass in the foundation of the dam.
- Mode 6 consists of shear along a planar discontinuity in the foundation, and a second discontinuity that daylights downstream of the dam and dips in the upstream direction.
- Mode 7 consists of toppling failure below the concrete foundation. This failure mode requires the existence of closely jointed rock with steeply dipping planes of weakness striking parallel to the axis of the dam.
- Mode 8 consists of rock in the foundation of the dam formed by two (2) discontinuities that intersect in a manner that creates a kinematically admissible rock wedge under the dam. For the rock wedge to be admissible, the line of intersection of the two (2) discontinuities needs to daylight downstream of the dam.

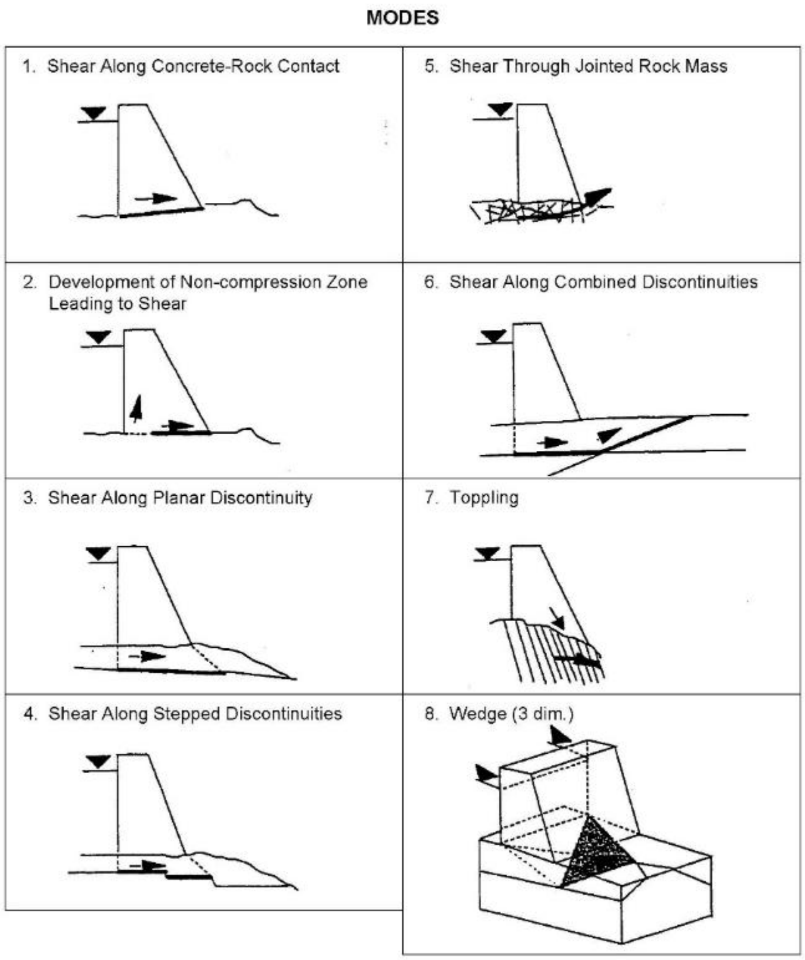

Exhibit 9-1: Potential Failure Modes for Concrete Gravity Dams (Fell, 2005)

Modes 1 and 2 consist of shearing along the concrete-to-rock interface. Hatch (2009) previously evaluated Modes 1 and 2 for normal, flood, probable maximum flood (PMF), and drain efficiency cases only. They did not evaluate a seismic case.

Mode 3 requires a planar discontinuity, parallel to the dam foundation, to extend over significant areas of the slope upon which the dam was constructed. The only area where this condition potentially exists at Upper Baker Dam is below the left abutment under Monoliths 17 through 24. Shear would occur along a sufficiently long foliation surface that would daylight under the dam. Despite the existence of rock containing foliation planes under Monoliths 14 through 16, this failure mode does not appear to be feasible under these monoliths as indicated in construction photographs and topographic maps, which display the unlikelihood that any one foliation plane is both long enough and in the proper orientation to daylight downstream of the dam.

Mode 4 also requires shear along planar discontinuities parallel to the dam foundation like that of Mode 3; however, this mode does not require that sliding take place along just one discontinuity. Rather, shearing can take place along multiple discontinuities with separation occurring along a second set of discontinuities or shearing through intact rock. At Upper Baker Dam, this condition could exist under Monoliths 18 through 24, with sliding along foliation and separation occurring on joints that are members of the joint sets that we have designated Joint Set 1, Joint Set 3, and Joint Set 4 (Exhibit 7-2). Mode 4 is a more likely condition to exist under the left abutment of the dam than Mode 3, as it does not require the existence of large-scale individual foliation planes longer than those observed in the construction photographs. As for Mode 3, it is unlikely that a combination of stepped foliation planes would be long enough and in the correct orientation to daylight downstream of the dam.

Mode 5 is not a feasible failure mode at Upper Baker Dam. Based on our observation of the rock cores, existing exposures, and construction photographs, the rock in the foundation is neither weak nor highly fractured as to make this failure mode feasible.

Likewise, Mode 7 is unlikely, as it requires a closely jointed or foliated rock mass with foliation striking approximately parallel to the dam axis. While the foliation in the east abutment is closely spaced, the strike of the foliation is about 90 degrees off the axis of the dam.

This study focuses on evaluating Modes 6 and 8. Mode 8 could exist anywhere under the dam where there are two (2) discontinuities with sufficiently long strike lengths and have the proper orientation to create a kinematically admissible wedge under the dam. For a kinematically admissible wedge to exist, the line of intersection of the wedge would need to daylight in the downstream direction of the dam, or intersect a joint or series of parallel joints oriented perpendicular to the intersection trendline and allow downstream movement to occur. We analyzed this mode of failure by checking if combinations of discontinuities make kinematically admissible wedges in the foundation of the left and right abutments. We concluded that the foliation planes, Joint Set 4, fault structures U1 and U2, as well as highly fractured zones in Monoliths 6 through 10, are large enough structures with the orientation to create a rock wedge under the dam. Mode 6 requires long, persistent discontinuities parallel to the rock surface on which the dam was built and a discontinuity that dips in the upstream direction and daylights downstream of the dam. Though the foliation in the left abutment is parallel to the rock surface, there does not appear to be a second discontinuity set that dips to the east or southeast in the upstream direction.

However, in accordance with reports by Stone & Webster (1960b and 1984, [revised 1987]), Joint Set 1 and Joint Set 3 were found to have soft, clay-like infillings and apertures up to 3 inches. Review of historical photographs and field mapping shows long, persistent discontinuities of Joint Set 1 and Joint Set 3 underneath the left abutment and toward the downstream edge. The presence of these soft-infilled joints, and possibly the U2 fault structure, create an open or compressible space for a rock mass to move into by compressing the joint infill and closing the apertures, creating a kinematically admissible wedge similar to Mode 6.

9.2 Addressed PFMs

This section discusses the specific PFMs addressed within this report. Our study focused on the identification of kinematically admissible blocks of rocks and stability analyses of rock wedges identified. Further details of the PFMs mentioned above and addressed within this report are as follows:

- PFMs N-UB-2A, F-UB-2A, and S-UB-2A: Shear displacement along a foliation surface within the rock mass below Monoliths 18/19. The presence of a non-daylighting wedge that has limited freedom to move has been proposed to explain the observed historical movement of Monolith 18. Data from the geotechnical instrumentation combined with observed offsets in drain holes and data from the boreholes, along with geotechnical laboratory testing, were used to refine the proposed wedge geometry.
- PFMs N-UB-2B, F-UB-2B, and S-UB-2B: Shear displacement along a discontinuity within the rock mass below Monoliths 9/10. The presence of a non-daylighting wedge is proposed that encompasses Monoliths 6 through 10 and may be constrained by Soft Seam D and the Block 10 Deformation Zone. Data from the geotechnical instrumentation combined with data from offsets observed in existing drain holes, new boreholes, geotechnical laboratory testing, geotechnical instrumentation, and piezometer information were used to refine the proposed wedge geometry.
- PFMs N-UB-2C, F-UB-2C, and S-UB-2C: Sliding along an adversely oriented discontinuity (or discontinuities) in the foundation below Monoliths 4/5. The potential for sliding is related to the depth, orientation, shear strength properties, groundwater uplift pressures along the sliding surface(s), and other external loading conditions. The geometry of the sliding surface(s) was based on the orientation of major and minor structures obtained from field mapping and downhole televiewer surveys. The major structure Soft Seam C and the Mylonitic Phyllite Zone are consistent with the general orientation of the foliation and do not form a kinematically admissible block of rock under the foundation of the dam.
- PFMs F-UB-3B and S-UB-3: Undermining of the spillway monoliths caused by continued spillway discharge eroding the rock foundation below the chute under dynamic loading in the spillway or earthquake loading. Data from the geotechnical instrumentation

combined with data from offsets observed in existing drain holes, new boreholes, geotechnical laboratory testing, geotechnical instrumentation, and piezometer information were used to refine the proposed wedge geometry.

- PFM F-UB-3A: Pertains to damage to the spillway structure during a large flood. In this PFM, the spillway is operated for an extended period. The dynamic forces on the spillway chute overstress the chute and it fails. Continued spillway discharge erodes the rock foundation below the chute and the erosion progresses upstream, eventually undermining the spillway monoliths; consequently, one or more monoliths fail resulting in downstream flooding. This report does not address the structural integrity of the spillway structure; however, options to improve the stability of the slope using either post-tensioned rock anchors or a grouted rock buttress will preclude foundation failure as a contributing factor to this PFM.
- PFM F-UB-3C: Pertains to stability of the slope downstream of the spillway with the potential to undermine and lead to damage or loss of the spillway and undermining of Monoliths 16 and 17. Data from new boreholes, geotechnical laboratory testing, and piezometer information were used to define the anticipated plane shear failure mode. Groundwater conditions are assumed based on surface water exposed on the upslope side of the spillway, seepage from existing drain holes in the concrete facing, and the tailrace water surface elevation.
- PFMs N-UB-8, F-UB-8, and S-UB-6: Introduced but are not addressed in this report.

10 GEOTECHNICAL ANALYSIS

10.1 Modes of Rock Slope Instability

Typical modes of rock slope instability include:

- Circular failures occur in highly weathered, altered, or fractured rock masses. In this failure mode, the rock mass behaves as a soil, and shear planes do not follow a single discrete structure or combination of discrete structures.
- Plane shear failures consist of a block of rock sliding on a single discontinuity, such as a joint, bedding plane, geologic contact, or fault dipping out of the slope face. The stability of the slope is dependent upon the following: (a) the orientation of the discontinuity with respect to that of the slope, (b) the shear strength of the discontinuity, (c) the weight of the block, and (d) the pressure due to water on the base of the block or in joints that could form tension cracks behind the rock face.
- Simple wedge failures consist of a block of rock sliding on two (2) discontinuities that intersect such that the intersection of the discontinuities plunges out of the slope face. The stability of the slope is dependent upon the same factors that determine stability for the plane shear type failure.

- Toppling failures consist of blocks of rocks that are formed by vertical or high-angle discontinuities, such as joints that dip into the slope. Topples can also occur where overhangs are created by poor blasting practices or the disintegration of weak, non-durable rock at the toe of the slope.

Instability could result from structures, such as contacts between geologic units, faults, and shear zones or rock mass discontinuities, that intersect the spillway slope in orientations that create plane shear, wedge sliding, and toppling failures. The rock at this site is neither so weathered, so altered, nor so fractured that a circular failure of the slope is likely. The other modes of failure—plane shear, wedge sliding, and toppling—are possible and were considered in our kinematic analyses.

10.2 Kinematic Analyses

Kinematic analyses were performed for the discontinuity data set described in Section 7.1 using the computer program Dips v. 8.021 (Rocscience, 2022). A kinematically admissible block is one in which the structure that bound the block is oriented in directions that allow the block to slide into free space, provided the forces that drive the block are sufficiently high. For the purpose of kinematic analysis, the structures are considered to be planar and through-going features. Kinematic analyses do not consider gravitational, hydrostatic, and seismic loading induced by the dam and other external driving forces.

Analyses of kinematically admissible wedges of rock for Upper Baker Dam were divided into groups of concrete monoliths; groups were based upon similarity in rock mass condition or by containing specific evaluated structures in the rock foundation below each monolith. Additionally, kinematic analyses of the spillway slope were performed to address PFMs S-UB-3 and F-UB-3B (HDR, 2019). Aforementioned, resources were used to delineate major mappable structures that were analyzed for formation of kinematically admissible rock wedges.

The investigation of failure planes included evaluations for sliding along major shear planes or prominent discontinuities at depth in the bedrock foundation. Sliding along or in proximity to the concrete/rock interface was addressed by Hatch and is not included in this report (Hatch, 2009). Five (5) areas were identified as susceptible to kinematically admissible failure modes and thus, areas of the foundation under the following monoliths were investigated: (1) Monoliths 1, 2, and 3; (2) Monoliths 4 and 5; (3) Monoliths 6 through 10; (4) Monoliths 17, 18, and 19; and (5) Monoliths 20 and 21. Additionally, kinematic analyses were performed for the spillway slope. Findings of this study are detailed in the following sections.

10.2.1 Monoliths 1, 2, and 3

10.2.1.1 Evaluation of Historical Photographs, Reports, Downhole Videos, and Borings

From the evaluation of historical photographs, previous reports, downhole camera videos, and borings, no kinematically admissible rock wedges formed by the intersection of major structures were identified. Historical photographs lacked sufficient detail and perspective to identify major structural features beyond what was presented in previous reports. Review of the downhole camera drains did not show the presence of any offsets or displacements in existing drain holes. However, several fractured zones were observed in drain holes and grout hole records that potentially coincide with major structure Soft Seam B (Shannon & Wilson, 2009; Stone & Webster, 1960b).

10.2.1.2 Evaluation of Major Structure

Two (2) major structures exist in the vicinity of Monoliths 1, 2, and 3: Fault A and Soft Seam B. These structures do not form a kinematically admissible wedge. Fault A dips into the right abutment at 73 degrees. While Fault A was reported to contain gouge and mud seams (Stone & Webster, 1960b), these conditions were not observed along the surface trace of Fault A downstream of the dam (Exhibit 10-1).

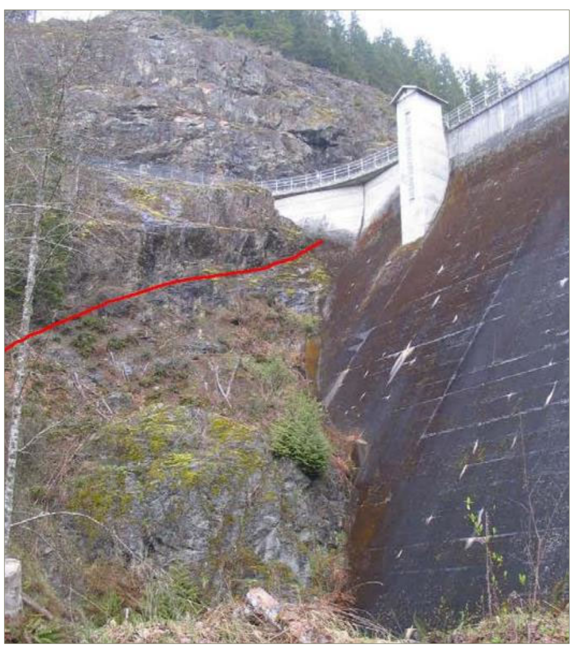

Exhibit 10-1: View of Right Abutment and Approximate Trace of Fault A (shown in red)

Fault A has a trace that runs approximately perpendicular to the axis of the dam and crosses the foundation in Monoliths 1 and 2. Soft Seam B was identified in grout holes only and was not exposed in the dam foundation during construction, nor is it observed in construction-era photographs (Stone & Webster, 1960b). Fractured zones were observed in drain hole videos that correspond to the interpreted location of Soft Seam B in Monolith 2. Soft Seam B has an apparent dip of 65 degrees and a dip direction of 215 degrees and is approximately parallel to the dam axis. Stone & Webster (1960b) states that Soft Seam B, which was observed in grout holes in Monoliths 2 and 3, but had no surface expression, was cleaned and grouted and does not extend above Elevation 680 feet or below Elevation 520 feet.

The theoretical intersection between Fault A and Soft Seam B occurs beneath Monolith 1. However, because Soft Seam B reportedly does not extend above an elevation of 680 feet, it is unlikely that these structures form a kinematically admissible rock wedge (Stone & Webster, 1960b). An objective of the geologic exploration program of boreholes BH-401, BH-402, and BH-403 was to ascertain the location and orientation of Soft Seam B. Soft Seam B was not intercepted in any of these boreholes and supports the conclusion from Stone & Webster that Soft Seam B does not extend below Elevation 520 feet and is in fact of limited persistence. A stereonet showing the concentration of minor structure in the right abutment, and the great circles and poles to the plane of Fault A and Soft Seam B are shown in Exhibit 10-2. This stereonet presents poles to the plane in a lower hemisphere equal-angle, polar projection.

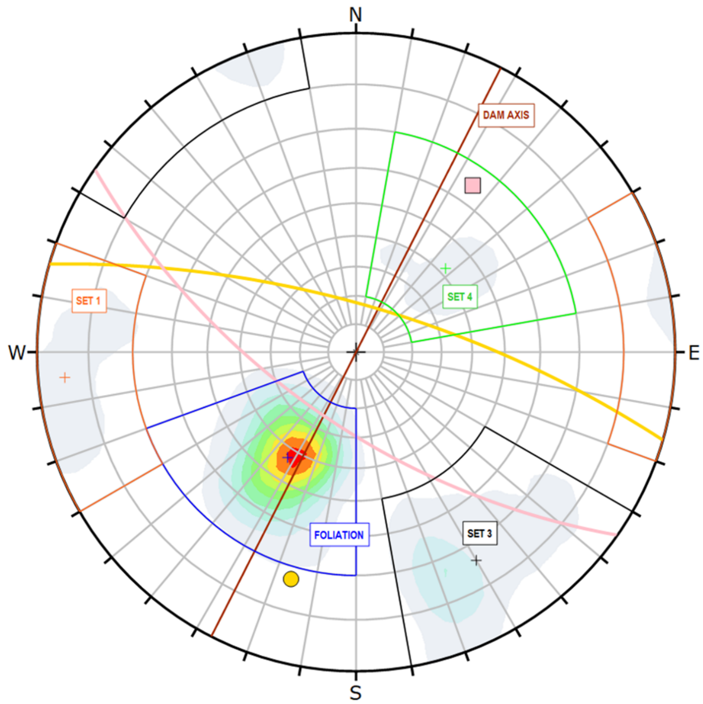

Symbol	LOCATION	Quantity
(yellow circle)	Fault A	1
(pink square)	Soft Seam B	1
	Others	2492

	Color	Dip	Dip Direction	Label
		User Planes		
4		90	297	Dam Axis
5		73	16	Fault A
6		65	215	Soft Seam B
		Mean Set Planes		
6m		42	227	Joint Set 4
8m		43	33	Foliation
9m		85	85	Joint Set 1
10m		74	330	Joint Set 3

Plot Mode	Pole Vectors
Vector Count	2494 (2494 Entries)
Hemisphere	Lower
Projection	Equal Angle

Exhibit 10-2: Lower Hemisphere Equal-Angle Polar Projection Showing Concentration of Minor Structure, and Great Circles and Poles to the Plane for Fault A and Soft Seam B

10.2.2 Monoliths 4 and 5

10.2.2.1 Evaluation of Historical Photographs, Reports, Downhole Videos, and Borings

From our evaluation of historical photographs, previous reports, downhole camera videos, and borings, no kinematically admissible rock wedges formed by the intersection of major structures were identified. Historical photographs lacked sufficient detail and orientation to identify major structural features beyond what was presented in previous reports. Review of downhole camera drains did not show the presence of any offsets or displacements in existing drain holes. An apparent soft seam was observed in B5-D3 that supports the presence of Soft Seam C.

10.2.2.2 Evaluation of Additional Borings, Instrumentation, and Major Structure

The following discussion pertains to PFMs N-UB-2C, F-UB-2C, and S-UB-2C. Two (2) major structures exist in the vicinity of Monoliths 4 and 5. These structures, with known orientations, were evaluated for the potential to form a kinematically admissible wedge. The two (2) major structures are Soft Seam C and a previously unidentified structure occupying the trough under Monolith 4, which is referred to as the Mylonite Zone. Soft

Seam C has a similar orientation to Fault A and crosses the dam foundation under Monoliths 4, 5, and 6. Soft Seam C strikes in proximity to the downslope edge of a trough under Monoliths 4 and 5. The trough is reported in construction-era documents as an area of soil or soft rock in Monoliths 4 and 5 that extends from approximately 480 to 500 feet in elevation (Stone & Webster, 1960b). Construction photographs and discussions in the Stone & Webster (1960b) report show the material there being excavated to sound rock and backfilled with concrete. A potential splay, or remnant portion, of the previously excavated Soft Seam C, and all that remains, was observed in boring IN-0500 from approximately 86 to 105 feet. Soft Seam C, with an estimated orientation of 83/054 degrees, is expressed as a mylonitic phyllite through this range. Manual inclinometer readings for IN-0500 do not indicate any displacement (Appendix K).

The Mylonite Zone was observed in BH-401 from approximately 17 feet down to a depth of 73 feet and in BH-402 from approximately 48 feet to the bottom of the boring at 153 feet. The Mylonite Zone occupies Monolith 4, with an approximate orientation of 59/028 degrees, and lines up with a regional structure observed in the lidar (Exhibit 6-7).
Exhibit 10-3 shows the concentration of minor structure in the right abutment, and the great circles and poles to the plane of Soft Seam C and the Mylonitic Zone.

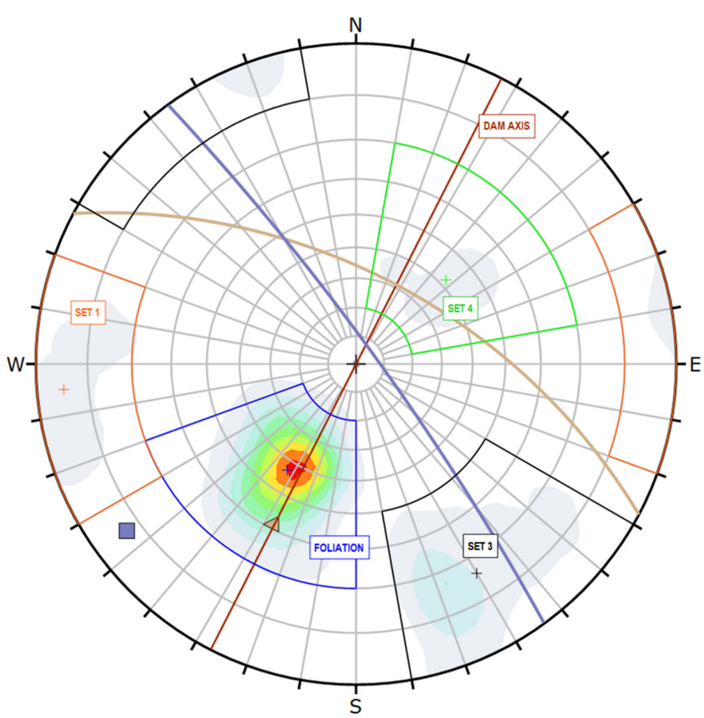

Symbol	LOCATION	Quantity
	Mylonite Zone	1
	Soft Seam C	1
	Others	2492

	Color	Dip	Dip Direction	Label
		User Planes		
4		90	297	Dam Axis
5		59	28	Mylonite Zone
6		83	54	Soft Seam C
		Mean Set Planes		
6m		42	227	Joint Set 4
8m		43	33	Foliation
9m		85	85	Joint Set 1
10m		74	330	Joint Set 3

Plot Mode	Pole Vectors
Vector Count	2494 (2494 Entries)
Hemisphere	Lower
Projection	Equal Angle

Exhibit 10-3: Lower Hemisphere Equal-Angle Polar Projection Showing Concentration of Minor Structure, and Great Circles and Poles to the Plane for Soft Seam C and the Mylonitic Zone

As presented in Exhibit 10-3, the major structure Soft Seam C and the Phyllite Zone are consistent with the general orientation of the foliation and do not form a kinematically admissible block of rock under the foundation of the dam. The wedge formed by these two (2) major structures has a favorable trend/plunge of 349/52 degrees and does not daylight downstream of the dam. This interpretation that a kinematically admissible wedge does not exist under Monoliths 4 and 5 supports listing PFMs N-UB-2C, F-UB-2C, and S-UB-2C as Category IV.

10.2.3 Monoliths 6 through 10

10.2.3.1 Evaluation of Historical Photographs, Reports, Downhole Videos, Additional Borings, and Instrumentation

The following discussion pertains to PFMs N-UB-2B, F-UB-2B, and S-UB-2B. From the evaluation of previous reports, historical photographs, downhole camera videos, and the recent boring exploration program, a potential kinematically admissible rock wedge has been inferred. An instrumentation program is currently in place to monitor displacements to assess specific depth ranges and zones of deformation, magnitudes of displacement, and the vector of movement, if any are occurring.

Stone & Webster (1963) observed that Monolith 10 had moved down relative to Monolith 9 by approximately 0.3 inch, and Monolith 9 had moved downstream relative to Monolith 8 by approximately 0.2 inch. During a review of downhole drain videos, offsets were observed in five (5) drain holes—B7-D1, B7-D2, B9-D2, B10-D1, and B10-D2—dating to the original construction of the dam and SD8-1 installed in 1963. These offsets in Monoliths 7, 8, 9, and 10 are shown in Appendix J, Figure J-1 (B7-D1, 41.5 feet; B7-D2, 23.2 feet; SD8-1, 24.5 feet; B9-D2, 32.5 feet; B10-D1, 29.5 feet) and Figure J-2 (B10-D2, 29 feet).

No offsets in either the downstream direction or parallel to the axis of the dam were observed in the additional drain holes drilled in 1963 to reduce high uplift pressures within Monoliths 7, 8, 9, and 10, except drain hole SD8-1; however, fracture zones were observed in several zones within these drains. The appearance of offset in only one drain hole, SD8-1, may indicate that the majority of displacement within Monoliths 6 through 10 primarily occurred prior to the drilling of these additional drain holes.

10.2.3.2 Evaluation of Major and Minor Structure

Two (2) major structures exist in the vicinity of Monoliths 6, 7, 8, 9, and 10: Soft Seam D and Block 10 Deformation Zone. Stone & Webster (1960b) identified Soft Seam D in the foundation during construction and in grout holes. Soft Seam D has an orientation of 83/162 degrees and crosses the dam foundation in Monoliths 6, 7, and 8. The dip direction of Soft

Seam D was determined based on the apparent dip of this structure identified in the "Report on Geology of Dam Site Record of Grout Curtain and Subsurface Drains" (Stone & Webster, 1960b) and on the trend of an interpreted extension of the Anderson Creek Fault (Exhibit 6-8). As discussed previously, this interpretation of the Anderson Creek Fault corresponds to a regional lineament observed in the lidar, the trend of the tailrace channel, and the apparent dip estimated by grout hole intersections (Drawing C-02). Block 10 Deformation Zone, with a modeled orientation of 53/047 degrees, was observed in borings IN-1000 and EX-1000. Similar to Soft Seam D, the dip direction was determined based on the trend of a similarly oriented regional lineament observed in bathymetry and the apparent dip estimated from EX-1000 and IN-1000. These two (2) major structures are displayed in Drawings C-01 and C-02, plan view and profile of the modeled structure under Upper Baker Dam.

A kinematic analysis of Block 10 Deformation Zone and Soft Seam D was performed to evaluate whether these two structures formed a kinematically admissible wedge. The lower hemisphere, equal-angle, polar projection stereonet showing the great circles and poles to the plane of Block 10 Deformation Zone, Soft Seam D, Fault U1, and the Block 6-10 Discontinuity used for the analysis is presented as Exhibit 10-4. The structure formed by the intersection of Soft Seam D and the Block 10 Deformation Zone is a steeply upstream-dipping wedge with a trend/plunge of 80/048 degrees. This wedge daylights underneath Monoliths 6, 7, 8, 9, and 10; therefore, this wedge is not admissible because it is confined by the dam.

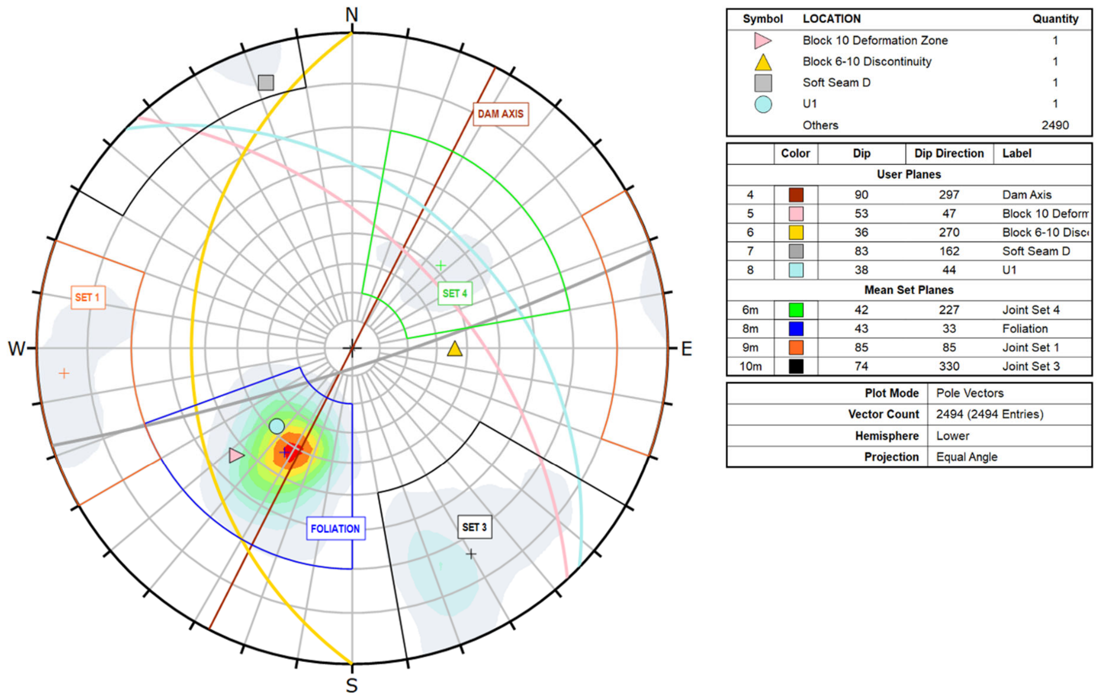

Exhibit 10-4: Lower Hemisphere Equal-Angle Polar Projection Showing Concentration of Minor Structure, and Great Circles and Poles to the Plane for Soft Seam D, the Block 10 Deformation Zone, the U1 Fault, and the Block 6-10 Discontinuity

In addition to evaluating the major structure in the vicinity of Monoliths 6, 7, 8, 9, and 10, a comparison of structure connecting the observed offsets in drain holes and structures observed in EX-1000, IN-1000, EX-0900, and IN-0900 indicates that the structure falls within Joint Set 4, has a modeled orientation of 36/270 degrees, and is furthermore referred to as the Block 6-10 Discontinuity.

10.2.3.3 Proposed Rock Wedge

As discussed above, the proposed rock wedge under Monoliths 6, 7, 8, 9, and 10 is formed by a combination of major structure, Block 10 Deformation Zone and Soft Seam D, and apparent movement along a highly persistent minor structure with an orientation similar to Joint Set 4. The current interpretation is that sliding of the foundation block along the Block 6-10 Discontinuity is bounded by Soft Seam D and the Block 10 Deformation Zone. The block geometry is presented below in Exhibit 10-5, Exhibit 10-6, and Drawings C-01 and C-02. Block 6-10 Discontinuity has an apparent dip parallel to the axis of the dam of about 21 degrees and an apparent dip perpendicular to the axis of the dam of about 34 degrees. The trend/plunge of the wedge formed by Block 6-10 Discontinuity, the Block 10 Deformation Zone, and Soft Seam D is 80/048 degrees. The current interpretation of historic displacement is that the rock wedge sliding along the Block 6-10 Discontinuity moved downstream as it compressed into Soft Seam D and the Block 10 Deformation Zone. As shown in Exhibit 10-5 and Exhibit 10-6, the block formed by Block 6-10 Discontinuity, Soft Seam D, and the Block 10 Deformation Zone does not daylight downstream and is fully located under the dam.

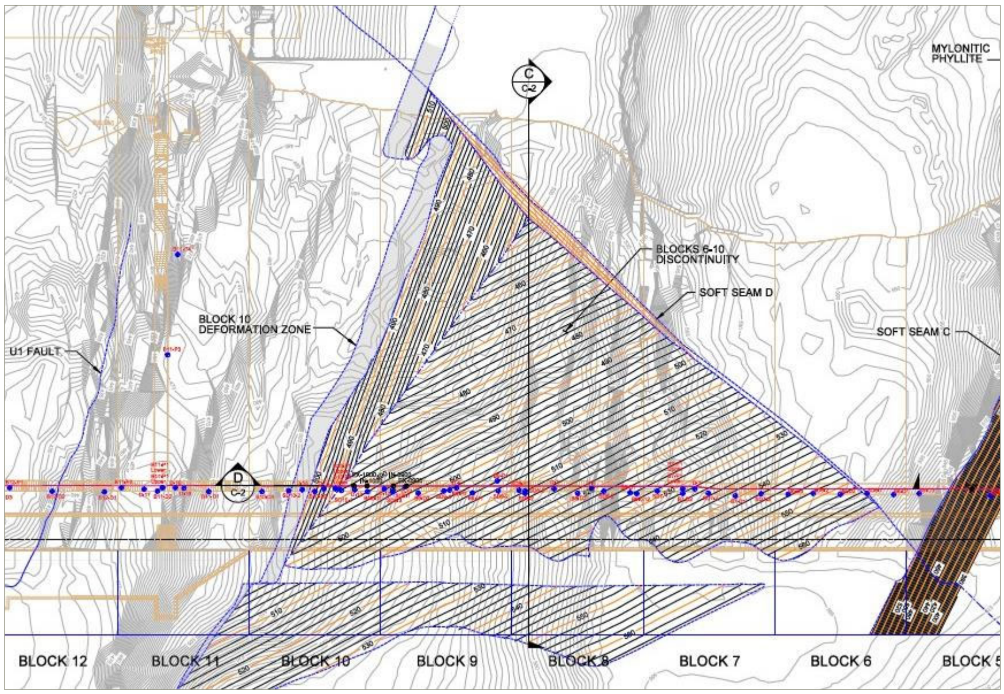

Exhibit 10-5: Plan View Showing Soft Seam D, Block 10 Deformation Zone, and the Block 6-10 Discontinuity

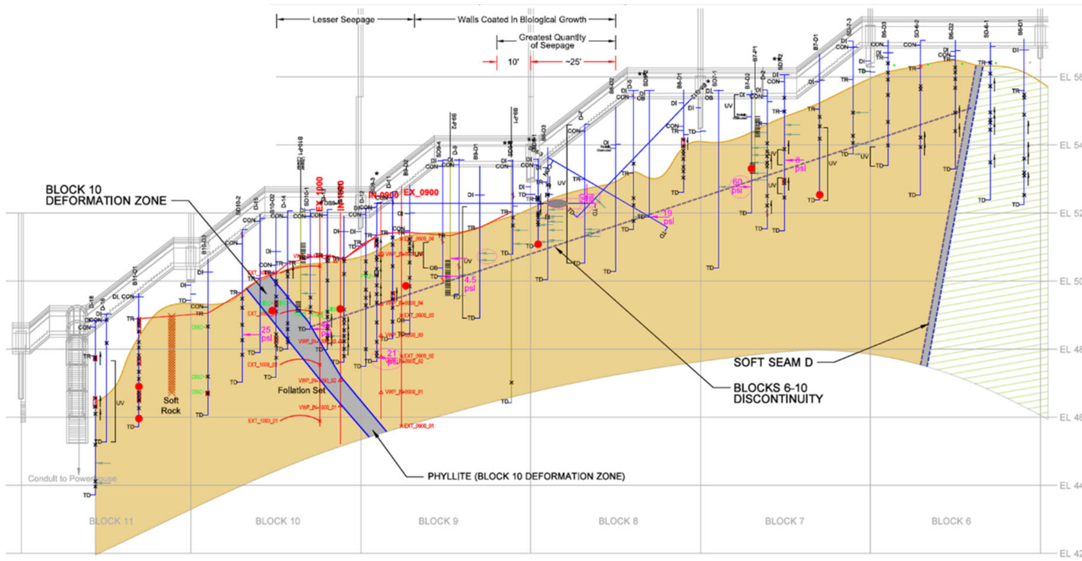

Exhibit 10-6: Section Showing Soft Seam D, Block 10 Deformation Zone, and the Block 6-10 Discontinuity

10.2.3.4 Review of Instrumentation Data

Review of manual inclinometer data and piezometer data indicates that recent displacements observed in IN-1000 at Elevation 491 feet, in EX-0900 between anchors 3 and 4, and in EX-1000 between anchors 2 and 3 are elastic and directly correlated to groundwater elevation measured in piezometer data (B7-P1, B11-P1 Lower, and IN-0900-4) and to reservoir elevation. The relationship between elastic displacements in IN-1000, and piezometer data and reservoir elevation is shown in Exhibit 10-7.

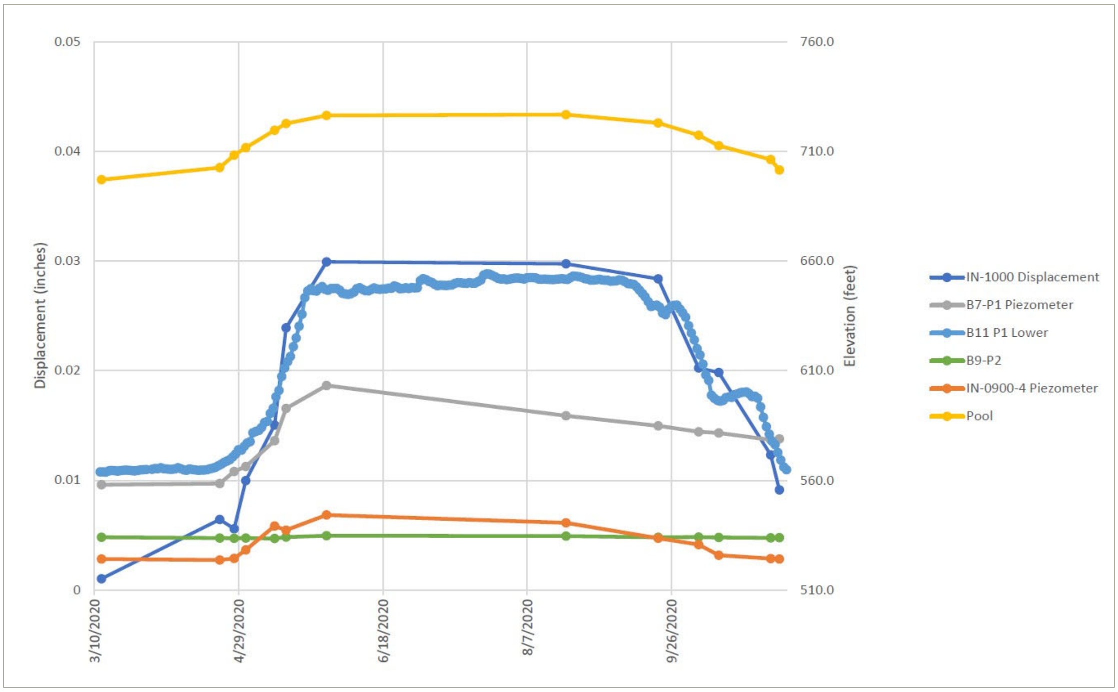

Exhibit 10-7: Elastic Displacement IN-1000 (Elevation 491 Feet) versus Selected Piezometers and Pool Elevation

Previously measured hydrostatic pressures in selected piezometers (B7-P1 Lower, VWP_IN-0900-4, and B11-P1 Lower) appear to have a direct connection to the reservoir. These piezometers are positioned or have a screened interval that cross, or are in proximity to, the Block 6-10 Discontinuity. In past years, as the Baker Lake pool is raised in the spring, the phreatic surface in B7-P1 Lower approaches Elevation 600 and remains high for a 2- to 3-week period and then drops to approximately Elevation 560 to 570 feet. However, after mid-May 2020 the phreatic surface in B7-P1 remained high, fluctuating between Elevation 595 and 609 feet, possibly indicating a continued connection to the reservoir and an opening of seepage pathway along the Block 6-10 Discontinuity. Exhibit 10-8 presents a section in Monolith 8 drawn perpendicular to the axis of the dam, which shows that Block 6-10 Discontinuity projects into the reservoir.

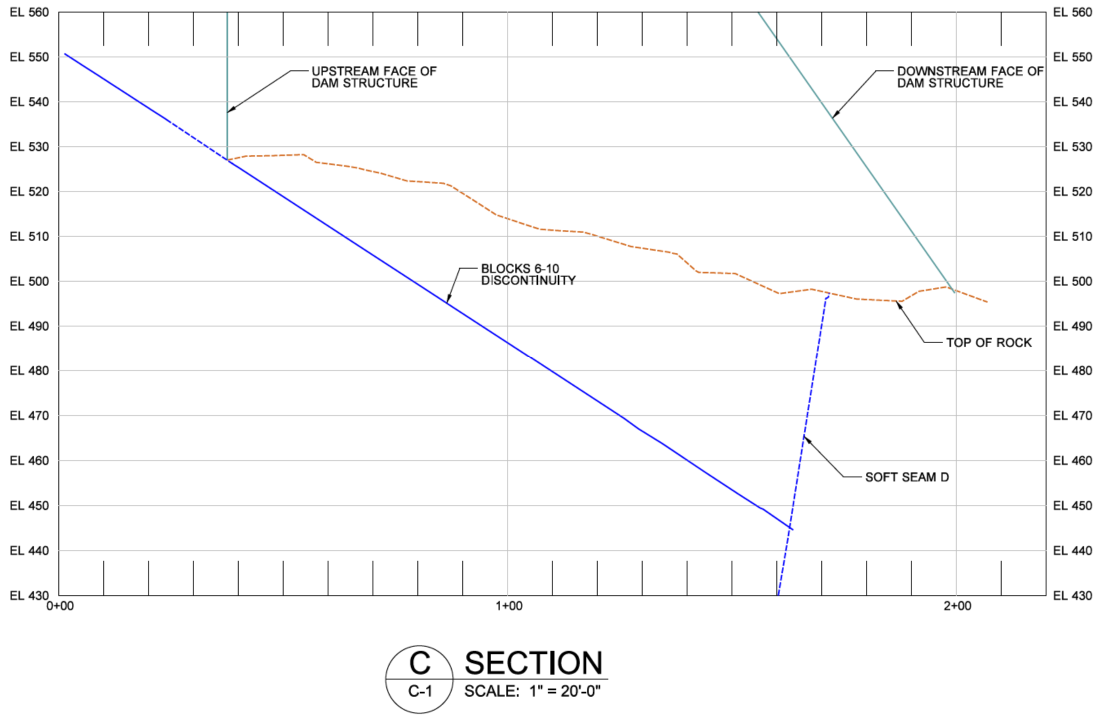

Exhibit 10-8: Section Perpendicular to the Dam Axis in Monolith 8 Showing the Apparent Dip of the Block 6-10 Discontinuity and Soft Seam D; Section is from Drawing C-02

In early 1963, it was recognized that a discontinuity projected into the reservoir and, in addition to adding more drain holes, a cinder blanket was constructed upstream of the dam that extended from the midpoint of Monolith 8 to the midpoint of Monolith 10. An illustration showing the cinder blanket relative to the monoliths is shown in Exhibit 10-9. Note that the cinder blanket does not extend into Monoliths 6 and 7, and does not cover the full projection of the Block 6-10 Discontinuity into the reservoir.

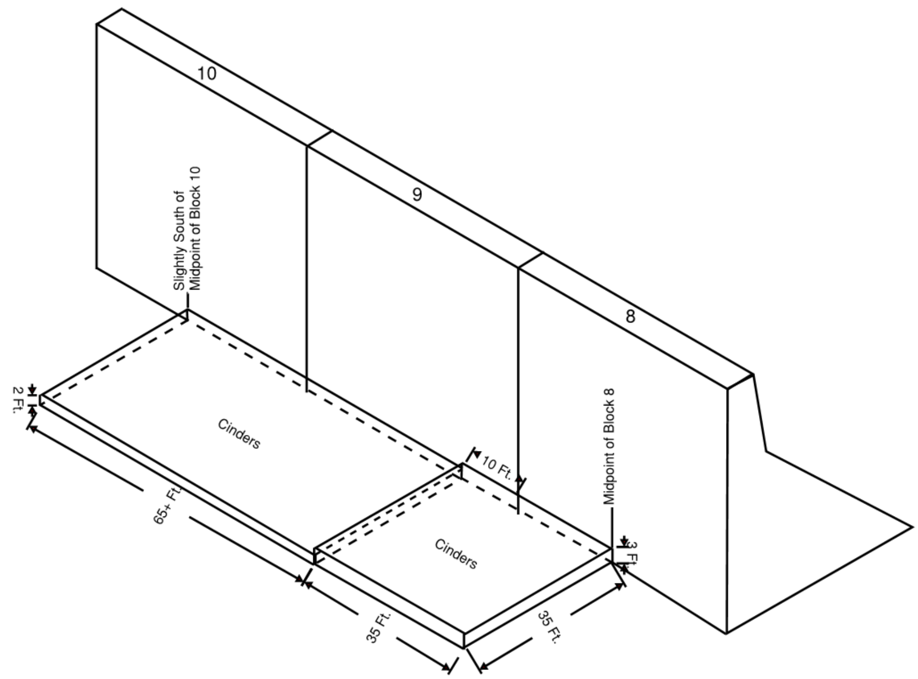

Exhibit 10-9: Illustration Showing the Coverage of the Cinder Blanket Installed Upstream of the Dam in 1963

10.2.3.5 Offsets in Monolith 11

During a recent review of drain hole videos, offsets were also observed in drain B11-D1 at depths of 27.6 and 37 feet (Shannon & Wilson, 2020a). Photographs of the offsets are shown in Appendix J, Figure J-2 (B11-D1, 27.6 feet; B11-D1, 37 feet). The locations of the offsets are also presented in Exhibit 10-6. The current interpretation is that sliding along the Block 6-10 Discontinuity is constrained between the Block 10 Deformation Zone and Soft Seam D. However, offsets in Drain B11-D1—in particular, the offset at 27.6 feet which appears to line up with the apparent dip of the Block 6-10 Discontinuity—suggest that the block may extend under Monolith 11. If the Block 6-10 Discontinuity extends into Monolith 11, then the U1 Fault may form the left plane of the wedge rather than the Block 10 Deformation Zone. In this case, the wedge will have similar geometry to the wedge formed by Soft Seam D, the Block 10 Deformation Zone, and the Block 6-10 Discontinuity, in that it will not daylight downstream from the dam and will almost be completely contained below the footprint of the dam. The extension of the Block 6-10 Discontinuity to the U1 Fault is illustrated in Exhibit 6-5.

10.2.4 Monoliths 17, 18, and 19

10.2.4.1 Evaluation of Historical Photographs, Reports, Downhole Videos, Additional Borings, and Instrumentation

The following discussion pertains to PFMs N-UB-2A, F-UB-2A, and S-UB-2A. From the evaluation of previous reports, historical photographs, downhole camera videos, and the recent boring exploration program, a potential kinematically admissible rock wedge has been inferred. An instrumentation program is currently in place that monitors displacements to assess specific depth ranges and zones of deformation, magnitudes of displacement, and the vector of movement, if any are occurring. The monitoring data collected between 2017 and 2020 from the extensometers and the inclinometers installed in 2016 indicate that the measured displacements are elastic and are in response to loading and unloading from the reservoir.

Stone & Webster (1963) observed that Monolith 18 had moved downstream relative to Monolith 19 by approximately 0.25 inch. Joint meters, across the monolith contraction joints, and extensometers were installed in the late 1960s to monitor any continued displacements of Monolith 18. Two (2) extensometers were anchored to the rock under Monolith 18 at an approximate depth of five (5) feet below the concrete-to rock-interface, and two (2) extensometers were anchored to the rock under Monolith 19 at an approximate depth of 80 feet below the concrete-to-rock interface. Extensometer readings indicate no movement relative to the anchor depths. Subsequent displacement measured at the contraction joint between Monolith 18 and 19 in the late 1960s indicated that the total block movement was on the order of approximately 0.5 inch. Evidence of continued downstream movement of Monolith 18 relative to 19, since the late 1960s, was considered to be inconclusive based on the extensometers' and joint meters' monitoring data prior to engineering analyses performed in 2015 and an analysis of Monoliths 18/19 movements by Hatch. Prior to 2008—when offsets were observed in drain holes—the exact location of movement was not known other than it occurred between five (5) and 80 feet below the concrete-to-rock interface.

During a review of videos obtained from a drain hole inspection in 2008, offsets were observed in two (2) drain holes, B18-D2 and B18-D3 (Shannon & Wilson, 2008). These drains date back to the original construction of the dam, and the offsets are most likely associated with the 1963 downstream movement of Monolith 18 relative to Monolith 19. Photographs of the offsets in Monolith 18 are shown in Appendix J, Figure J-2 (B18-D2, 36 feet), and Figure J-3 (B18-D3, 31.2 feet).

10.2.4.2 Proposed Rock Wedge

No offsets in either the downstream direction or parallel to the axis of the dam were observed in the other drains of Monoliths 17, 18, or 19. The discrete offsets identified in the two (2) borings and the highly fractured zones in two (2) adjacent borings, all located in Monolith 18, combine to form a plane with an apparent dip of 45 degrees and a surface approximately parallel to foliation. The apparent dip of this structure is presented in Exhibit 10-10.

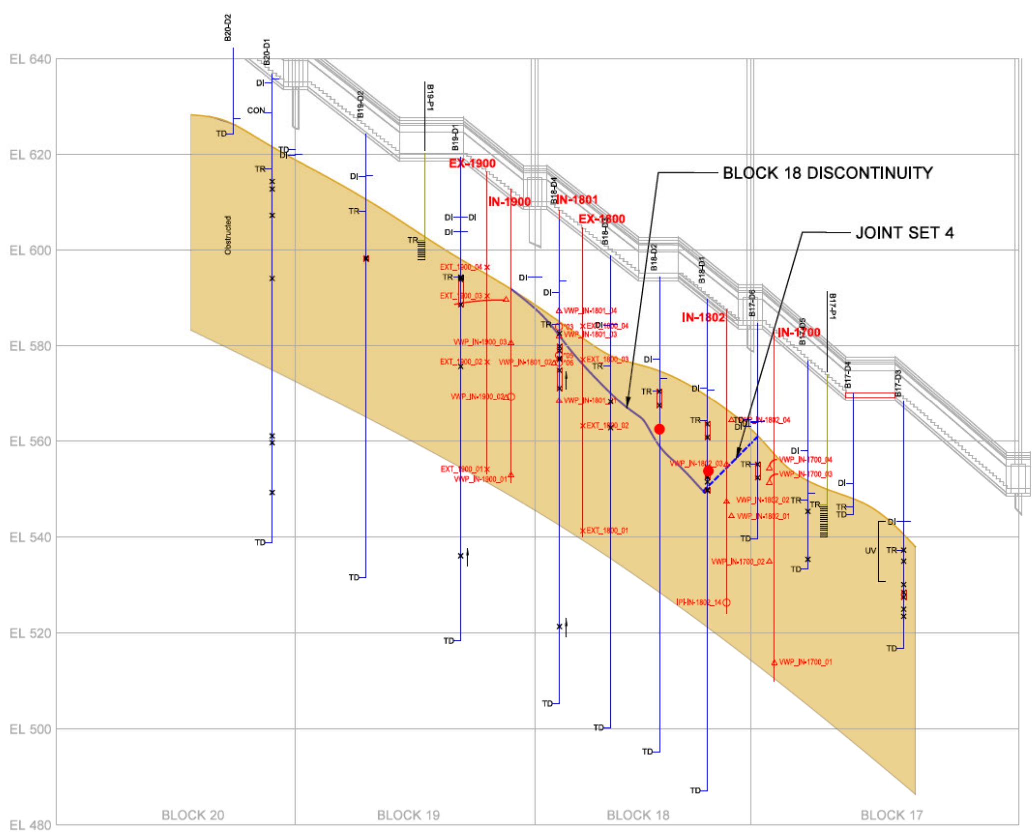

Exhibit 10-10: Cross Section Along Gallery of Monolith 18 Showing Inferred Slide Plane and Features Observed in Drain Review; Red Dots Indicate Observed Offsets in Drains

For movement to occur, this surface would either have to daylight downstream or combine with one or more discontinuities to daylight or allow movement downstream. Through an iterative process of plotting the surface trace of valid foliation orientations, an orientation that aligns with the crack development in Monoliths 18 and 19 was observed. This particular foliation plane was selected for modeling by Hatch in their 3D numerical model;

while it is not an exact match to the model, the geometry of the block generally satisfies both the observations in the drain holes and the cracking in the concrete monoliths (Hatch, 2015). Furthermore, it was determined that in the direction of Monolith 18 downstream movement, the sliding surface dips in a downstream direction and will therefore not daylight in the slope downstream in proximity to the dam.

Numerous steeply dipping and persistent joints, generally corresponding to Joint Set 1 and Joint Set 3, are variously described as mud seams or cracks where grout return was observed during construction of the dam. While these joints are too steeply dipping to satisfy daylighting downstream, it is our current understanding that these open joints, and possibly the U2 Fault, could compress to allow movement of the rock wedge along foliation in a general downstream direction. The U2 Fault and plan view of the inferred rock wedge is presented in Exhibit 10-11. A section oriented perpendicular to the axis of the dam is presented in Exhibit 10-12. The monitoring data collected between 2017 and 2020 from the extensometers and the inclinometers installed in 2016 do not indicate permanent, ongoing displacement under Monoliths 18 and 19. This is similar to a statement made by Hatch that "the wedge is locked in place and no further deformation is expected" (Hatch, 2015). Hatch states their model should be "considered approximate given the uncertainty of extent of wedges under these blocks [monoliths]" and recommends continued monitoring of displacement using high-precision instruments (Hatch, 2015). The lower hemisphere, equal-angle, polar projection stereonet showing the great circles and poles to the plane of the Block 18 Discontinuity and Fault U2 used for the analysis is presented as Exhibit 10-13.

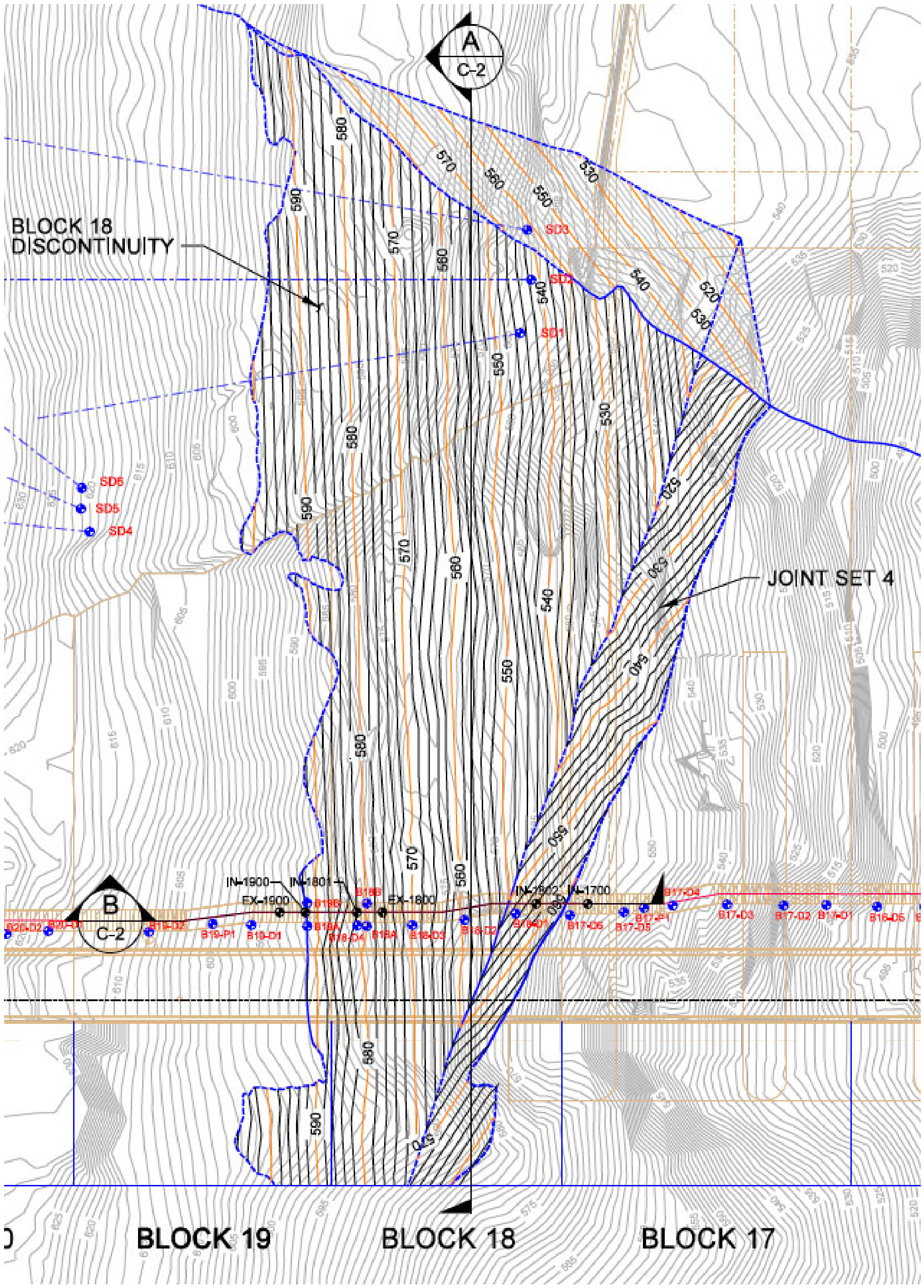

Exhibit 10-11: Plan View of Extent of Inferred Rock Wedge under Monolith 18; Green Lines are Topographic Expression of Foliation Slip Surface; Purple Lines Represent the Side-Release Plane Along J4

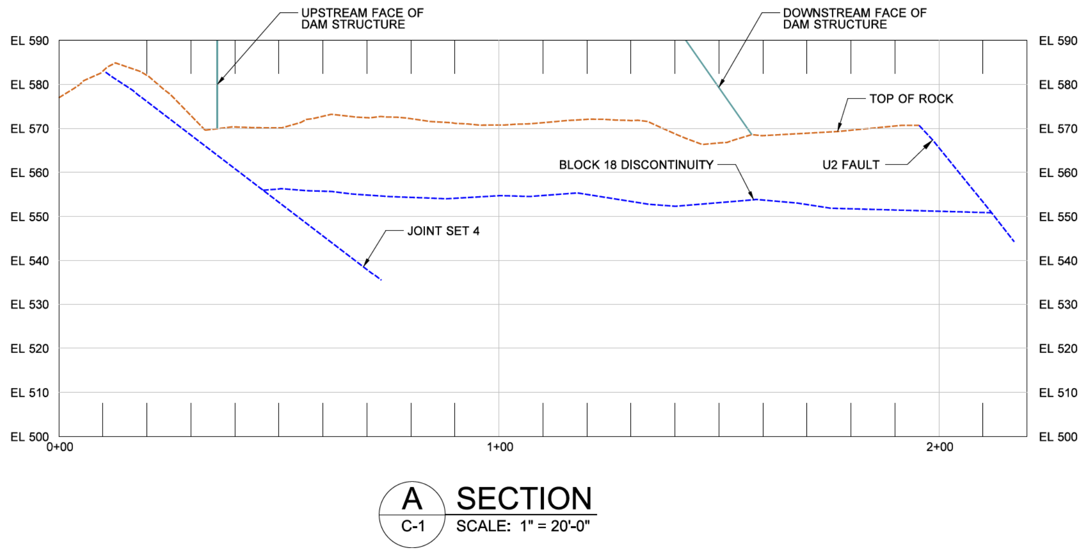

Exhibit 10-12: Cross Section along C-C' Showing Slip Surface of Foliation Plane and Vertical to Near-Vertical Joints of J1/J3

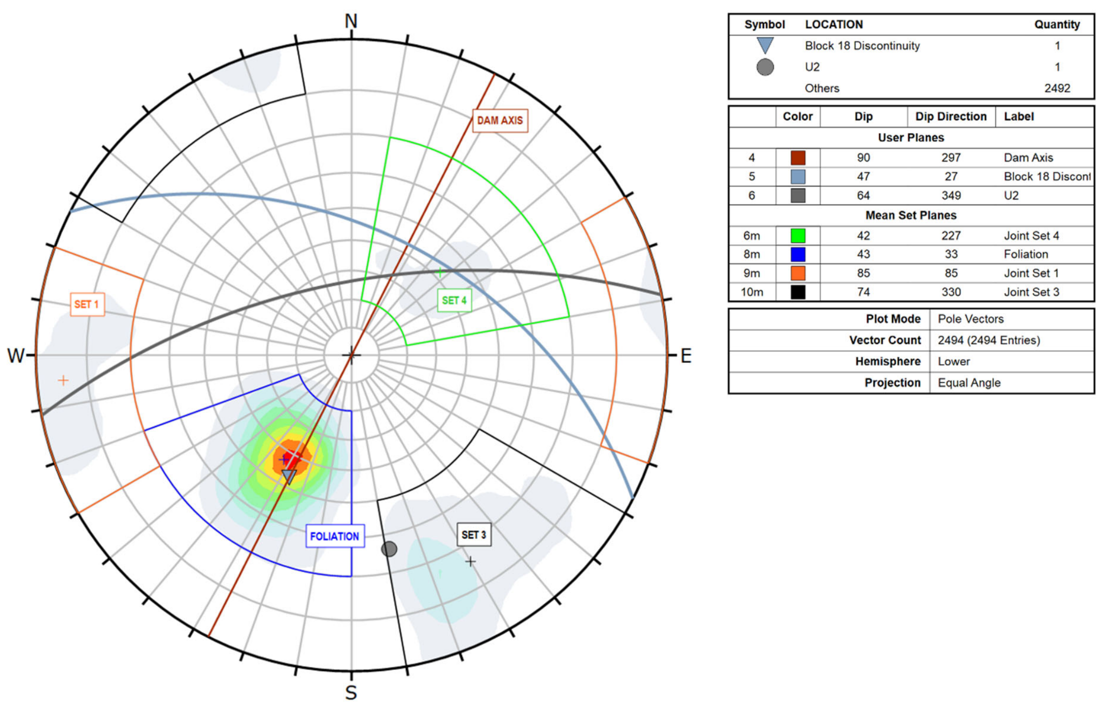

Exhibit 10-13: Lower Hemisphere Equal-Angle Polar Projection Showing Concentration of Minor Structure, and Great Circles and Poles to the Plane for Block 18 Discontinuity and U2 Fault

10.2.5 Monoliths 20 and 21

During a recent review of drain hole videos, offsets were also observed in drain B20-D4 at a depth of 84 feet and in B21-D1 at a depth of 77 feet (Shannon & Wilson, 2020a). Photographs of the offsets are shown in Appendix J, Figure J-3. The locations of the offsets are also presented in Drawing C-02. Displacement of Monolith 20 relative to Monolith 21 was reported to be of similar magnitude to the displacement measured in Monoliths 18 and 19 (Stone & Webster, 1972). Offsets observed in B20-D1 and B21-D4 may be related to this historic movement. The apparent dip of a surface drawn through the offsets is approximately 50 degrees, which is within the range of dip of foliation. Offsets are located between 20 and 23 feet below the concrete-to-rock interface. Joint meters installed at the contraction joint between Monoliths 20 and 21 show elastic movement related to reservoir and temperature fluctuations, but no permanent displacement has been measured in the joint meters since April 2015.

10.2.6 Spillway Slope

PFMs S-UB-3, F-UB-3A, and F-UB-3B identified in the PFMA identified a kinematically admissible plane shear sliding failure mode of the foliation in the spillway slope (HDR, 2019). To evaluate these PFMs, we performed kinematic analyses of the spillway slope using the discontinuity data set described in Section 7.1.

The results of the plane shear sliding, flexural toppling, and wedge sliding kinematic analyses of the spillway slope are presented as Exhibit 10-14, Exhibit 10-15, and Exhibit 10-16, respectively. Results of the kinematic analyses are displayed on lower-hemisphere, equal-angle, polar projection stereonets where structure orientations are plotted as poles to the planes. The orientation of a kinematically admissible failure is illustrated as the red-shaded region.

The results of the kinematic analyses demonstrate that, while both the plane shear and wedge sliding modes of failure could occur on the spillway slope, the plane shear mode of failure is the dominant failure mode. Historic photographs of the spillway excavation were reviewed to identify a major geologic structure that could provide lateral release planes or back release planes resulting in sliding along foliation in plane shear orientation. Structures identified in historic photographs and their relationship to existing joint sets are displayed in Exhibit 7-2. Plane shear failures have also occurred previously along foliation immediately downstream of the spillway.

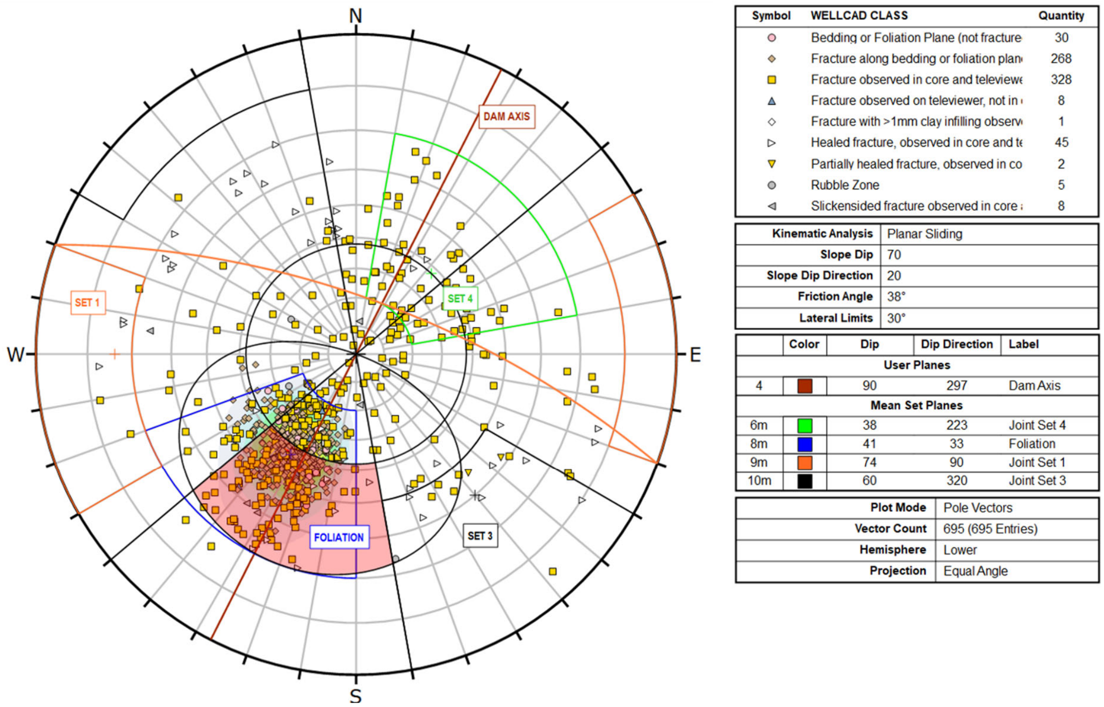

Exhibit 10-14: Plane Shear Sliding Kinematic Analysis of the Spillway Slope

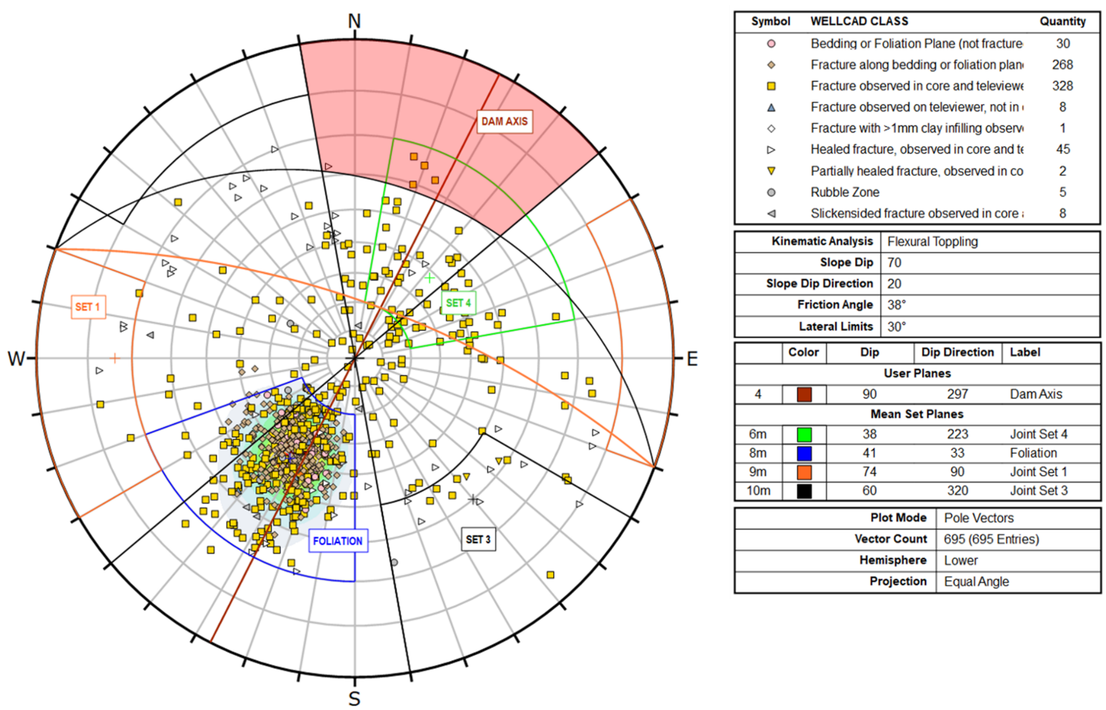

Exhibit 10-15: Flexural Toppling Kinematic Analysis of the Spillway Slope

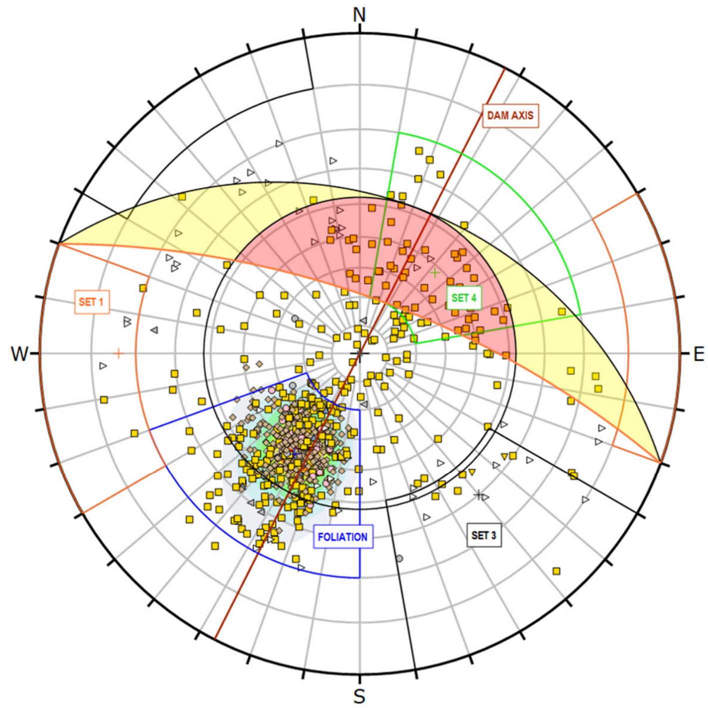

Symbol	WELLCAD CLASS	Quantity
○	Bedding or Foliation Plane (not fractured)	30
◇	Fracture along bedding or foliation plane,	268
□	Fracture observed in core and televiewer	328
△	Fracture observed on televiewer, not in cc	8
◇	Fracture with >1mm clay infilling observec	1
▷	Healed fracture, observed in core and tele	45
▽	Partially healed fracture, observed in core	2
○	Rubble Zone	5
◁	Slickensided fracture observed in core an	8

Kinematic Analysis	Wedge Sliding
Slope Dip	70
Slope Dip Direction	20
Friction Angle	38°

	Color	Dip	Dip Direction	Label
User Planes				
4		90	297	Dam Axis
Mean Set Planes				
6m		38	223	Joint Set 4
8m		41	33	Foliation
9m		74	90	Joint Set 1
10m		60	320	Joint Set 3

Plot Mode	Pole Vectors
Vector Count	695 (695 Entries)
Hemisphere	Lower
Projection	Equal Angle

Exhibit 10-16: Wedge Sliding Kinematic Analysis of the Spillway Slope

10.3 Limit Equilibrium Analyses of Spillway Support

10.3.1 General

To address the identified PFM of plane shear sliding of the spillway along a foliation surface that daylights in the foundation below Monoliths 16/17 (PFMs S-UB-3 and F-UB-3B described in Section 1.4.34), we reviewed historic photographs of the spillway excavation to identify a major geologic structure that could provide lateral release planes or back release planes that result in sliding along foliation in plane shear orientation. Structures identified in historic photographs and their relationship to existing joint sets are displayed in Exhibit 7-2. Plane shear failures have occurred previously along foliation immediately downstream of the spillway.

We performed two-dimensional (2D) limit equilibrium stability analyses using Slide (v. 9.023) by Rocscience (2022). The spillway slope—a steep slope parallel to the centerline of the spillway—presents the appropriate geometry for 2D stability evaluation perpendicular to the centerline of the spillway. Additionally, 2D evaluation of the plane shear failure mode does not consider side-release planes and their respective contributions to rock block stability; therefore, the most adverse plane shear condition is evaluated. Input-output files for each Slide slope stability analysis are provided in Appendix N.

In our kinematic analyses, we concluded the rock mass is unlikely to produce a circular failure in any of the slopes; thus, we employed non-circular failure surface searching methods in our models and constrained the inclination of the sliding planes between 35 and 45 degrees to simulate failures along foliation planes. We selected the generalized limit equilibrium (GLE)/Morgenstern-Price (Morgenstern) as the vertical slice limit equilibrium analysis method (Abramson, Lee, Sharma, and Boyce, 2001); the GLE/Morgenstern method of slope stability analysis was selected because it accommodates non-circular failure surfaces and is generally considered the most robust limit equilibrium method, as it resolves both force and moment vertical slice equilibrium.

No distress or movement of the concrete facing or spillway has been documented. An inspection performed by Vertical Access in 2015 concluded, "The concrete surfaces of the upper Baker Dam Spillway are in very good condition. There is narrow cracking at the ogee face and training walls, some with associated efflorescence, but none of significant depth" (Vertical Access, 2015). Analyses of spillway stability included several conditions such as:

- Existing Conditions;
- Rock Anchor Support Case (1 ¾-inch Anchors):
  - Static Analysis under Usual Loading Conditions,
  - Static Analysis under PMF Unusual Loading Conditions,
  - Pseudo-Static Analysis of 84th percentile Maximum Credible Earthquake (MCE) (Extreme Loading Conditions),
  - Static Analysis using Post-Earthquake Material Properties;
- Rock Anchor Support Case (8 Strand Anchors):
  - Static Analysis under Usual Loading Conditions,
  - Static Analysis under PMF Unusual Loading Conditions,
  - Pseudo-Static Analysis of 84th percentile MCE (Extreme Loading Conditions),
  - Static Analysis using Post-Earthquake Material Properties;
- Grouted Rock Buttress Support Case (Global Failure with Dowel Supports at the base of the Grouted Rock Buttress):
  - Static Analysis under Usual Loading Conditions,
  - Static Analysis under PMF Unusual Loading Conditions,
  - Pseudo-Static Analysis of 84th percentile MCE (Extreme Loading Conditions),
  - Static Analysis using Post-Earthquake Material Properties.

10.3.2 Summary of Previous Limit Equilibrium Analyses

The previous limit equilibrium analyses of the spillway utilized laboratory testing that was initially selected to evaluate the behavior of the rockmass under the monoliths of the dam and an assumed phreatic surface based on surficial observations. The laboratory testing indicated a base friction angle for the rock mass on sawed surfaces that ranged from 15 to 34 degrees, with a mean friction angle of 26 degrees. Due to higher normal stresses used in previous laboratory testing, the resulting base friction angles from these tests range lower than those determined in later spillway testing. The normal stresses used in direct shear testing on samples collected from the spillway borings reflect the range of normal stresses acting along the slip surfaces in the spillway slope. The lower friction angle used in the original analyses (based on direct shear testing at higher normal stress) resulted in the requirement that, for the slope to have a factor of safety equal to 1.0, the shear strength along foliation incorporates rock bridging and scaled shear strength. The need to accept rock bridges in our interpretation of the shear strength properties was consistent with an interpretation of the rock mass at that time and because the factor of safety for existing conditions is not less than 1.0. Details of the scaled strength material properties previously used are described in subsequent sections. Exhibit 10-17 below presents a summary of FSs from previous limit equilibrium analyses using scaled strength properties.

Exhibit 10-17: Summary of Limit Equilibrium Analyses from Previous Limit Equilibrium Analyses using Scaled Strength Properties

Loading Condition	FS Criteria	Existing Conditions	Grouted Rock Buttress		Anchor-Supported
			Below Buttress	Above Buttress	
Usual	1.5	0.97	1.52	1.82	1.75
Unusual	1.3	NA	1.49	1.75	1.66
Pseudo-static	1.1	NA	1.12	1.30	1.11
Post-Earthquake	1.3	NA	1.35	1.37	1.46

All the previous analyses met the target factors of safety using a scaled strength property approach and using a phreatic surface in the slope based on observations and engineering judgment. However, because of the uncertainty related to the groundwater conditions, additional field investigations and analyses were performed to better define the phreatic surface and the impact on the stability of the spillway.

10.3.2.1 Scaled Strength

The formulas for scaled cohesion (c) and scaled friction angle (Φ) are based on an approximation of scaled strength property formulation (Jennings, 1970):

Scaled C = (%Rock Bridge) x Rock Mass Cohesion + (1-%Rock Bridge) x Joint Cohesion

Scaled Φ = tan-1{(%Rock Bridge x tan(Phi Rock Mass)) + (1-%Rock Bridge x tan(Phi Joint))}

The percent rock bridges depends on the length of the slide plane, the discontinuity persistence, and discontinuity spacing. Rock bridges are calculated as follows: discontinuity length and discontinuity spacing are determined by field mapping of the exposed slope. The number of steps, or rock bridges, is determined by dividing the length of the slide plane by the mean discontinuity length. The number of rock bridges is multiplied by the median discontinuity spacing, resulting in the length of intact rock that must be broken for failure to occur along the slide plane. The length of intact rock is divided by the slide plane length (and multiplied by 100) to calculate the percent rock bridges.

In the previous analyses for the existing static condition, the FS against sliding failure equal to approximately 1.0 (0.97) was achieved with foliation shear strength of 1,649 psf cohesion and a joint friction angle of 33 degrees, approximately equivalent to 5% rock bridges.

10.3.3 Limit Equilibrium Methodology

10.3.3.1 Modifications to Previous Analyses

In addition to installing vibrating wire piezometers to monitor groundwater conditions underneath the spillway, the additional geotechnical explorations enabled us to perform additional laboratory testing specific to the rockmass under the spillway and refine the material properties to reflect spillway specific stresses and properties. The direct shear testing normal stresses were lowered from a range of 50 to 300 psi conducted for the previous sample suite to a range of 25 to 100 psi to reflect the lower normal stress the spillway exerts on the rockmass. The reduction in normal stresses increased the frictional shear strength and as a result, scaled shear strength and rock bridges were no longer needed for the spillway to have an existing factor of safety of 1.0 under existing and historically observed conditions. These updated limit equilibrium (LE) analyses utilized frictional only shear strength along discontinuities to enable a comparison to the previously evaluated scaled strength material property models.

10.3.3.2 Design Criteria

The limit equilibrium analyses were performed according to the guidelines presented in the Geotechnical Design Memorandum GD-1, Rev. 1 – Spillway Support Analyses Criteria (Shannon & Wilson, 2022; Appendix M) with the following design criteria for factor of safety (FS):

- FS for Usual (Static) Loading Conditions greater than or equal to 1.5,
- FS for Unusual (Static, PMF) Loading Conditions greater than or equal to 1.3,
- FS for Post-Earthquake (Static) Loading Conditions greater than or equal to 1.3, and
- FS for Extreme (Pseudo-Static) Loading Conditions greater than or equal to 1.1.

10.3.3.3 Slope Geometry

The slope geometry evaluated is based on two (2) cross sections taken through the spillway slope, perpendicular to its axis, in the vicinity of the 2021 spillway borings: (1) Section 1 was taken through borings BH-16-1 and BH-17-1 from the toe of the slope at an approximate elevation of 430 feet to an elevation of approximately 630 feet, and (2) Section 2 was taken through borings BH-16-2 and BH-17-2 from the toe of the slope at an approximate elevation of 430 feet to an elevation of approximately 615 feet. The topography of these sections is based on surveying completed by Pacific Geomatics in December 2014 (Pacific Geomatics, 2014). A concrete facing was placed over the rock slope downslope of the spillway during construction. The thickness of this facing ranges from approximately five (5) to 20 feet, but it is not known if any rock bolts tie the concrete to the slope. The height of the spillway above the diversion channel invert ranges from about 110 to 115 feet. This surface has an average slope inclination of about 50 degrees, a maximum slope of about 70 degrees, and an average dip direction of 25 degrees, which is nearly parallel to the mean dip direction of the foliation. Because the dip of the foliation ranges from 15 to 60 degrees, and the slope inclination ranges from 50 to 70 degrees, a plane shear failure mode is kinematically admissible for all or a portion of the spillway width over the full range of foliation dip observed in outcrop.

10.3.3.4 Rock Mass Properties

As previously stated, we concluded in our kinematic analyses the rock mass is unlikely to produce a circular failure in any of the slopes; thus, we employed non-circular failure surface searching methods in our models and constrained the inclination of the sliding planes between approximately 30 and 45 degrees to simulate failures along foliation planes.

Additionally, we modeled the phyllite shear strength as an anisotropic strength comprised of two components: discontinuity shear strength and rock mass shear strength. Discontinuity shear strength was applied in the analyses as weak planes at inclinations of approximately 30, 35, 40, and 45 degrees. Specific foliation structures with dip inclinations greater than 45 degrees were observed within the geotechnical borings and modeled explicitly. The additional foliation surfaces with an inclination greater than 45 degrees were modeled due to forming a kinematically admissible rock block that daylights adjacent to or partially under the spillway. For all other inclinations, phyllite rock mass shear strength values were applied. Discontinuity shear strength with a joint friction angle of 48 degrees for phyllite was used when modeling usual (static), unusual (PMF), and extreme (pseudo-static) loading conditions. To model the slope with reduced foliation shear strength following an earthquake event (post-earthquake loading condition), a joint friction angle of 41 degrees for phyllite was applied to the model.

10.3.3.5 Seismic Loading Conditions

According to the Baker River Project Updated Deterministic Seismic Hazard Analysis, the appropriate ground motion for use in pseudo-static analyses of Upper Baker Dam is the 84th Percentile Maximum Credible Earthquake, with a peak ground acceleration (PGA) equal to 0.45 (Shannon & Wilson, 2020b). The horizontal seismic coefficient, k_h, for use in analyses is equal to two-thirds (2/3) of the PGA: 0.3 g (Kramer, 1996; Shannon & Wilson, 2022).

10.3.3.6 Groundwater Conditions

The piezometric head for each boring was selected to be used in the spillway slope analyses and stabilization design as the maximum groundwater elevation measured in any of the three (3) VWPs from December 14, 2021, through July 5, 2022. The design piezometric head between the two (2) measured groundwater elevation measurements in each boring was approximated based on engineering judgment and understanding of the site history of the spillway slope. Piezometric head levels in BH-17-1 and BH-17-2 indicated artesian groundwater pressures originating from upslope of the spillway structure; therefore, it modeled as a piezometric head as opposed to being modeled as a groundwater table. Each analysis was performed with the approximated piezometric surface based on measurements from the VWPs in the spillway borings.

10.3.3.7 Other Loading Conditions

In addition to the static and pseudo-static loading conditions, we evaluated a PMF (unusual) loading condition. In the case of the PMF, a full spill through the gates would yield an approximately 1,100 pounds per square foot (psf) distributed load across the width of the spillway (Falvey, 2019).

10.3.4 Existing Conditions Analysis

The initial input parameters for the existing conditions case were selected based on field observations of geologic mapping, core logging, laboratory testing of intact rock and concrete samples, and as-built drawings of the concrete spillway liner. This includes observations of the spillway and slope that show no signs of slope failure or distress in the spillway's concrete. Therefore, back-calculations were performed based on the available data and as presented in section 8 to evaluate the stability of the spillway under existing conditions and given the assumed groundwater conditions which are based on VWP measurements.

As illustrated in Exhibit 10-18, a static FS against sliding failure equal to approximately 1.0 (1.02) was achieved for Section 1 with a foliation shear strength of 0 cohesion and a joint friction angle of 48 degrees. As illustrated in Exhibit 10-19, a static FS against sliding failure equal to approximately 1.1 (1.11) was achieved for Section 2 with the same material properties. Existing condition model results and stability analysis reports from Slide (v. 9.023) by Rocscience are presented in Appendix N.

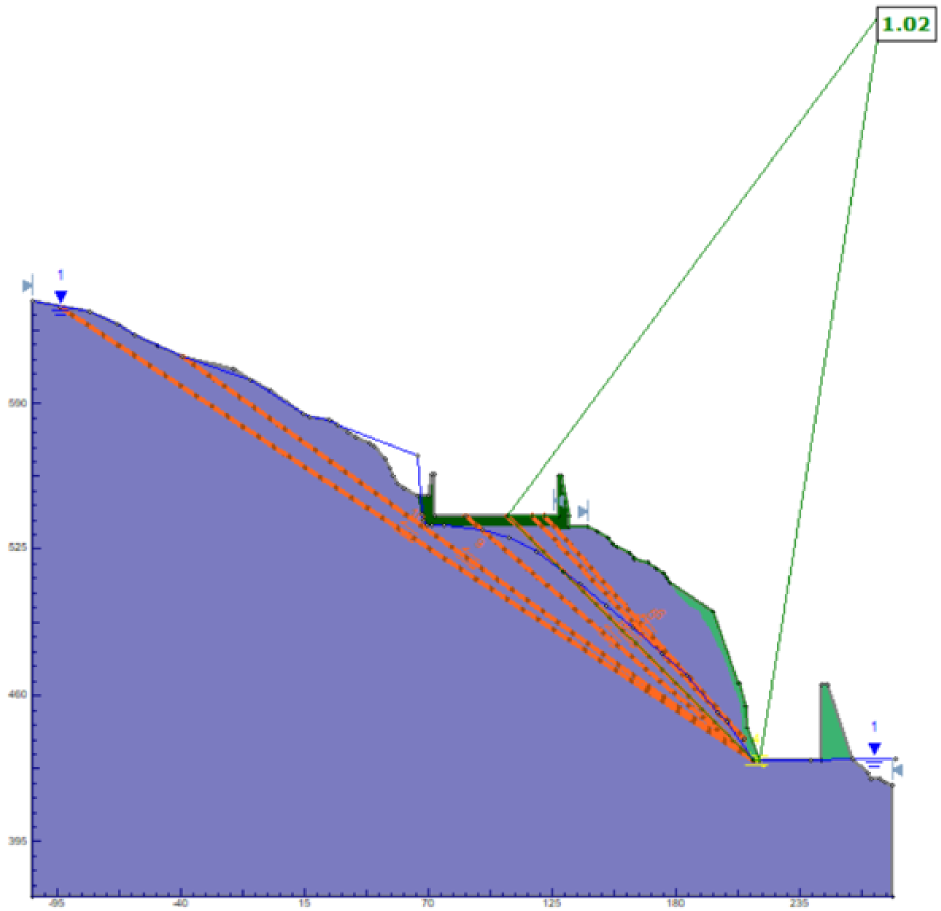

Material Name	Color	Unit Weight (lbs/ft3)	Strength Type	Cohesion (psf)	Phi (deg)	UCS (psf)	GSI	mi	D	Water Surface	Generalized Anisotropic
Foliation - Mohr-Coulomb		170	Mohr-Coulomb	0	48					Piezometric Line 1	
Concrete		150	Mohr-Coulomb	21620	0					Piezometric Line 1	
Rock Mass		170	Generalized Hoek-Brown			460800	60	7	0	Piezometric Line 1	
Spillway Concrete		150	Generalized Anisotropic							Piezometric Line 1	User Defined 1
Base Concrete		150	Mohr-Coulomb	0	35					Piezometric Line 1	

Exhibit 10-18: Existing Conditions Analysis for Section 1. Artesian groundwater pressures have been measured in the VWP upslope of the spillway (boring BH-17-1). In Slide, artesian groundwater conditions are modeled using a piezometric head line, shown as the blue boundary, which accounts for the artesian pore pressures without contributions from the additional weight of the water (i.e., pooled water).

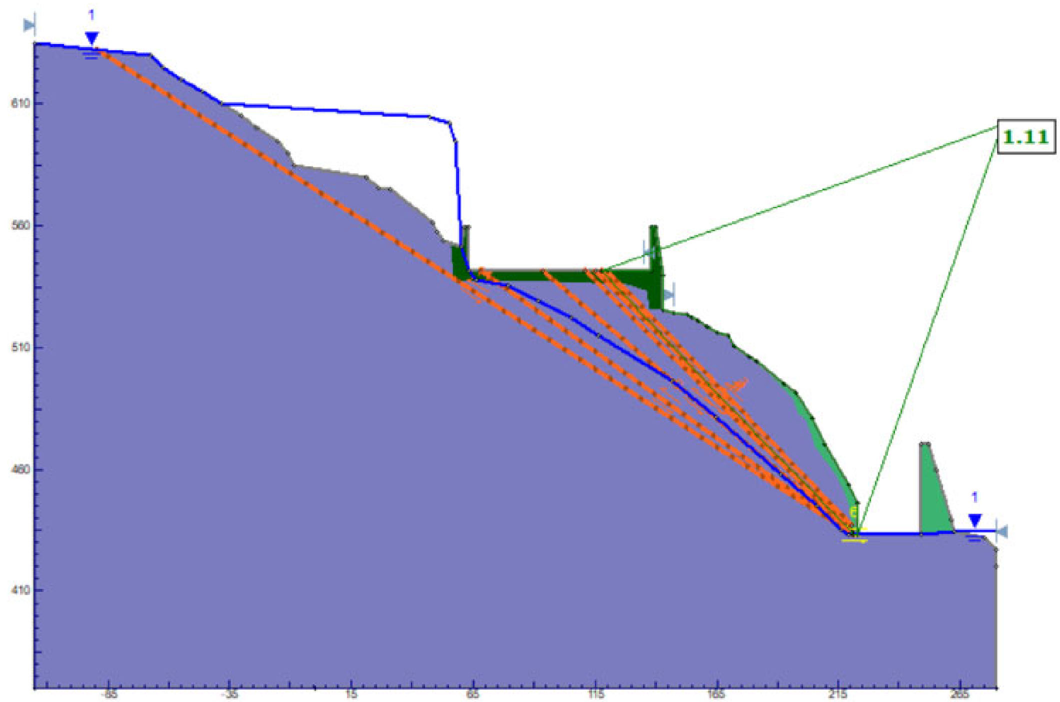

Material Name	Color	Unit Weight (lbs/ft3)	Strength Type	Cohesion (psf)	Phi (deg)	UCS (psf)	GSI	mi	D	Water Surface	Generalized Anisotropic
Foliation - Mohr-Coulomb		170	Mohr-Coulomb	0	48					Piezometric Line 1	
Concrete		150	Mohr-Coulomb	21620	0					Piezometric Line 1	
Rock Mass		170	Generalized Hoek-Brown			460800	60	7	0	Piezometric Line 1	
Spillway Concrete		150	Generalized Anisotropic							Piezometric Line 1	User Defined 1
Base Concrete		150	Mohr-Coulomb	0	35					Piezometric Line 1	

Exhibit 10-19: Existing Conditions Analysis for Section 2. Artesian groundwater pressures have been measured in the VWP upslope of the spillway (boring BH-17-2). In Slide, artesian groundwater conditions are modeled using a piezometric head line, shown as the blue boundary, which accounts for the artesian pore pressures without contributions from the additional weight of the water (i.e., pooled water).

The limit equilibrium analysis used anisotropic strength to model the phyllite rock, and the strength of concrete was modeled as a Mohr-Coulomb material as recommended by RocData (Rocscience, 2019):

- Rock mass shear strength with an intact UCS of 460,800 psf, GSI of 60, material constant (mi) of seven (7), and unit weight equal to 170 pounds per cubic foot (pcf);
- Foliation shear strength with zero (0) psf cohesion and a joint friction angle of 48 degrees and unit weight equal to 170 pcf;
- Concrete shear strength is equal to two times the square root of the UCS of concrete having cohesion of 21,620 psf, friction angle equal to zero (0) degrees, and unit weight equal to 120 pcf (Shannon & Wilson, 2022); and
- Base concrete-to-rock shear strength of 35 degrees with zero (0) cohesion and unit weight equal to 150 pcf.

Highly persistent minor structure displayed in Exhibit 7-1 show that there are several long joints striking parallel to Joint Set 1 or 3 (and parallel to the direction of sliding), which would provide lateral release for plane shear sliding along foliation. Foliation could daylight both downslope of the spillway and just on the upslope edge of the spillway, as shown in Exhibit 7-1, Exhibit 7-2, and Drawing C-02.

10.3.5 Rock Anchor Support Analyses

10.3.5.1 Support Design

One proposed alternative to stabilize the existing spillway slope is to support the slope with post-tensioned rock anchors. Two different anchor supported slope options were modeled with tensioned rock anchors installed on 8-foot centers with a bond length of over 20 feet declined at 15 degrees from horizontal. One anchor-supported slope option was modeled as Grade 150, 1 ¾-inch anchors with a bond strength equal to 18,095 lbs/ft over the 20-foot bond length. The second anchor-supported slope option was modeled as 8 Strand anchors, also having a bond strength of 18,095 lbs/ft over the 20-foot bond length. The bottom row of anchors is modeled at an approximate elevation of 440 feet in Section 1 and 445 feet in Section 2.

The limit equilibrium analyses for the rock anchor support design were performed according to the guidelines presented in the Geotechnical Design Memorandum GD-1, Rev. 1: Spillway Support Analyses Criteria (Shannon & Wilson, 2022). The rock anchor support pattern was designed to meet the criteria established in GD-1, Rev. 1, such that the presented design meets or exceeds the required FSs under usual, unusual, and extreme loading conditions (Shannon & Wilson, 2022). Model results and stability analysis reports from Slide (v. 9.023) by Rocscience for the rock anchor-supported rock buttress design are presented in Appendix N.

10.3.5.2 Static Analysis under Usual Loading Conditions

For an anchor-supported slope using 1 ¾-inch, Grade 150 anchors under usual loading conditions, the static FS (GLE/Morgenstern):

- For Section 1 is 2.2 and
- For Section 2 is 2.3.

The Slide results for a 1 ¾-inch, Grade 150 anchor-supported slope are presented in Exhibit 10-20 and Exhibit 10-21, respectively. The proposed rock anchor support pattern exceeds the required FS of 1.5 under usual loading conditions established by GD-1, Rev. 1 (Shannon & Wilson, 2022) for both Section 1 and Section 2.

For an anchor-supported slope using 8 Strand anchors under usual loading conditions, the static FS (GLE/Morgenstern):

- For Section 1 is 2.4 and
- For Section 2 is 2.7.

The Slide results for an 8 Strand anchor-supported slope are presented in Exhibit 10-22 and Exhibit 10-23, respectively. The proposed rock anchor support pattern exceeds the required FS of 1.5 under usual loading conditions established by GD-1, Rev. 1 (Shannon & Wilson, 2022) for both Section 1 and Section 2.

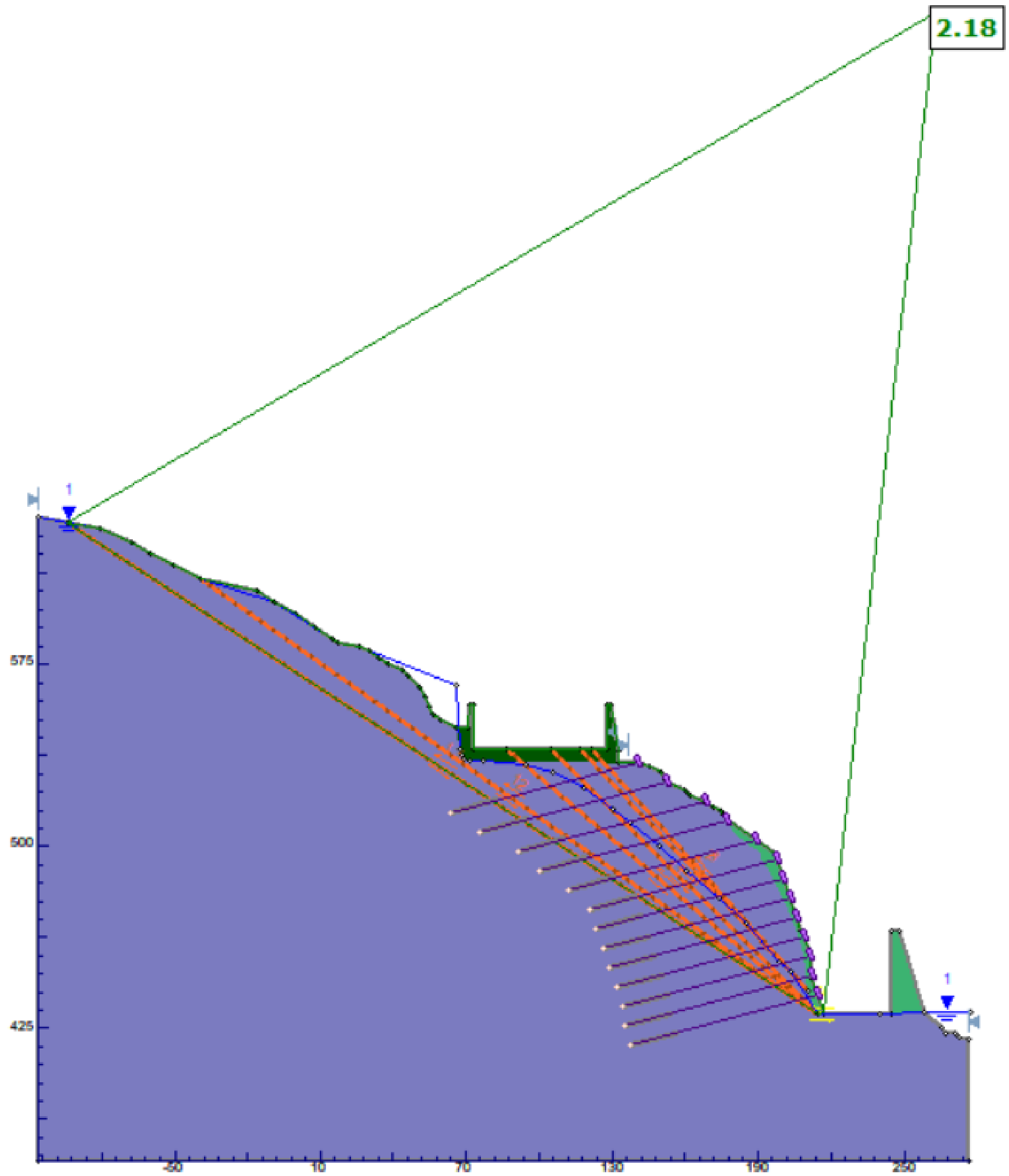

Exhibit 10-20: Limit Equilibrium Results for the Static Analysis of the 1 ¾-inch, Grade 150 Anchor-Supported Slope under Usual Loading Conditions for Section 1. Artesian groundwater pressures have been measured in the VWP upslope of the spillway (boring BH-17-1). In Slide, artesian groundwater conditions are modeled using a piezometric head line, shown as the blue boundary, which accounts for the artesian pore pressures without contributions from the additional weight of the water (i.e., pooled water).

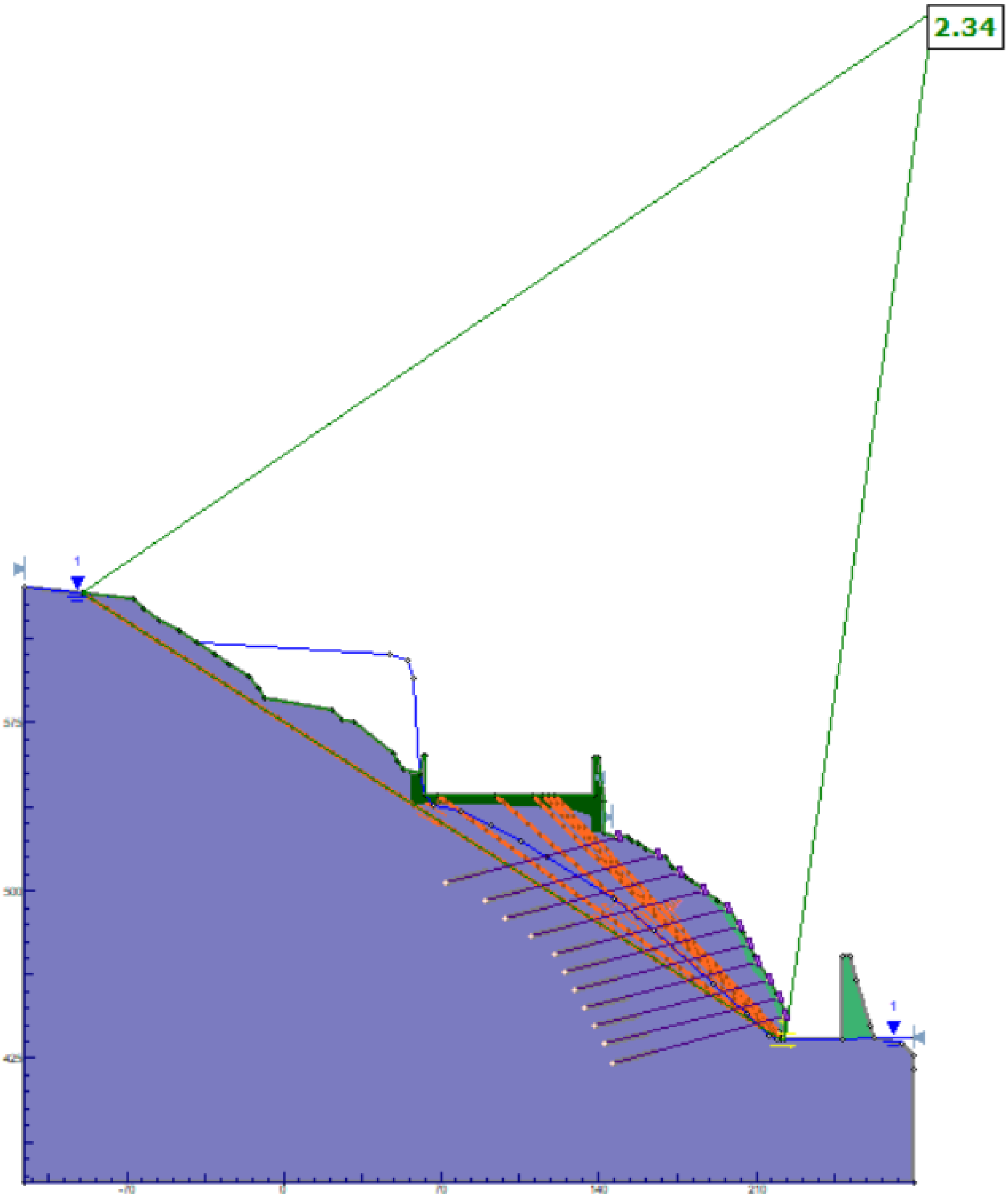

Exhibit 10-21: Limit Equilibrium Results for the Static Analysis of the 1 ¾-inch, Grade 150 Anchor-Supported Slope under Usual Loading Conditions for Section 2. Artesian groundwater pressures have been measured in the VWP upslope of the spillway (boring BH-17-2). In Slide, artesian groundwater conditions are modeled using a piezometric head line, shown as the blue boundary, which accounts for the artesian pore pressures without contributions from the additional weight of the water (i.e., pooled water).

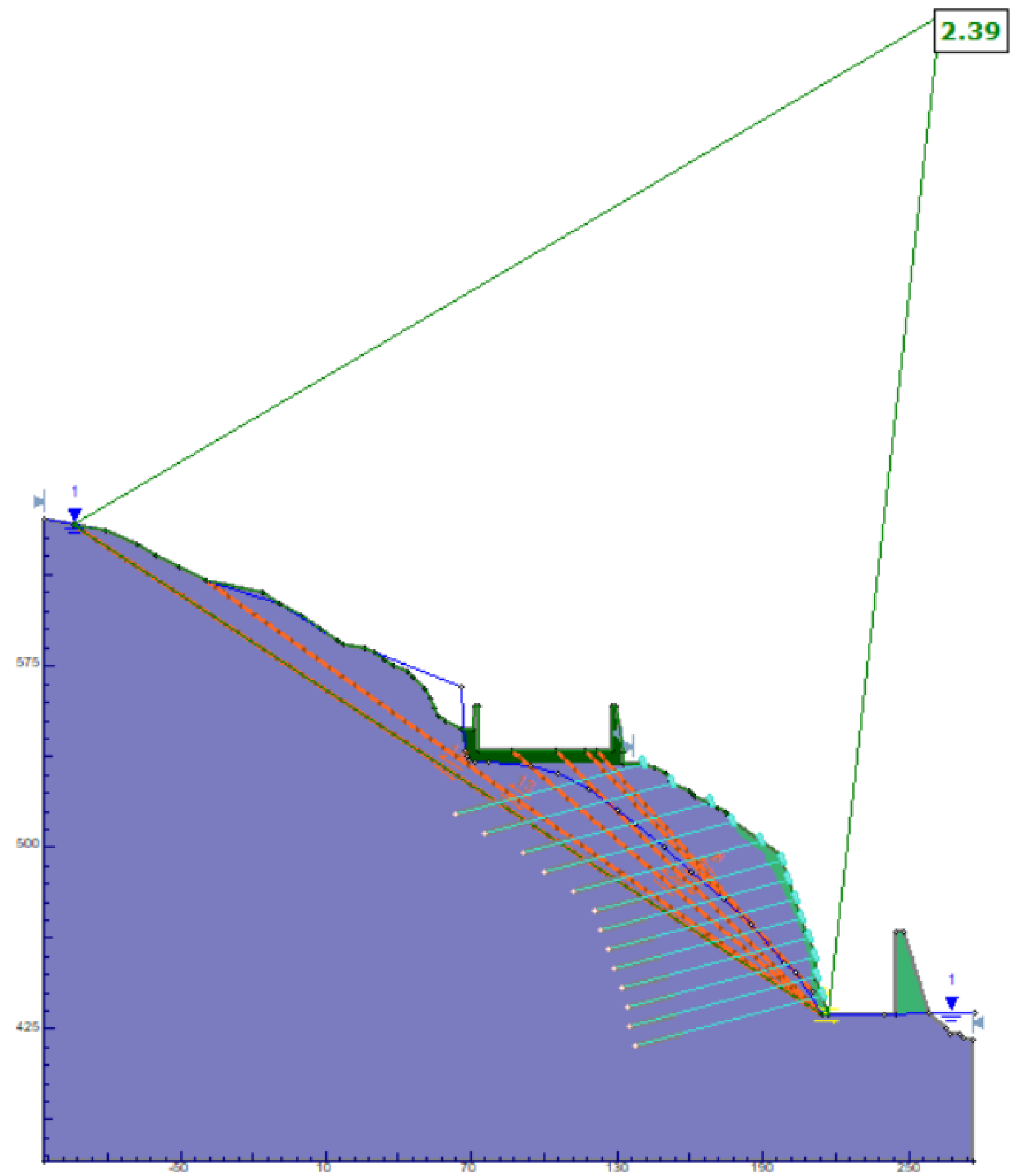

Exhibit 10-22: Limit Equilibrium Results for the Static Analysis of the 8 Strand Anchor-Supported Slope under Usual Loading Conditions for Section 1. Artesian groundwater pressures have been measured in the VWP upslope of the spillway (boring BH-17-1). In Slide, artesian groundwater conditions are modeled using a piezometric head line, shown as the blue boundary, which accounts for the artesian pore pressures without contributions from the additional weight of the water (i.e., pooled water).

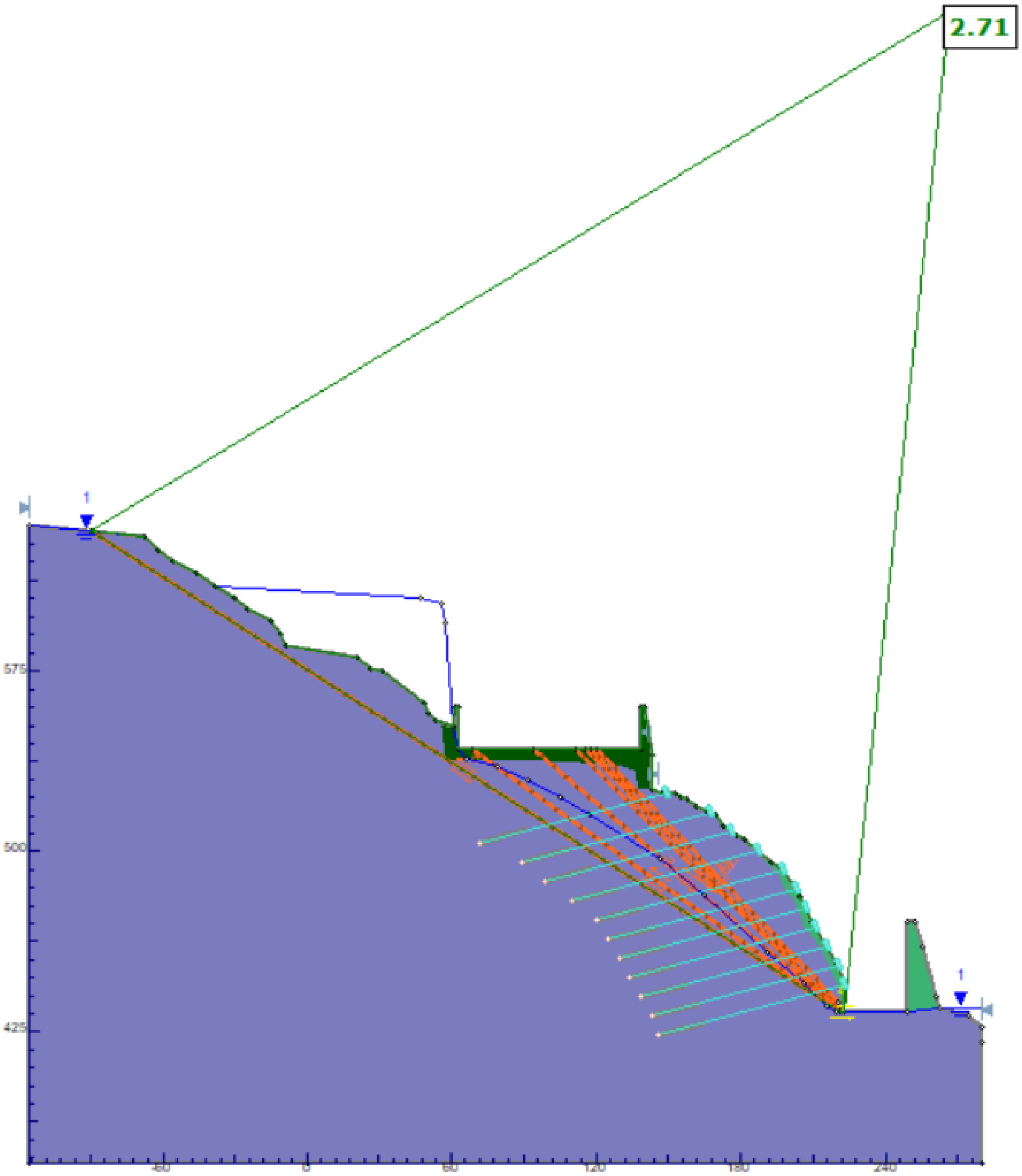

Exhibit 10-23: Limit Equilibrium Results for the Static Analysis of the 8 Strand Anchor-Supported Slope under Usual Loading Conditions for Section 2. Artesian groundwater pressures have been measured in the VWP upslope of the spillway (boring BH-17-2). In Slide, artesian groundwater conditions are modeled using a piezometric head line, shown as the blue boundary, which accounts for the artesian pore pressures without contributions from the additional weight of the water (i.e., pooled water).

10.3.5.3 Static Analysis under Probable Maximum Flood Unusual Loading Conditions

For an anchor-supported slope using 1 ¾-inch, Grade 150 anchors under unusual, PMF loading conditions, the static FS (GLE/Morgenstern):

- For Section 1 is 2.2 and
- For Section 2 is 2.3.

The Slide results for a 1 ¾-inch, Grade 150 anchor-supported slope are presented in Exhibit 10-24 and Exhibit 10-25, respectively. The proposed rock anchor support pattern exceeds the required FS of 1.3 under unusual loading conditions established by GD-1, Rev. 1 (Shannon & Wilson, 2022) for both Section 1 and Section 2.

For an anchor-supported slope using 8 Strand anchors under unusual, PMF loading conditions, the static FS (GLE/Morgenstern):

- For Section 1 is 2.4 and
- For Section 2 is 2.6.

The Slide results for an 8 Strand anchor-supported slope are presented in Exhibit 10-26 and Exhibit 10-27, respectively. The proposed rock anchor support pattern exceeds the required FS of 1.3 under unusual loading conditions established by GD-1, Rev. 1 (Shannon & Wilson, 2022) for both Section 1 and Section 2.

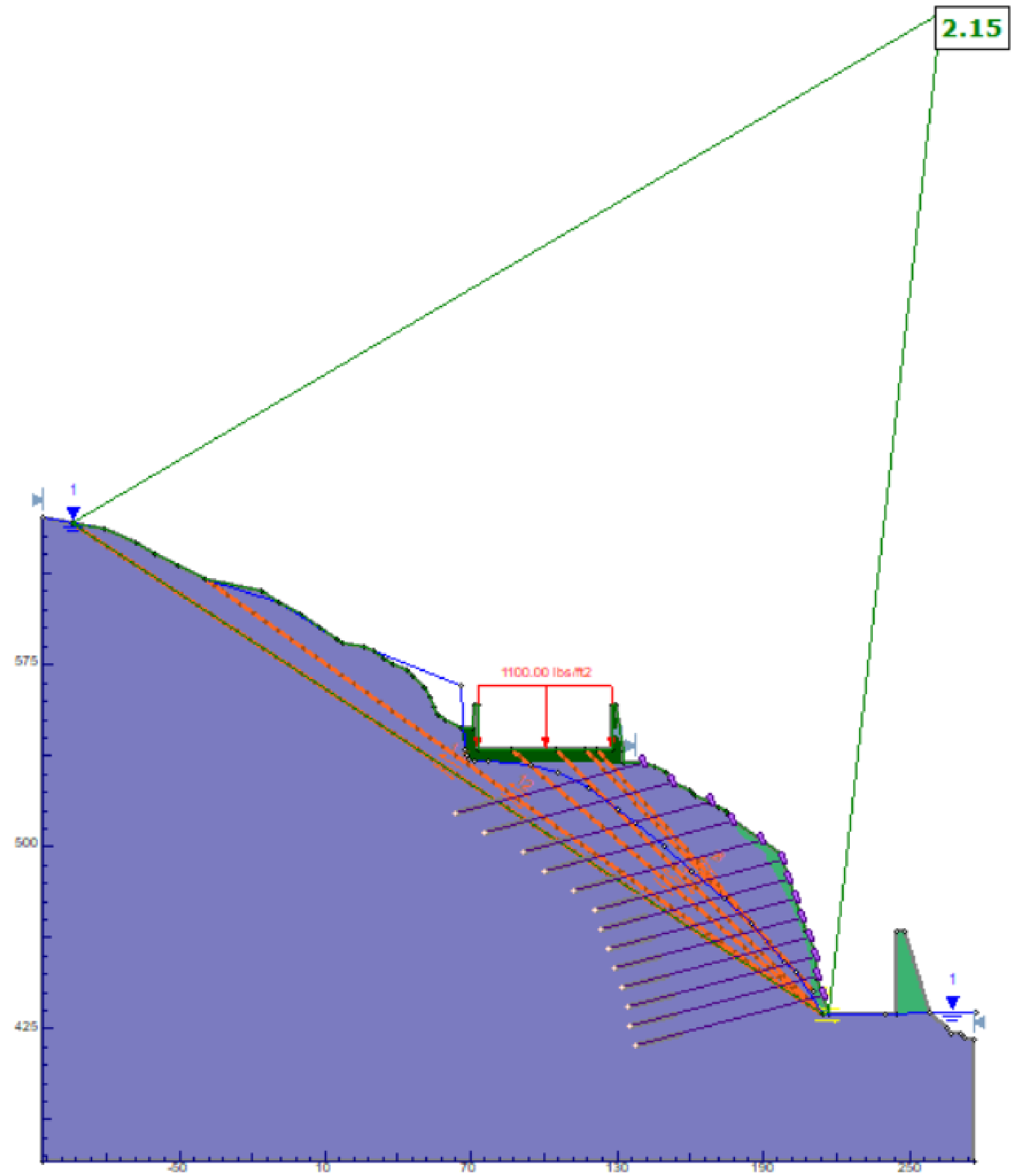

Exhibit 10-24: Limit Equilibrium Results for the Static Analysis of the 1 ¾-inch, Grade 150 Anchor-Supported Slope under Unusual Loading Conditions for Section 1. Artesian groundwater pressures have been measured in the VWP upslope of the spillway (boring BH-17-1). In Slide, artesian groundwater conditions are modeled using a piezometric head line, shown as the blue boundary, which accounts for the artesian pore pressures without contributions from the additional weight of the water (i.e., pooled water).

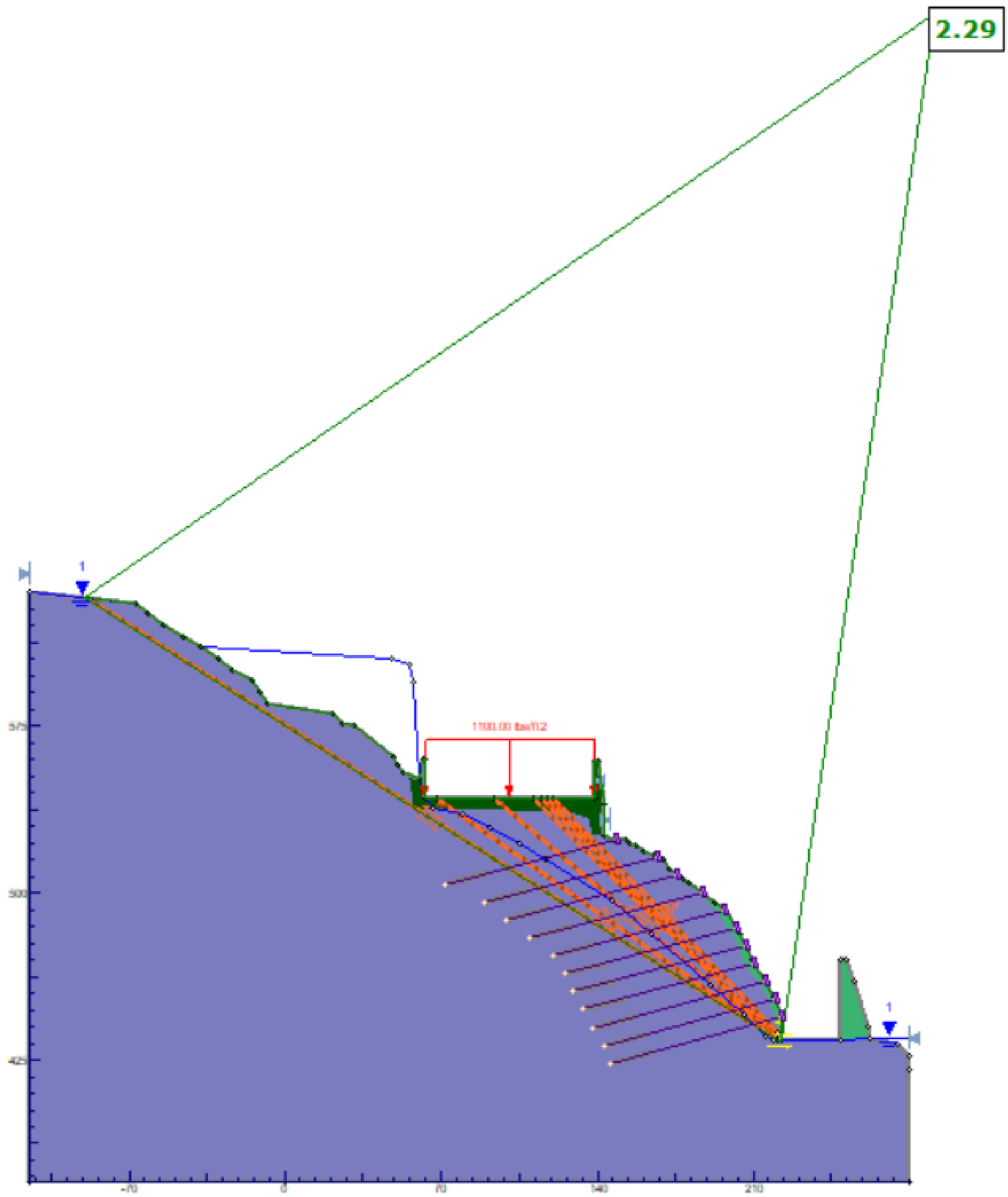

Exhibit 10-25: Limit Equilibrium Results for the Static Analysis of the 1 ¾-inch, Grade 150 Anchor-Supported Slope under Unusual Loading Conditions for Section 2. Artesian groundwater pressures have been measured in the VWP upslope of the spillway (boring BH-17-2). In Slide, artesian groundwater conditions are modeled using a piezometric head line, shown as the blue boundary, which accounts for the artesian pore pressures without contributions from the additional weight of the water (i.e., pooled water).

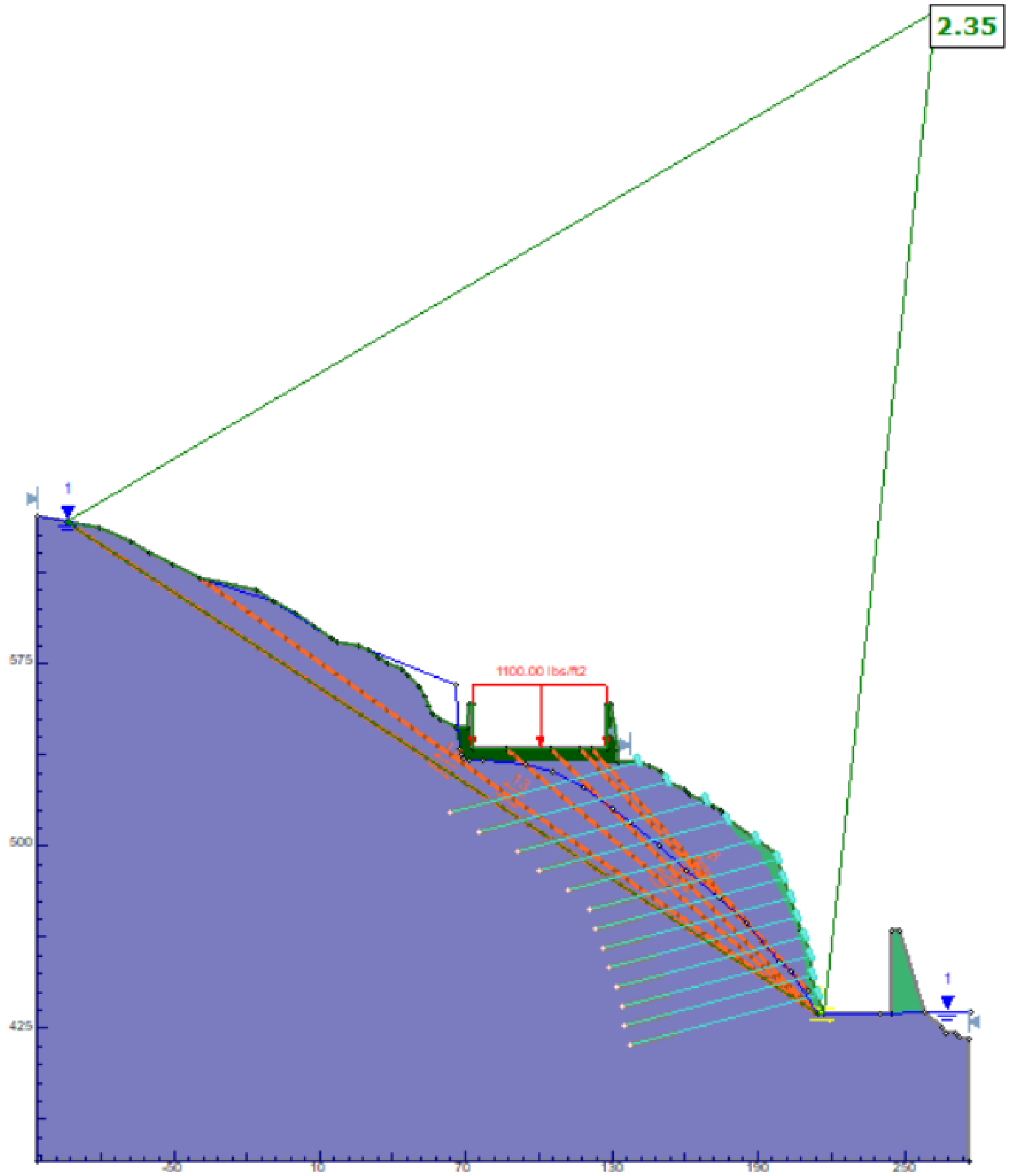

Exhibit 10-26: Limit Equilibrium Results for the Static Analysis of the 8 Strand Anchor-Supported Slope under Unusual Loading Conditions for Section 1. Artesian groundwater pressures have been measured in the VWP upslope of the spillway (boring BH-17-1). In Slide, artesian groundwater conditions are modeled using a piezometric head line, shown as the blue boundary, which accounts for the artesian pore pressures without contributions from the additional weight of the water (i.e., pooled water).

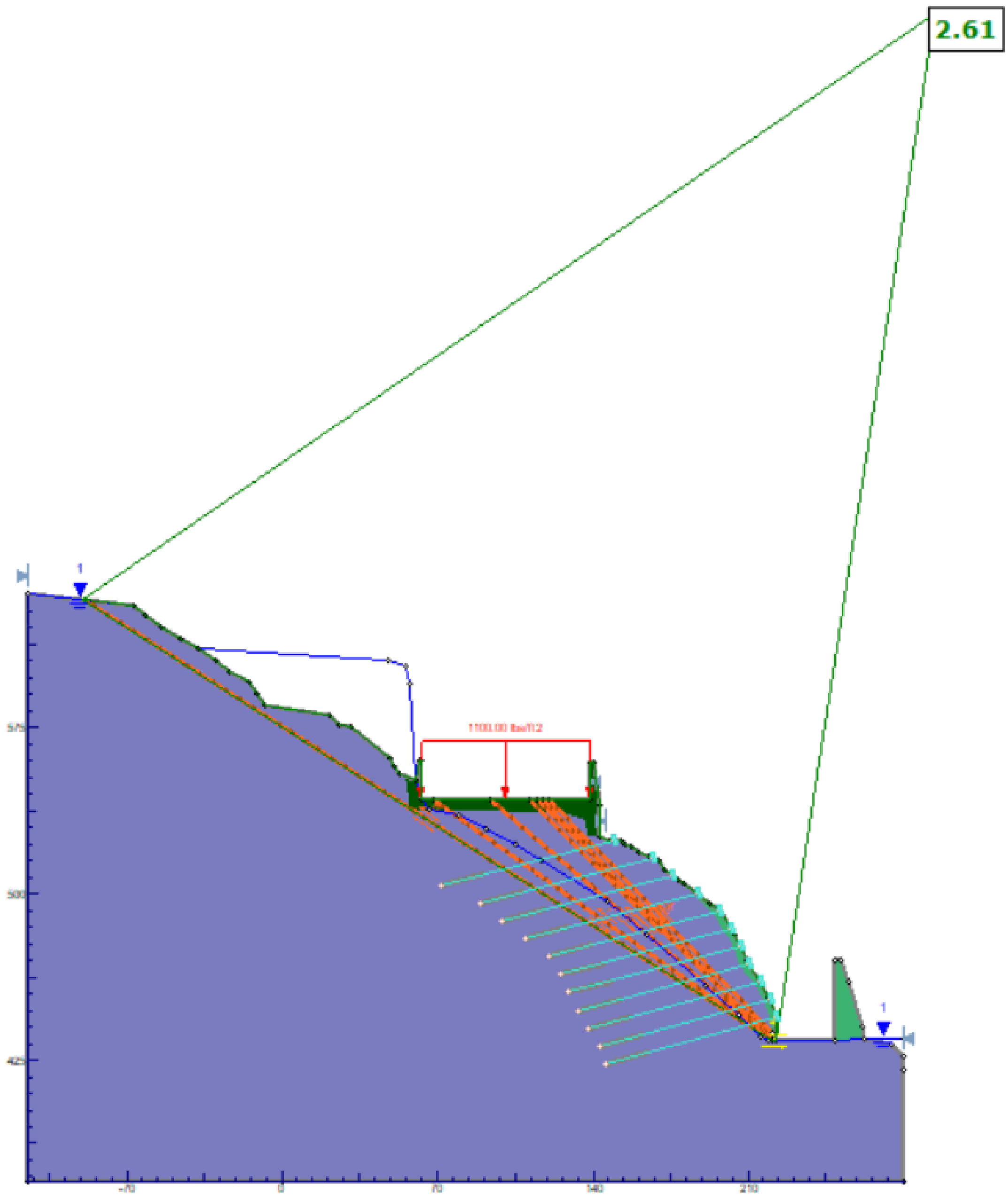

Exhibit 10-27: Limit Equilibrium Results for the Static Analysis of the 8 Strand Anchor-Supported Slope under Unusual Loading Conditions for Section 2. Artesian groundwater pressures have been measured in the VWP upslope of the spillway (boring BH-17-2). In Slide, artesian groundwater conditions are modeled using a piezometric head line, shown as the blue boundary, which accounts for the artesian pore pressures without contributions from the additional weight of the water (i.e., pooled water).

10.3.5.4 Pseudo-Static Analysis under Extreme Loading Conditions

For an anchor-supported slope using 1 ¾-inch, Grade 150 anchors under extreme loading conditions, the pseudo-static FS (GLE/Morgenstern):

- For Section 1 is 1.1 and
- For Section 2 is 1.2.

The Slide results for a 1 ¾-inch, Grade 150 anchor-supported slope are presented in Exhibit 10-28 and Exhibit 10-29, respectively. The proposed rock anchor support pattern meets the required FS of 1.1 under extreme pseudo-static loading conditions established by GD-1, Rev. 1 (Shannon & Wilson, 2022) for Section 1 and exceeds the required FS of 1.1 for Section 2.

For an anchor-supported slope using 8 Strand anchors under extreme loading conditions, the pseudo-static FS (GLE/Morgenstern):

- For Section 1 is 1.1 and
- For Section 2 is 1.3.

The Slide results for an 8 Strand anchor-supported slope are presented in Exhibit 10-30 and Exhibit 10-31, respectively. The proposed rock anchor support pattern meets the required FS of 1.1 under extreme pseudo-static loading conditions established by GD-1, Rev. 1 (Shannon & Wilson, 2022) for Section 1 and exceeds the required FS of 1.1 for Section 2.

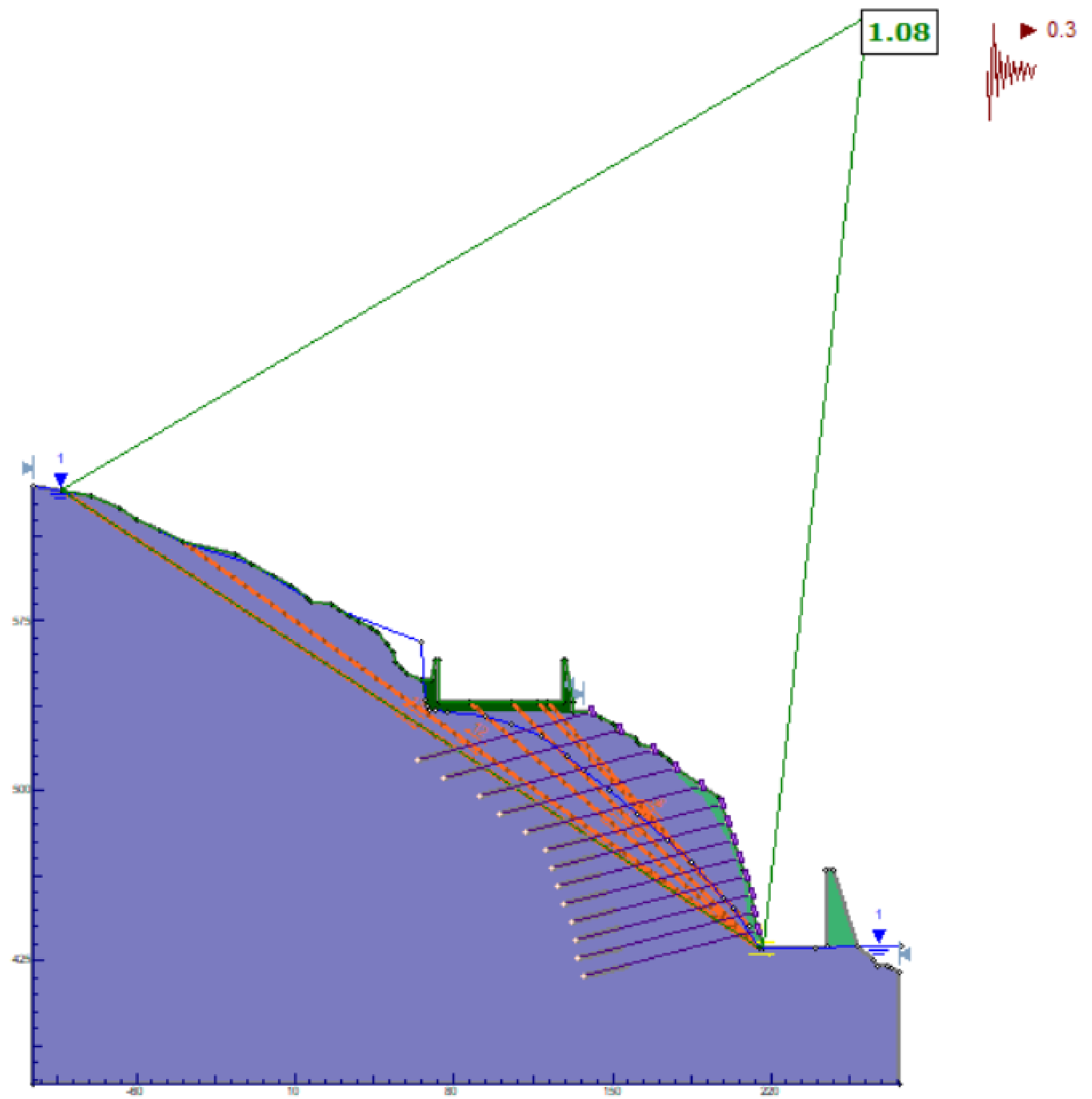

Exhibit 10-28: Limit Equilibrium Results for the Pseudo-Static Analysis of the 1 ¾-inch, Grade 150 Anchor-Supported Slope under Extreme Loading Conditions for Section 1. Artesian groundwater pressures have been measured in the VWP upslope of the spillway (boring BH-17-1). In Slide, artesian groundwater conditions are modeled using a piezometric head line, shown as the blue boundary, which accounts for the artesian pore pressures without contributions from the additional weight of the water (i.e., pooled water).

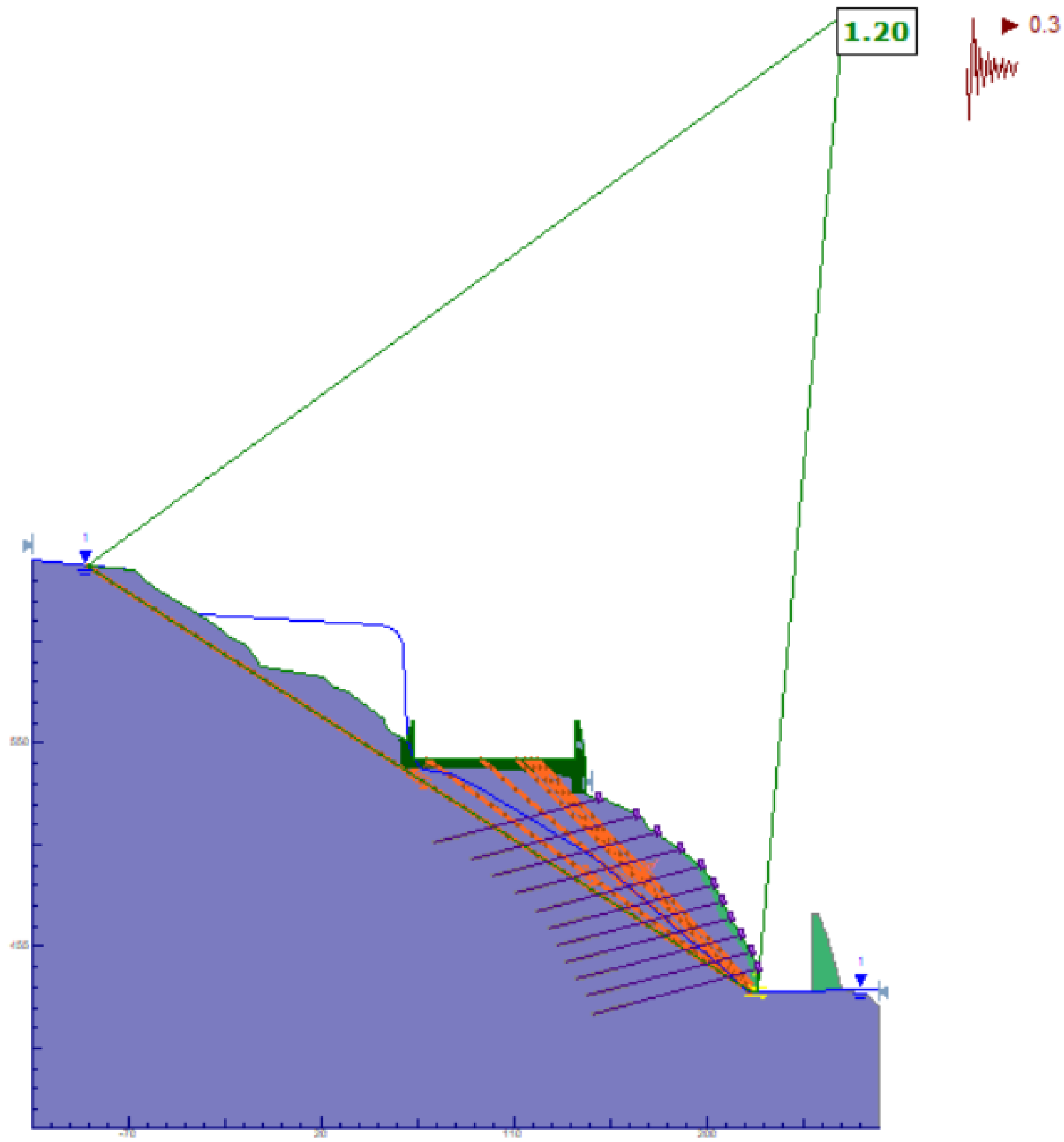

Exhibit 10-29: Limit Equilibrium Results for the Pseudo-Static Analysis of the 1 ¾-inch, Grade 150 Anchor-Supported Slope under Extreme Loading Conditions for Section 2. Artesian groundwater pressures have been measured in the VWP upslope of the spillway (boring BH-17-2). In Slide, artesian groundwater conditions are modeled using a piezometric head line, shown as the blue boundary, which accounts for the artesian pore pressures without contributions from the additional weight of the water (i.e., pooled water).

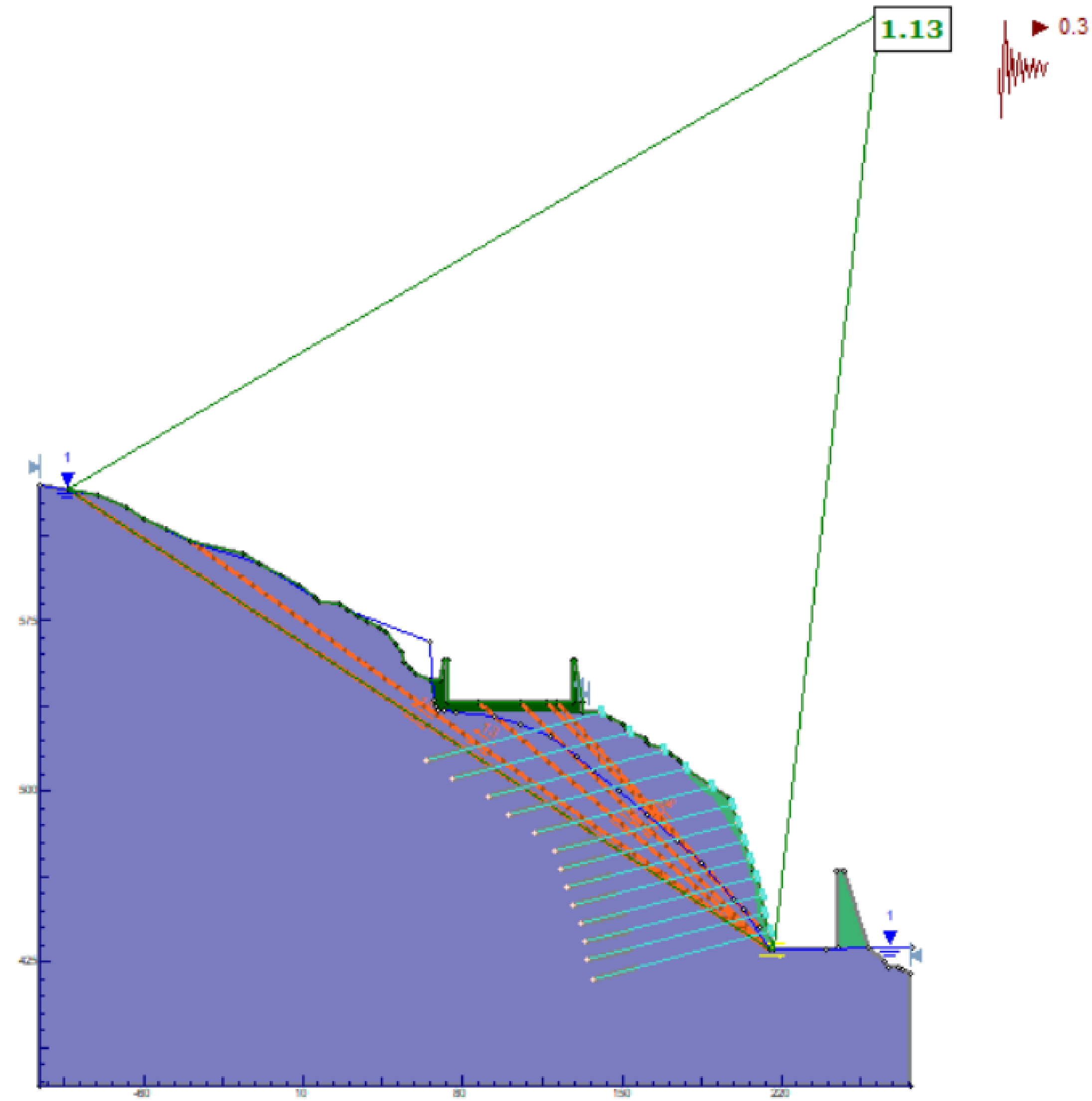

Exhibit 10-30: Limit Equilibrium Results for the Pseudo-Static Analysis of the 8 Strand Anchor-Supported Slope under Extreme Loading Conditions for Section 1. Artesian groundwater pressures have been measured in the VWP upslope of the spillway (boring BH-17-1). In Slide, artesian groundwater conditions are modeled using a piezometric head line, shown as the blue boundary, which accounts for the artesian pore pressures without contributions from the additional weight of the water (i.e., pooled water).

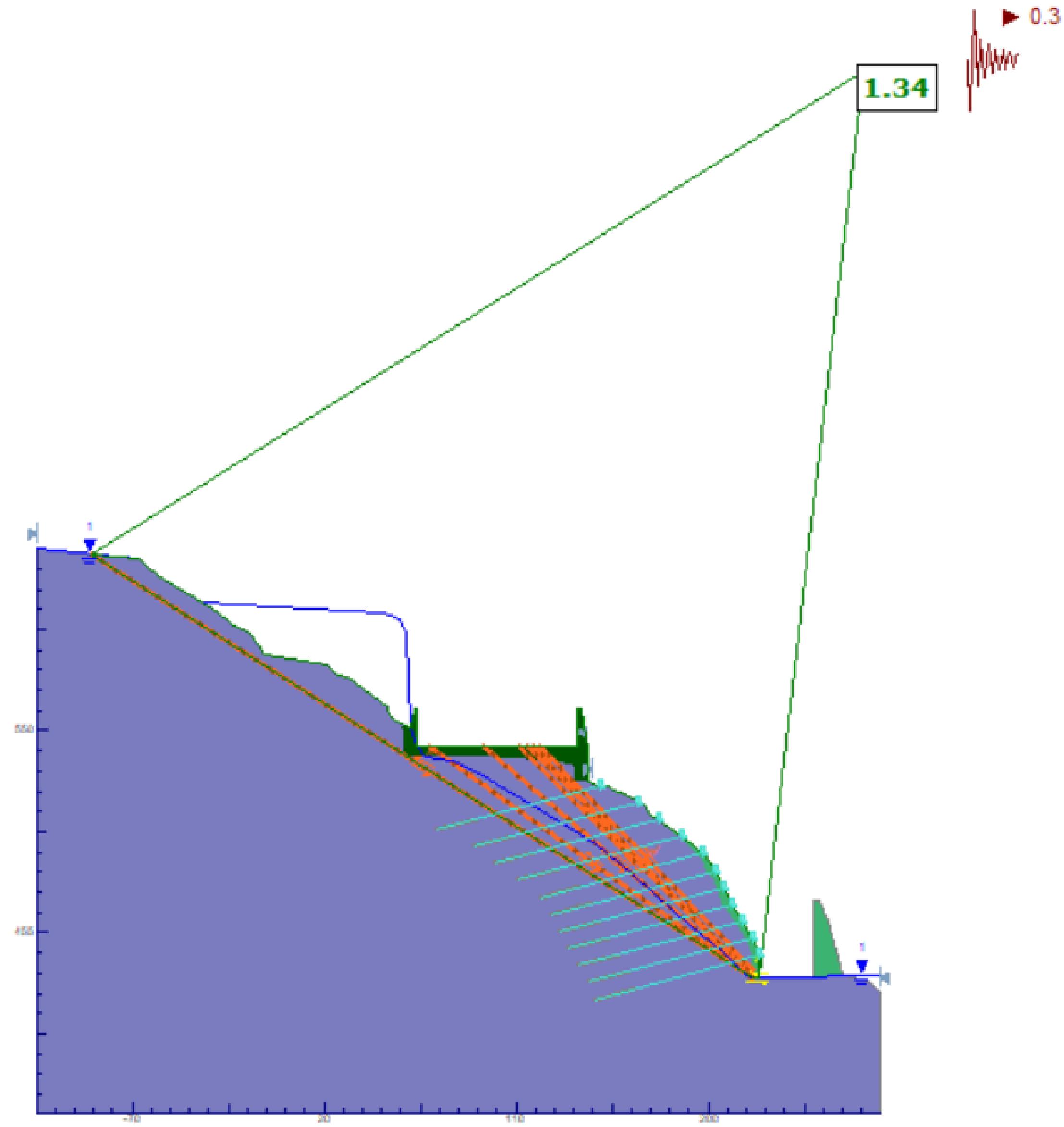

Exhibit 10-31: Limit Equilibrium Results for the Pseudo-Static Analysis of the 8 Strand Anchor-Supported Slope under Extreme Loading Conditions for Section 2. Artesian groundwater pressures have been measured in the VWP upslope of the spillway (boring BH-17-2). In Slide, artesian groundwater conditions are modeled using a piezometric head line, shown as the blue boundary, which accounts for the artesian pore pressures without contributions from the additional weight of the water (i.e., pooled water).

10.3.5.5 Static Analysis using Post-Earthquake Material Properties

For an anchor-supported slope using 1 ¾-inch, Grade 150 anchors with post-earthquake material properties under usual loading conditions, the static FS (GLE/Morgenstern):

- For Section 1 is 1.6 and
- For Section 2 is 1.8.

The Slide results for a 1 ¾-inch, Grade 150 anchor-supported slope are presented in Exhibit 10-32 and Exhibit 10-33, respectively. The proposed rock anchor support pattern exceeds the required FS of 1.3 under usual loading conditions with post-earthquake material established by GD-1, Rev. 1 (Shannon & Wilson, 2022) for both Section 1 and Section 2.

For an anchor-supported slope using 8 Strand with post-earthquake material properties under usual loading conditions, the static FS (GLE/Morgenstern:

- For Section 1 is 1.9 and
- For Section 2 is 2.1.

The Slide results for an 8 Strand anchor-supported slope are presented in Exhibit 10-34 and Exhibit 10-35, respectively. The proposed rock anchor support pattern exceeds the required FS of 1.3 under usual loading conditions with post-earthquake material established by GD-1, Rev. 1 (Shannon & Wilson, 2022) for both Section 1 and Section 2.

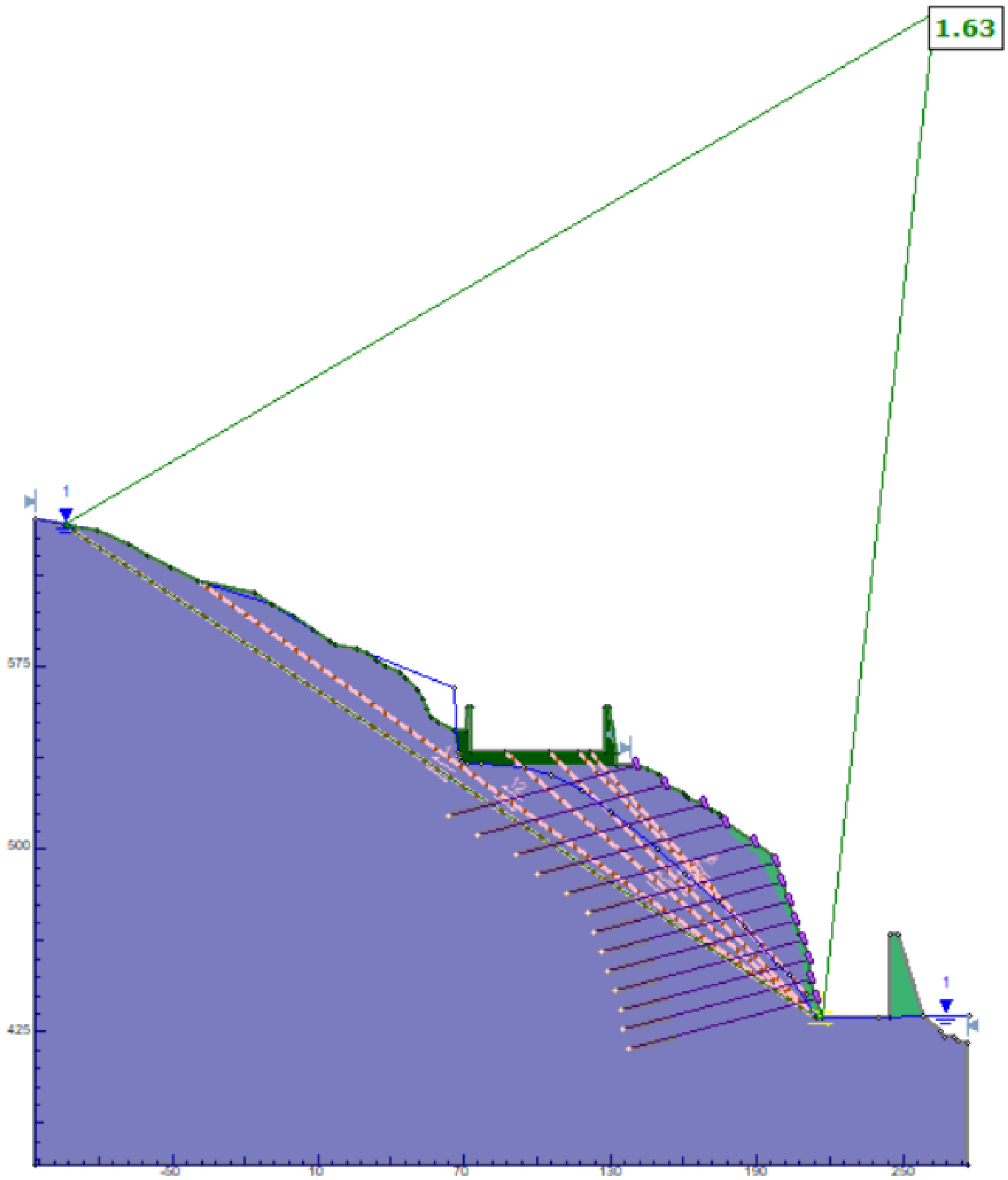

Exhibit 10-32: Limit Equilibrium Results for the Static Analysis of the 1 ¾-inch, Grade 150 Anchor-Supported Slope under Usual Loading Conditions with Post-Earthquake Material Properties for Section 1. Artesian groundwater pressures have been measured in the VWP upslope of the spillway (boring BH-17-1). In Slide, artesian groundwater conditions are modeled using a piezometric head line, shown as the blue boundary, which accounts for the artesian pore pressures without contributions from the additional weight of the water (i.e., pooled water).

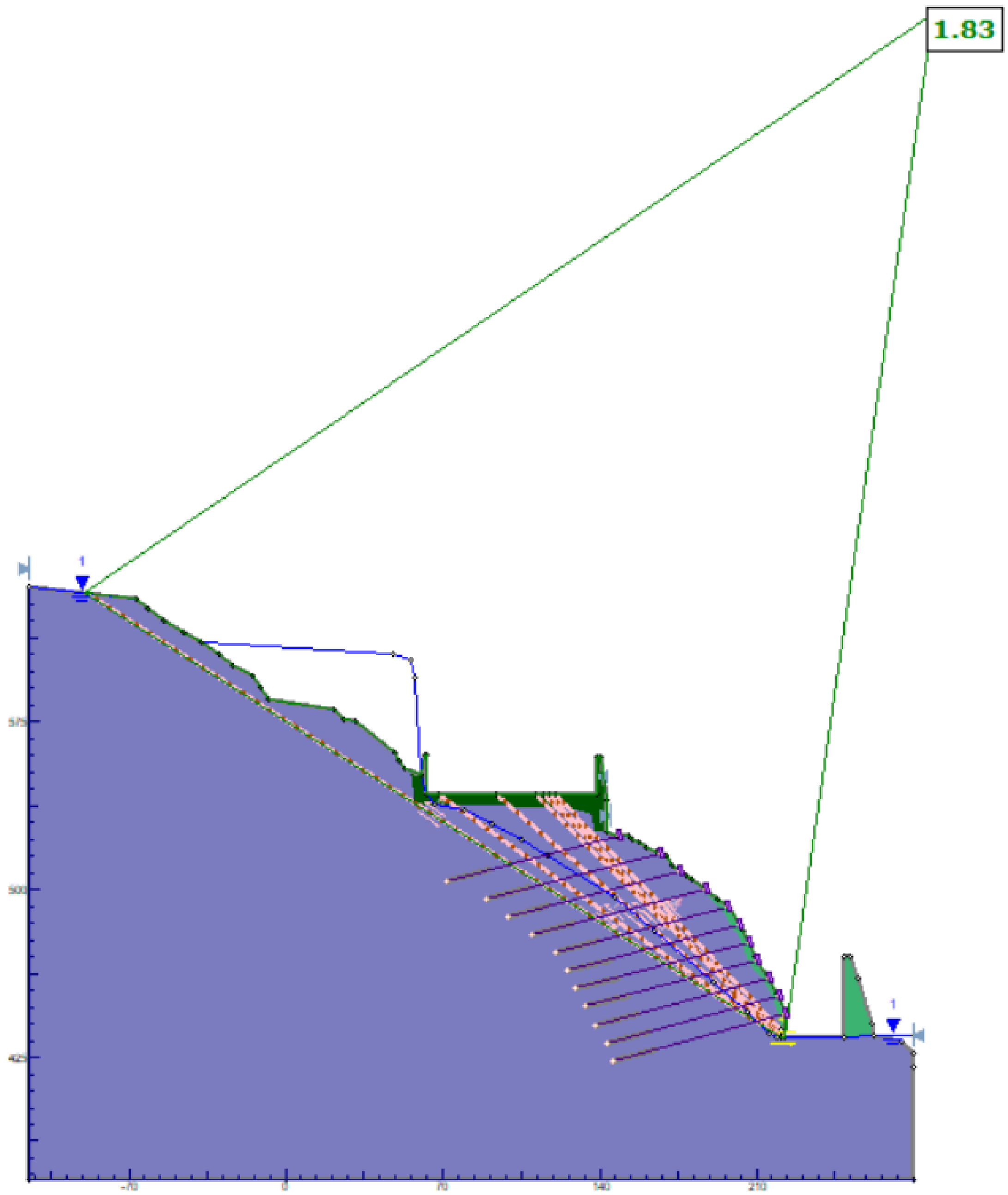

Exhibit 10-33: Limit Equilibrium Results for the Static Analysis of the 1 ¾-inch, Grade 150 Anchor-Supported Slope under Usual Loading Conditions with Post-Earthquake Material Properties for Section 2. Artesian groundwater pressures have been measured in the VWP upslope of the spillway (boring BH-17-2). In Slide, artesian groundwater conditions are modeled using a piezometric head line, shown as the blue boundary, which accounts for the artesian pore pressures without contributions from the additional weight of the water (i.e., pooled water).

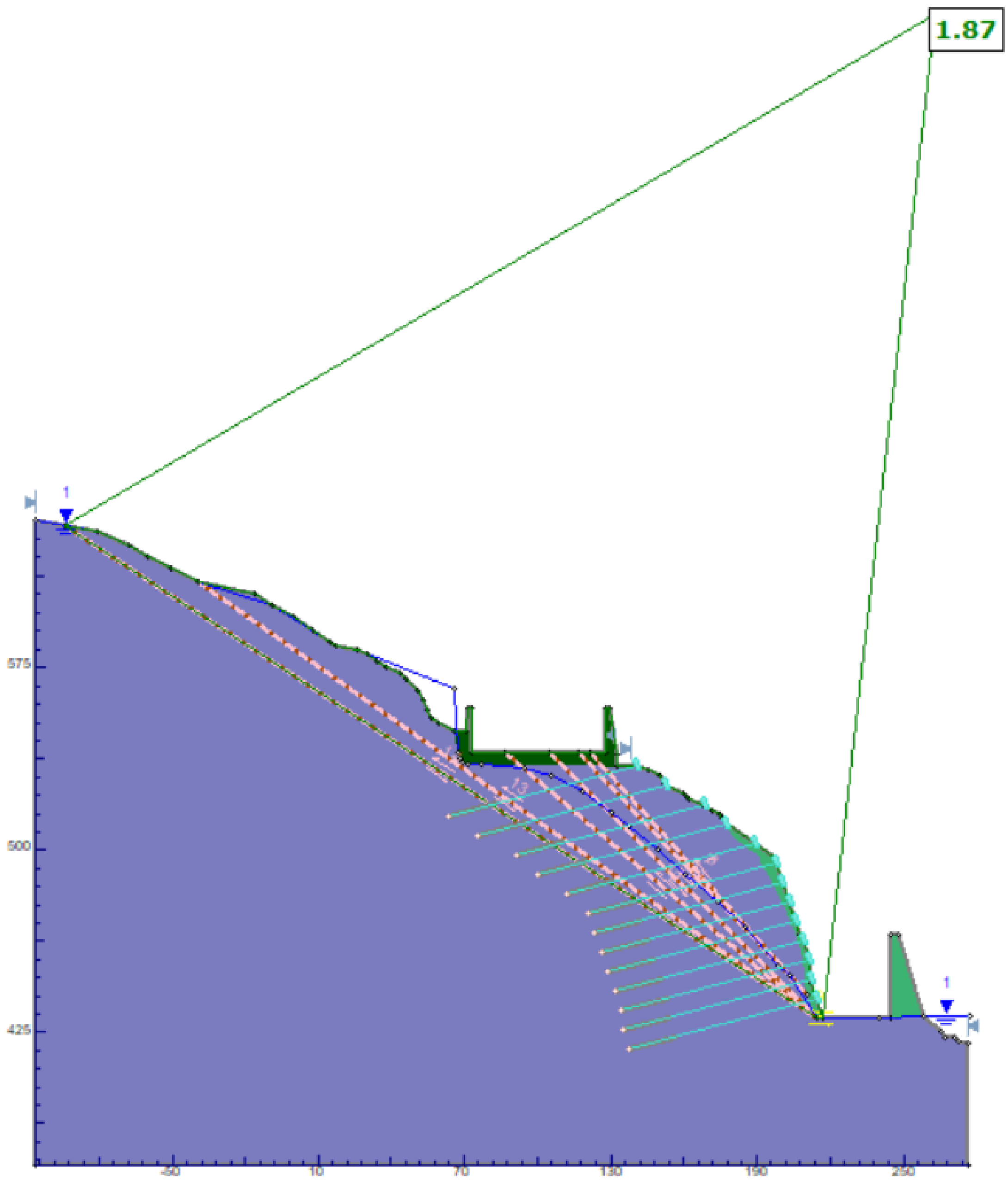

Exhibit 10-34: Limit Equilibrium Results for the Static Analysis of the 8 Strand Anchor-Supported Slope under Usual Loading Conditions with Post-Earthquake Material Properties for Section 1. Artesian groundwater pressures have been measured in the VWP upslope of the spillway (boring BH-17-1). In Slide, artesian groundwater conditions are modeled using a piezometric head line, shown as the blue boundary, which accounts for the artesian pore pressures without contributions from the additional weight of the water (i.e., pooled water).

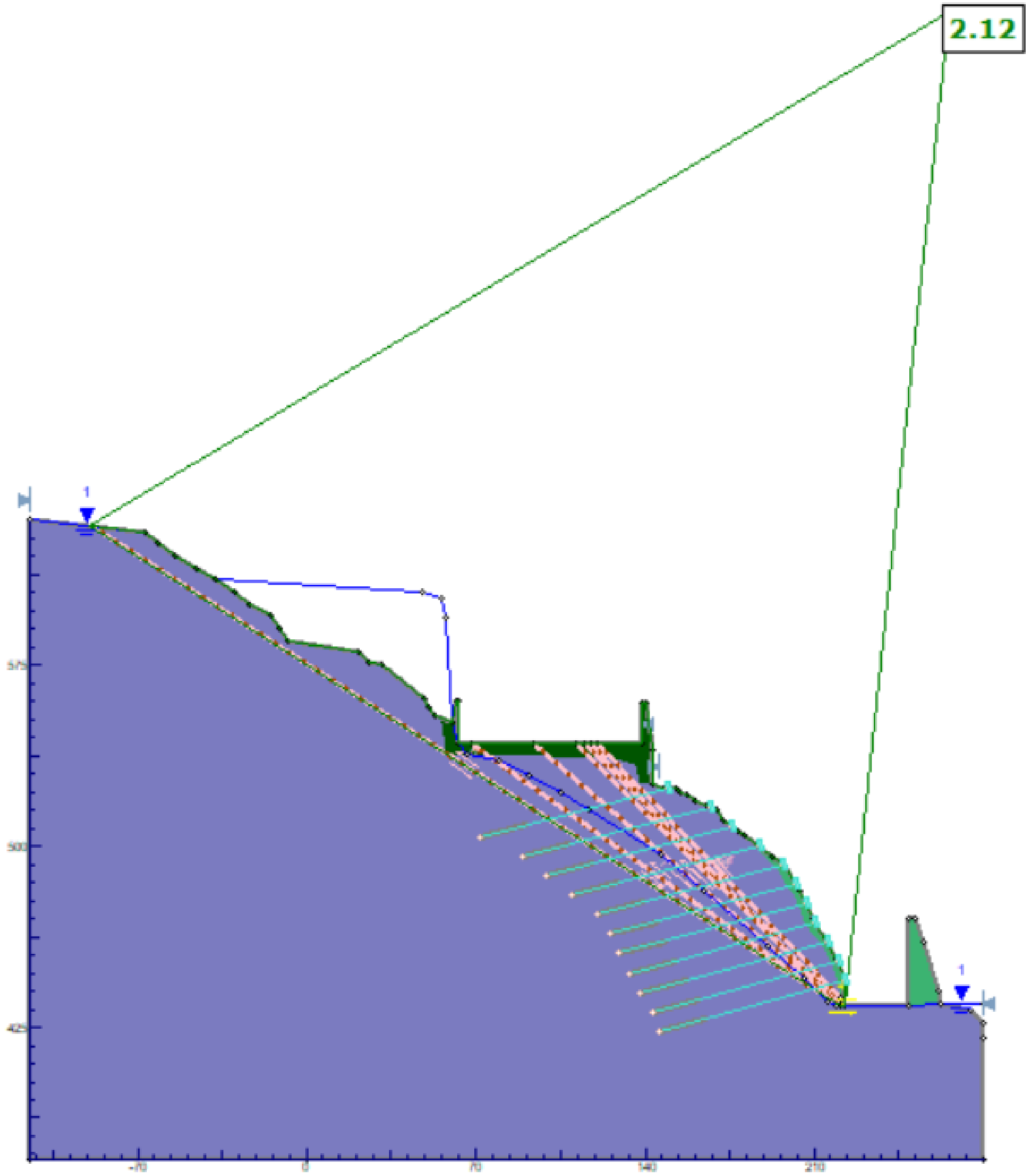

Exhibit 10-35: Limit Equilibrium Results for the Static Analysis of the 8 Strand Anchor-Supported Slope under Usual Loading Conditions with Post-Earthquake Material Properties for Section 2. Artesian groundwater pressures have been measured in the VWP upslope of the spillway (boring BH-17-2). In Slide, artesian groundwater conditions are modeled using a piezometric head line, shown as the blue boundary, which accounts for the artesian pore pressures without contributions from the additional weight of the water (i.e., pooled water).

10.3.6 Grouted Rock Buttress Support Analyses

10.3.6.1 Support Design

The second proposed alternative for stabilizing the existing spillway slope is to fill the existing sluiceway structure with concrete and rock rubble, creating a grouted rock buttress to support the base of the slope. A cost comparison was performed to evaluate which of the two proposed support options had an estimated lower construction cost, with the grouted rock buttress being the lower cost option. We recommend this option as the preferred mitigation alternative.

To provide drainage to the buttress a total of 21, 60-foot weep holes will be installed below the top of the buttress in two rows along the 130-foot length of the sluiceway. One row of 11 weep holes will be installed at an elevation of 440 feet and a second row of 10 weep holes will be installed at an elevation of 450 feet. To provide additional drainage to the spillway, three sets of three, 80-foot weep holes drilled in a fan arrangement with a 10 degree splay between each weep hole will be installed above the buttress at an elevation of 470 feet. To provide additional shear resistance against sliding for the grouted rock buttress, two rows of 20-foot-long (embedded 10 feet into the sluiceway and extending 10 feet into the buttress), Grade 150, 1¾-inch rock dowels were modeled on 5-foot centers. Using the limit equilibrium model, we estimated the shear resistance required per foot along the longitudinal axis of the buttress to satisfy global stability requirements under the varying loading (Usual, Unusual PMF, Seismic, and Post-Earthquake). The maximum shear resistance required by the dowels to meet the target factors of safety was 108,850 pounds per foot. We then selected a rock dowel configuration that provides the required shear demand and performed hand calculations to check sliding and overturning stability. The required development length of the rock dowels was calculated as nine (9) feet using the relationships presented in Wyllie (1999) (Equations 9.11-9.14). However, it was decided that a minimum anchor length of 10 feet should be used for a 1 ¾-inch based on minimum bond length recommendations in PTI (2014); Sabatini, Pass, and Bachus (1999); USACE (1994); and Xanthakos (1991). Rock dowel shear pins are modeled as pile/micro-piles within Slide providing a shear resistance of approximately 228,000 pounds each. The shear resistance follows relationships between ultimate tensile strength and shear strength as suggested in Georgi Genov's 2020 technical report, Revisiting the Rule-of-Thumb Dependencies of Shear Strength and the Hardness on the Yield and the Ultimate Strengths (Genov, 2020). This translates to an additional shear resistance per foot along the longitudinal axis of the buttress of approximately 91,200 pounds.

The limit equilibrium analyses for the grouted rock buttress support design were performed according to the guidelines presented in the Geotechnical Design Memorandum GD-1, Rev.

1: Spillway Support Analyses Criteria (Shannon & Wilson, 2022). The grouted rock buttress was designed to meet the criteria established in GD-1, Rev. 1 such that the presented design meets or exceeds the required FSs under usual, unusual, and extreme loading conditions (Shannon & Wilson, 2022). For the grouted rock buttress support design, limit equilibrium analyses were performed to evaluate failure surfaces through the concrete lining above the grouted rock buttress and global failure of the grouted rock buttress with dowel supports. Model results and stability analysis reports from Slide (v. 9.023) by Rocscience for the grouted rock buttress design are presented in Appendix N.

10.3.6.2 Static Analysis under Usual Loading Conditions

Under usual loading conditions, the static FS (GLE/Morgenstern) for Section 1:

- Against failure through the concrete lining above the grouted rock buttress is 1.6 and
- Against global failure of the dowel-supported grouted rock buttress is 2.0.

The Slide results for failure cases above and through the dowel-supported grouted rock buttress are presented in Exhibit 10-36 and Exhibit 10-37. The proposed dowel-supported grouted rock buttress design exceeds the required FS of 1.5 under usual loading conditions established by GD-1, Rev. 1 (Shannon & Wilson, 2022) for Section 1.

Under usual loading conditions, the static FS (GLE/Morgenstern) for Section 2:

- Against failure through the concrete lining above the grouted rock buttress is 2.8 and
- Against global failure of the dowel-supported grouted rock buttress is 2.3.

The Slide results for failure cases above and through the dowel-supported grouted rock buttress are presented in Exhibit 10-38 and Exhibit 10-39. The proposed dowel-supported grouted rock buttress design exceeds the required FS of 1.5 under usual loading conditions established by GD-1, Rev. 1 (Shannon & Wilson, 2022) for Section 2.

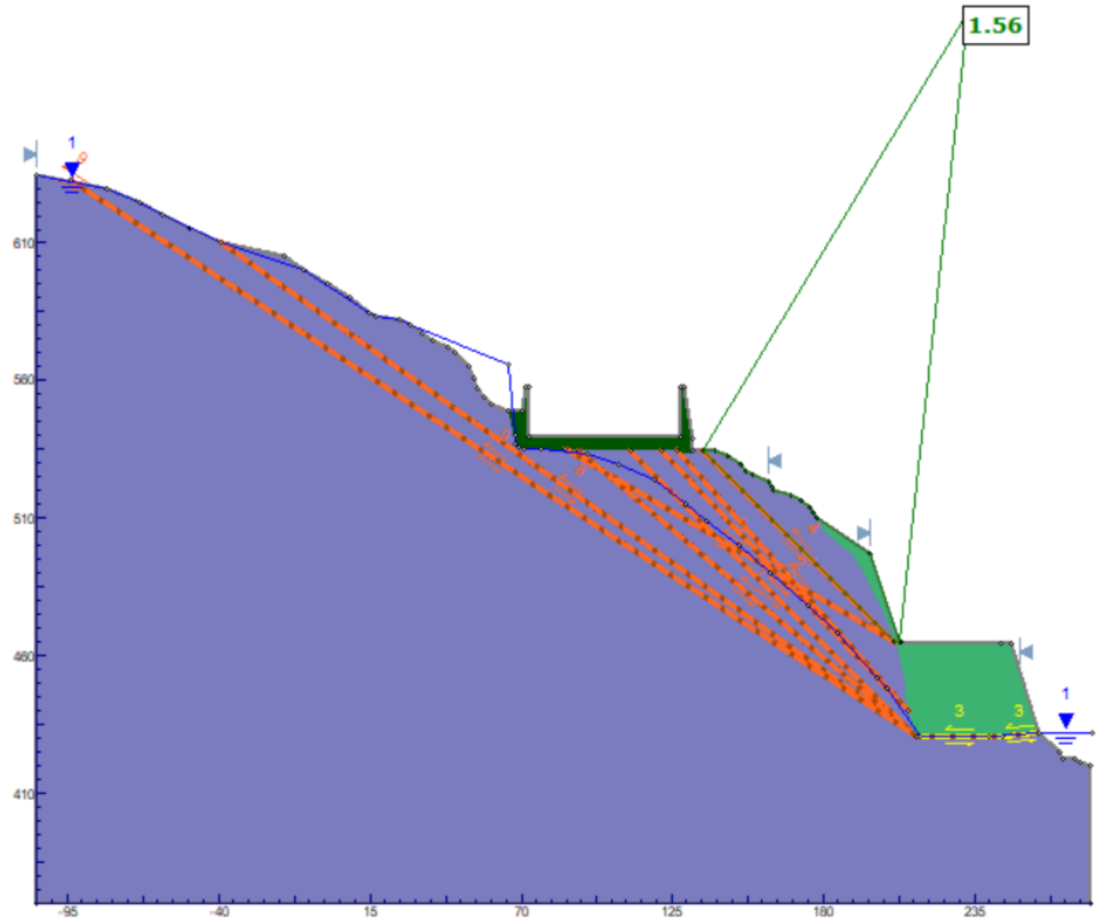

Exhibit 10-36: Limit Equilibrium Results for the Static Analysis of Failure Above the Dowel-Supported Grouted Rock Buttress under Usual Loading Conditions for Section 1. Artesian groundwater pressures have been measured in the VWP upslope of the spillway (boring BH-17-1). In Slide, artesian groundwater conditions are modeled using a piezometric head line, shown as the blue boundary, which accounts for the artesian pore pressures without contributions from the additional weight of the water (i.e., pooled water).

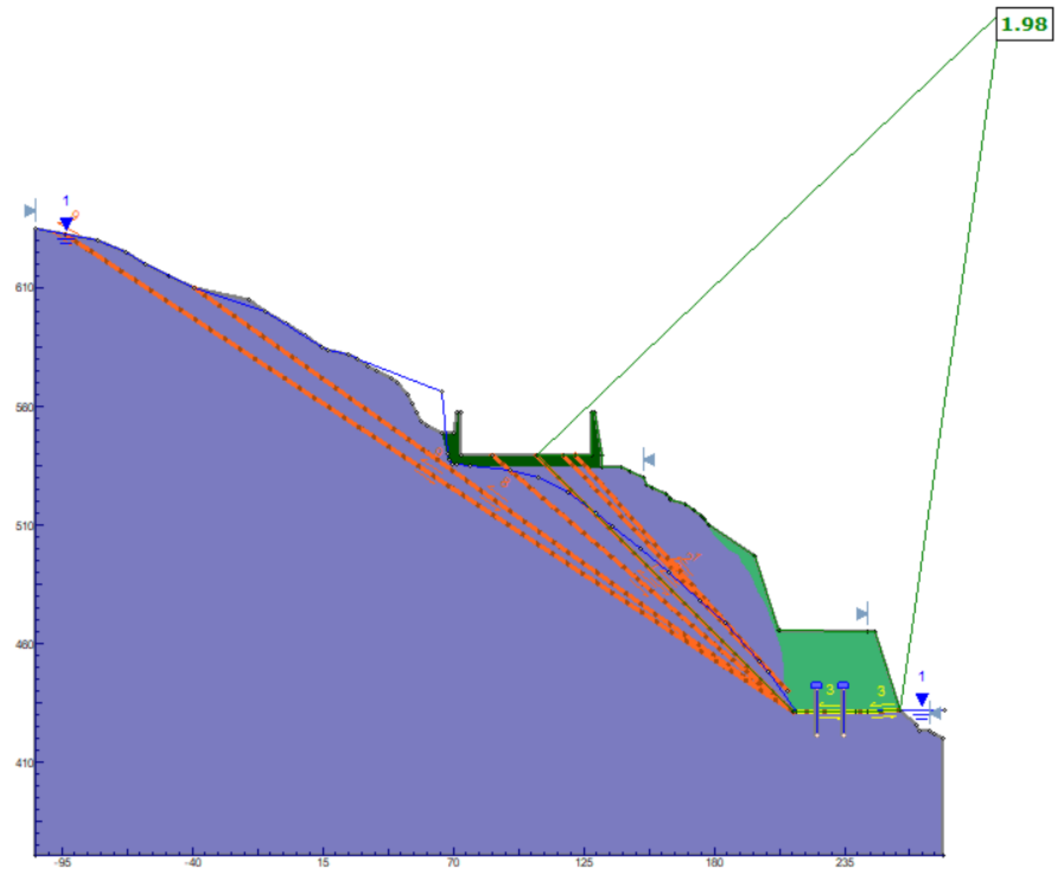

Exhibit 10-37: Limit Equilibrium Results for the Static Analysis of Failure Through the Dowel-Supported Grouted Rock Buttress under Usual Loading Conditions for Section 1. Artesian groundwater pressures have been measured in the VWP upslope of the spillway (boring BH-17-1). In Slide, artesian groundwater conditions are modeled using a piezometric head line, shown as the blue boundary, which accounts for the artesian pore pressures without contributions from the additional weight of the water (i.e., pooled water).

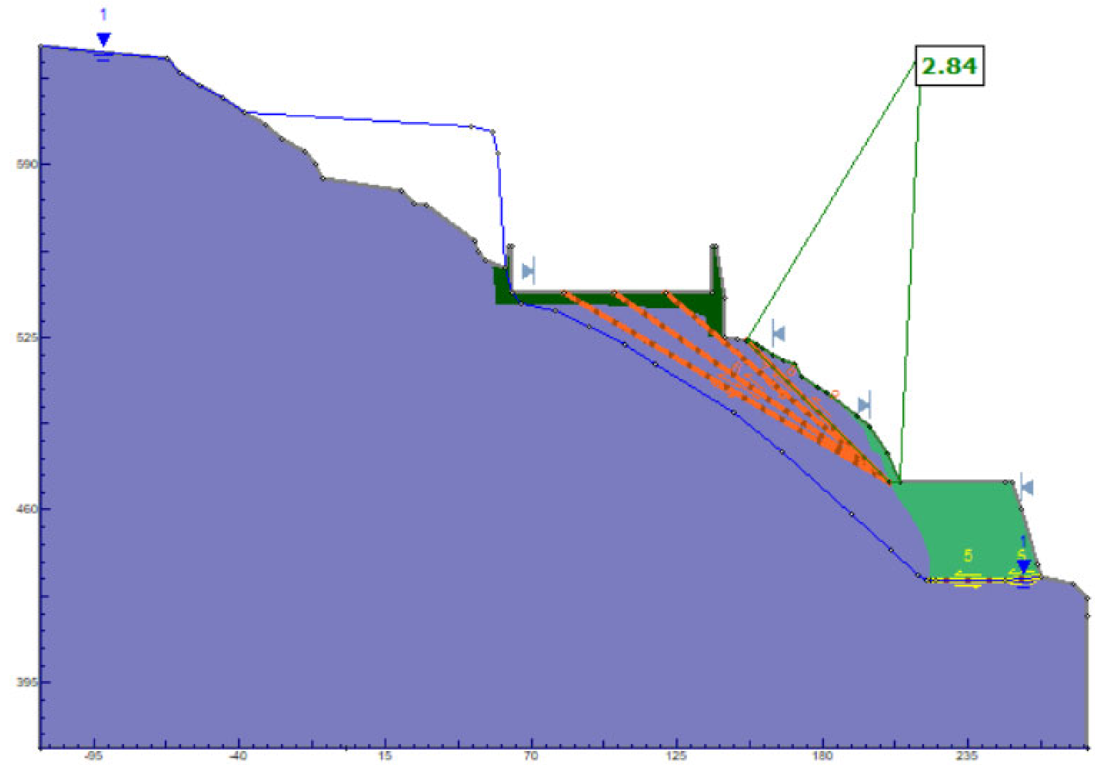

Exhibit 10-38: Limit Equilibrium Results for the Static Analysis of Failure Above the Dowel-Supported Grouted Rock Buttress under Usual Loading Conditions for Section 2. Artesian groundwater pressures have been measured in the VWP upslope of the spillway (boring BH-17-2). In Slide, artesian groundwater conditions are modeled using a piezometric head line, shown as the blue boundary, which accounts for the artesian pore pressures without contributions from the additional weight of the water (i.e., pooled water).

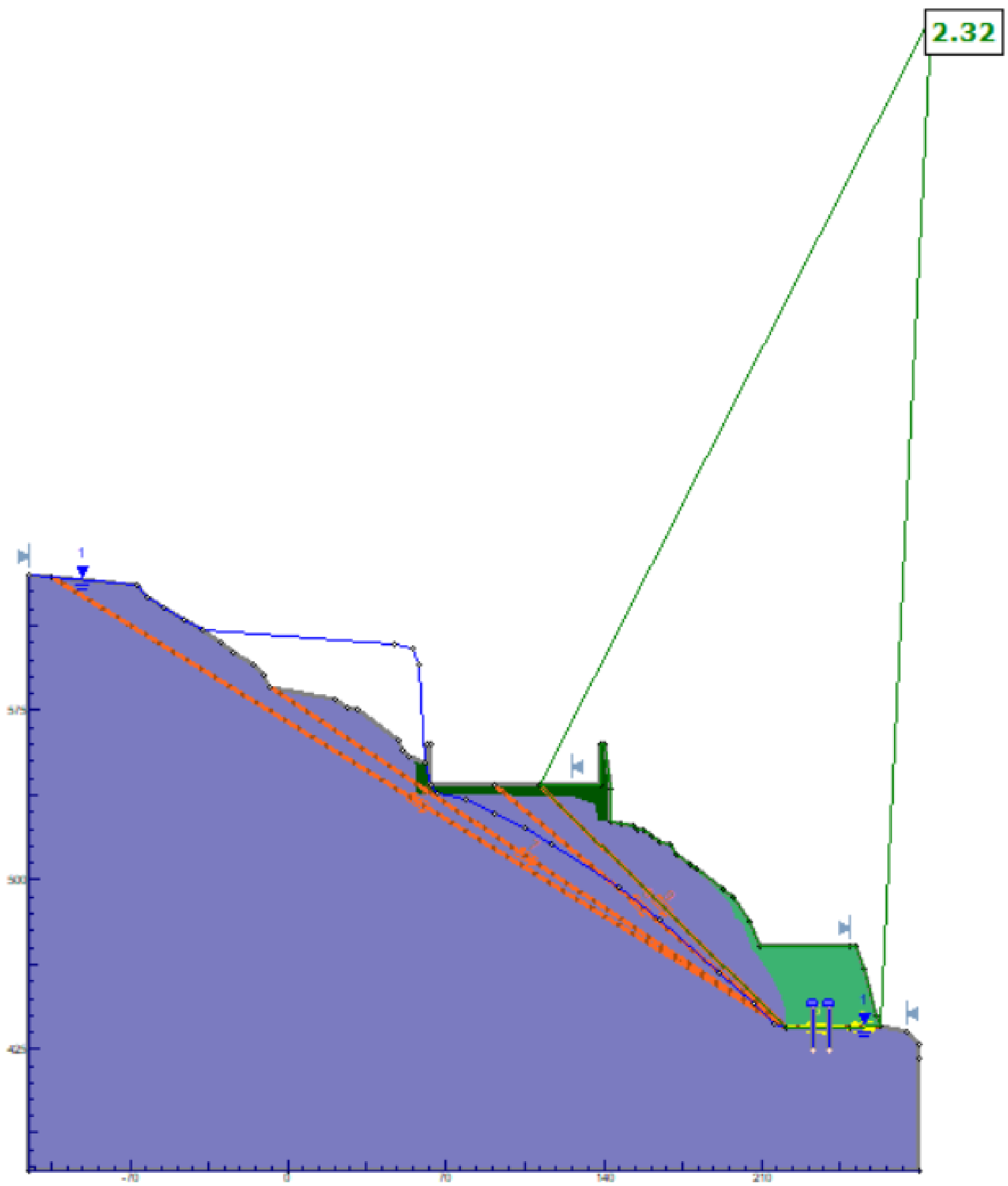

Exhibit 10-39: Limit Equilibrium Results for the Static Analysis of Failure Through the Dowel-Supported Grouted Rock Buttress under Usual Loading Conditions for Section 2. Artesian groundwater pressures have been measured in the VWP upslope of the spillway (boring BH-17-2). In Slide, artesian groundwater conditions are modeled using a piezometric head line, shown as the blue boundary, which accounts for the artesian pore pressures without contributions from the additional weight of the water (i.e., pooled water).

10.3.6.3 Static Analysis under Probable Maximum Flood Unusual Loading Conditions

Under unusual, PMF loading conditions, the static FS (GLE/Morgenstern) for Section 1:

- Against failure through the concrete lining above the grouted rock buttress is 1.6 and
- Against global failure of the dowel-supported grouted rock buttress is 2.0.

The Slide result for failure cases above and through the dowel-supported grouted rock buttress are presented in Exhibit 10-40 and Exhibit 10-41. The proposed dowel-supported grouted rock buttress design exceeds the required FS of 1.3 under unusual, PMF loading conditions established by GD-1, Rev. 1 (Shannon & Wilson, 2022) for Section 1.

Under unusual, PMF loading conditions, the static FS (GLE/Morgenstern) for Section 2:

- Against failure through the concrete lining above the grouted rock buttress is 2.8 and
- Against global failure of the dowel-supported grouted rock buttress is 2.3.

The Slide result for failure cases above and through the dowel-supported grouted rock buttress is presented in Exhibit 10-42 and Exhibit 10-43. The proposed dowel-supported grouted rock buttress design exceeds the required FS of 1.3 under unusual, PMF loading conditions established by GD-1, Rev. 1 (Shannon & Wilson, 2022) for Section 2.

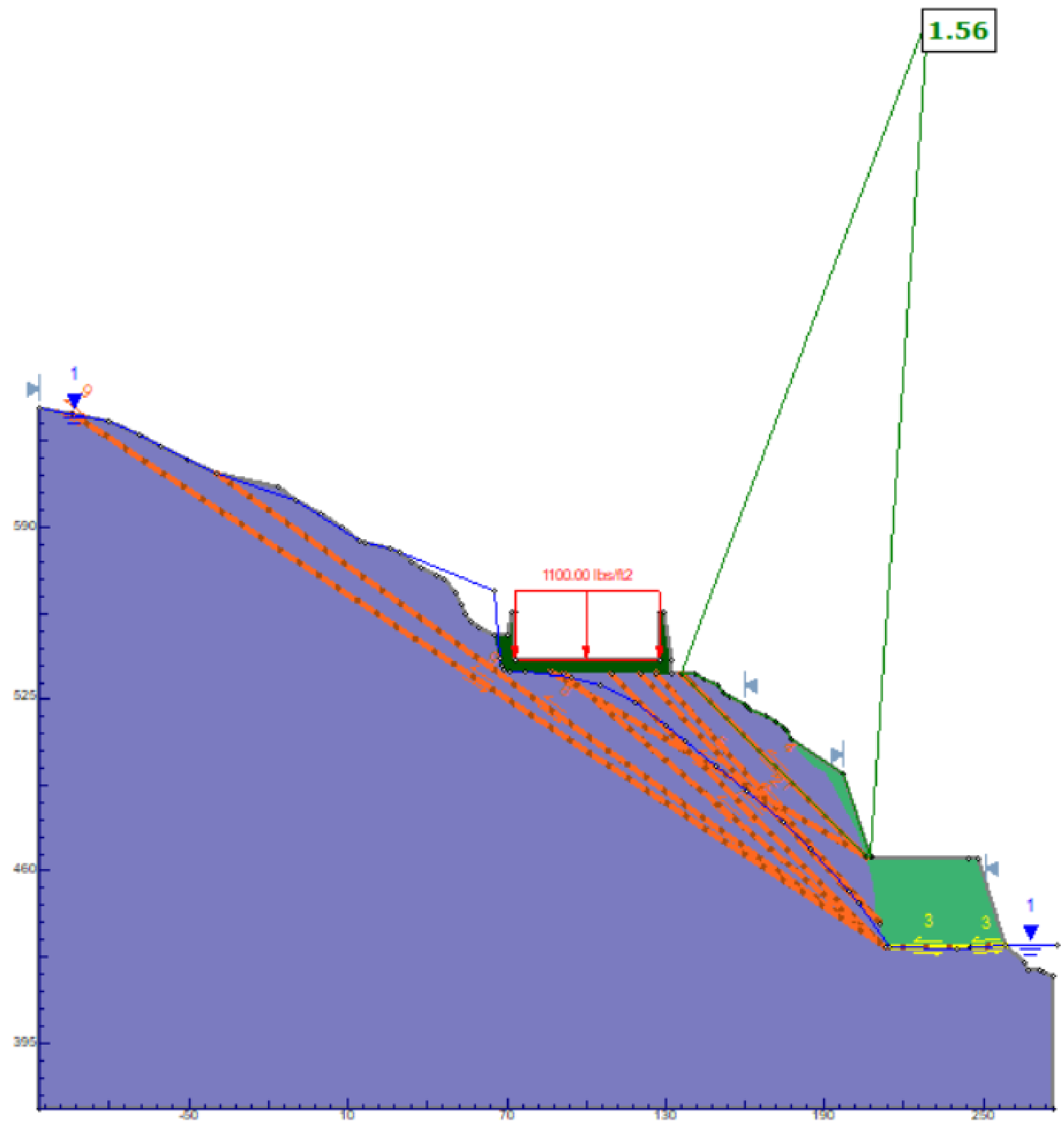

Exhibit 10-40: Limit Equilibrium Results for the Static Analysis of Failure Above the Dowel-Supported Grouted Rock Buttress under Unusual Loading Conditions for Section 1. Artesian groundwater pressures have been measured in the VWP upslope of the spillway (boring BH-17-1). In Slide, artesian groundwater conditions are modeled using a piezometric head line, shown as the blue boundary, which accounts for the artesian pore pressures without contributions from the additional weight of the water (i.e., pooled water).

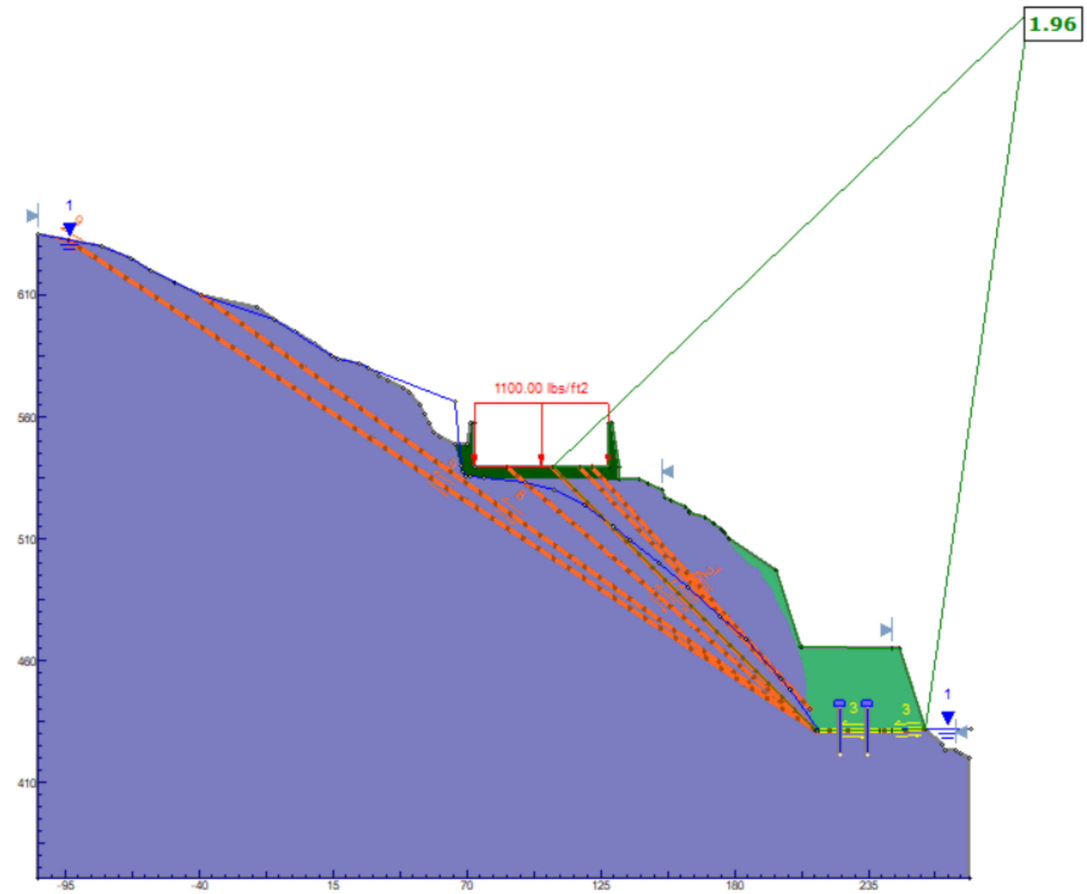

Exhibit 10-41: Limit Equilibrium Results for the Static Analysis of Failure Through the Dowel-Supported Grouted Rock Buttress under Unusual Loading Conditions for Section 1. Artesian groundwater pressures have been measured in the VWP upslope of the spillway (boring BH-17-1). In Slide, artesian groundwater conditions are modeled using a piezometric head line, shown as the blue boundary, which accounts for the artesian pore pressures without contributions from the additional weight of the water (i.e., pooled water).

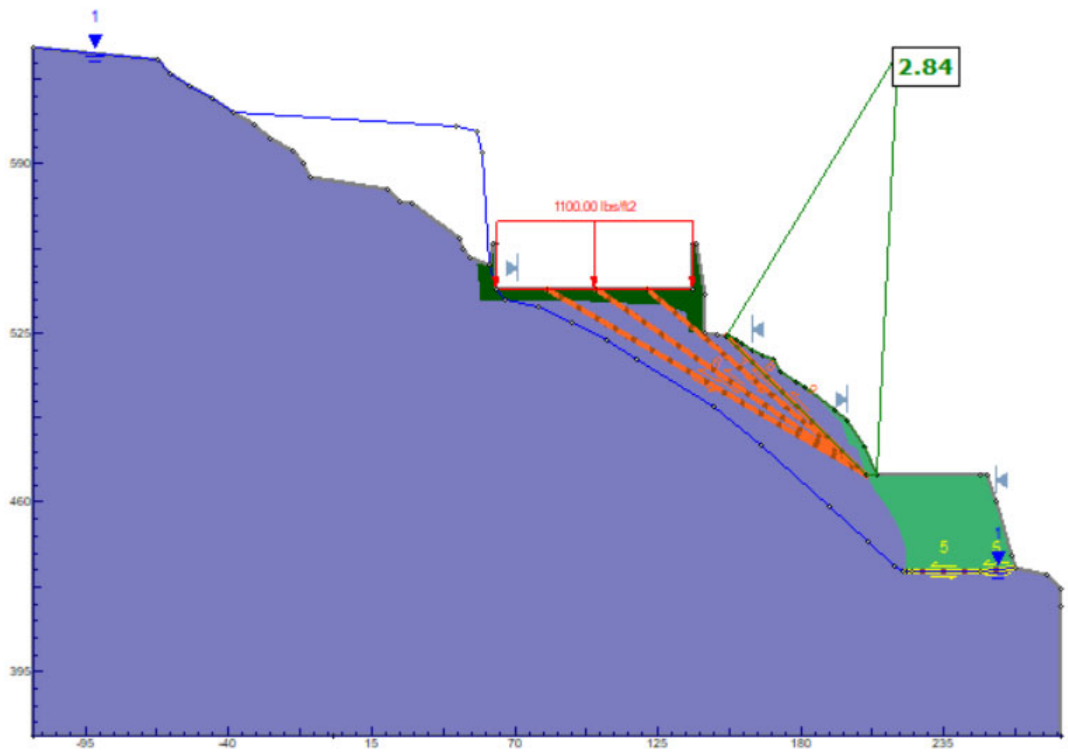

Exhibit 10-42: Limit Equilibrium Results for the Static Analysis of Failure Above the Dowel-Supported Grouted Rock Buttress under Unusual Loading Conditions for Section 2. Artesian groundwater pressures have been measured in the VWP upslope of the spillway (boring BH-17-2). In Slide, artesian groundwater conditions are modeled using a piezometric head line, shown as the blue boundary, which accounts for the artesian pore pressures without contributions from the additional weight of the water (i.e., pooled water).

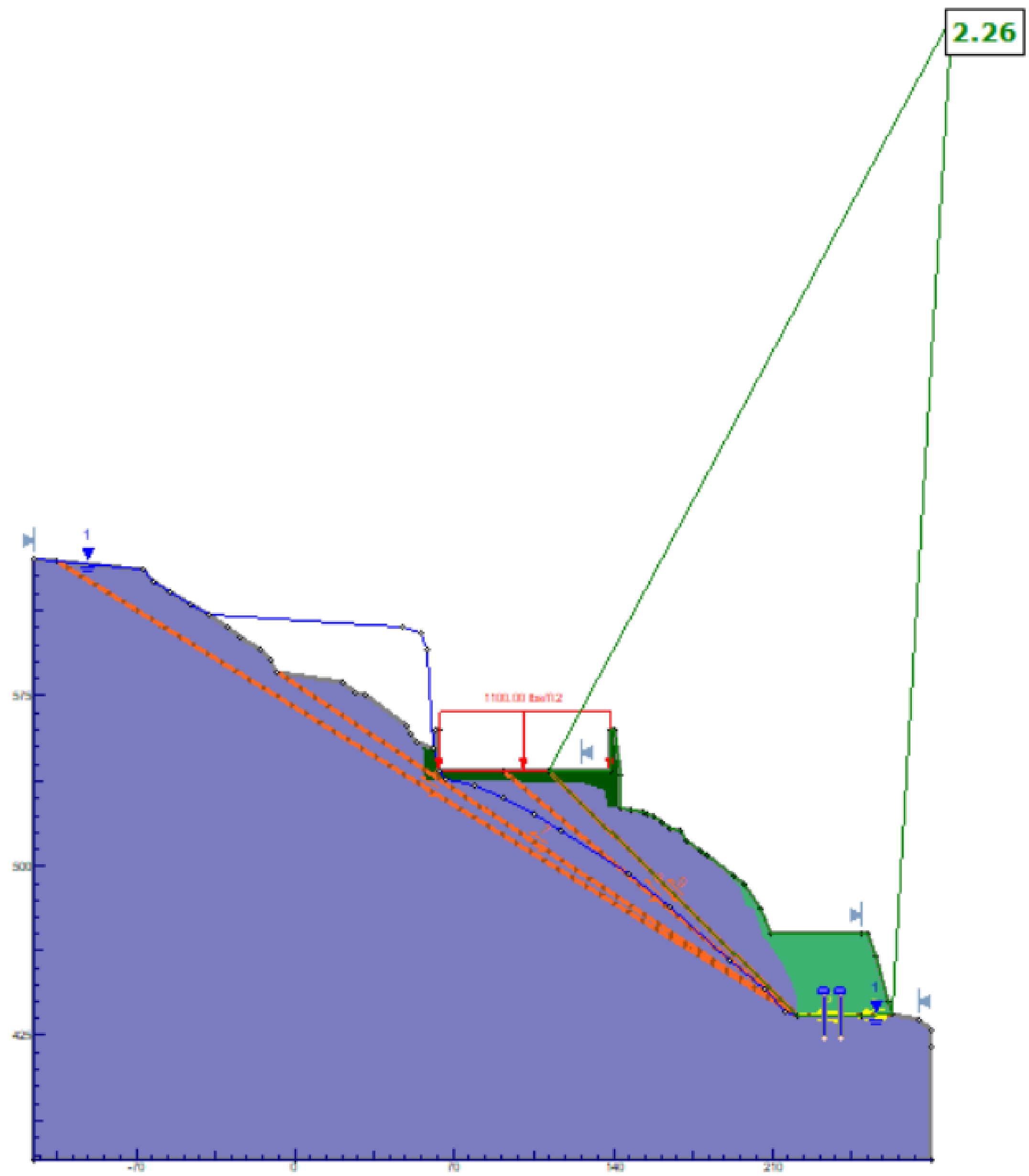

Exhibit 10-43: Limit Equilibrium Results for the Static Analysis of Failure Through the Dowel-Supported Grouted Rock Buttress under Unusual Loading Conditions for Section 2. Artesian groundwater pressures have been measured in the VWP upslope of the spillway (boring BH-17-2). In Slide, artesian groundwater conditions are modeled using a piezometric head line, shown as the blue boundary, which accounts for the artesian pore pressures without contributions from the additional weight of the water (i.e., pooled water).

10.3.6.4 Pseudo-Static Analysis under Extreme Loading Conditions

Under extreme loading conditions, the pseudo-static FS (GLE/Morgenstern) for Section 1:

- Against failure through the concrete lining above the grouted rock buttress is 1.1 and
- Against global failure of the dowel-supported grouted rock buttress is 1.3.

The Slide results for failure cases above and through the dowel-supported grouted rock buttress are presented in Exhibit 10-44 and Exhibit 10-45. The proposed dowel-supported grouted rock buttress design exceeds the required FS of 1.1 under extreme, pseudo-static loading conditions established by GD-1, Rev. 1 (Shannon & Wilson, 2022) for Section 1. Additionally, we evaluated the seismic conditions of the sluiceway slope using conventional Newmark sliding block deformation analysis according to Newmark (1965), described in Section 10.3.4.

Under extreme loading conditions, the pseudo-static FS (GLE/Morgenstern) for Section 2:

- Against failure through the concrete lining above the grouted rock buttress is 2.0 and
- Against global failure of the dowel-supported grouted rock buttress is 1.5.

The Slide results for failure cases above and through the dowel-supported grouted rock buttress are presented in Exhibit 10-46 and Exhibit 10-47. The proposed dowel-supported grouted rock buttress design exceeds the required FS of 1.1 under extreme, pseudo-static loading conditions established by GD-1, Rev. 1 (Shannon & Wilson, 2022) for Section 2. Additionally, we evaluated the seismic conditions of the sluiceway slope using conventional Newmark sliding block deformation analysis according to Newmark (1965), described in Section 10.3.8.

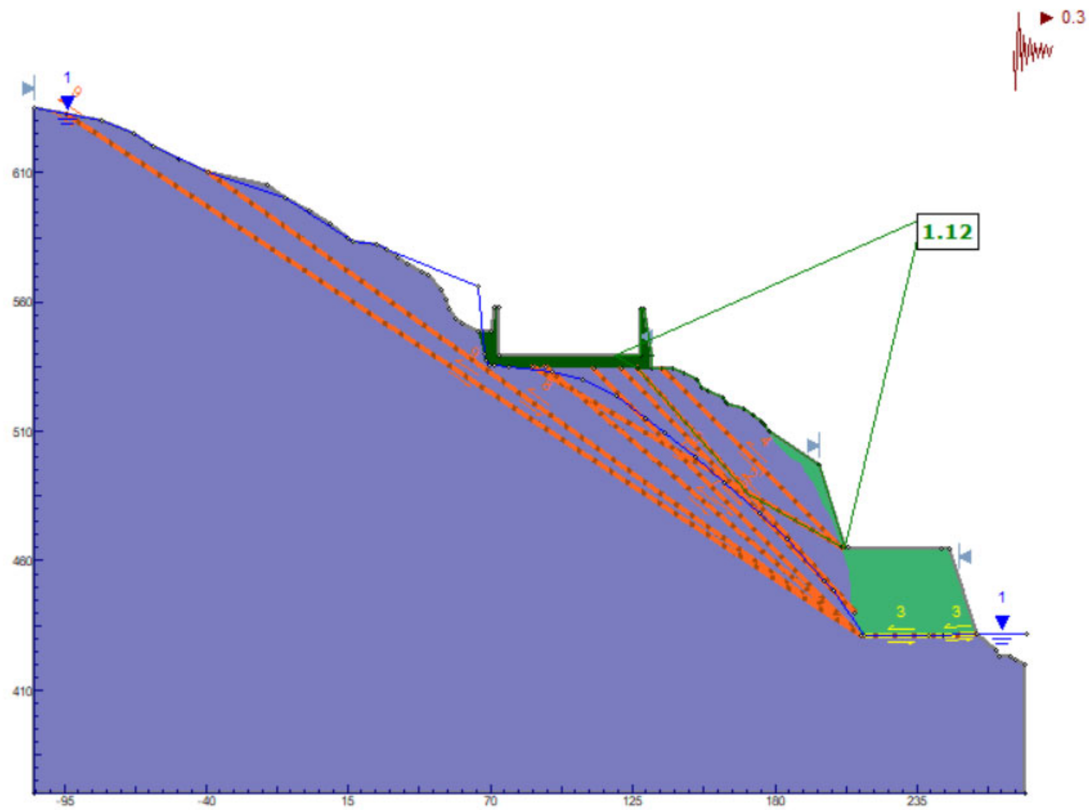

Exhibit 10-44: Limit Equilibrium Results for the Static Analysis of Failure Above the Dowel-Supported Grouted Rock Buttress under Extreme Loading Conditions for Section 1. Artesian groundwater pressures have been measured in the VWP upslope of the spillway (boring BH-17-1). In Slide, artesian groundwater conditions are modeled using a piezometric head line, shown as the blue boundary, which accounts for the artesian pore pressures without contributions from the additional weight of the water (i.e., pooled water).

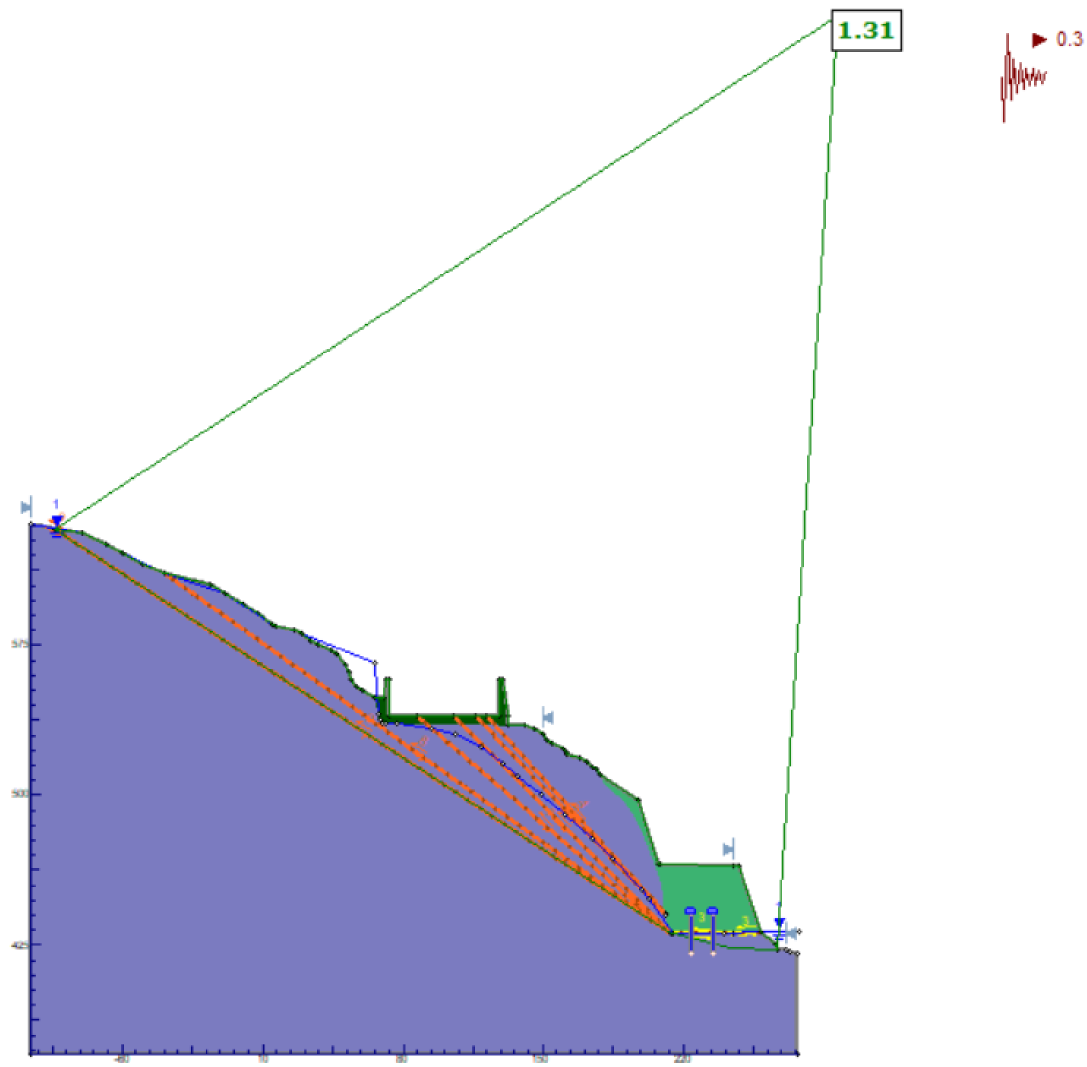

Exhibit 10-45: Limit Equilibrium Results for the Static Analysis of Failure Through the Dowel-Supported Grouted Rock Buttress under Extreme Loading Conditions for Section 1. Artesian groundwater pressures have been measured in the VWP upslope of the spillway (boring BH-17-1). In Slide, artesian groundwater conditions are modeled using a piezometric head line, shown as the blue boundary, which accounts for the artesian pore pressures without contributions from the additional weight of the water (i.e., pooled water).

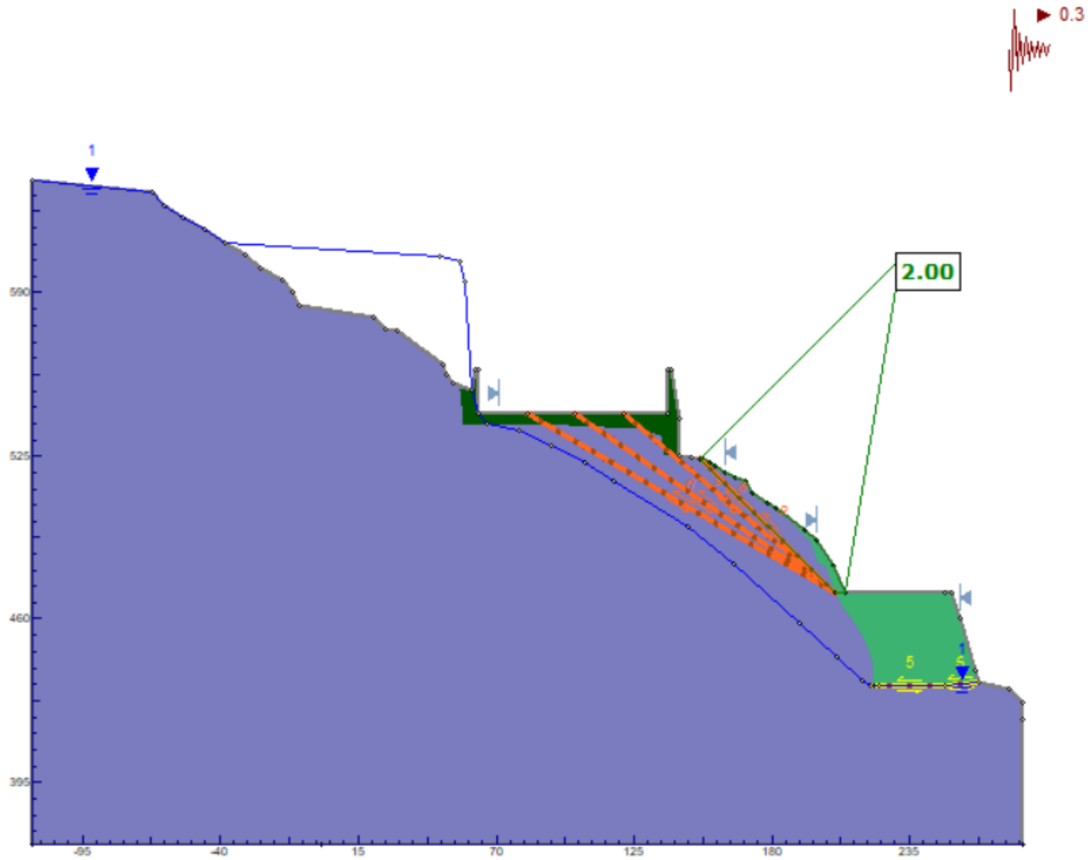

Exhibit 10-46: Limit Equilibrium Results for the Static Analysis of Failure Above the Dowel-Supported Grouted Rock Buttress under Extreme Loading Conditions for Section 2. Artesian groundwater pressures have been measured in the VWP upslope of the spillway (boring BH-17-2). In Slide, artesian groundwater conditions are modeled using a piezometric head line, shown as the blue boundary, which accounts for the artesian pore pressures without contributions from the additional weight of the water (i.e., pooled water).

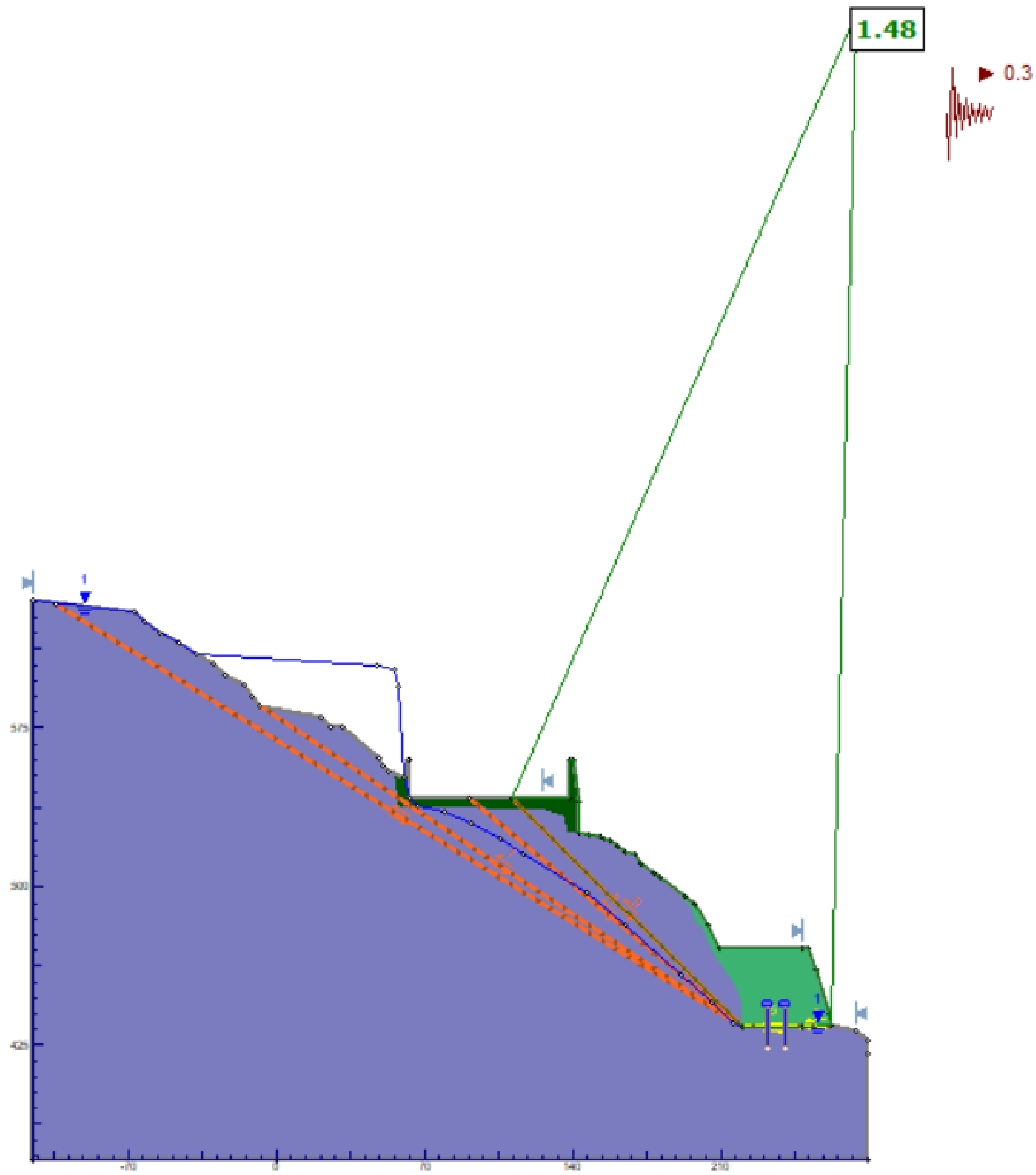

Exhibit 10-47: Limit Equilibrium Results for the Static Analysis of Failure Through the Dowel-Supported Grouted Rock Buttress under Extreme Loading Conditions for Section 2. Artesian groundwater pressures have been measured in the VWP upslope of the spillway (boring BH-17-2). In Slide, artesian groundwater conditions are modeled using a piezometric head line, shown as the blue boundary, which accounts for the artesian pore pressures without contributions from the additional weight of the water (i.e., pooled water).

10.3.6.5 Static Analysis using Post-Earthquake Material Properties

Under usual loading conditions with post-earthquake material, the static FS (GLE/Morgenstern) for Section 1:

- Against failure through the concrete lining above the grouted rock buttress is 1.4 and
- Against global failure of the dowel-supported grouted rock buttress is 1.8.

The Slide results for failure cases above and through the dowel-supported grouted rock buttress are presented in Exhibit 10-48 and Exhibit 10-49. The proposed dowel-supported grouted rock buttress design exceeds the required FS of 1.3 under usual loading conditions with post-earthquake material established by GD-1, Rev. 1 (Shannon & Wilson, 2022) for Section 1.

Under usual loading conditions with post-earthquake material, the static FS (GLE/Morgenstern) for Section 2:

- Against failure through the concrete lining above the grouted rock buttress is 2.6 and
- Against global failure of the dowel-supported grouted rock buttress is 2.1.

The Slide results for failure cases above and through the dowel-supported grouted rock buttress are presented in Exhibit 10-50 and Exhibit 10-51. The proposed dowel-supported grouted rock buttress design exceeds the required FS of 1.3 under usual loading conditions with post-earthquake material established by GD-1, Rev. 1 (Shannon & Wilson, 2022) for Section 2.

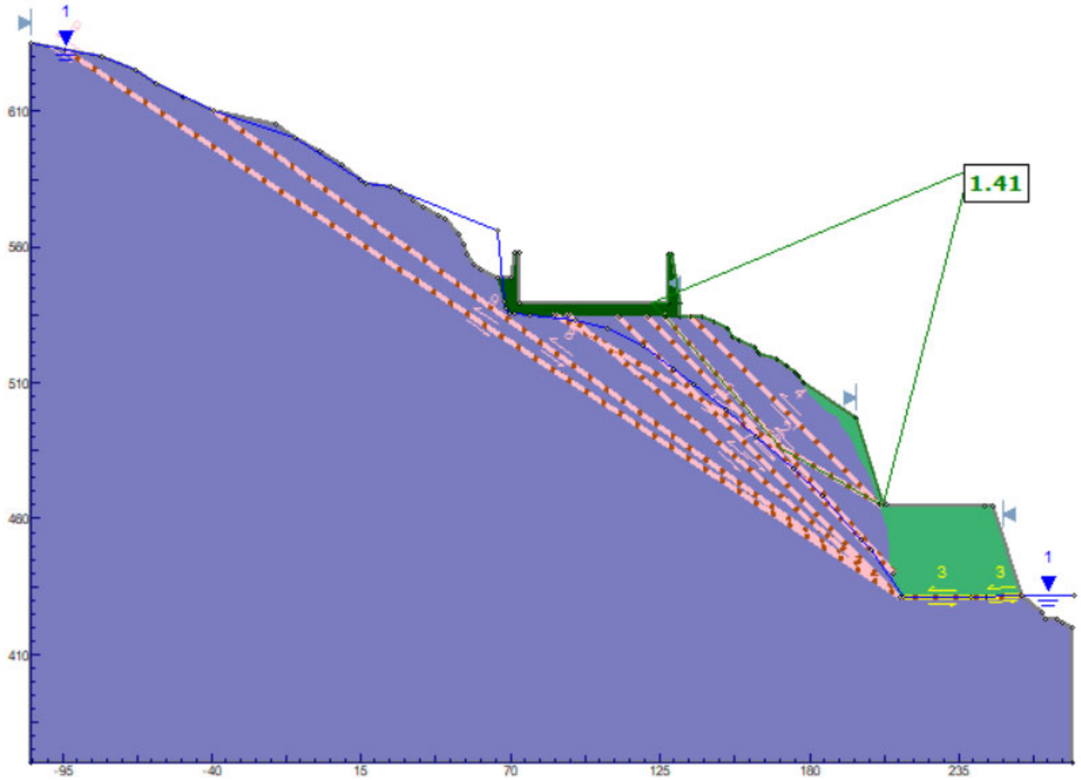

Exhibit 10-48: Limit Equilibrium Results for the Static Analysis of Failure Above the Dowel-Supported Grouted Rock Buttress under Usual Loading Conditions with Post-Earthquake Material Properties for Section 1. Artesian groundwater pressures have been measured in the VWP upslope of the spillway (boring BH-17-1). In Slide, artesian groundwater conditions are modeled using a piezometric head line, shown as the blue boundary, which accounts for the artesian pore pressures without contributions from the additional weight of the water (i.e., pooled water).

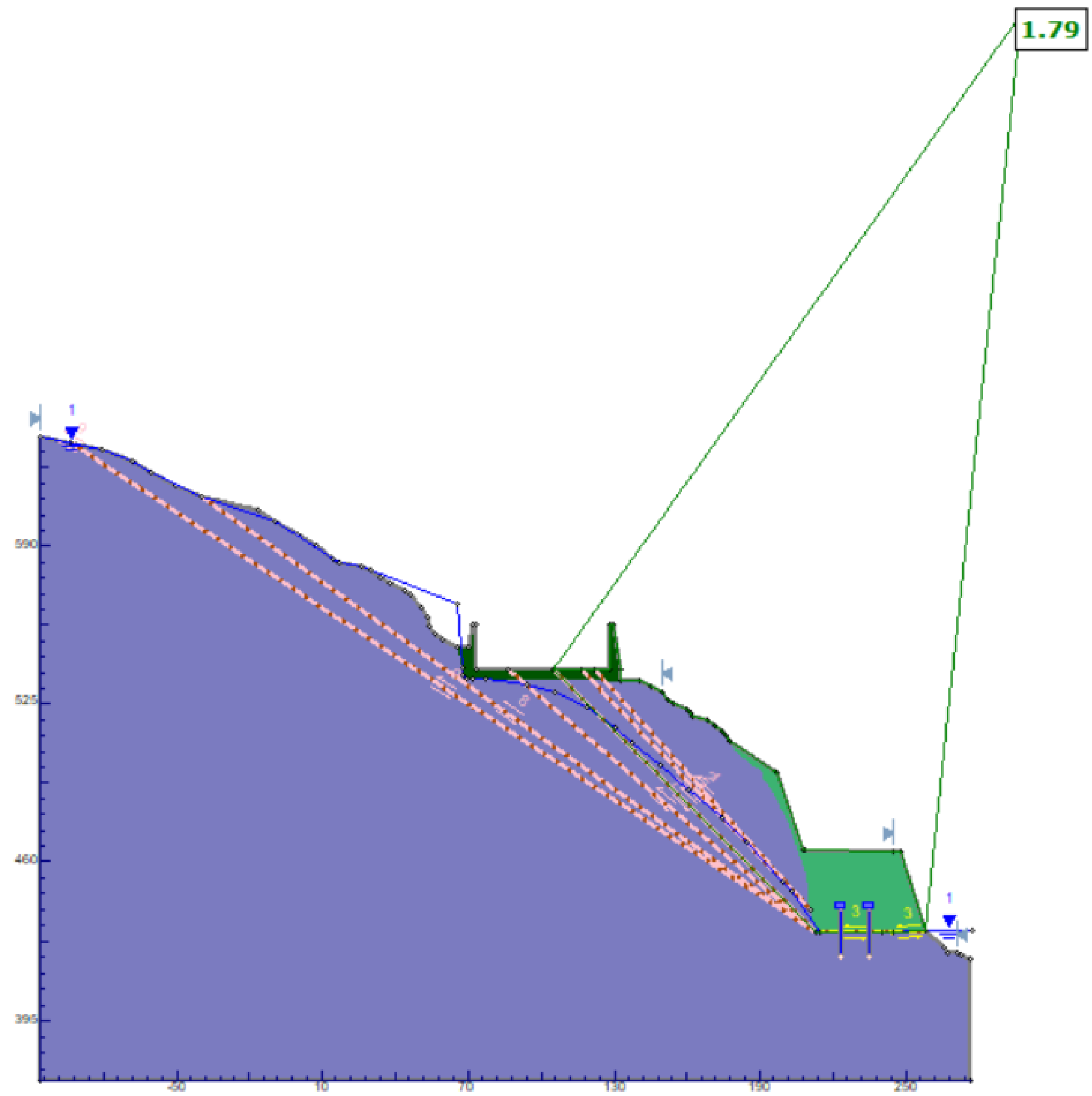

Exhibit 10-49: Limit Equilibrium Results for the Static Analysis of Failure Through the Dowel-Supported Grouted Rock Buttress under Usual Loading Conditions with Post-Earthquake Material Properties for Section 1. Artesian groundwater pressures have been measured in the VWP upslope of the spillway (boring BH-17-1). In Slide, artesian groundwater conditions are modeled using a piezometric head line, shown as the blue boundary, which accounts for the artesian pore pressures without contributions from the additional weight of the water (i.e., pooled water).

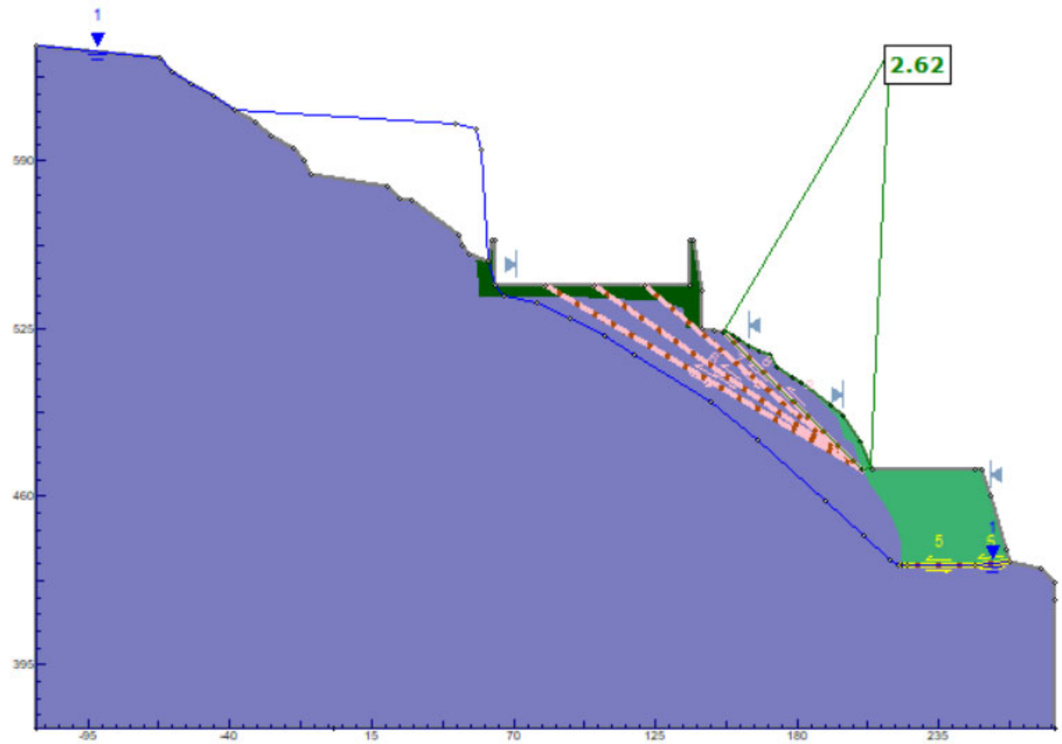

Exhibit 10-50: Limit Equilibrium Results for the Static Analysis of Failure Above the Dowel-Supported Grouted Rock Buttress under Usual Loading Conditions with Post-Earthquake Material Properties for Section 2. Artesian groundwater pressures have been measured in the VWP upslope of the spillway (boring BH-17-2). In Slide, artesian groundwater conditions are modeled using a piezometric head line, shown as the blue boundary, which accounts for the artesian pore pressures without contributions from the additional weight of the water (i.e., pooled water).

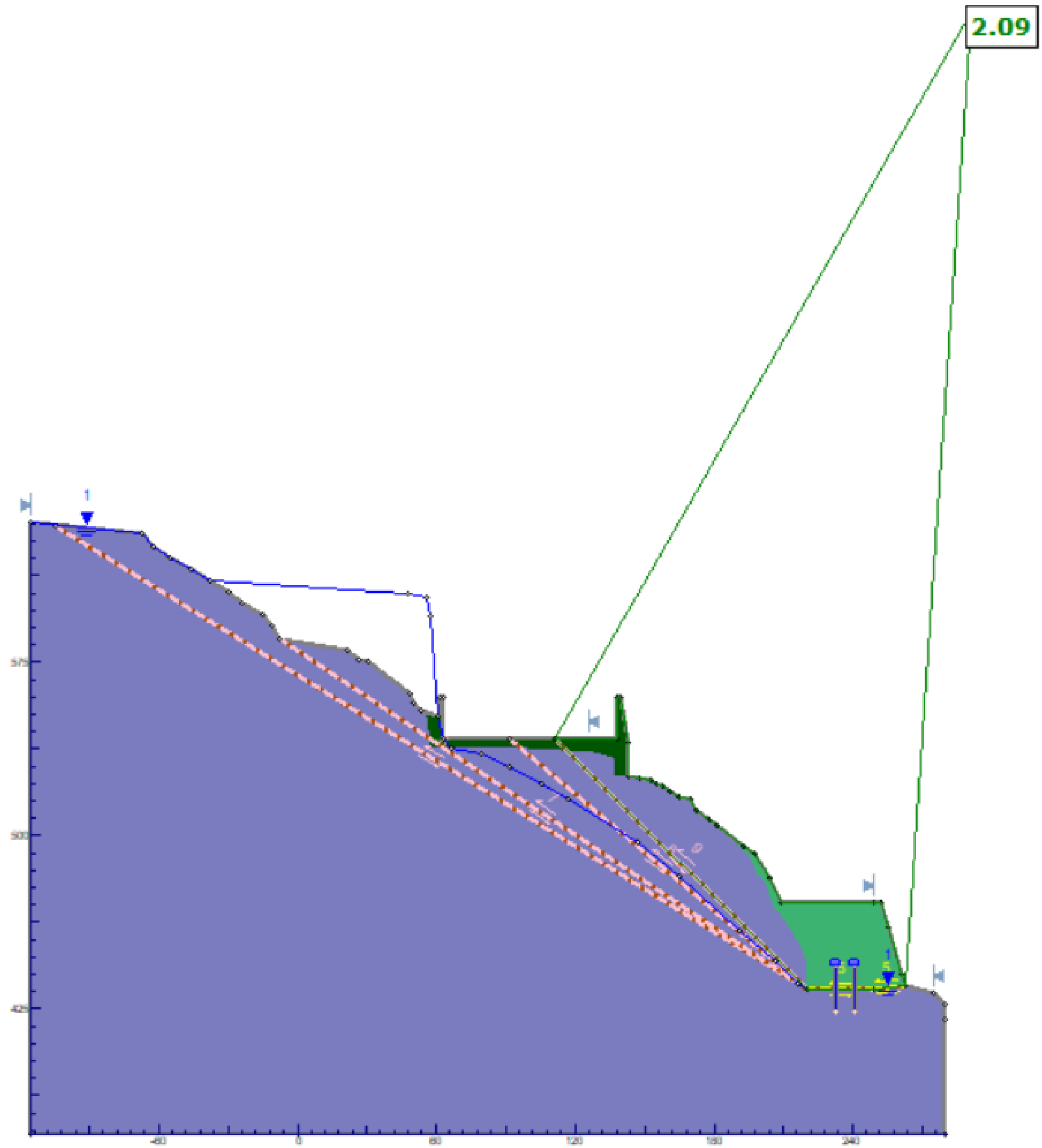

Exhibit 10-51: Limit Equilibrium Results for the Static Analysis of Failure Through the Dowel-Supported Grouted Rock Buttress under Usual Loading Conditions with Post-Earthquake Material Properties for Section 2. Artesian groundwater pressures have been measured in the VWP upslope of the spillway (boring BH-17-2). In Slide, artesian groundwater conditions are modeled using a piezometric head line, shown as the blue boundary, which accounts for the artesian pore pressures without contributions from the additional weight of the water (i.e., pooled water).

10.3.7 Newmark Analyses of Existing Conditions and Spillway Support Options

Upper Baker Dam is in a high seismicity area according to FERC (2006); therefore, dynamic analysis is required for evaluation of seismic loading effects. Seismic effects were evaluated for the sluiceway slope using conventional Newmark sliding block displacement analyses (Newmark, 1965). The Newmark analyses were performed using a built-in module in Slide (v. 9.023) by Rocscience (2022) and are provided in Appendix O.

The Newmark sliding block analysis method estimates permanent displacements of slopes during seismic loading and is an extension of the pseudo-static analysis method. Because earthquake accelerations vary with time, a FS computed using a pseudo-static analysis would vary throughout an earthquake. If the inertial forces acting on a potential failure mass caused by earthquake loading exceed the resisting forces, the FS would become less than 1.0, and the potential failure mass is no longer in equilibrium. The failure mass would be accelerated by the unbalanced force, resulting in permanent deformations. This situation is analogous to a block resting on an inclined plane; thus, the method is typically referred to as the "Newmark sliding block analysis." The magnitude of the displacement is obtained by integrating twice—acceleration is the second time derivative of displacement—the difference of the applied acceleration and the critical acceleration with respect to time (Kramer, 1996). Slide implements a Newmark seismic displacement analysis using the code developed for the program SLAMMER (Jobson and others, 2013) developed by the USGS.

Time and acceleration data were input into Slide for these analyses by importing time history records for seven (7) ground motion sets developed for the Baker River Project. Using two orthogonal horizontal components from each ground motion set, a total of 14 time histories were developed for the Baker River Project (Shannon & Wilson, 2019). These time histories were developed using FERC guidelines (Idriss and others, 2018) and the following process:

- Develop Target Spectra: Develop horizontal and vertical deterministic target spectra for time history spectral matching. The horizontal target spectrum is developed as an envelope of two 84th percentile deterministic crustal background Maximum Credible Earthquake (MCE) events. The vertical target spectrum corresponds to the same horizontal MCE scenarios.
- Select Reference Time Histories: Select seven (7) 3-component ground motion sets consistent with the MCE target spectra. Each ground motion set includes two orthogonal horizontal components and one vertical component. Only the two orthogonal horizontal components were used in our analyses.
- Spectrally Match Time Histories: Modify each selected reference time history so that its acceleration response spectrum matches the corresponding target spectrum.

- Post-Process Time Histories: Process the spectrally matched acceleration time histories to eliminate potential drift in velocity and displacement time histories.

The time histories were developed for National Earthquake Hazards Reduction Program Site Class A/B (hard rock/soft rock) boundary conditions with a time-weighted average shear wave velocity in the upper 30 meters of a soil/rock profile (VS30) of 1,500 meters per second, or approximately 5,000 feet per second. This site condition was selected after reviewing the foundation conditions at Baker River Hydroelectric Project structures and considering ground motion models' capabilities in modeling this site condition. The selected reference ground motions (Shannon & Wilson, 2019) are listed in Exhibit 10-52.

Exhibit 10-52: Selected Time Histories

Mechanism	Reverse Oblique	Reverse Oblique	Reverse	Reverse	Reverse	Reverse	Reverse
Earthquake	Loma Prieta	Loma Prieta	San Fernando	Chuetsu-oki_ Japan	Iwate_ Japan	Iwate_ Japan	Chuetsu-oki_ Japan
Earthquake Date	1989	1989	1971	2007	2008	2008	2007
Station Name	Gilroy Array #6	San Jose – Santa Teresa Hills	Lake Hughes #4	Kawaguchi	IWT010	Yuzawa	Joetsu Oshimaku Oka
M_W	6.93	6.93	6.61	6.8	6.9	6.9	6.8
R_{rup} (km)	18.33	14.69	25.07	29.25	16.27	25.56	22.48
R_{jb} (km)	17.92	14.18	19.45	23.63	16.26	22.41	15.62
V_{S30} (m/sec)	663.31	671.77	600.06	640.14	825.83	655.45	610.05
PGA (g)	0.428	0.426	0.438	0.446	0.445	0.436	0.460
1st Horizontal Component	LOMAP_ G06000	LOMAP_ SJTE225	SFERN_ L04111	CHUETSU_ 65042NS	IWATE_ IWT010NS	IWATE_ 44BC1NS	CHUETSU_ 65008NS
2nd Horizontal Component	LOMAP_ G06090	LOMAP_ SJTE315	SFERN_ L04201	CHUETSU_ 65042EW	IWATE_ IWT010EW	IWATE_ 44BC1EW	CHUETSU_ 65008EW
Vertical Component	LOMAP_ G06-UP	LOMAP_ SJTE-UP	SFERN_ L04DWN	CHUETSU_ 65042UD	IWATE_ IWT010UD	IWATE_ 44BC1UD	CHUETSU_ 65008UD

NOTES:
g = standard acceleration of gravity; km = kilometer; m/sec = minutes per second; M_w = moment magnitude; PGA = peak ground acceleration; R_{jb} = Joyner-Boore distance; R_{rup} = source-to-site rupture distance; V_{S30} = velocity in upper 30 meters of soil/rock profile

The results of the Newmark displacement analyses are presented in Appendix O and summarized in Exhibit 10-53 and Exhibit 10-54. Chapter 4 Embankment Dams states that "The deformations calculated for potential failure masses by Newmark… should normally not exceed 2 feet…," (FERC, 2006). According to Wyllie and Mah (2004), the Newmark method of analysis should be considered order-of-magnitude estimates of field behavior, and the following guidelines should be used to anticipate likely slope behavior (California Division of Mines and Geology [CDMG], 1997):

- Slope displacements of zero (0) to 4 inches (0 to 100 millimeters [mm]) are unlikely to correspond to serious landslide movement;
- Slope displacements of 4 to 40 inches (100 to 1,000 mm) may be sufficient to cause serious ground cracking or enough strength loss to result in continuing post-seismic failure; and
- Slope displacements greater than 40 inches (>1,000 mm) may yield damaging landslide movement and such slopes should be considered unstable.

We performed analyses in Slide (v. 9.023) by Rocscience (2022) using Generalized Limit Equilibrium (GLE) and Janbu-simplified methods to estimate the yield acceleration of the slope designs in both Section 1 and Section 2. Furthermore, we performed Newmark analyses for both sections using the built-in Newmark Analyses feature of Slide (v. 9.023) by Rocscience (2022) as well as a Python code by Shannon & Wilson that generated acceleration, velocity, and displacement (AVD) time histories, and the 14 time histories developed for Upper Baker by Shannon & Wilson (2019); Newmark analyses were only performed with the Janbu-simplified limit equilibrium method which generally yields a more conservative result.

For Section 1 and Section 2, the maximum permanent displacement estimated for the 14 time histories for the existing spillway condition is approximately 66.5 and 11.0 inches, for the time histories RSN5618_IWATE_IWT010NS and RSN4869_CHUETSU_65042EW, respectively. Newmark analyses were performed on the existing spillway condition to evaluate the reduction of slope displacement as a result of mitigation methods. The results of the Newmark analyses for the existing slope condition and mitigation alternatives are presented in Exhibit 10-53 and Exhibit 10-54 for Section 1 and 2, respectively.

For Section 1 and Section 2, the maximum permanent displacement estimated for the 14 time histories from all presented stabilization designs is approximately 0.12 inches for a failure above the grouted rock buttress for the time history, RSN4869_CHUETSU_65042NS. However, for both sections, the maximum permanent displacement estimated for the 14 time histories is equal to 0.1 inch for both anchor-supported designs as well as for the dowel-supported grouted rock buttress. Therefore, according to the CDMG (1997) guidelines, the buttress-supported and the anchor-supported slopes are unlikely to correspond to serious slope movement.

Exhibit 10-53: Summary of Estimated Seismic Displacement for Section 1 using Newmark Analysis

Section 1 – Estimate Seismic Displacement of Failure Mass (inches)					
		Anchor-supported		Buttress-supported	
Time History	Existing Spillway Condition	1 ¾-inch Anchors	8 Strand Anchors	Above	Dowel Supported
RSN72_SFERN_L04111	34.4	< 0.1	< 0.1	< 0.1	0.1
RSN72_SFERN_L04201	31.7	<0.1	< 0.1	< 0.1	< 0.1
RSN769_LOMAP_G06000	48.8	< 0.1	< 0.1	< 0.1	< 0.1
RSN769_LOMAP_G06090	48.1	< 0.1	< 0.1	< 0.1	< 0.1
RSN801_LOMAP_SJTE225	36.8	< 0.1	< 0.1	< 0.1	< 0.1
RSN801_LOMAP_SJTE315	47.0	< 0.1	< 0.1	< 0.1	< 0.1
RSN4845_CHUETSU_65008NS	27.4	< 0.1	< 0.1	< 0.1	< 0.1
RSN4845_CHUETSU_65008EW	26.0	< 0.1	< 0.1	< 0.1	< 0.1
RSN4869_CHUETSU_65042NS	50.6	< 0.1	< 0.1	< 0.1	0.1
RSN4869_CHUETSU_65042EW	56.4	< 0.1	< 0.1	< 0.1	< 0.1
RSN5618_IWATE_IWT010NS	66.5	< 0.1	< 0.1	< 0.1	< 0.1
RSN5618_IWATE_IWT010EW	51.7	< 0.1	< 0.1	< 0.1	< 0.1
RSN5815_IWATE_44BC1NS	50.5	< 0.1	< 0.1	< 0.1	< 0.1
RSN5815_IWATE_44BC1EW	45.2	< 0.1	< 0.1	< 0.1	< 0.1

NOTE:
Reported values calculated in Slide v. 9.023 (Rocscience, 2022).

Exhibit 10-54: Summary of Estimated Seismic Displacement for Section 2 using Newmark Analysis

Section 2 – Estimate Seismic Displacement of Failure Mass (inches)					
		Anchor-supported		Buttress-supported	
Time History	Existing Spillway Condition	1 ¾-inch Anchors	8 Strand Anchors	Above	Dowel Supported
RSN72_SFERN_L04111	6.2	0.1	< 0.1	0.1	< 0.1
RSN72_SFERN_L04201	7.1	< 0.1	< 0.1	< 0.1	< 0.1
RSN769_LOMAP_G06000	6.2	< 0.1	< 0.1	< 0.1	< 0.1
RSN769_LOMAP_G06090	6.2	< 0.1	< 0.1	< 0.1	< 0.1
RSN801_LOMAP_SJTE225	7.0	< 0.1	< 0.1	0.1	< 0.1
RSN801_LOMAP_SJTE315	7.9	< 0.1	< 0.1	0.1	< 0.1
RSN4845_CHUETSU_65008NS	4.2	< 0.1	< 0.1	< 0.1	< 0.1
RSN4845_CHUETSU_65008EW	7.7	< 0.1	< 0.1	< 0.1	< 0.1
RSN4869_CHUETSU_65042NS	5.3	0.1	< 0.1	0.1	< 0.1
RSN4869_CHUETSU_65042EW	11.0	< 0.1	< 0.1	< 0.1	< 0.1
RSN5618_IWATE_IWT010NS	9.6	< 0.1	< 0.1	0.1	< 0.1
RSN5618_IWATE_IWT010EW	7.8	< 0.1	< 0.1	< 0.1	< 0.1
RSN5815_IWATE_44BC1NS	9.2	< 0.1	< 0.1	0.1	< 0.1
RSN5815_IWATE_44BC1EW	7.9	< 0.1	< 0.1	0.1	< 0.1

NOTE:
Reported values calculated in Slide v. 9.023 (Rocscience, 2022).

The acceleration time histories with yield accelerations, the velocity time histories, and displacement time histories (AVD time histories) with cumulative permanent deformation are presented for each support scenario and earthquake motion in Appendix O. Slide does not include the time histories as outputs from the program; therefore, we produced the AVD time histories by integrating the acceleration time history for accelerations greater than the yield acceleration to calculate the velocity time history and then integrating velocity to calculate the displacement time history in both the positive and negative directions. The yield acceleration of 1 ¾-inch, Grade 150 and 8 Strand anchor-supported slopes for Section 1 are 0.32 and 0.37 g, respectively. The yield acceleration of the dowel-supported grouted rock buttress slope for Section 1 is 0.30 g. The yield acceleration of 1 ¾-inch, Grade 150 and 8 Strand anchor-supported slopes for Section 2 are 0.30 and 0.35 g, respectively. The yield acceleration of the dowel-supported grouted rock buttress slope for Section 2 is 0.40 g.

10.3.8 Summary of Limit Equilibrium Analyses

As a comparison to the previously evaluated limit equilibrium analyses, we ran the existing conditions model, as presented in Section 10.3.4, with the previously utilized scaled strength material properties and revised piezometric surface. The resultant factors of safety are presented below in Exhibit 10-55.

Exhibit 10-55: Summary of Existing Condition Limit Equilibrium Analyses

Section	Loading Condition	Previous LE Scaled Strength	Current LE	Current LE
			Scaled Strength	Friction Only Strength
Section 1	Usual – Existing Condition	0.97	1.17	1.02

By keeping the material properties the same, the only appreciable difference between the previous suite of limit equilibrium models and our updated analyses is the piezometric surface. We see an increase of 0.2 in the factor of safety from the previously scaled strength LE analyses and the updated scaled strength LE analyses for the existing usual loading condition. This indicates that the previously assumed groundwater conditions were more adverse than what has been recorded via the VWPs and utilized for the updated LE analyses. Furthermore, we switched to frictional shear strength for our LE analyses which thus assumed that the existing spillway under the usual loading condition had a factor of safety of approximately 1.0. This indicates that our current LE analyses are more conservative with respect to the available shear strength along foliation as to the previously accepted scaled strength material properties which resulted in a factor of safety of approximately 1.2 in the current model.

Based on the evaluated geometry, groundwater conditions, and material and support properties, both the grouted rock buttress (with shear rock dowels) and the anchor-supported slope meet all factors of safety for the evaluated loading conditions. The following exhibit (Exhibit 10-56) presents a summary of the resultant factors of safety (rounded down to the nearest tenth) of the limit equilibrium analyses.

Exhibit 10-56: Summary of Resultant Factors of Safety of the Limit Equilibrium Analyses

Section	Loading Condition	FS Criteria	Grouted Rock Buttress		Anchor-Supported Slope	
			Above Buttress	Dowel Supported	1 ¾-inch, Grade 150	8 Strand
Section 1	Usual	1.5	1.6	2.0	2.2	2.4
	Unusual	1.3	1.6	2.0	2.2	2.4
	Pseudo-static	1.1	1.1	1.3	1.1	1.1
	Post-Earthquake	1.3	1.4	1.8	1.6	1.9
Section 2	Usual	1.5	2.8	2.3	2.3	2.7
	Unusual	1.3	2.8	2.3	2.3	2.6
	Pseudo-static	1.1	2.0	1.5	1.2	1.3
	Post-Earthquake	1.3	2.6	2.1	1.8	2.1

As presented in Exhibit 10-56, all supported cases meet the design factors of safety for each loading condition. For usual loading conditions with a target FS of 1.5, the FSs range from 1.6 to 2.8 for both sections (Section 1 and Section 2) for all spillway support designs. For unusual loading conditions (PMF) with a target FS of 1.3, the FSs range from 1.6 to 2.8 for both sections for all spillway support designs. For extreme (pseudo-static) loading conditions with a target FS of 1.1, the FSs range from 1.1 to 2.0 for both sections for all spillway support designs. For post-earthquake loading conditions with a target FS of 1.3, the FSs range from 1.4 to 2.6 for both sections for all spillway support designs.

10.3.9 Action Level Limit Equilibrium Analyses of VWPs

As part of the required information to be provided to FERC, we performed an additional suite of analyses to evaluate the piezometric head in each of the VWPs of the additional spillway borings to meet Action Levels (wherein an Action Level is defined as a factor of safety of 1.2 under usual static conditions) for the grouted rock buttress with shear rock dowels. It was assumed that there is connectivity between VWPs vertically such that only one piezometric surface needs to be determined for each section (i.e., Section 1 or Section 2). Furthermore, it is assumed that there is lateral connectivity between VWPs for each section of the spillway such that there would be an observable rise in the hydrostatic head of adjacent VWPs. As a result, the action level elevations for VWPs in the recommended grouted rock buttress case, presented below as Exhibit 10-57, are for the two sets of VWPs;

16-1 & 17-1, and 16-2 & 17-2. For example, if you have a 21-foot rise in BH-16-1 and a 69-foot rise in BH-17-1, then the FS for Section 1 would be reduced to 1.2.

Exhibit 10-57: VWP Action Levels for Spillway Borings

Section	Action Level Elevation (feet)		Head Above Observed Historic High (feet)	
	BH-16 Borings	BH-17 Borings	BH-16 Borings	BH-17 Borings
Section 1 (BH-16-1 & BH-17-1)	530	635	21	69
Section 2 (BH-16-2 & BH-17-2)	535	635	39	33

10.3.10 Proposed Spillway Support Design

Based on the evaluated geometry, groundwater conditions, and material and support properties, the dowel-supported grouted rock buttress and the two anchor-supported slope scenarios meet all factors of safety for the evaluated loading conditions. However, from review of past projects and construction-related costs, we recommend stabilizing the existing spillway slope with a grouted rock buttress by filling the existing sluiceway structure with concrete and rock rubble and installing 20-foot-long shear pins on 5-foot centers (embedded 10 feet into the sluiceway and extending 10 feet into the buttress). A suite of weep holes as discussed previously will be installed to aid in drainage of the spillway rockmass and assist in lowering hydrostatic pressures (Shannon & Wilson, 2021).

10.4 Downstream Spillway Protection

This section addresses erosion downstream of the spillway that is related to the failure mode described in PFM F-UB-3C. Plane shear is an active and ongoing failure mode in the slopes downstream of the spillway. This failure mode is visible in construction photographs and is evident by the existing rock pile at the base of the slope resulting from these plane shear failures (Exhibit 10-58). Accumulated rock blocks at the base of the slope range from slabs a few feet thick—measured perpendicular to foliation—to blocks up to two (2) feet to 10 feet wide—measured parallel to foliation. Mitigation to avoid damage to the spillway was addressed during original construction by extending the concrete apron around the downstream end of the spillway casting against the foliation plane. While this has been largely successful over the years, PSE remains concerned that plane shear failures may progress beyond the existing concrete apron and undermine the end of the spillway. Hydraulic and limit equilibrium analyses were performed to evaluate global stability of the slope downstream of the spillway. Details of these analyses, and mitigation efforts designed to improve stability of the slope and protect the downstream spillway from further erosion, are presented in the following sections.

Exhibit 10-58: Photo of Slope Downstream of the Spillway with Rock Pile at Base of Slope

10.4.1 Hydraulic Analysis

A hydraulic analysis was performed by Dr. Henry Falvey (Falvey, 2016) to evaluate the force imparted on the rock downstream of the spillway. The hydraulic analysis considered different flow rates, stream trajectories, and landing locations on the downstream spillway slope for normal operations (usual loading conditions). The purpose of the hydraulic analysis was to estimate the stream power, which is an index of the force and erosive ability of a flowing body of water acting on the spillway. Given the stream power, mitigation measures were then designed to support and protect the slope downstream of the spillway from further erosion. The most adverse loading condition was used to evaluate global stability and the integrity of the proposed mitigation measures in our analyses. The details and assumptions of the analysis are included in Dr. Falvey's report, which is presented as Appendix G.

10.4.2 Limit Equilibrium Analyses

We performed 2D limit equilibrium stability analyses using Slide (v. 7.009) by Rocscience (2017) and selected GLE/Morgenstern as the vertical slide limit equilibrium analysis method (Abramson, Lee, Sharma, and Boyce, 2001). To adequately capture the plane shear failures, we employed non-circular failure surface searching methods in our models. We selected the GLE/Morgenstern method of slope stability analysis because it accommodates non-circular failure surfaces and is generally considered the most robust limit equilibrium method, as it resolves both force and moment vertical slice equilibrium. We performed a 2D evaluation of the plane shear failure mode which does not consider side-release planes and their respective contributions to rock block stability; thus, the most adverse plane shear condition is evaluated.

Analyses of spillway stability included:

- Existing conditions, with and without hydraulic loading, and
- A rock bolt support with concrete facing case (static support case).

10.4.2.1 Design Criteria

Due to uncertainty in the groundwater conditions, mitigation measures were designed to achieve a target FS of 2.0 for global stability of the slope instead of the typical FS of 1.5 for usual (static) loading conditions. Seismic and post-seismic conditions were not considered.

10.4.2.2 Slope Geometry

Slope geometry and cross sections used in our analyses were based on survey work performed by Orion Geomatics in October of 2016. The surface has an average inclination of about 40 degrees and steepens to about 55 degrees near the toe of the slope. The average dip direction is about 25 degrees, which is roughly parallel to the mean dip direction of the rock foliation. The dip of the foliation ranges from 15 to 60 degrees. Therefore, the foliation can daylight in the slope, making a plane shear failure mode kinematically admissible. Foliation and a more steeply inclined joint set that acts as a release plane, with dips ranging from about 60 to 85 degrees, were considered in our analyses as discussed in the next section.

10.4.2.3 Rock Mass Properties

We used an anisotropic strength function to incorporate the rock mass shear strength and foliation/discontinuity strength into our global stability model. The discontinuity shear strength was applied over dips ranging from 30 to 50 degrees for foliation and 70 to 80 degrees for the more steeply inclined release plane joint set. These ranges were selected based on the density of discontinuity measurements within the discontinuity sets. The discontinuity friction angle, of 25 degrees, applied to these dip ranges was based on estimates of the base friction angle for phyllite from laboratory testing. Cohesion, representing rock bridges along the discontinuity planes, was estimated to be about 1,400 psf, established from analyses of the existing conditions under hydraulic loading as described in the next section. For all other inclinations, phyllite rock mass shear strength values were applied using equivalent Mohr-Coulomb properties of 17,800 psf for cohesion and a friction angle of 50 degrees.

10.4.2.4 Groundwater Conditions

As previously mentioned, the groundwater conditions within the slope downstream of the spillway are unknown. Due to this uncertainty, groundwater was not modeled in our analyses. Instead, we increased the target FS to 2.0 for design.

10.4.2.5 Existing Conditions

While slope failures have occurred along the foliation planes downstream of the spillway, they have been relatively small, with volumes typically less than 10 cubic yards, and the slope downstream of the spillway is not actively failing. This indicates that the slope is generally stable under existing conditions but becomes periodically unstable. Reasons for the instability range from an increase in driving forces (i.e., groundwater conditions or force from spilling water) or a reduction in the resisting forces (i.e., weathering of the rock mass or fracture propagation through cyclic loading of the rock mass). As such, it was assumed that the FS under a flow of approximately 4,000 cubic feet per second (Falvey, 2016) is slightly higher than 1.0, indicating failure may occur under these loading conditions. The stream from the spillway impacts a horizontal width slightly larger than the 50-foot spillway width due to gravity and dispersion of the water as it runs off the spillway edge. This results in an approximately 70-foot slope length being impacted by the spillway discharge with an equivalent water pressure of 4,000 psf. As illustrated in Exhibit 10-59, a static FS against sliding failure slightly higher than 1.0 (1.09) was achieved with discontinuity shear strengths of 1,400 psf cohesion and a joint friction angle of 25 degrees. For a larger failure, spanning about half the slope, a FS of about 1.2 (1.23) exists for this loading condition.

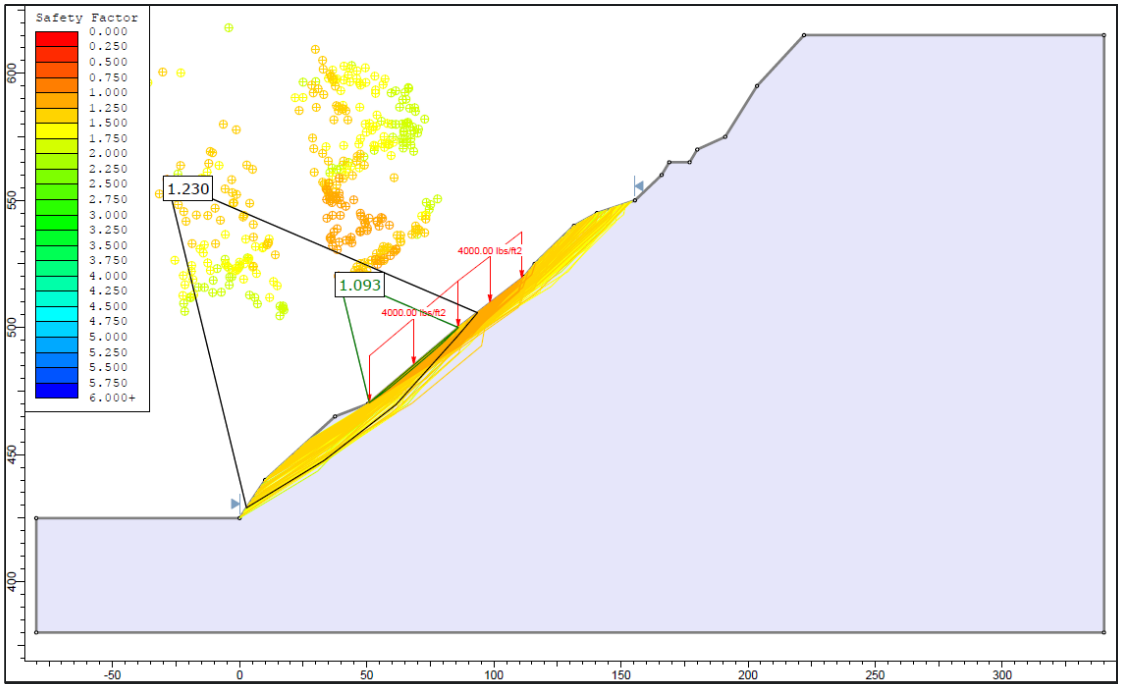

Exhibit 10-59: Existing Conditions with Hydraulic Loading Analysis

We also checked the FS for the existing slope without hydraulic loading from the spillway. The results of that analysis are presented in Exhibit 10-60. For this case of the existing slope without hydraulic loading, the FS is about 2.1 (2.14).

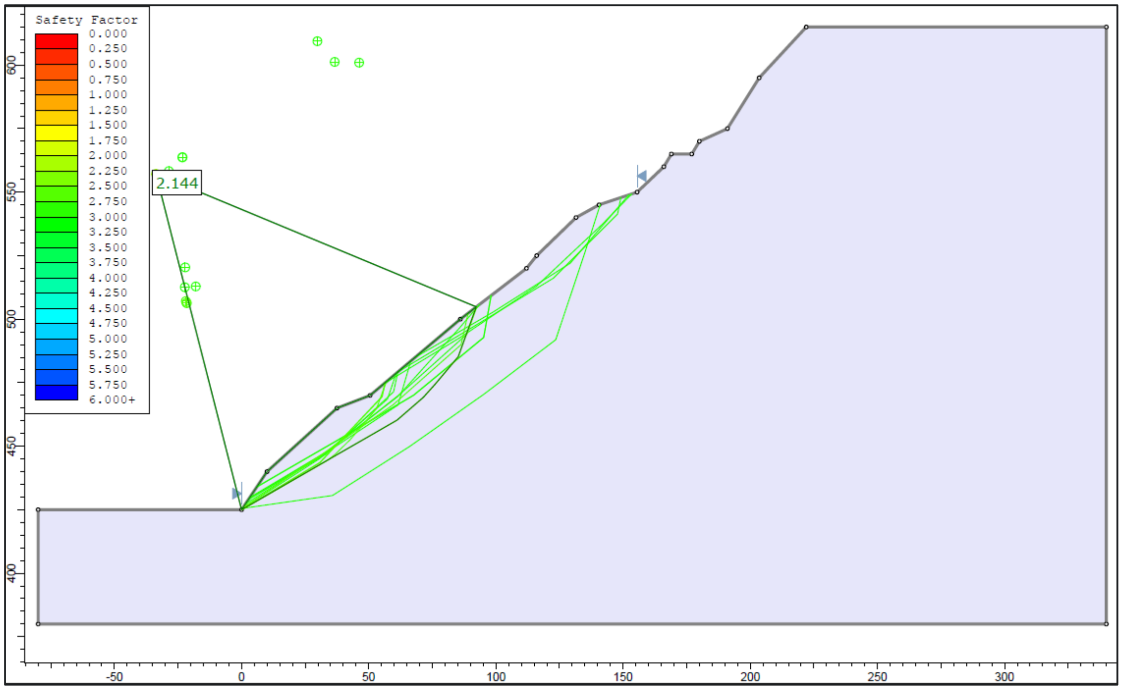

Exhibit 10-60: Existing Conditions without Hydraulic Loading Analysis

10.4.2.6 Static Support Case

The limit equilibrium analyses performed to evaluate the mitigation measure required to achieve a FS of 2.0 used the same cross-section, material properties, assumed failure mechanism, and groundwater conditions as the existing conditions case. The mitigation measure considered included pattern rock bolting with a concrete reinforcement pad along the surface of the slope, as discussed further in the next section. Based on the geometry of the slope, concrete pad, and rock bolts, three types of failure could develop:

- Failure Surface 1: Failure surface initiates and terminates below the concrete facing,
- Failure Surface 2: Failure surface initiates below the concrete facing and terminates outside of the concrete facing, and
- Failure Surface 3: Failure surface encompasses or goes around the concrete facing.

We modeled the concrete to have no strength to allow all three failure surface types to develop in our model. However, for a rock sliding failure to occur along a failure surface that initiates and terminates below the concrete facing (Failure Surface 1), the concrete facing would have to be compromised and therefore not designed correctly. For this reason, we targeted a FS of 2.0 for the other two failure surfaces (Failure Surface 2 and Failure Surface 3) and checked the FS value for Failure Surface 1 for the case in which the concrete facing provides no resistance. The results of the analysis are presented in Exhibit 10-61.

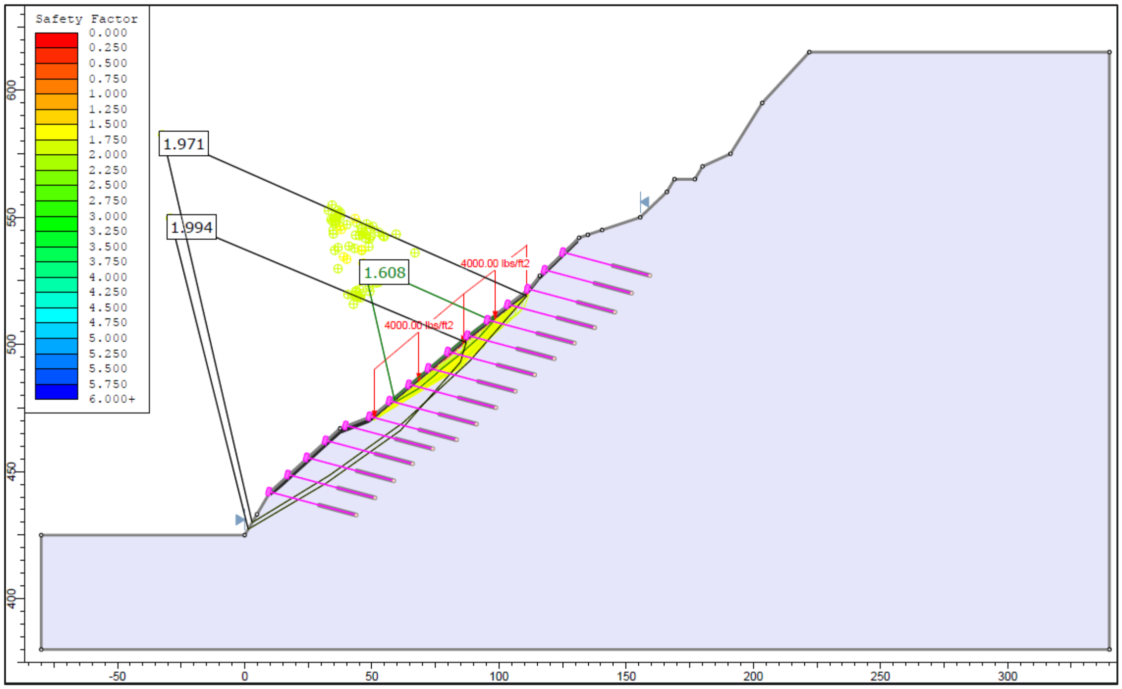

Exhibit 10-61: Static Support Case Analysis

Rock dowels modeled in our analysis were representative of 1⅜-inch, Grade 150 bars spaced in a 10-foot square pattern, along and perpendicular to the slope. The strength, length, and spacing of the rock dowels were adjusted until a FS of 2.0 was achieved for the controlling failure surface, which initiates below the concrete facing and extends below the concrete facing toward the toe of the slope. For this support pattern, a FS of 1.6 (1.61) was achieved for a failure surface initiating and terminating below the concrete facing, and a FS of 1.9 (1.97) was achieved for a failure surface encompassing the concrete facing. A minimum unbonded length of 20 feet is required to achieve these FSs.

A separate set of analyses was performed to evaluate the required bond length of the dowels. The analyses evaluated the grout-to-ground stress and bar-to-grout stress of the dowels. A minimum bond length of 15 feet is required to exceed stresses developed in the dowels.

10.4.3 Concrete Reinforcement Pad

In assessing mitigation measures, we recognized that a typical rock dowel design would not provide an adequate service life for PSE due to the erosive capacity of water hitting the rock surface downstream of the spillway. The continual force of the water acting on the dowel heads and foliation surface could, over time, cause blocks of rock to fail in between the dowel locations and fail the dowels through cyclic bending. The mitigation measure proposed is a reinforced concrete slab to protect the rock surface, dowel heads, and to distribute the impact force of the water.

BergerABAM under contract to Shannon & Wilson performed analyses to evaluate shear loading on the dowels imparted by spillway hydraulic loading and sliding along the concrete pad to rock interface (Appendix L). They considered the weight of concrete as well as horizontal and vertical forces imparted on the concrete by water coming from the spillway. Considering allowable bar strengths and sliding resistance between the concrete and rock, BergerABAM calculated that a 2¼-inch, Grade 150 bar spaced on a 10-foot grid would be required (Appendix L). As an additional supportive measure to resist straining and movement of the concrete pad atop the downstream spillway surface toward the toe of the slope, a row of micropiles were designed at the toe of the slope to carry the load of the concrete pad.

10.4.4 Proposed Downstream Protection Support Design

To provide adequate support to the downstream spillway foliation surface, we recommend pattern rock dowel installation of Grade 150, 2¼-inch bars on a 10-foot spacing. Each rock dowel should have a minimum length of 35 feet, with a 20-foot-long unbonded zone and a minimum 15-foot-long bonded zone. The minimum hole diameter of each dowel is 5 inches. The heads of the rock dowels should be encapsulated in an approximately 2-foot-thick reinforced concrete pad. A double row of micropiles should be installed at the toe of the slope once loose rock debris has been removed. To alleviate water pressures that may build up behind the concrete pad, weep holes, 40 feet in length and spaced on a 20-foot grid, should be drilled.

According to the PFMA, this PFM was classified as Category IV because a failure of the rockslide area would not affect the operation or use of the spillway, the erosion path is very long, and the 3DEC analysis does not account for the presence of the spillway (HDR, 2019). For these reasons, and because historic erosion (monitored using lidar surveys since 2015) has shown that erosion has not encroached within 15 feet of the spillway, PSE has adopted a monitoring approach to the downstream spillway slope prior to implementation of slope stabilization measures. The approach is presented in Exhibit 10-60. If new erosion events encroach to the line in Exhibit 10-62 marked "Threshold Limit," then PSE proposes to complete final design of the facing systems. Facing system construction would be implemented if erosion encroaches on the line marked "Action Limit."

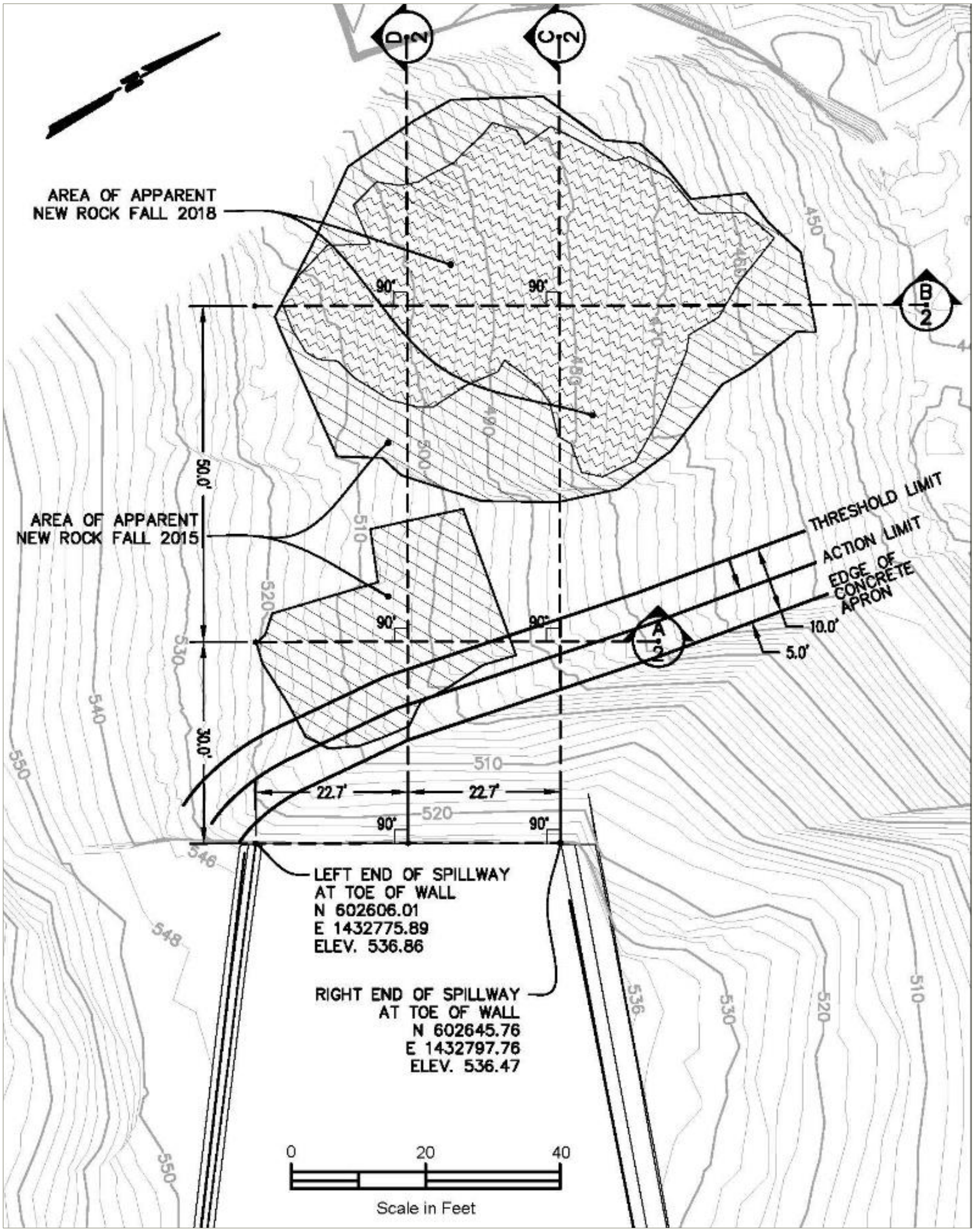

Exhibit 10-62: Downstream Erosion Monitoring Program

11 CONCLUSIONS

This report addressed the following PFMs:

- PFMs N-UB-2A, F-UB-2A, and S-UB-2A, which pertain to shear displacement along a foliation surface within the rock mass below Monoliths 18/19;
- PFMs N-UB-2B, F-UB-2B, and S-UB-2B, which pertain to shear displacement along a discontinuity within the rock mass below Monoliths 9/10;
- PFMs N-UB-2C, F-UB-2C, and S-UB-2C, which pertain to sliding along an adversely oriented discontinuity (or discontinuities) in the foundation below Monoliths 4/5;
- PFMs S-UB-3 and F-UB-3B, which pertain to stability of the spillway slope downstream of Monoliths 16/17 or erodibility of the slope downstream of the spillway with the potential to undermine and lead to damage or loss of the spillway and undermining of Monoliths 16/17;
- PFM F-UB-3A is introduced but is not directly addressed in this report;
- PFM F-UB-3C, which pertains to stability of the slope downstream of the spillway with the potential to undermine and lead to damage or loss of the spillway and undermining of Monoliths 16/17; and
- PFMs N-UB-8, F-UB-8, and S-UB-6 are introduced but are not addressed in this report.

No kinematically admissible rock wedges formed by the intersection of major structures were identified in Monoliths 1, 2, and 3 nor in Monoliths 4 and 5. Two (2) major structures exist in the vicinity of Monoliths 1, 2, and 3: Fault A and Soft Seam B; these structures do not form a kinematically admissible wedge. Two (2) major structures also exist in the trough under Monolith 4 and 5: Soft Seam C and a previously unidentified structure, referred to as the Mylonite Zone; again, these structures do not form a kinematically admissible wedge.

11.1 PFMs N-UB-2A, F-UB-2A, and S-UB-2A

Based on a review of previous reports, historical photographs, downhole camera videos, location of observed offsets in drain holes, and the recent boring exploration program, a block under Monoliths 17, 18, and 19 has been identified. The block is formed by foliation and Joint Set 4, and the current interpretation is that the block does not daylight downstream. Hatch also used this geometry in their 3D numerical model and determined that Monolith 18 is locked up against Monolith 19, such that further displacement of Monolith 18 was not anticipated (Hatch, 2015). Inclinometer and joint meters installed at monolith contraction joints indicate that all displacements are elastic, and no permanent displacement has occurred.

During a review of drain holes, offsets were observed in existing drain holes in Monoliths 20 and 21 that may be related to monolith displacements recorded in 1963. The apparent dip of a surface connecting the offsets is consistent with the dip of the foliation set. Joint meter instruments installed at the contraction joint between Monoliths 20 and 21 indicate elastic movement related to reservoir and temperature fluctuations, although no permanent displacement has been measured in the joint meters since April 2015.

Because no permanent displacement has been measured in Monoliths 17, 18, and 19, and no permanent displacement has been measured between Monoliths 20 and 21 since April 2015, PFMs N-UB-2A, F-UB-2A, and S-UB-2A should be considered for reclassification in the next PFMA.

11.2 PFMs N-UB-2B, F-UB-2B, and S-UB-2B

Based on previous reports, historical photographs, downhole camera videos, and the recent boring exploration program, two (2) major structures exist in the vicinity of Monoliths 6, 7, 8, 9, and 10: Soft Seam D and Block 10 Deformation Zone. These major structures, combined with the Block 6-10 Discontinuity interpreted from existing drain offsets, form a rock wedge with a trend/plunge of 80/048 degrees. This wedge daylights underneath Monoliths 6, 7, 8, 9, and 10, and is therefore not admissible because it is confined by the dam.

The current interpretation of historic displacement is that the rock wedge sliding along the Block 6-10 Discontinuity moved downstream as it compressed into Soft Seam D and the Block 10 Deformation Zone. Review of manual inclinometer data and piezometer data indicates that recent displacements observed in IN-1000 at Elevation 491 feet, in EX-0900 between anchors 3 and 4, and in EX-1000 between anchors 2 and 3 are elastic and directly correlated to groundwater elevation measured in piezometer data in B7-P1, B11-P1 Lower, and IN-0900-4 and to reservoir elevation. These piezometers are positioned or have a screened interval that cross or are in proximity to the Block 6-10 Discontinuity. In past years, as the Baker Lake pool is raised in the spring, the phreatic surface in B7-P1 Lower approaches Elevation 600 and remains high for a two (2) to three (3) week period and then drops to approximate Elevation 560 to 570 feet. However, after mid-May 2020, the phreatic surface in B7-P1 remained high, fluctuating between Elevation 595 and 609 feet, possibly indicating a continued connection to the reservoir and an opening of seepage pathway along the Block 6-10 Discontinuity.

A review of drain holes identified an offset in B11-D1 at a depth of 27.6 feet that appears to line up with the Block 6-10 Discontinuity. The offset of this feature is less than offsets observed in drain holes in Monoliths 7, 9, and 10. If the Block 6-10 Discontinuity extends into Monolith 11, then the U1 Fault may form the left plane of the wedge rather than the

Block 10 Deformation Zone. In this case, the wedge will have similar geometry to the wedge formed with the Block 10 Deformation Zone, will not daylight downstream of the dam, and will almost entirely be contained under the footprint of the dam. Installation of inclinometer casings and MPBXs adjacent to contraction joints in Monoliths 10/11 and 11/12 is not recommended at this time. Installation of this instrumentation should be considered if permanent displacement is observed in the existing joint meters installed at the Monolith 10/11 and 11/12 contraction joints.

Because the wedge formed by Soft Seam D and Block 10 Deformation Zone daylights underneath Monoliths 6, 7, 8, 9, and 10—and is therefore not admissible because it is confined by the dam—PFMs N-UB-2B, F-UB-2B, and S-UB-2B should be considered for reclassification in the next PFMA.

11.3 PFMs N-UB-2C, F-UB-2C, and S-UB-2C

Based on previous reports, historical photographs, downhole camera videos, and the recent boring exploration program, two (2) major structures exist in the vicinity of Monoliths 4 and 5: Soft Seam C and the Mylonite Zone. These structures are consistent with the general orientation of the foliation and do not form a kinematically admissible block of rock under the foundation of the dam. Review of manual inclinometer data for IN-0500 does not indicate any displacement. Because no displacement has been measured in the inclinometer readings and the wedge formed by Soft Seam C and the Mylonite Zone does not form a kinematically admissible block of rock under the foundation of the dam, PFMs N-UB-2C, F-UB-2C, and S-UB-2C should be considered for reclassification in the next PFMA.

11.4 PFMs S-UB-3, F-UB-3B, and F-UB-3A

PFMs S-UB-3 and F-UB-3B pertain to sliding of the spillway along a foliation surface that daylights in the foundation below Monoliths 16/17. Two alternatives are presented to stabilize the existing spillway. The first alternative is to support the slope with Grade 150, 1¾-inch-diameter, post-tensioned rock anchors installed on 8-foot centers with a bond length of over 20 feet. The preferred alternative is to fill the existing sluiceway structure with rock excavated from the tailrace channel, encapsulate the rock rubble with concrete to create a grouted rock buttress to support the base of the slope, and install 20-foot-long shear pins on 5-foot centers (embedded 10 feet into the sluiceway and extending 10 feet into the buttress).

PFM F-UB-3A is introduced in this report but is not addressed as it pertains to damage to the spillway structure during a large flood. This report does not address the structural integrity of the spillway structure; however, options to improve the stability of the slope using either post-tensioned rock anchors or a grouted rock buttress will preclude foundation failure as a contributing factor to this PFM.

11.5 PFM F-UB-3C

This failure mode relates to loss of material downslope of the spillway as a result of extended spillway flows. The erosion progresses upstream, undermining the spillway, and possibly the monoliths. According to the PFMA, this PFM was classified as Category IV because a failure of the rockslide area would not affect the operation or use of the spillway, the erosion path is very long, and the 3DEC analysis does not account for the presence of the spillway (HDR, 2019).

Two alternatives to address this PFM are proposed. The first proposed option is to construct a reinforced concrete pad on the slope beyond the spillway structure. The second proposed option is to adopt a monitoring approach that includes monitoring performance of the slope after spill events. If the erosion encroaches to a "Threshold Limit" line (Exhibit 10-62), then design of the facing system would be finalized. If erosion encroaches to the "Action Limit" line, then a facing system would be implemented. Because historic erosion (monitored using lidar surveys since 2015) has shown that erosion has not encroached within 15 feet of the spillway, and due to the Category IV criteria presented in the PFMA and as previously discussed, PSE has adopted the second option.

12 REFERENCES

Abramson, L.W., Lee, T.S., Sharma, S., and Boyce, G.M., 2001, Slope Stability and Stabilization Methods, 2nd edition, John Wiley & Sons.

ASTM International, 2008, Standard test method for performing laboratory direct shear strength tests of rock specimens under constant normal force, D5607-08: West Conshohocken, Pa., ASTM International, Annual book of standards, v. 04.08, soil and rock (I): D420 - D5876, 8 p., available: www.astm.org.

ASTM International, 2010a, Standard practice for sonic drilling for site characterization and the installation of subsurface monitoring devices, D6914-04(2010): West Conshohocken, Pa., ASTM International, Annual book of standards, v. 04.09, soil and rock (II): D5877-latest, 11 p., available: www.astm.org.

ASTM International, 2010b, Standard test methods for laboratory determination of water (moisture) content of soil and rock by mass, D2216-10: West Conshohocken, Pa., ASTM International, Annual book of standards, v. 04.08, soil and rock (I): D420 - D5876, 7 p., available: www.astm.org.

ASTM International, 2014a, Standard practice for rock core drilling and sampling of rock for site exploration, D2113-14: West Conshohocken, Pa., ASTM International, Annual book of standards, v. 04.08, soil and rock (I): D420 - D5876, 20 p., available: www.astm.org.

ASTM International, 2014b, Standard test method for compressive strength and elastic moduli of intact rock core rock specimens under varying states of stress and temperatures, D7012-14: West Conshohocken, Pa., ASTM International, Annual book of standards, v. 04.09, soil and rock (II): D5877-latest, 9 p., available: www.astm.org.

Barton, N.; Lien, R.; and Lunde, J., 1974, Engineering Classification of Rock Masses for the Design of Tunnel Support in Rock Mechanics 6(4), p. 189-239.

Barton, Nick and Bandis, Stavros, 1993, Effects of block size on the shear behavior of jointed rock, in Goodman, R. E. and Heuze, F. E., eds., Issues in rock mechanics, 23rd Symposium on Rock Mechanics, 1982, Berkeley, Calif., Proceedings: N.Y., Society of Mining Engineers of the American Institute of Mining, Metallurgical and Petroleum Engineers, Inc., p. 739-760.

Brown, E.H. et al., 1987, Geologic map of the Northwest Cascades, Washington, Geological Society of America, Map and Chart Series MC-61.

California Division of Mines and Geology (CDMG), 1997, Guidelines for Evaluating and Mitigating Seismic Hazards in California, California Div. of Mines and Geology, Special Publication 117, www/consrv.ca.gov/dmg/pubs/sp/117/

Deere, D.U. and Miller, R.P., 1966, Engineering classification and index properties for intact rock: Kirtland Air Force Base, New Mexico, Air Force Weapons Laboratory, Report no. AFWL-TR-65-116, NTIS Report no. AD 646-610, 308 p.

Federal Energy Regulatory Commission (FERC), Office of Energy Projects, Division of Dam Safety, and Inspections, 2008, Dam safety inspection report: Portland, Ore., FERC, project No. 2150 WA.

Fell, R., MacGregor, P., Stapledon, D., and Bell, G., 2005, Geotechnical Engineering of Dams: Leiden, A.A. Balkema, 912 p.

Forest Service, 2002, Baker River watershed analysis, Mt. Baker-Snoqualmie National Forest, Pacific Northwest Region, Seattle, WA, August.

Genov, G., 2020, Revisiting the rule-of-thumb dependencies of the shear strength and the hardness of the yield and the ultimate strengths, University of Bergen – Department of Physics and Technology, Norway.

Goodman, R.E., and Powell, Chris, 2003, Investigations of blocks in foundations and abutments of concrete dams: Journal of Geotechnical and Geoenvironmental Engineering, v. 129, no. 2, p. 105-116.

Hatch Energy Services, Inc., 2009, Stress and stability analysis, final report, Upper Baker Dam: Report prepared for Puget Sound Energy, Bellevue, Wash., Rev. 2, June.

Hatch Energy Services, Inc., 2015, Draft Structural Analysis of Upper Baker Dam Blocks 18 and 19: Report prepared for Puget Sound Energy, Bellevue, Wash., Rev. B, April 6.

HDR Engineering, Inc., 2019, Baker River Hydroelectric Project, Upper Baker Development FERC Project No. 2150 Potential Failure Modes Analysis Report; Report prepared by HDR Engineering, Inc., Bellevue, Wash., for Puget Sound Energy, Bellevue, Wash., November.

Henry T. Falvey & Associates, Inc., 2016, Estimate of Stream Power, Conifer, CO, June.

Henry T. Falvey & Associates, Inc., 2019, Memorandum Pressures on Invert of Upper Baker Dam Spillway, Conifer, CO, April.

Hoek, E.; Carter, T.G.; and Diederichs, M.S., 2013, Quantification of the Geological Strength Index chart, in 47th US Rock Mechanics/Geomechanics Symposium, San Francisco, Calif., 2013, Proceedings: Alexandria, Va., American Rock Mechanics Association, paper 13 672, 8 p.

Hoek, Evert; Kaiser, P.K.; and Bawden, W F., 1995, Support of underground excavations in hard rock: Brookfield, Vt., A. A. Balkema Publishers, 215 p.

Idriss, I. M.; Archuleta, R.J.; Abrahamson, N.A., 2018, Engineering guidelines for the evaluation of hydropower projects, Chapter 13 - Evaluation of earthquake ground motions (final): Washington, D. C., FERC, available: https://www.ferc.gov/industries/hydropower/safety/guidelines/eng-guide.asp.

International Commission on Large Dams (ICOLD), 2017, Internal erosion of existing dams, levees and dikes, and their foundations, Bulletin 164, 288 p.

Jennings, J.E., 1970, A Mathematical theory for the calculation of the stability of slopes in open cast mines, in Planning of Open Pit Mines Proceedings, Johannesburg; p. 87-102.

Jobson, R.W.; Rathje, E. M.; Jibson, M.W.; and Lee, Y.W., 2013, SLAMMER – Seismic Landslide Movement Modeled using Earthquake Records (ver. 1.1, November 2014): U.S. Geological Survey Techniques and Methods, Book 12, Chapter B1, unpaginated.

Kramer, S.L., 1996, Geotechnical earthquake engineering: Upper Saddle River, N. J., Prentice Hall, 653 p.

Leonard, Boudinot, and Skodje, 2008, NAVD88 – 2006 Survey for Upper and Lower Baker Facilities, Report prepared by Leonard, Boudinot, and Skodje, Inc., Mt. Vernon, Wash., for Puget Sound Energy, Inc., Bellevue, Wash., April.

MWH Americas, Inc., 2004, Baker River hydroelectric project, Upper baker development FERC part 12 safety inspection report: Report prepared by MWH Americas, Inc., Bellevue, Wash., for Puget Sound Energy, Inc., Bellevue, Wash., October.

MWH Americas, Inc., 2009, Baker River hydroelectric project, Upper Baker Dam evaluation of sliding stability: Report prepared by MWH Americas, Inc., Bellevue, Wash., for Puget Sound Energy, Inc., Bellevue, Wash., June.

Newmark, N.M., 1965, Fifth Rankine lecture: Effects of earthquakes on dams and embankments: Geotechnique, v. 15, no. 2, p. 139-160.

Pacific Geomatics Services, Inc., 2014, Plate set, Upper Baker Dam abutments topographic overview and notes: Plates prepared by Pacific Geomatic Services, Inc., Mountlake Terrace, Wash., 1305901_TOPO.DWG, for Puget Sound Energy, Bellevue., Wash., January 4p.

Post-Tensioning Institute (PTI), 2014, Recommendations for prestressed rock and soil anchors (5th ed.): Phoenix, Ariz., Post-Tensioning Institute, 110 p.

Puget Sound Energy (PSE), 1960, Upper Baker Dam, Concrete, Washington, construction photos: Photos from Puget Sound Energy Board of Consultants meeting no. 1, available: Shannon & Wilson, Inc. project file, 21-1-09014-100 [UBK Construction Photos.pdf].

Puget Sound Energy (PSE), 2009, History of Block 18/19 Relative Movements, Upper Baker River Project 2150: Report prepared by Puget Sound Energy, Bellevue, Wash., project no. 2150, for Federal Energy Regulatory Commission, Portland, Oreg., May 6.

Puget Sound Energy (PSE), 2013, Baker River development FERC no. 2150, Upper Baker Dam schematic section view (Rev. 2): Bellevue, Wash., Puget Sound Energy, drawing no. PTS-0157, sheet 2 of 4.

Puget Sound Energy (PSE), 2014, Geotechnical report, 2013 dam safety surveillance and monitoring report: Report prepared by Puget Sound Energy, Bellevue, Wash., BAK.2014.0430.0681.PSE.FERC-PRO, for the Federal Energy Regulatory Commission, Portland, Ore., April, 7 p.

Rocscience, Inc., 2017, Slide, v. 7.0, 2D Limit Equilibrium Slope Stability Analysis Toronto, Ontario, Rocscience, Inc.

Rocscience, Inc., 2019, RocData, v. 5.0, Rock, Soil and Discontinuity Strength Analysis, Toronto, Ontario, Rocscience, Inc.

Rocscience, Inc., 2020a, Dips, v. 8.006, Graphical and Statistical Analysis of Orientation Data Toronto, Ontario, Rocscience, Inc.

Rocscience, Inc., 2022, Slide2, v. 9.023, 2D Limit Equilibrium Slope Stability Analysis Toronto, Ontario, Rocscience, Inc.

Rocscience, Inc., 2022, Dips, v. 8.021, Graphical and Statistical Analysis of Orientation Data Toronto, Ontario, Rocscience, Inc.

Sabatini, P.J., Pass, D.G., and Bachus, R.C., 1999, Ground anchors and anchored systems: Washington, D. C., U.S. Federal Highway Administration, report no. FHWA-IF-99-015, Geotechnical Engineering Circular no. 4, 281 p.

Shannon & Wilson, 2008, Concrete-rock Interface, Upper Baker Dam, Concrete, Washington (DRAFT): Report prepared by Shannon & Wilson, Inc., Seattle, Wash., 21 1 20972-002, for Puget Sound Energy, Inc., Bellevue, Wash., October.

Shannon & Wilson, 2009, Foundation Drain Inspection, Upper Baker Dam, Concrete, Washington (DRAFT): Report prepared by Shannon & Wilson, Inc., Seattle, Wash., 21 1 20972-001, for Puget Sound Energy, Inc., Bellevue, Wash., February.

Shannon & Wilson, 2010, Rock abutment stability assessment (Revision 2), Upper Baker Dam, Concrete, Washington: Report prepared by Shannon & Wilson, Inc., Seattle, Wash., 21-1-20972-003, for Puget Sound Energy, Inc., Bellevue, Wash., November.

Shannon & Wilson, 2012, Geotechnical report, rock abutment stability assessment supplement, Upper Baker Dam, Concrete, Washington: Report prepared by Shannon & Wilson, Inc., Seattle, Wash., 21-1-20972-003, for Puget Sound Energy, Bellevue, Wash., August, 5 p.

Shannon & Wilson, 2013, Geotechnical draft report, camera inspection of drains near block 18, Upper Baker Dam, Concrete, Washington (DRAFT): Report prepared by Shannon & Wilson, Inc., Seattle, Wash., 21-1-09014-010, for Puget Sound Energy, Bellevue, Wash., December, 12 p.

Shannon & Wilson, 2015a, Draft assessment of failure modes, Upper Baker Dam, Concrete, Washington: Report prepared by Shannon & Wilson, Inc., Seattle, Wash., 21-1-21988-004, for Puget Sound Energy, Bellevue., Wash., April.

Shannon & Wilson, 2015b, Final Report, Baker River Projects, Probabilistic Seismic Hazard Analysis and Updated Deterministic Seismic Hazard Analysis; Report prepared by Shannon & Wilson, Inc., Seattle, Wash., 21-1-21999-004, for Puget Sound Energy, Bellevue., Wash., April.

Shannon & Wilson, 2016, Phase 2 Instrumentation Design Report, Upper Baker Dam, Concrete, Washington: Report prepared by Shannon & Wilson, Inc., Seattle, Wash., 21-1-21988-103, for Puget Sound Energy, Bellevue, Wash., September.

Shannon & Wilson, 2018, Dam Safety Instrumentation Upgrades, Upper Baker Dam, Concrete, WA: Report prepared by Shannon & Wilson, Inc., Seattle, Wash., 21-1-21988-235, for Puget Sound Energy, Bellevue, Wash., October.

Shannon & Wilson, 2019, Draft earthquake time history development for the Baker River project, Concrete, Washington: Prepared by Shannon & Wilson, Inc., Seattle, Washington, 21-1-22284-004, for Puget Sound Energy, July.

Shannon & Wilson, 2020a, Summary Report Upper Baker Dam Drain Scoping, Concrete, Washington: Report prepared by Shannon & Wilson, Inc., Seattle, Wash., 103486-001, for Puget Sound Energy, Bellevue, Wash., August.

Shannon & Wilson, 2020b, Geotechnical Report, Earthquake Time History Development for Baker Project, Concrete, Washington, Prepared by Shannon & Wilson, Inc., Seattle Wash., 21-1-22284-004 for Puget Sound Energy, Bellevue, Wash., November.

Shannon & Wilson, 2022, Geotechnical Design Memorandum GD-1, Rev. 1, Upper Baker Dam, Concrete, Washington, Spillway Support Analyses Criteria: Memorandum prepared by Shannan & Wilson, Inc., Seattle, Wash., 105102-033, for Puget Sound Energy, Bellevue, Wash., October.

Stone & Webster Engineering Corporation, 1960a, Foundation drainage dam: Drawing prepared by Stone & Webster for Puget Sound Energy & Light Company, number 9548-7H-7D, May 5.

Stone & Webster Engineering Corporation, 1960b, Report on geology of dam site record of grout curtain and subsurface drains, Baker River Project, Upper Baker River Plant, Puget Sound Power & Light Company: Report prepared by Stone & Webster, Boston, Mass., job no. J.O. No. 9548.01, for Puget Sound Power & Light Company, Seattle, Wash., October 26.

Stone & Webster Engineering Corporation, 1963, Report on additional drainage – blocks 5 through 10, Upper Baker Dam, for Puget Sound Power & Light Company, Seattle, Washington: Report prepared by Stone & Webster, Boston, Mass., for Puget Sound Power & Light Company, Seattle, Wash., August 27.

Stone & Webster Engineering Corporation, 1972, Report on analysis of movements, Upper Baker Dam: Report prepared for Puget Sound Power & Light, Seattle, Wash., October.

Stone & Webster Engineering Corporation, 1978, Geotechnical report, periodic safety inspection report no. 3, Baker River development, FERC project no. 2150: Report prepared by Stone & Webster, Denver, Colo., J.O. no. 13135, for Puget Sound Power & Light Company, Bellevue, Wash., Sept, 7 p.

Stone & Webster Engineering Corporation, 1983, Geotechnical report, periodic safety inspection report no. 4, Baker River development, FERC project no. 2150: Report prepared by Stone & Webster, Denver, Colo., J.O. no. 14390.05, for Puget Sound Power & Light Company, Bellevue, Wash., August, 18 p.

Stone & Webster Engineering Corporation, 1984, Seismic analyses of the Baker River Dams, volume three, Upper Baker Dam: Report prepared by Stone & Webster, Denver, Colo., for Puget Sound Power & Light Company, Bellevue, Wash., January (revised November 1987).

Stone & Webster Engineering Corporation, 1988a, Geotechnical report, periodic safety inspection report no. 5, Baker River development, FERC project no. 2150: Report prepared by Stone & Webster, Denver, Colo., J.O. no. 18069, for Puget Sound Power & Light Company, Bellevue, Wash., August, 19 p.

Stone & Webster Engineering Corporation, 1988b, Upper Baker Dam drainage system study: report prepared by Stone & Webster, Denver, Colo., Sept, 5 p.

Stone & Webster Engineering Corporation, 1990, Foundation drainage investigation, Upper Baker River Dam, final report: Report prepared by Stone & Webster, Denver, Colo., for Puget Sound Power & Light Company, Bellevue, Wash., November.

Tabor, R.W, Haugerud; R.A., Hildreth, W; and Brown, E.H., 2003, Geologic Map of the Mount Baker 30- by 60-Minute Quadrangle, Washington, USGS Pamphlet to accompany Geologic Investigations Series I-2660.

U.S. Army Corps of Engineers (USACE), 1994, Engineering and design – Rock Foundations: U.S. Army Corps of Engineers, Engineer Manual EM 1110-1-2908, 1 v, November 30.

Vertical Access, 2015, Condition Survey Report, Upper Baker Dam, Whatcom County, WA, September.

Wyllie, D.C., 1999, Foundations on Rock (2nd ed.): London, Spon Press, p. 401

Wyllie, D.C. and Mah, C.W., 2004, Rock slope engineering - civil and mining (4th ed.): London, Spon Press, 431 p.

Xanthakos, 1991, Ground Anchors and Anchored Structures, p. 141.